Development of an Antibody Reformatting Strategy for use in Targeted Protein Degradation Therapies for Neurodegenerative Diseases

Caitlin May O'Shea

A thesis submitted for the degree of PhD Molecular and Cell Biology

School of Life Sciences

University of Essex

Date of Submission for Examination: September 2025

Word count: 32,804

Abstract

Neurodegenerative diseases (NDDs) such as Parkinson's disease (PD) and amyotrophic lateral sclerosis (ALS) are a leading cause of global mortality and place a great financial and emotional burden on healthcare systems and support networks. Misfolded insoluble aggregates and toxic soluble proteins are central hallmarks of these NDDs. α-Synuclein aggregation drives Parkinson's disease pathology and is a suitable target for selective protein clearance. Biological proteolysis targeting chimeras (bioPROTACs) aim to eliminate disease-causing intracellular proteins using host cell ubiquitination and degradation pathways.

Here, I describe a bioPROTAC comprising the E3 ubiquitin ligase domain of CHIP (carboxy terminus of Hsc70-interacting protein) fused to NbSyn87, a nanobody specific for α-synuclein. Successful target degradation was achieved using the CHIP-NbSyn87 bioPROTAC. In contrast, CHIP-based bioPROTACs targeting SOD1, a ubiquitously expressed protein prone to misfold and aggregate in ALS, failed to degrade its target. This work highlighted key parameters for consideration during BioPROTAC design including target half-life and solubility, recognition domain binding affinity, molecular chaperone activity, and interdomain linker optimisation.

A strategy for rational repurposing of conformation-specific antibodies into soluble, functional intrabodies was also developed. Candidate antibodies were reformatted into scFvs and their solubility and specificity tested. A panel of misfolding-specific SOD1 intrabodies and conformation-specific α-synuclein intrabodies are described. Almost any antibody can be reformatted as a highly soluble (>70 %) and intracellularly stable intrabody using the described approach, based on the discovery

of a strong negative correlation between net charge and intrabody solubility in cell models.

Table of Contents

Statement of Originality

Unless otherwise stated in the text, this thesis is the result of my own work.

Acknowledgements

I want to extend my heartfelt thanks to my supervisor Gareth Wright, for all your support and guidance over the past three years. You've taught me to have a lot more faith in myself, to have fun and have helped me to become a better writer, presenter, teacher, and a better scientist.

I would like to especially thank my supervisor Leo Schalkwyk and panel chair Greg Brooke, who were able to give invaluable advice during panel meetings. Thank you to our lab technician Julie for teaching me everything health and safety and more importantly, for her incredible cakes. I would like to thank our specialist lab technician Rushba Shahzad for her motivation and support during the time we were working together; the memories made in the past two years are something I will always be thankful for. I would like to express how grateful I am for all the friendships I have made during these three years at Essex.

Mum, Rob and Dad: thanks for keeping my bank balance topped up while I spent my stipend on coffee and pastries. Thank you for your unwavering love and support, and for believing in me, so that I could chase my childhood dream. I would like to thank Teg Owen; who's 99 years of life experience and advice has shaped me into the woman I am today.

And lastly I would like to acknowledge my little (big) brother Talan who always had one piece of advice for me: "Stay weird".

List of Figures

List of Tables

List of Appendices

Glossary of Abbreviations

Abbreviation	Full name
AAV	Adeno-associated virus
AbRSA	Antibody Region-Specific Alignment
AD	Alzheimer's Disease
AF	AlphaFold
AI	Artificial intelligence
ALS	Amyotrophic Lateral Sclerosis
ALSFRS-R	Amyotrophic Lateral Sclerosis Functional Rating Scale - Revised
AMPK	AMP-activated protein kinase
ANOVA	Analysis of Variance
ApoE4	Apolipoprotein E4
AR	Androgen Receptor
ATP	Adenosine triphosphate
AU	Absorbance Units
AUTAC	Autophagy targeting chimera
AUTOTAC	Autophagy targeting chimera
BBB	Blood brain barrier
BCA	Bicinchoninic Acid
bioPROTAC	Biological proteolysis targeting chimera
BRCA1	Breast cancer gene 1
BRD4	Bromodomain-containing protein 4
C-terminal	Carboxy-terminal
C9ORF72	Chromosome 9 open reading frame 72

cDNA	Complementary DNA
CDR	Complementarity determing region
CETSA	Cellular Thermal Shift Assay
CHIP	Carboxy-terminus of Hsc70-interacting protein
CI-M6PR	cation-independent mannose-6-phosphate receptor
cm	centimetres
CMA	Chaperone mediated autophagy
CNS	Central Nervous System
CO_2	Carbon dioxide
CRBN	Cereblon
CRISPR	Clustered Regularly Interspaced Short Palindromic Repeat
CSF	Cerebrospinal fluid
DEPTAC	Dephosphorylation targeting chimera
DLB	Dementia with Lewy Bodies
DMEM	Dulbecco's Modified Eagle Medium
DMSO	Dimethyl sulphoxide
DNA	Deoxyribonucleic acid
DTT	Dithiothreitol
E. coli	*Escherichia coli*
ECL	Enhanced chemiluminescence
EDTA	Ethylenediaminetetraacetic acid
ER	Oestrogen Receptor
Fab	Fragment antigen-binding
fALS	Familial amyotrophic lateral sclerosis
FBS	Foetal bovine serum

Fc	Fragment crystallisable
FDA	Food and Drug Administration
FTD	Frontotemporal dementia
FUS	Fused in sarcoma
GAPDH	Glyceraldehyde-3-phosphate dehydrogenase
GFP	Green fluorescent protein
GRAVY	Grand Average of Hydropathy
hCCS	Human copper chaperone for SOD1
HCl	Hydrochloric acid
HECT	Homologous to E6AP C-terminus
HEK293	Human Embryonic Kidney 293
HER2	Human epidermal growth factor
HIF1a	Hypoxia-inducible factor 1 subunit alpha
HRP	Horseradish peroxidase
Hsc70	Heat shock cognate 70
IAP	Inhibitor of Apoptosis
IFN	Interferon
IgG	Immunoglobulin G
IκBa	Inhibitor of κB alpha
IP	Immunoprecipitation
iPSC	Induced pluripotent stem cells
IPTG	Isopropyl β-d-1-thiogalactopyranoside
IRES	Internal Ribosome Entry Site
kDa	KilaDalton
KRAS	Kirsten rat sarcoma virus

LB	Luria Broth
LBD	Lewy Body Disease
LC3	Microtubule-associated protein 1 light chain 3
LRRK2	Leucine rich repeat kinase 2
LYTAC	Lysosome targeting chimera
mA	milli-Amps
mAb	Monoclonal antibody
MBP	Maltose Binding Protein
MDM2	Mouse double minute 2 homolog
MetAp-2	Methionine aminopeptidase 2
min	Minutes
ml	Millilitres
MPNN	Message Passing Neural Network
mRNA	Messenger RNA
Mut	Mutant
N-terminal	NH_2-terminal
NAC	Non-amyloid component
NaCl	Sodium Chloride
Nb	Nanobody
NBR1	Neighbour of Brca1 gene 1
NDD	Neurodegenerative Disease
NEDD4	Neural Precursor Cell Expressed, Developmentally Down-regulated 4
NFkB	Nuclear Factor kappa-light-chain-enhancer of activated B cells
NLS	Nuclear localisation signal

NFT	Neurofibrillary tangles
NP-40	Nonidet P-40
OD600	Optical Density at 600 nm
OPTN	Optineurin
P/S	Penicillin/Streptomycin
PBS	Phosphate Buffered Saline
PCNA	Proliferating nuclear cell antigen
PCR	Polymerase chain reaction
PD	Parkinson’s Disease
PDB	Protein DataBank
PDD	Parkinson’s Disease with dementia
PFF	Pre-formed Fibrils
POI	Protein of interest
PolyUb	Polyubiquitination
PP2A-B	Protein Phosphatase 2A
PROTAC	Proteolysis targeting chimera
PTM	Post-translational modification
RAS	Rat sarcoma
RBR	RING-between-RINGs
REM	Rapid eye movement
RING	Really interesting new gene
RNA	Ribonucleic acid
Rpm	Revolutions per minute
sALS	Sporadic ALS
SCF	Skp1-Cullin-F box complex containing Hrt1

scFv	Single chain variable fragment
SDS	Sodium dodecyl sulfate
SDS-PAGE	Sodium dodecyl sulfate – polyacrylamide gel electrophoresis
siRNA	Small interfering RNA
SOD1	Superoxide dismutase 1
SPOP	Speckle-type POZ protein
SQSTM1	Sequestome 1
STAND	Ultra-stable cytoplasmic antibody
TBK1	TANK-binding kinase 1
TBS	Tris buffered saline
TBS-t	Tris buffered saline with tween
TDP-43	TAR DNA-binding protein 43
TEV	Tobacco Etch Virus
UBE2C	Ubiquitin-conjugating enzyme E2 C
UPS	Ubiquitin proteasomal degradation system
UTR	Untranslated region
v/v	Volume/volume
VEGF	Vascular Endothelial Growth Factor
VH	Variable Heavy
VHL	Von Hippel Landau
VL	Variable Light
w/v	Weight/volume
WHO	World Health Organisation
WT	Wild type

Chapter I: Introduction

Neurodegenerative diseases (NDD) are collectively a group of disorders that cause neural cell damage leading to physical and cognitive dysfunction (Erkkinen et al., 2018). The World Health Organisation (WHO) predicts that NDDs will collectively be the second most common cause of death over the next two decades (Durães et al., 2018). Generally, current treatments aim to alleviate symptoms and cannot reverse disease pathology (Van Bulck et al., 2019). A central causative agent of NDDs are misfolded protein aggregates, considered “undruggable” by conventional small-molecule inhibitors and agonists, in that they lack a target ligand-binding site for pharmacological modulators (Tomoshige and Ishikawa, 2021).

1.1 Parkinson’s disease

1.1.1 Epidemiology

Lewy body diseases (LBDs) are a heterogenous group of disorders that encompass Parkinson disease (PD), PD with dementia (PDD) and dementia with Lewy bodies (DLB) (Lashuel et al., 2013). PD can be characterised by accumulation of the presynaptic protein α-synuclein, and progressive degeneration of dopaminergic neurons in the substantia nigra Accumulation of α-synuclein aggregates and fibrils leads to the eventual degradation of neocortical, limbic, and nigral-striato circuitries, a critical step before the onset of declining motor function. Parkinson’s disease can be generally characterised as a loss of dopaminergic neurons in the substantia nigra located in the midbrain, which is associated with Lewy body formation and pathological aggregation of α-syn (Fearnley and Lees, 1991; Spillantini et al., 1998). PD is

classified as the second most common NDD and as the global population ages, prevalence of PD is predicted to dramatically increase, with number of cases projected to increase 112% by 2050 (Su et al., 2025). Therefore, the emotional and economic burden of PD will likely escalate in tandem without more effective treatments or preventative measures identified.

Clinical diagnosis of PD primarily relies on manifestations such as bradykinesia and progressive resting tremor, coupled with non-motor features such as depression and REM sleep behaviour disorder which can present several years before motor deficits (Kouli et al., 2018). In later stages of the disease additional manifestations such as autonomic dysfunction and progressive cognitive decline also appear (Sung and Nicholas, 2013). This suggests that loss of dopaminergic neurons and dopaminergic terminals in the basal ganglia are crucial for the loss of motor functions, as opposed to loss of neurons in the substantia nigra (Marras et al., 2018). Like most NDDs, PD exhibits a multifactorial aetiology often resulting from genetic and environmental risk factors.

1.1.2 Pathology

Abnormal accumulation and misfolding of α-syn is a neuropathological hallmark of PD. The formation of cytoplasmic Lewy bodies is associated with dysfunction and eventual degeneration of PD neurons. Overexpression of α-syn also increases mitochondrial reactive oxygen species (ROS) and inhibits mitochondrial function (Zhu et al., 2011). Mutations in the PARKIN and PINK1 genes are known causes of early onset autosomal recessive PD (Kitada et al., 1998; Valente et al., 2004). Both genes regulate the mitophagic degradation pathway involving preferential degradation in

lysosomes, where a loss of function in either gene results in impaired mitophagy and accumulating dysfunctional mitochondria (Vincow et al., 2013). LRRK2 mutations lead to deposition of α-synuclein on the outer mitochondrial membrane (Li et al., 2014).

Neuroinflammation plays a mechanistic role in PD pathogenesis. Protein aggregates accumulating in the substantia nigra, and high levels of reactive microglia are found in postmortem PD brain tissue, reviewed by Caggiu et al., (2019), inciting the same question as to whether dysfunctional neuroinflammatory events trigger PD pathogenesis or are an unsuccessful response triggered by the detection of toxic misfolded proteins. This further reinforces the multifactorial heterogeneity of PD, with many influential genetic and environmental pathways converging on specific pathways such as protein aggregation, neuroinflammation and impaired autophagy.

1.1.3 α-Synuclein

α-Synuclein is a 140 amino acid protein with three distinct structural regions: the N-terminal region, the non-amyloid component, and the C-terminal region. The N-terminal region is positively charged and has an alpha-helicoidal structure allowing it to bind to lipid membranes, necessary for protein function and prevents aggregation (Meade et al., 2023). The C-terminal region however is negatively charged and subject to posttranslational modifications in disease conditions. Phosphorylation at serine 129 accelerates formation of toxic inclusions and loss of dopaminergic neurons *in vivo* (Sato et al., 2011). Soluble α-synuclein is naturally unfolded and monomeric, and while difficult to replicate has also been shown to form a stable helical structure by associating as a homotetramer (Wang et al., 2011). Under physiological conditions,

α-synuclein resides in presynaptic terminals and its proposed role is to regulate synaptic vesicles trafficking and neurotransmitter release (Bendor et al., 2013; Maroteaux and Scheller, 1991). Its role in promotion of SNARE-complex assembly, essential for synaptic vesicles release, supports efficient exocytosis and maintains presynaptic homeostasis (Burré et al., 2010) . Overall, α-synuclein is an important modulator of synaptic transmission and knockout mice are observed to experience age-dependent cognitive decline where the role of α-synuclein is dispensable in younger mice and becomes essential in aging mice, suggesting that α-synuclein ensures normal synaptic function during the ageing process (Burré et al., 2010).

α-Synuclein is the primary component of Lewy body inclusions in all PD patients, Spillantini et al., (1998), and can be observed to form fibrillar aggregates *in vitro*. α-Synuclein was first reported within neurofibrillary tangles (NFTs) with immunohistochemical studies demonstrating its presence in the substantia nigra (Wakabayashi et al., 2000). Number of inclusions was found to correlate with disease severity (Wakabayashi et al., 2000). This finding was later confirmed by double-immunolabeling and electron microscopy studies (Arima et al., 2000). Two key missense mutations in the α-synuclein protein, have been linked to autosomal dominant early onset PD: α-syn^{A30P} and α-syn^{A53T} (Krüger et al., 1998; Polymeropoulos et al., 1997). Other mutations in the same region are also linked to PD: α-syn^{G51D,} α-syn^{E46K,} α-syn^{H50Q}. Although these mutations are rare, it remains clear that α-syn is a critical component of Lewy bodies in both sporadic and inherited cases, (Sanderson et al., 2020).

Emerging evidence indicates that α-synuclein exists within cells in a dynamic continuum of monomeric, oligomeric, and aggregated states each contributing differently to toxicity and propagation (Rana et al., 2025). Typically, these aggregates range in size from tens to hundreds of nanometers to a few micrometers and are highly heterogenous. The small non-fibrillar α-synuclein aggregates, often denoted as soluble oligomers are proposed to be highly toxic and drive disease pathogenesis and neurotoxicity, (Emin et al., 2022). While there is no refined definition of oligomers, the term oligomers refers to any soluble aggregate of an intermediate size between monomers and insoluble fibrils (Du et al., 2020).

1.1.4 Current therapeutic options

Current treatment of PD centres around pharmacological replacement of dopamine, although other neurotransmission pathways such as serotonin and acetylcholine systems are implicated in Parkinson's disease and can explain why some symptoms are not managed well by dopamine-based therapies (Armstrong and Okun, 2020)., Dopamine agonists such as levodopa taken in combination with carbidopa (a decarboxylase inhibitor) are useful initial therapies that alleviate symptoms associated with the loss of neurotransmitter dopamine (Salat and Tolosa, 2013). However, several studies report adverse events such as impulse control disorders, described as excessive and uncontrollable gambling, shopping and hypersexuality and serious withdrawal symptoms (Pondal et al., 2013). A longitudinal study described the 5-year cumulative incidence of impulse control disorders to be approximately 46% and strongly associated with dopamine agonist use (Corvol et al., 2018). While levodopa is most likely to lead to functional improvements, PD patients will typically have to increase Levodopa frequency and dosage as the disease

progresses (Chou et al., 2018). Deep brain stimulation and rehabilitative therapeutic approaches provide effective relief in patients with disabling tremors and complement pharmacological interventions but no disease modifying treatment for PD is available. Unfortunately, deep brain stimulation does not halt disease progression or improve non-motor symptoms associated with PD, but can provide relief from motor symptoms such as bradykinesia and tremor (Hitti et al., 2019).

Monoclonal antibodies are of high interest as a potential PD therapeutic. BIIB054, also referred to as cinpanemab, is an aggregated α-synuclein specific monoclonal antibody (Brys et al., 2019). Recently, results from a phase II clinical trial testing cinpanemab as a treatment for PD showed that cinpanemab was an unsuccessful intervention and no significant changes in clinical measures of disease progression were reported in comparison to placebo groups (Lang et al., 2022). More recently, Biogen chose to discontinue development of cinpanemab. Another monoclonal antibody targeting aggregated α-synuclein is also being investigated for its use as a disease modifying PD therapeutic. PRX002, also referred to as prasinezumab, also targets aggregated α-synuclein but has high affinity for the C-terminus and binds to both monomeric and aggregated α-synuclein (Pagano et al., 2021). Results from a Phase IIB trial of prasinezumab for treatment of early stage PD reported no significant differences between placebo and test groups and adverse effects following infusions (Pagano et al., 2022). However, post-hoc analysis revealed that over a 1-year duration, prasinezumab might reduce motor degeneration progression to a greater extent in individuals with rapidly progressive PD, despite initial trial results showing limited impact on primary patient outcomes, (Xiao and Tan, 2025). Phase III clinical trials are ongoing (Pagano et al., 2024).

1.2 Amyotrophic lateral sclerosis (ALS)

1.2.1 Epidemiology

ALS is a fatal motor neuron disease characterised by degenerative alterations in both upper and lower motor neurons (Rowland and Shneider, 2001). Clinical manifestation of ALS usually presents in middle to late stages of life, presenting as a widespread progressive muscle atrophy and systemic weakness and in most cases disease survival is limited to 2-5 years due to eventual debilitating effects of degeneration on respiratory muscle tissue (Vasta et al., 2025). Progressive paralysis of the limbs, speech impairment and difficulty swallowing are also common features of ALS (Kiernan et al., 2011).

1.2.2 Pathology

More than fifty disease causative or modifying genes have been identified in relation to familial ALS (fALS) cases. A range of mutations have been found to cause ALS, in particular mutations in SOD1, chromosome 9 open reading frame 72 (C9ORF72), fused in sarcoma (FUS), TANK-binding kinase 1 (TBK1), and TAR DNA-binding protein 43 (TDP43) occur most frequently, and most variants in other genes are largely uncommon (Boylan, 2015). Different SOD1 mutations are associated with different rates of disease progression and varied disease severity, (Huang et al., 2024). This highlights the high degree of disease heterogeneity among patients in addition to the vastly diverse nature of clinical manifestations such as age of onset and disease severity. A hexanucleotide repeat expansion in the C9ORF72 gene is most commonly observed: accounting for up to 50% of fALS cases and 20% of

sporadic ALS (sALS) cases (Masrori and Van Damme, 2020). Protein aggregation in degenerating motor neurons and oligodendrocytes is a central feature of ALS pathology, predominantly comprised of ubiquitinated aggregates called Lewy body-like hyaline inclusions (Blokhuis et al., 2013). The aetiology of ALS is highly complex; neuroinflammation, glutamate-induced neurotoxicity and metabolic impairment are key pathological mechanisms (Kiernan et al., 2011). TDP-43 aggregation occurs in both sporadic and familial forms of ALS.

1.2.3 SOD1

Mutations and aggregation of SOD1 can be found in both fALS and sALS cases with SOD1 mutations accounting for approximately 5% of all ALS cases. Superoxide dismutase 1 (SOD1) is a cytosolic and mitochondrial enzyme which protects cells from oxidative stress by converting superoxide radicals into hydrogen peroxide, which can then be broken down by other enzymes such as catalase (Corson et al., 1998). SOD1 misfolded conformers and aggregates become toxic to cells, and degeneration of motor neurons can be observed (Bruijn et al., 1998). While the exact mechanism of SOD1 aggregation requires further exploration, several lines of evidence propose that SOD1 mutations lead to conformational changes within the native protein structure of SOD1, causing ALS through a toxic gain of function. This toxicity linked to ALS is likely to arise from SOD1 misfolding, induced by dominant point mutations or aberrant post-translational modifications, which may be relevant in cases of ALS lacking SOD1 mutations (Rotunno et al., 2014). Dominant point mutations make up part of over 210 ALS-related mutations, which also include deletions and insertions, deletions of base pairs in the 3'-UTR and premature truncations (Shaw et al., 1997; Shi et al., 2004).

Overexpression of $SOD1^{WT}$ causes ALS-like disease features in transgenic mice, and mutations exhibiting similar biophysical properties to $SOD1^{WT}$ such as D90A, C6S, E100K, and L117V cause ALS, providing supporting evidence that $SOD1^{WT}$ contributes to ALS pathology (Paré et al., 2018). Additionally, abundant aggregates containing misfolded $SOD1^{WT}$ can be found in patients harbouring ALS-related mutations other than SOD1, such as C9ORF72 and FUS (Forsberg et al., 2019).

ALS is often referred to as a prion disease, in that misfolded proteins can propagate to other cells and spread pathology, acting as a transmissible agent between cells facilitated by extracellular vesicle and unconventional secretory pathways (Wenzhi et al., 2024). SOD1 displays prion-like properties both *in vitro* and *in vivo*, indicating its role in pathogenesis of sALS (McAlary et al., 2019). Accumulating SOD1 aggregates in motor neurons may contribute to the progression of ALS, and clearance of toxic aggregates may improve ALS pathology to treat the disease.

1.2.4 Current therapeutic options

Treatment for ALS primarily focuses on respiratory support in later stages of disease and symptom management. Riluzole and edravone aim to provide modest symptomatic relief but is not always effective in all patients. Riluzole is a glutamate antagonist aimed at improving the survival rate in ALS patients, but has only a significantly small effect (Vasta et al., 2025). Riluzole does not improve muscle strength or respiratory function, and pivotal studies found that patient survival was only extended by 2-3 months, while more recent studies found patient survival was extended by 6-19 months (Bensimon et al., 1994; Andrews et al., 2020). High doses

of riluzole were found to prolong later stage ALS in a dose-ranging trial rather than slowing disease progression (Fang et al., 2018).

To date over 40 clinical trials studying ALS treatments have had negative results, due to the heterogenous nature of the disease and the complex underlying disease mechanisms. Several novel therapies are being pursued that focus on clearance of aggregated protein in order to treat neurodegenerative diseases such as ALS. Recent findings from a phase III clinical trial investigating the effect of antisense oligonucleotide (tofersen) intrathecal administration for mutant SOD1 ALS patients revealed that despite significantly reduced concentrations of SOD1 in CSF clinical end points did not improve and several adverse effects were experienced during the study (Miller et al., 2022). Tofersen aims to reduce synthesis of SOD1 by inducing RNase H-mediated degradation of SOD1 mRNA, as it is hypothesised that progressive neurodegeneration in ALS could be due to a toxic gain of function in the mutant SOD1 protein (Rinaldi and Wood, 2018; Sau et al., 2007). Previous *in vitro* and *in vivo* findings showed significant reductions in SOD1 concentrations in response to tofersen administration (McCampbell et al., 2018). However, no significant difference was observed in changes to ALSFRS-R scores between tofersen-treated and placebo subgroups, although observed trends showed a reduction in decline of measures of clinical function. FDA granted accelerated approval of tofersen due to reductions in the neurodegeneration marker plasma neurofilament light chain observed in treated patients in an open-label extension study (Miller et al., 2022). Approval was supported by integrated results from the VALOR and open-label extension studies suggesting that earlier initiation of tofersen compared to delayed start initiation were associated with trends in reduction in ALSFRS-R scores.

Other approaches such as CRISPR and small interfering RNAs (siRNAs) that inhibit SOD1 production may also improve disease pathology in ALS animal models. However, no effective therapy is yet available that effectively degrades aggregated protein at the post-translational level or halt disease progression. Most recently, a Cas13 nuclease ortholog (RfxCas13d) targeting SOD1 reduced SOD1 mRNA and protein in mice spinal cords and had positive effects on outcomes in a SOD1 mouse model (Powell et al., 2022). Interestingly, it was also shown that a RfxCas13d variant led to a 50% reduction in huntingtin, exhibiting the versatile ability of programmable CRIPSR effector proteins for the reduction of target protein mRNA and subsequent translation of aberrant proteins.

1.3 Protein degradation pathways

1.3.1 Ubiquitin proteasomal degradation

Approximately 80-90% of proteins in eukaryotic cells are degraded by the ubiquitin proteasomal degradation system (UPS), an ATP dependent degradation system crucial to maintaining protein homeostasis (Chen et al., 2016). Ubiquitination is a post-translational modification (PTM), where ubiquitin is covalently attached to lysine residues on a target protein, through an ATP-dependent cascade involving E1 activating, E2 conjugating and E3 ligase enzymes (**Fig.1**). It generally operates through polyubiquitination of a target protein and hydrolysis of that protein by the 26S proteolytic enzyme complex (reviewed by Zhang et al., 2022). First, ubiquitin is activated by E1, entering a thioester linkage with a catalytic cysteine, before transferring through a trans-esterification reaction to an E2 conjugating enzyme (**Fig.1**) (Komander and Rape, 2012)**.** Monomeric ubiquitin can be further modified by forming

isopeptide bonds between one of the internal lysine residues or N-terminal methionine and the C-terminal carboxylic acid of another ubiquitin molecule, with each lysine-linked ubiquitination creating distinct degradation signals (**Table.1**) (Komander, 2009; Mulder et al., 2020). For example, K11 and K48-linked polyubiquitination provides a degradation signal allowing ubiquitinated target proteins to be recognised and promptly degraded by the 26S proteasome (Flick et al., 2006).

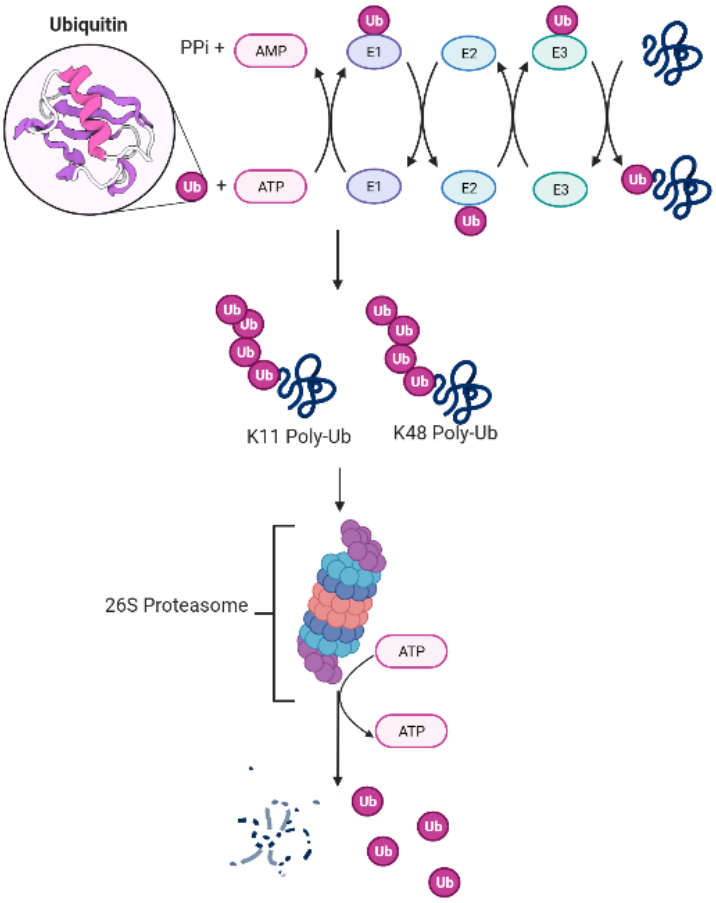

Figure 1.1. Ubiquitin-proteasomal degradation pathway. *Produced in BioRender.*

Table 1. Ubiquitin linkage sites and their associated functions in protein degradation and signalling. *Ubiquitin can be assembled into polymeric chains through ubiquitination of seven lysine residues or the primary methionine on ubiquitin, with each distinct polyubiquitination linkage serving a different cellular function (Damgaard, 2021).*

Ubiquitin linkage type	**Role in degradation**	**Other functions**	**References**
Met1		Regulation of NFkB and IFN signalling	(Komander and Rape, 2012)
Lys6		DNA damage response	(Morris *et al.,* 2004)
Lys11	Proteasomal degradation	Regulation of cell cycle and membrane trafficking	(Wickcliffe *et al.,* 2011; Yang *et al.,* 2021)
Lys27		Protein secretion regulation, DNA damage repair, mitochondrial damage and innate immune response	(Geisler *et al.,* 2010)
Lys29	Proteasomal degradation	Regulation of AMPK-related kinases, innate immune response	(Yu *et al.,* 2016)
Lys33		Innate immune response (type I IFN signalling), intracellular trafficking	(Lin *et al.,* 2016; Yuan *et al.,* 2014; Yang *et al.,* 2021)
Lys48	Proteasomal degradation		(Jacobson *et al.,* 2009)
Lys63	Autophagic degradation signalling	DNA damage repair, cytokine signalling	(Chen *et al.,* 2009; Jacobson *et al.,* 2009; Grice *et al.,*2016)

E3 ligases can be categorised into three families: RING-, HECT-, and RING-between-RINGs type (RBR-type), based on their mechanism of action (Morreale and Walden, 2016). The really interesting new gene (RING) E3 transfer mechanism is deemed more simplistic compared to HECT and RBR type mechanisms, involving the transfer of ubiquitin directly from the E3-E3-ubiquitin complex to a lysine residue on the bound substrate, making them potentially attractive targets for modifying and harnessing E3 ligase ubiquitination and subsequent degradation. HECT E3 and RBR-like E3 ligases require an additional process: transthiolation from an E2 ligase cysteine residue to a cysteine on the E3 ligase ubiquitylation domain prior to transfer to the substrate (Potjewyd and Axtman, 2021).

Protein degradation processes such as the UPS are often disrupted in neurodegenerative disease pathology. When the efficiency of protein homeostasis systems is perturbed in disease, misfolded and damaged protein aggregates rise to toxic levels within the cell, leading to progressive neuronal cell death and neurodegeneration (Layfield et al., 2005). Soluble forms of aggregated proteins, denoted oligomers, are implicated in the pathogenesis of neurodegenerative diseases (Haass and Selkoe, 2007). It is well understood that impaired proteasomal degradation is present in neurodegenerative diseases, as reviewed by (Rousseau and Bertolotti, 2018). Although ageing is multifactorial, there is likely an association between general ageing and a decline in proteasomal degradation and regulation (Saez and Vilchez, 2014).

1.4 Autophagy-lysosomal degradation

Autophagy is a cellular waste disposal system in which damaged

macromolecules such as proteins become wrapped in bilayered autophagosomes and engulfed by lysosomes for degradation (**Fig.2**). There are three main subtypes of autophagic degradation: Macroautophagy (often commonly referred to as autophagy), microautophagy and chaperone-mediated autophagy (CMA). Microautophagy is a non-selective process differing from typical autophagy-lysosomal degradation in that the lysosomal membrane directly engulfs small autophagic cargo rather than generating autophagosomes (Li et al., 2011).

Autophagy is a crucial process for protein homeostasis, clearing protein aggregates or damaged organelles but is often disrupted in NDD states (Guo et al., 2017). In normal conditions, the formation of a double-membrane phagophore begins the autophagy process, coordinated by core autophagy related proteins (Hollenstein and Kraft, 2020). The phagophore closes to engulf material, becoming an autophagosome which fuses with a lysosome leading to degradation of the contained cargo (Parzych and Klionsky, 2014). The lysosome contains hydrolases and enzymes that degrade the enclosed protein upon fusion. Based on the observations that autophagy-defective mice exhibit manifestations of neurodegeneration, Kuma et al., (2017), and that genetic mutations of autophagic receptors such as sequestome 1 (SQSTM1), optineurin (OPTN), and neighbour of BRCA1 gene 1 (NBR1) are highly associated with NDDs suggest that defective autophagy is an important aetiological factor of NDDs (Deng et al., 2019).

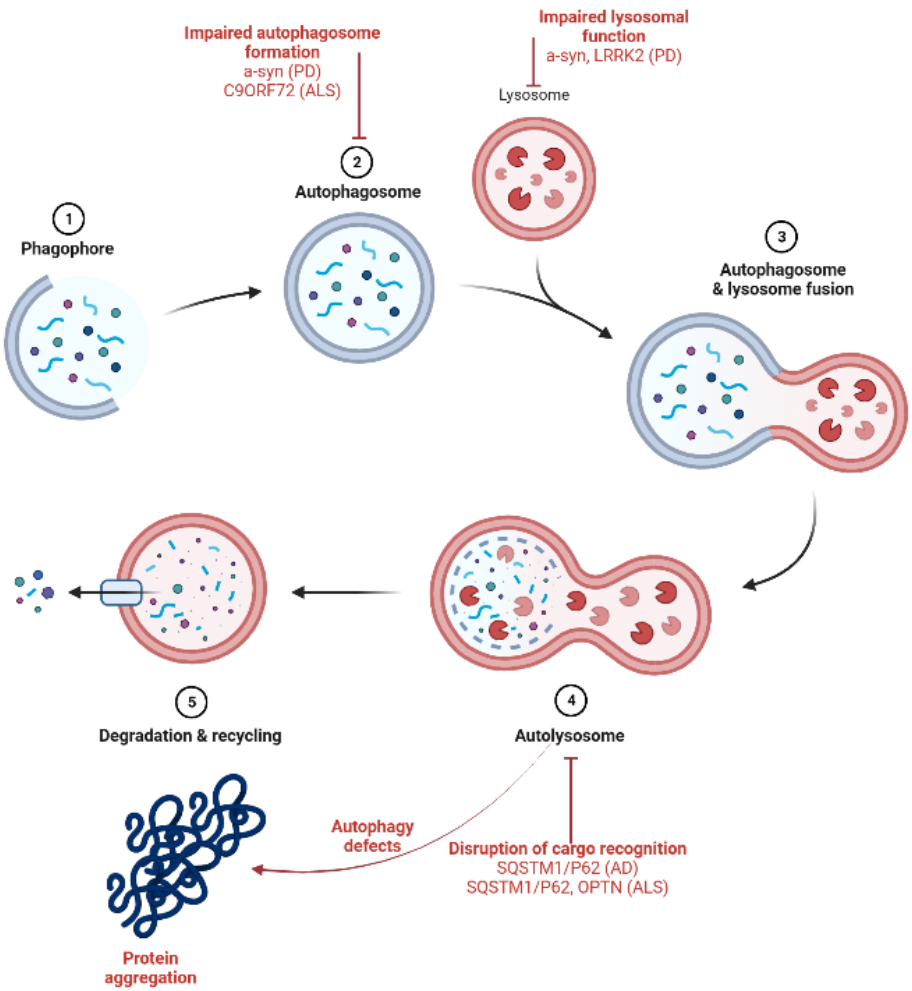

Figure 1.2. Autophagy process schematic. *Examples of perturbed autophagy in NDD conditions and affected genes are depicted. The phagophore is an active sequestering compartment which closes to form and autophagosome before fusing with the lysosome, leading to cargo degradation. Produced in BioRender.*

Because neurons are terminally differentiated and cannot dilute damaged proteins or organelles through cell division, they depend strongly on constitutive autophagic pathways for bulk clearance of misfolded proteins and defective organelles. This makes autophagy a potentially attractive therapeutic target for ND treatment, particularly chaperone-mediated autophagy (CMA). CMA is a more specialised subgroup of autophagy, a highly selective process in which damaged

cytosolic proteins, in addition to certain transcription factors and signalling molecules are degraded under certain conditions such as starvation and stress. Damaged or misfolded proteins containing a consensus CMA binding motif KFERQ sequence are recognised by chaperone heat shock cognate 70 (Hsc70) and co-chaperones, followed by delivery and internalisation into lysosomes via lysosome-associated membrane protein type 2a leading to lysosomal degradation (**Fig.3**) (Sinha et al., 2017).

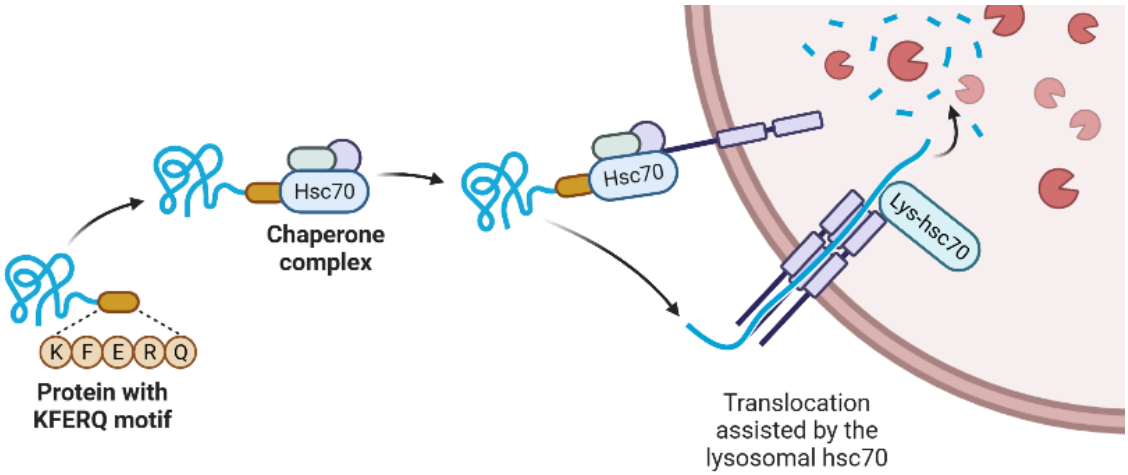

Figure 1.3. Chaperone-mediated autophagy mechanism*. Produced in BioRender.*

1.4 Targeted protein degradation therapies for neurodegenerative diseases

1.4.1 Proteolysis targeting chimeras (PROTACs)

1.4.1.1 Structure

Interestingly, Pfizer has removed all efforts towards neuroscience drug discovery and development, halting eight Phase I and Phase II clinical trials to redirect funding due to lack of efficacy (Mullard, 2018). This reinforces the demand for research into non-drug therapeutic mechanisms to address this gap in the field, perhaps

achievable with targeted protein degradation tools such as PROTACs that act catalytically as opposed to pharmacologically inhibiting or agonising a target. The possibilities of this approach are illustrated by an Arvinas and Pfizer collaboration to develop and commercialise the PROTAC ARV-471, targeting the oestrogen receptor for degradation for the treatment of oestrogen receptor positive (ER+)/human epidermal growth factor receptor negative (HER2-) breast cancer.

PROTACs are heterobifunctional molecules consisting of an E3 ligase moiety and a target protein binding domain connected by a linker domain, that can effectively degrade the protein of interest (POI) through E3 ligase recruitment and utilisation of the UPS (**Fig.4**). Targeted protein degradation approaches have the potential to yield potent and highly selective removal of disease-causing proteins. PROTACs effectively reprogram E3 ligases to degrade specific substrates with a high catalytic turnover rate, requiring low PROTAC concentrations to give a high standard of efficacy (Bondeson et al., 2015). The high catalytic substrate turnover rate of PROTACs is highly beneficial for the long-term clearance of pathological aggregating proteins in neurodegenerative disease states. This in turn overcomes the current therapeutic paradigm where large pharmacological drug concentrations are required to maximise drug-receptor occupancy and achieve a clinical benefit, often accompanied by adverse effects. Additionally, many proteins affected in NDDs are structurally disordered or misfolded, making generating high affinity small molecule ligands difficult. PROTACs can additionally cross the BBB, as demonstrated by AD-targeting PROTAC XL01126 are of high therapeutic potential, overcoming potential pitfalls of pharmacological agents that cannot penetrate the BBB (Liu et al., 2022).

1.4.1.2 Mechanism of action

Based on their mechanism of action, PROTACs can potentially target any protein including previously “undruggable” targets, providing that a low molecular weight ligand can be generated for the protein of interest (POI), with the advantage that low affinity ligands are suitable as they make transient interactions with the target protein (Collins et al., 2017). For efficient degradation, the PROTAC must enter a cell and interact with both the POI and the E3 ligase in a ternary complex to trigger ubiquitination of the target (**Fig.4**). Following ubiquitination, the POI is degraded by the proteasome. The PROTAC mechanism of action allows the molecule to be recycled and involved in several catalytic reactions to degrade several target proteins, which depending on PROTAC stability can lead to a longer duration of action within the cell.

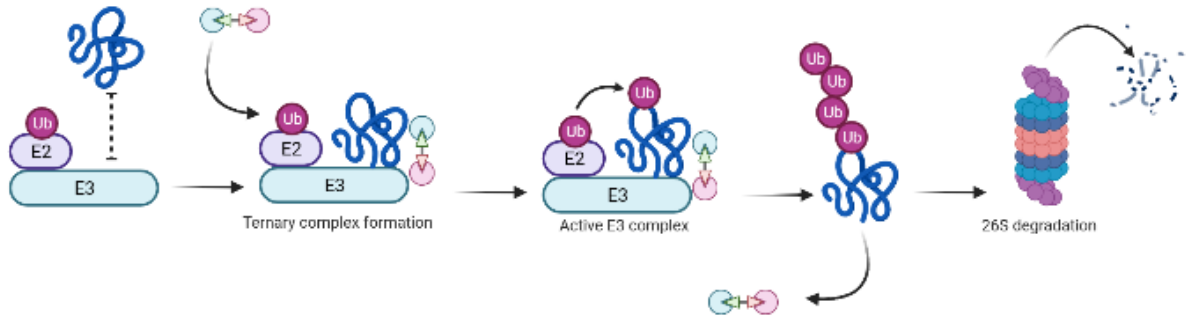

Figure 1.4. PROTAC mechanism of action*. An E3 ubiquitin ligase cannot ubiquitinate a target distant protein. Upon PROTAC expression and binding to the target protein, E3 ubiquitin ligases are brought into proximity and can successfully ubiquitinate the target protein, leading to its degradation. The PROTAC can then form E3 complexes with new target proteins and E3 ligases.*

1.4.1.3 Early PROTAC design

An early study proposed harnessing the UPS to facilitate targeted protein degradation, by modifying ubiquitin-conjugating enzymes (E2 ligases), demonstrating that E2 target recognition can be engineered to facilitate targeted ATP-dependent degradation *in vitro* (Gosink and Vierstra, 1995).

The PROTAC concept was first proposed by Crews and Deshaies research group in which the first PROTAC molecule was synthesised and shown to successfully degrade its target, MetAp-2, by recruiting MetAp-2 to the ubiquitin ligase complex SCF (Skp1-Cullin-F box complex containing Hrt1) (Sakamoto et al., 2001). By designing a chimeric molecule containing an ovalicin motif to recruit MetAp2 and an IkBa phosphopeptide to recognise the SCF ubiquitin ligase complex, Sakamoto et al., (2001), successfully induced degradation of MetAp2 *in vitro* and laid the foundation for further PROTAC design and testing. Although the phosphopeptide-containing PROTAC designed in this study was unlikely to penetrate cells and required further modification beyond the F-box fusion approach, this study provided an early basis for designing and testing PROTACs *in vivo* as a tool for degradation targeted proteins.

The development of new peptide based PROTACs quickly ensued including PROTACs targeting androgen receptors and oestrogen receptors (Schneekloth et al., 2004). Again, these PROTACs were chemically unstable with a low cell permeability but provided further proof of concept for targeted ubiquitination and degradation of selected proteins. In this early study microinjection was used to demonstrate PROTAC functionality within an intact cell, but further studies incorporating a HIF1a peptide fragment to recruit VHL E3 ligases within a cell surpassed the need to use

microinjection (Schneekloth et al., 2004). The first nonpeptidic, small-molecule PROTAC replaced the HIF1a peptide used in previous studies with a newly developed small molecule ligand for VHL retaining the hydroxyproline crucial for VHL ligand binding (Buckley et al., 2012). These 1st generation PROTACs were only effective at low micromolar ranges with cellular permeability and activity, however the first small molecule based PROTACs targeting AR and ER were developed and exhibited a higher degree of cell penetrability (Pettersson and Crews, 2019). With the introduction of second-generation PROTACs degradation efficacy improved but molecular weight ultimately remained relatively high limiting specificity and harbouring its own toxicity problems.

Most recently, Arvinas developed an oestrogen receptor (ER) targeting PROTAC, named ARV-471 which potently degraded ER with high specificity leading to reduced tumour burden in patient-derived xenograft models (Snyder et al., 2025). ARV-110 (bavdeglutamide) was also developed to specifically target androgen receptor (AR) as a novel metastatic castration-resistant prostate cancer therapy and has also reached Phase II clinical trials (NCT03888612) (Neklesa et al., 2019). ARV-110 exhibited high levels of efficacy in patients harbouring AR^{T878X} and AR^{H875Y} mutations, leading to resistance to currently available AR targeting therapies. However, grade 3/4 elevations in liver enzymes and acute renal failure were observed in two patients, which was attributed to be due to a drug interaction with rosuvastatin, a commonly used cholesterol lowering medication. This result collectively reinforces the promising alternative approach for targeting ‘undruggable’ protein targets that PROTAC technology can provide (Kelm et al., 2023).

CRBN and VHL-based PROTACS largely dominate the field of PROTAC design, along with IAP and MDM2-based PROTACs, as they allow for the ubiquitylation and following degradation of new substrates at nanomolar and even picomolar doses (Hughes et al., 2021). These E3 ligands are likely only suitable for some types of PROTAC design.

1.4.1.4 Tau-targeting PROTACs

In 2016, a pioneering study demonstrated the efficacy of TH006 against the elimination of Tau through the recruitment of the VHL E3 ligase (Chu et al., 2016). Among the series of molecules designed and tested in the study, TH006 had the highest potency due to its ability to increase polyubiquitination of tau in cells and reduce cytotoxicity mediated by amyloid-beta (Chu et al., 2016). A small molecule PROTAC was developed by Arvinas to degrade pathological tau in homozygous JNPL3 tauopathy mice models potently. Preclinical *in vivo* studies revealed that the Arvinas small molecule PROTAC degraded over 95% of pathological tau species (Cacace et al., 2019).

More recently, dephosphorylation targeting chimeras (DEPTACs) have been introduced as a novel strategy to selectively target hyperphosphorylated tau as a therapy for AD. Zheng et al., (2021), produced a DEPTAC consisting of a tau-binding and PP2A-B recruiting domain connected by a linker domain, which exhibited a high degree of efficiency in dephosphorylating tau by facilitating the binding of tau to PP2A-Ba, the most active tau dephosphorylating protein *in vitro* and *in vivo* (Wang et al., 2021). More studies incorporating more physiologically relevant models using iPSCs are necessary to assess if DEPTAC mediated tau degradation improves pathology.

1.4.1.5 Lysosome targeting chimera

Typical PROTAC design is limited to targeting proteins that contain cytoplasmic domains with ligands that can successfully bind to necessary intracellular machinery, which propelled the design of lysosome-targeting chimeras (LYTACs) in order to establish targeted degradation of extracellular or membrane-associated proteins. LYTACs consist of an antibody or small targeting molecule fused to synthetic glycopeptide ligands that are cation-independent mannose-6-phosphate receptor (CI-M6PR) agonists to shuttle secreted and membrane-associated proteins to lysosomes (Banik et al., 2020). This was successfully applied to Apolipoprotein E4 (ApoE4) which increased ApoE4 trafficking to lysosomes 13 fold, Banik et al., (2020), broadly providing early evidence that LYTACs may be useful in directing extracellular proteins implicated in neurodegenerative for lysosomal degradation, if modulation of pharmacokinetic properties to limit off-target clearance and stoichiometries relative to the lysosome-targeting receptor can be fine-tuned for more effective degradation.

1.4.1.6 Current Limitations

Recent evidence demonstrates that some designed PROTACs are not completely specific to the target protein of interest, especially if another protein is in close proximity to the PROTAC or is part of the same complex as a target protein (Hsu et al., 2020). CRBN-based PROTACs are a well-documented example of off target protein degradation, since CRBN ligands such as thalidomide analogues are known to recruit various neo-substrates for degradation by CRBN (Sievers et al., 2018). Off target degradation is a likely outcome of PROTAC administration. Maniaci et al., (2017), report findings suggesting that ‘bystander degradation’ can occur when

degradation of a protein is observed that is not directly bound to the PROTAC but can become ubiquitinated and hence degraded as part of the PROTAC-POI complex.

The Hook effect was defined by Douglass et al., (2013) which can be observed when the PROTAC saturates binding to the target and E3 ligase resulting in the formation of binary complexes instead of the productive degrading ternary complex, preventing target ubiquitination and degradation (Paiva and Crews, 2019). While more likely to occur at high PROTAC concentration, a resulting E3-PROTAC binary complex may lead to increased off target degradation of lower affinity targets. The hook effect could be alleviated by increasing protein-protein interaction or cooperativity of the ternary complex, Park et al., (2022), however this has not yet been displayed *in vivo*. While this may negatively affect PROTAC efficacy, it is not yet clear if this has any safety or toxicological dangers.

1.4.2 Autophagy targeting chimera (AUTAC)

1.4.2.1 Structure and mechanism of action

AUTACs are heterobifunctional small molecule compounds consisting of a targeted warhead and autophagy recruiter, such as the guanine derivative degradation tag employed by Takahashi et al., (2019), connected to a substrate-binding small unit by a flexible linker domain to trigger the autophagolysosomal degradation of a target protein (**Fig.5**). The AUTAC molecule triggers K63-linked polyubiquitination, which subsequently is recognised by autophagy receptor SQSTM1/p62 to be recruited into autophagosomes for lysosome-mediated degradation.

AUTACs were first developed by Takahashi et al., (2019) and present a novel targeted degradation strategy that can potentially degrade proteins independent of the UPS by instead utilising autophagic clearance. 8-nitro-cGMP guanylation promoted ubiquitination of Group A *streptococcus* in previous observations, which propelled the investigation of employing guanine derivatives as a tag for targeted K63-linked ubiquitination and recruitment of autophagy systems (Takahashi and Arimoto, 2021). S-guanylation utilised by these AUTACs remains dependent on ubiquitination of the target protein (Ji et al., 2022).

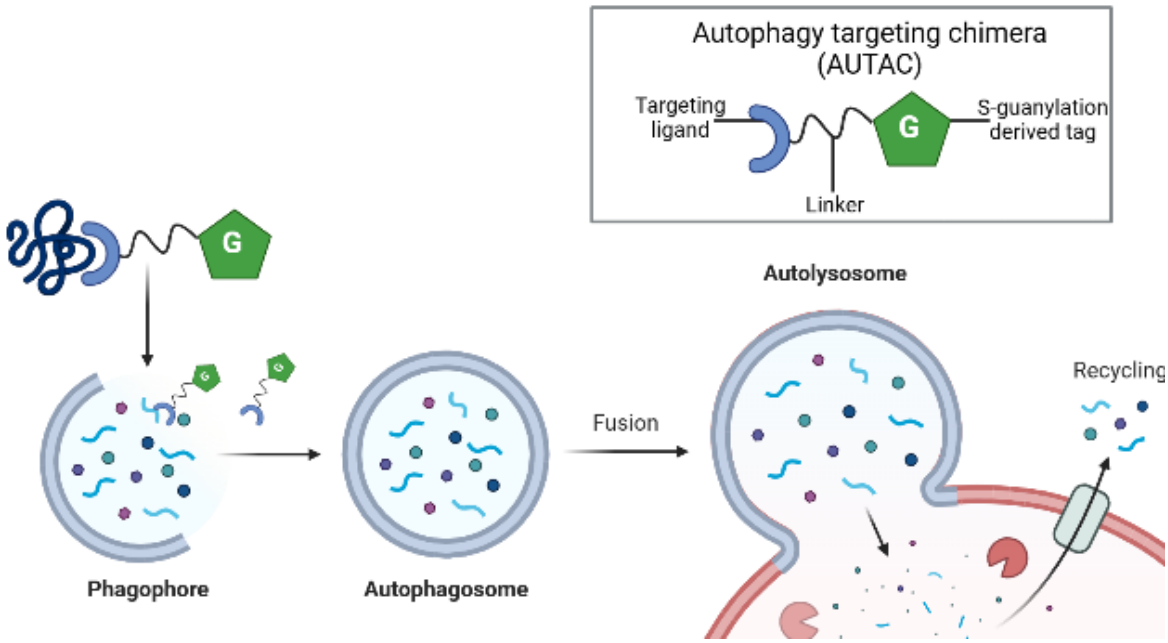

Figure 1.5. AUTAC structure and mechanism*. Simplified schematic of AUTAC structures. A targeting ligand is flexibly linked to a guanine-derived tag that recruits the autophagy system. (Adapted from Takahasi & Arimoto, 2021). Produced in BioRender.*

1.4.2.2 Current applications of AUTACs

Shortly after a novel AUTAC was developed to degrade bromodomain-containing protein 4 (BRD4) by targeting LC3 and demonstrated significant anti-

proliferative activity in triple negative breast cancer cell line MDA-MB-231 (Pei et al., 2021). In a similar study, small molecule glue tethering compounds that bind LC3 to mutant huntingtin led to effective degradation of mutant huntingtin *in vitro* (Tomoshige et al., 2017).

Despite effective autophagic degradation of target proteins mediated by LC3 binding, these AUTACs have no impact on autophagy flux of cells. To address this Ji *et al.,* (2022), present an AUTOTAC (AUTOphagy-TArgeting Chimera) that binds the ZZ domain of autophagy receptor SQSTM1/p62 (Sequestome-1) to accelerate self-oligomerisation, LC3 binding, and autophagosome generation, as N-terminal arginylation through the p62-ZZ domain conformationally activates p62, facilitating autophagy and increasing cellular autophagic flux (Varshavsky, 2019). This AUTOTAC model successfully degraded aggregation-prone tau species *in vitro* and *in vivo,* however off -target degradation issues were not fully investigated (Ji et al., 2022).

PROTACs importantly can potentially degrade “undruggable” targets in the human proteome, and development of AUTACs and bioAUTACs may provide new advantages as a broader range of substrates can be degraded by the autophagic system. Currently the literature surrounding AUTAC design and ubiquitin ligase selectivity is limited, and further work is necessary to identify E3 ubiquitin ligases that accelerate selective clearance of target proteins via the autophagic system, and researching surrounding AUTACs is currently limited to preclinical stages. The application of AUTACs to degrade protein aggregates such as those observed in NDD has not yet been addressed in the literature. In addition, a lack of detailed understanding surrounding mechanisms of AUTAC action is evident from the

literature, however it is currently speculated that AUTACs induce proximity between a target protein and ubiquitin ligase using distinct mechanisms differing largely from PROTACs (Takahashi and Arimoto, 2021).

1.4.3 Biological proteolysis targeting chimera (BioPROTAC)

1.4.3.1 Structure

Biological proteolysis targeting chimeras (BioPROTAC)s are engineered fusion proteins comprised of a target binding domain that selectively binds to the target protein and is connected to an E3 ubiquitin ligase domain (Lim et al., 2020). Target binding domains can be derived from nanobodies, intrabodies, chaperone proteins and other relevant protein domains. BioPROTACs contain an entire E3 ligase or an E3 ligase ubiquitylation domain as part of their structure rather than an E3 ligase binding moiety and therefore do not require the recruitment of endogenous E3 ligase to initiate degradation (**Figure 1.6**). Upon BioPROTAC administration to cells, usually by an encoding vector such as AAV, brings the POI into proximity with the E3 ligase, which subsequently ubiquitinates the protein, directing the targeted protein to proteasomal degradation by the host cell (Rambacher et al., 2021). It is not always necessary to incorporate a linker region reducing any variability associated with differing length and attachment sites of linkers. Currently less than 2% of the 600 available human E3 ligases have been incorporated into PROTAC design, Wang et al., (2022), and new bioPROTAC design presents an opportunity to exploit new E3 ligases for highly selective degradation. HECT E3 ligases may be less suitable for PROTAC and bioPROTAC design as the formation of additional thioester intermediates is necessary before E2 ubiquitin transfer and isopeptide bond formation (Buckley and Crews, 2014).

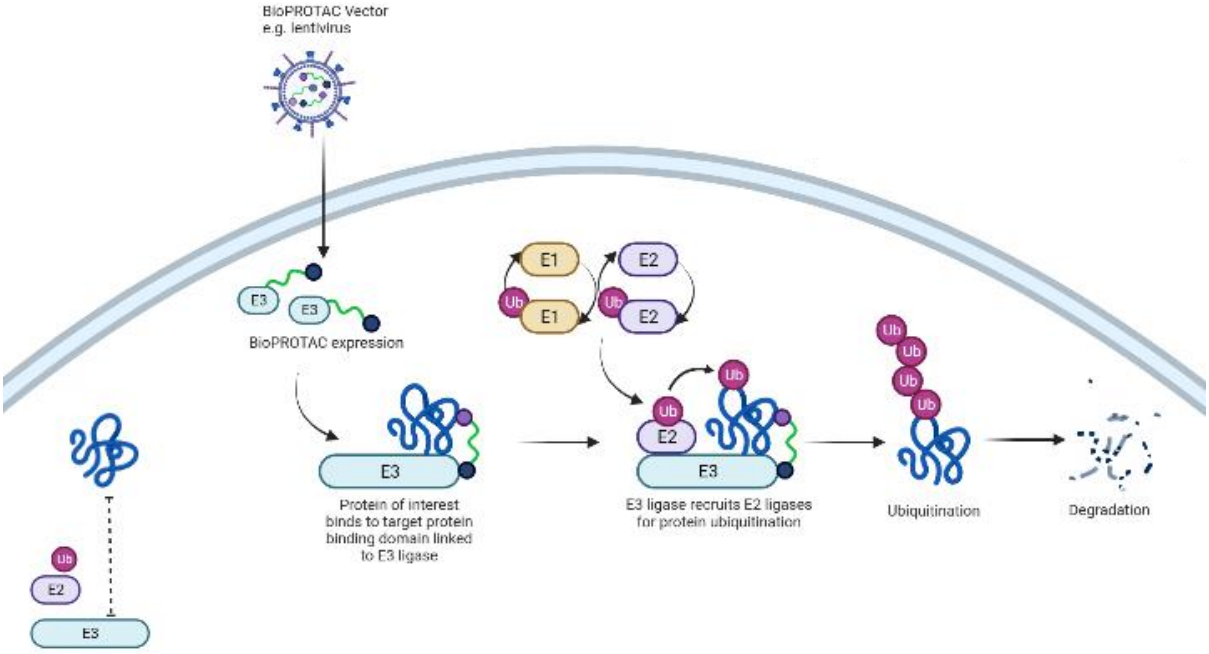

Figure 1.6. BioPROTAC mechanism of action*. When expressed in cells, the bioPROTAC brings the POI into close proximity with the fused E3 ligase. Subsequently, E2 ligases can be recruited for protein ubiquitination and subsequent degradation.*

1.4.3.2 Current applications of BioPROTACs

Proliferating cellular nuclear antigen (PCNA) is an attractive oncological target as it is overexpressed in dividing tumour cells and is associated with a poor prognosis (Moldovan *et al.,* 2007; Wang *et al.,* 2016). A PCNA-targeting bioPROTAC exhibited superior pharmacological effects over stoichiometric inhibition of PCNA. By incorporating Con1, a high affinity peptide ligand of PCNA, and E3 adaptor protein SPOP (speckle type POZ protein), rapid degradation of PCNA could be achieved *in vitro* (Lim et al., 2020).

The oncogenic protein KRAS is found to be mutated in 86% of RAS-altered cancers, and RAS protein are associated with up to 16% of cancers (Kargbo, 2020). It is of high therapeutic value but has been considered undruggable due to its lack of sites amenable for binding small molecules. The ability of bioPROTACs to potentially target these undruggable targets such as KRAS was demonstrated by Bery et al., (2020), whose work provides evidence that bioPROTACs can degrade undruggable targets such as KRAS with varying degrees of efficacy. A variety of E3 ligases were initially incorporated into the study providing further evidence that bioPROTACs can engage a wide range of novel E3 ligases beyond small molecule PROTAC design.

Bacterial E3 ligase mimetics have also been incorporated into targeted protein degradation strategies, exhibiting highly potent target degradation with little variability compared to other human E3 ligases in the literature, demonstrated by (Ludwicki et al., 2019). IpaH9.8-based ubiquibodies have also been repurposed as bioPROTACs targeting ubiquitin conjugating enzyme E2 C (UBE2C) (Wang et al., 2023). UBE2C targeted degradation is a crucial example where bioPROTAC design is advantageous as UBE2C does not possess the small molecule binding sites needed for standard PROTAC development (Bekes *et al.,* 2022).

bioPROTACs targeting α-synuclein have been demonstrated to successfully degrade their target and reduce pathology, preventing pre-formed fibril aggregation in primary neuron models (Carton et al., 2025). Other PROTACs and small molecule degraders have been reported to degrade α-synuclein. Using the cereblon E3 ligase and a single domain antibody targeting α-synuclein, proteasomal degradation of α-synuclein can be facilitated (Jiang et al., 2024). Additionally, the first SOD1-targeting

bioPROTAC exhibiting mutant specificity has been developed, utilising a CHIP E3 ligase domain and misfolded SOD1 specific intrabody (Chisholm et al., 2025).

While bioPROTACs are currently experimental and have not yet reached clinical trials, the bioPROTAC concept presents an emerging technology that address some of the current pitfalls of small molecule PROTACs. Most importantly, bioPROTACs can potentially target currently undruggable targets that PROTACs cannot selectively degrade with such high selectivity limiting the likelihood of off-target degradation.

Synonymous to bioPROTACs, ubiquibodies aim to target and degrade specific pathological proteins with high selectivity and specificity. By effectively reprogramming the substrate specificity of a E3 ubiquitin ligase by replacing the wildtype substrate binding domain with a single-chain variable fragment (scFv) intrabody, the respective target protein can be degraded by the E3 ligase with high affinity (Portnoff *et al.,* 2014). A ubiquibody targeting α-synuclein was developed by fusing an anti-α-syn scFv to the NEDD4 E3 catalytic domain to target α-synuclein for ubiquitination and degradation, and it was shown that directing targeted ubiquitination to the non-amyloid component of α-synuclein (Nac32HECT) had a positive effect on intracellular α-synuclein levels and partially rescued α-synuclein over expression *in vitro* (Vogiatzis et al., 2021). Ubiquibodies hold great promise as an effective therapeutic strategy for clearance of aggregated proteins in NDD conditions such as PD, Vogiatzis et al., (2021), yet further research is required to determine safety and specificity and determine optimal delivery of ubiquibodies.

1.4.3.3 Nanobodies

Nanobodies are described as a more versatile antibody form consisting only of a single antigen-binding domain, derived from the variable domain of heavy-chain-alone antibodies (Muyldermans, 2021). With a molecular weight of ~15kDa, nanobodies are promising tools for gene therapy approaches and bioPROTAC design. Their ability to bypass the BBB and engage with host protein degradation systems adds to their therapeutic value (Chatterjee et al., 2018). Recent success of targeted protein degradation in preclinical models of PD and AD demonstrate their therapeutic potential in the context of NDDs, however their use in targeting SOD1 degradation is more limited. In a recent study conducted by Kumar et al., (2022), anti-SOD1 nanobodies were developed that alleviated pathogenic features of mutant SOD1 *in vivo,* through mitigation of the misfolded conformation of SOD1. It is well understood that levels of mutant SOD1 instability correlates with disease severity, Wang et al., (2008), therefore improving levels of functional natively folded SOD1 and restoration of mutant SOD1 to typical subcellular locations may be a viable therapeutic approach for ALS.

1.5 Antibody and scFv structure

The rapid development of monoclonal antibody technologies has led to the expansion of a toolkit of high-affinity binders against a wide range of disease relevant proteins, with promising therapeutic potentials. Over 160 antibodies are currently approved for clinical use and over three billion antibodies have been sequenced to date (Briney et al., 2019; Carter and Rajpal, 2022). This interactome encompasses antibodies that have a high affinity for specific conformational states, including but not limited to varying protein aggregation states or toxic misfolded conformers. This

degree of specificity is especially important in the context of neurodegenerative disease, where toxic misfolded species are conformationally distinct from the native wildtype protein.

An IgG antibody is the most abundant monoclonal antibody (mAb isotype) and is composed of two heterodimeric antigen binding fragments (Fab region) and one homodimeric fragment crystallisable region (Fc) domain that confers overall stability of the mAb molecule. In idealised conditions, each antibody recognises a specific antigen unique to its target, although in practice antibodies can exhibit a degree of cross-reactivity, binding to similar epitopes with lower affinity (Notkins, 2004). The paratope or antigen-binding site of the antibody is specific for a particular epitope displayed on the antigen (Edelman, 1973; Teillaud et al., 1983). Complementarity determining regions (CDRs) are highly diverse antibody regions that determine antigen recognition and binding, giving rise to the diverse antibody interactome (Polonelli et al., 2008). Antibody numbering schemes based on structural similarities of immunoglobulin frameworks and sequence alignments are employed to label antibody CDRs. Chothia and enhanced Chothia (Martin) CDR numbering systems are commonly used, although other systems such as Kabat and IMGT can be used to locate and number CDR from a given antibody sequence (Abhinandan and Martin, 2008; Chothia and Lesk, 1987; Kabat and Wu, 1971; Lefranc et al., 1999). In all systems, CDRs are numbered one to three on both VH and VL chains. Among the six CDRs, the VH chain CDR3 typically contributes highest structural diversity, playing a central role in antigen specificity, whereas CDR1 and CDR2 are more cross-reactive (Xu and Davis, 2000).

Single chain variable fragments (scFvs) are 25-35kDa molecular weight synthetic constructs composed of immunoglobulin variable heavy chain (VH) and variable light chain (VL) regions retaining parent antibody CDRs that confer antigen specificity (**Figure 5.1**), CDR numbers. The VH and VL domain are typically connected by a flexible repeating glycine-serine linker $(G_4S)_3$, forming the scFv (Bird et al., 1988; Huston et al., 1988). In the first description of scFvs, truncated antibody cDNA sequences were expressed in yeast mutants, as stable truncated heavy and light chains that assemble and bind to a target antigen (Carlson, 1988). Specificity is determined by Fv variable regions derived from the parent antibody. CDR3 from both the VH and VL domains mediate the majority of interactions with antigen and are critical for successful target interaction (Jones et al., 1986; MacCallum et al., 1996). Four cysteines comprise two disulphide bonds that connect the two β-sheets and stabilise the Ig fold (Wörn and Plückthun, 1998a).

scFvs lack the Fc antibody fragment, minimising immunogenicity from binding of the Fc region to complement proteins. In the extracellular environment, scFvs also have a shorter half-life than antibodies due to the absent Fc region, potentially preventing undesirable immune responses (Go et al., 2024).

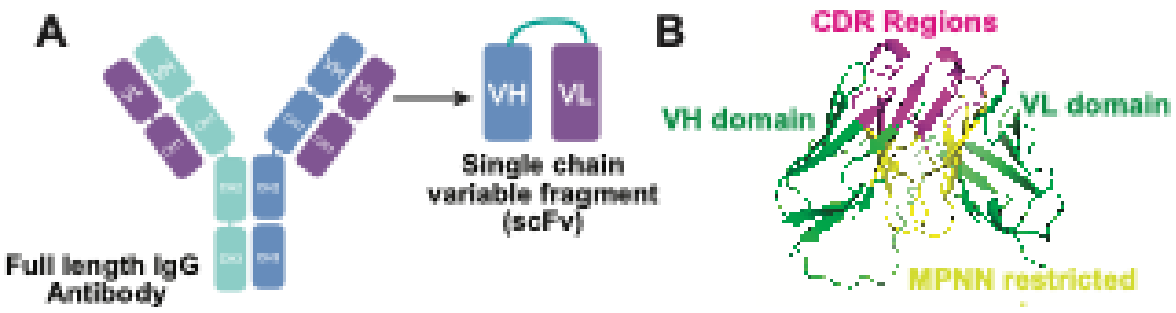

Figure 1.7. Schematic representing scFv derivation and scFv construct design. *A, Schematic depicting the full-length IgG antibody and derivation of a VHVL oriented scFv. B, AlphaFold 3 predicted scFv structure, visualised in ChimeraX. Green represents VH and VL framework regions and pink regions indicate the three CDR loops.*

The use of scFvs to treat neurodegenerative disorders is of high therapeutic potential. This may be through inhibition of aberrant protein-protein interactions or preventing transitions to protein misfolding or aggregation. Targeting at the protein level using scFv intrabodies offers the advantage of targeting distinct protein conformations, post-translational modifications and different misfolding exposed epitopes, allowing interference with disease pathogenesis at the intracellular origin. While small molecule drugs may target a protein directly, it is well understood that approximately 85% of the human proteome is considered undruggable (Neklesa et al., 2017). This estimate originates from studies citing that only 3,000-4,500 proteins encompass the targetable human proteome, while the remainder of the proteome lack suitable binding pockets or accessibility (Finan et al., 2017; Hopkins and Groom, 2002). Not all proteins have accessible sites for small molecule interaction and protein-

protein interaction. Further, aberrant conformations make it more challenging to target neurodegenerative disease-causing proteins with small molecule drugs.

Currently, there is no reliable method to engineer stable cytoplasmic intrabodies in mammalian cells. scFv solubility remains a major challenge, due to their tendency to form insoluble aggregates in the cytoplasm many techniques have been implemented to overcome this, by either altering the scFv amino acid sequences or adding solubilisation tags, chaperone proteins, or modifying the expression system itself. Upon defining how scFvs are generated, the currently available methods by which scFv solubility has been successfully optimised will be investigated and current limitations or shortfalls of described optimisation strategies will be reviewed.

1.6 Limitations of scFvs

scFvs are notoriously insoluble when expressed in the reducing cytoplasm (Cardinale et al., 2001). The redox environment of the mammalian cytoplasm hinders disulfide bond formation, which contributes 4-6kcal/mol to the stability of typical antibody domains (Wörn and Plückthun, 1998b). VH and VL domains are removed from their natural antibody formation within immunoglobulin folds, and the properties of each VH and VL domain individually may impede folding and stability (Dudgeon et al., 2009; Ewert et al., 2003). Additionally, the crowded cytoplasm may promote aggregation as a consequence of increased protein-protein interactions (Ellis, 2001). Often, efforts to optimise scFv solubility results in low expression and yield in bacterial systems. Furthermore, sensitivity to protease degradation and molecular chaperones can further hinder stability and expression of scFvs.

1.7 scFv solubility optimisation strategies

1.7.1 scFv linker peptide optimisation

Intrabody VH and VL domains are connected by a flexible peptide linker to form a scFv (**Figure 1.8**). Perhaps overlooked, the linker peptide can be an important factor in influencing scFv properties such as solubility and binding affinity (Chen et al., 2013). Length and composition of the peptide linker can influence stability, affinity, expression yield and correct folding of the scFv (Chen et al., 2013). The most commonly used linker is the $(G_4S)_3$ linker (**Figure 1.9**) which provides sufficient flexibility to correctly orientate the two domains, often used for intracellular *E. coli* expression (Bird et al., 1988; Huston et al., 1988). Glycine is a small, flexible amino acid that does not carry charge or any side chain, providing rotational freedom and making it a favourable selection for repeating linker peptides. The incorporation of a polar serine residue provides some hydrophilicity to the scFv, reducing hydrophobic interactions.

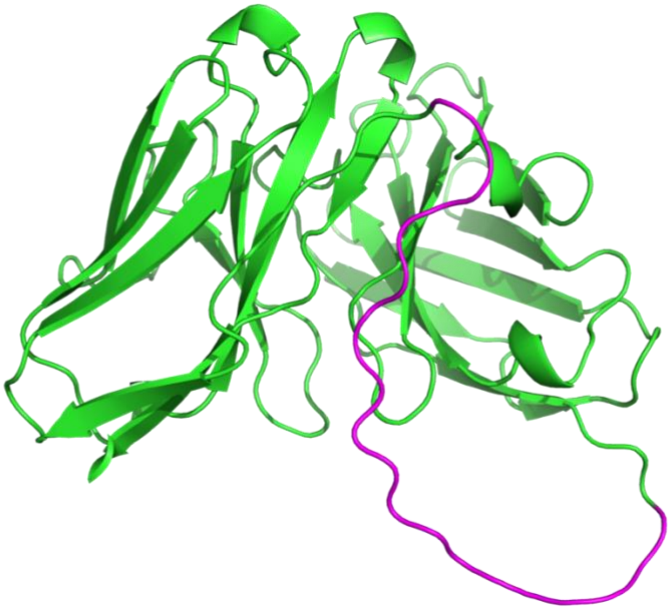

Figure 1.8. The flexible scFv peptide linker. *Predicted structure of an scFv in VH-VL orientation. In pink, the linker peptide joining the VH and VL domain is highlighted.*

AlphaFold 3 was used to determine predicted structure, and structures were visualised using ChimeraX.

Amino acids such as threonine and alanine have also been used in scFv linker peptides, with reportedly improved stability (Luz et al., 2018). However, the test construct (VL-VH) was in a different orientation to the control (VH-VL) and contained an additional N-terminal FLAG tag which may have influenced solubility of the test construct containing the non-conventional linker. The more hydrophilic linker used in this work (**Figure 1.9; LLB17**) was reportedly less flexible than a type G_4S linker, which may contribute to increased domain stability (Zhao et al., 2008).

Linkers with non-repeating units may harbour a similar flexibility to standard peptide linkers with reduced immunogenicity and be preferred when using PCR-based engineering approaches (Hennecke et al., 1998). One study demonstrated that in comparison to a $(G_3S)_4$ linker, (**Figure 1.9C; L1**), non-repetitive linker incorporation, (**Figure 1.9C; L2**), generated a more thermally stable anti-VEGF scFv, but there were no significant differences in *in vivo* efficacy in zebrafish models (Arslan et al., 2022). While the percentage of scFv monomer was significantly higher when the non-repetitive linker was used, there was no difference in percentage of insoluble aggregates found between repetitive and non-repetitive linker scFvs. The non-repetitive linker used in this work was generated by Hennecke et al., (1998), who presented three alternative linkers (**Figure 1.9B**), that were proposed as equivalent to standard $(G_4S)_3$ linkers, although this work was completed using bacterial scFv expression.

Linker length, in addition to linker composition, has an influential effect on specificity and binding affinity. A study completed by the Tanaka group demonstrated an interesting relationship between linker peptide length and scFv reactivity in *E. coli*. scFvs against daidzin were generated with either 1, 3, 5, or 7 GGGGS repeats (**Figure 1.9D**). Results demonstrate that reactivity to daidzin increased with increased linker peptide length, but specificity slightly decreased with increased linker length (Yusakul et al., 2016). Increased linker length may allow greater flexibility and improved domain organisation and hence binding affinity. Conversely, scFvs with very short linkers (less than 12 residues) may be more susceptible to scFv dimerisation (Hudson and Kortt, 1999).

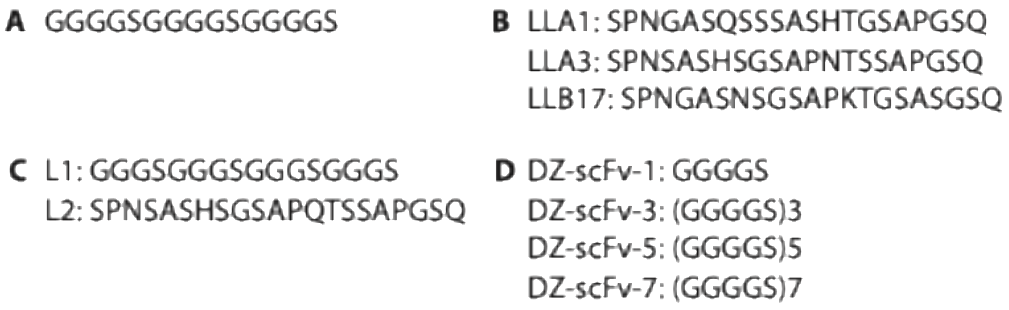

***Figure 1.9. scFv linker peptide alternative constructs**. Repeat length and linker composition alter scFv biophysical properties. **A**; Typically used glycine repeat linker. **B**; non-repeating unit linker alternatives. **C**; An alternative repeating linker with three glycines per unit rather than 4. **D**; Linkers of different length containing repeating units.*

1.7.2 Directed Evolution

Early scFv optimisation strategies were predominantly founded on directed evolution, the means of mimicking natural selection to evolve proteins toward a more desirable function or property. Through iterative cycles of mutagenesis, selection, and

amplification, scFv variants can be generated with enhanced solubility in bacterial expression systems (Wang et al., 2018). In more detail, mutations are introduced through methods such as PCR and SDM, before expressing variants in bacteria, yeast or phage display systems and screening for improved properties such as improved solubility. Further repeating rounds of iterative cycles of mutagenesis is then employed to progressively enrich variants with improved traits. Directed evolution approaches can be employed to improve binding affinity, scFv folding, expression levels or reduce immunogenicity in addition to solubility enhancement.

Directed evolution of an anti-carcinoembryonic antigen scFv, was found to generate a scFv fragment with increased affinity and extended half-life compared to the wildtype scFv. Further, soluble expression of the scFv was increased 100-fold through screening generated mutant libraries for increased yeast surface display levels, using iterative rounds of flow cytometry (Chao et al., 2006; Graff et al., 2004).

Phage display technology was employed by the Winter group to isolate variable heavy domain fragments with increased thermostability (Jespers et al., 2004). Arg28 was identified as a key residue that conferred resistance to increased temperature and reduced aggregation (Famm et al., 2008). This suggests that changing biophysical properties of the variable heavy domain can increase thermostability and aggregation resistance, hence improving scFv solubility.

A combination of structure- and sequence-based methods were used to generate a more focused library of mutant scFvs that were expressed in *E. coli* and subsequently screened for thermal stability and retained binding affinity (Miller et al.,

2010). A selection of single mutations was identified that increased the melting temperatures of variable domains by more than 14 ^{o}C, and these mutations could also be combined to further increase melting temperature cumulatively (Miller et al., 2010). All mutations identified in this study significantly stabilised the variable heavy scFv domain, which further suggests that VH stability or even solubility is predictive of whole molecule solubility. However, some of the most stabilising mutations identified were found to reside within CDR loops, consistent with reports the CDR sequences heavily influence thermodynamic stability (Honegger et al., 2009). Altering CDR sequences may disrupt antigen binding affinity.

A phage display system was used by Christ's group in order to identify mutations that render variable domains more resistant to aggregation and their thermostability was tested using previously described methods of superantigen capture to identify scFv domains that were correctly folded and not aggregated (Christ et al., 2007). Critical residues were identified and selected for substitution to aspartic or glutamic acid before screening for increased heat resistance (Dudgeon et al., 2012). This study provided evidence that introduction of charge at the antigen binding site can increase aggregation resistance, and that aspartic acid mutations were favourable to glutamic acid mutations and positively charged residues. However, studies also describe increased aggregation resistance with addition of charged terminal peptide tags to antibodies which is not positional (Schaefer and Plückthun, 2012). It is clear that net charge may influence aggregation propensity, but position of net charge does not seem to have a determinate effect.

Currently, there is no reliable method to engineer stable cytoplasmic scFvs in mammalian cells. The screening of stable scFvs from hybridoma clones or use of yeast and phage display libraries described here is laborious and the success rate not predictable.

1.7.3 Bacterial co-expression chaperones

Co-expression of bacterial chaperones can be used to assist scFv folding in *E. coli* recombinant protein production systems. Molecular chaperones are proteins that bind to non-native protein conformers and promote correct folding to the native steric structure, or provide a surface for the native fold to assemble correctly (Saibil, 2013). Expression in the oxidative periplasmic space, reduced culture temperatures, engineered *E. coli* variants, and fusion solubility tags have also been implemented as strategies to improve scFv solubility and expression in bacterial systems (Gil and Schrum, 2013).

Skp is a periplasmic holdase that stabilises newly synthesised outer membrane proteins during translocation and folding and has been demonstrated to improve scFv folding in the periplasm (Hayhurst and Harris, 1999). For example, periplasmic co-expression of the chaperone Skp led to a 3–4-fold increase in scFv binding activity in comparison to the native scFv counterpart, and solubility of the expressed scFv was highest when co-expressed with the Skp chaperone (Wang *et al.,* 2013). This finding was supported in a study developing a soluble 3A21-targeting scFv, where scFv binding activity was significantly increased in the obtained soluble fractions (Sonoda *et al.,* 2011). Interestingly, co expression of the scFv with Skp and other molecular chaperones such as FkpA does not have a synergistic effect (Sonoda *et al.,* 2011).

Additionally, cytoplasmic molecular chaperones were reported to be ineffective with regards to secretory periplasmic production. FkpA co expression also has reported notable effects on scFv solubility in the periplasmic space (Ramm and Pluckthun, 2000).

Small affinity tags such as the 33-residue P17 peptide tag have also been documented to increase scFv solubility, sometimes more effectively than other chaperoning fusion tags such as MBP, although this is dependent on the scFv in question and expression system used. In Shuffle T7 *E. coli*, solubility of the G12 scFv used throughout the study increased from 14.9 % to 45 % through the addition of a C-terminal P17 tag (Wang et al., 2022). While this is a considerable increase in solubility, it is clear however that solubility enhancement of scFvs is dependent on expression system and scFv characteristic; a notoriously insoluble scFv was not successfully optimised through addition of the P17 tag and solubility for other scFvs was only improved in Shuffle T7 (Wang et al., 2022). Addition of the P17 tag also modestly increased melting temperature by 2.3 ^{o}C, indicating that stability of the scFv was increased, which suggests type I intramolecular chaperone activity by the tag.

GroEL chaperone complex expression aims to assist folding of non-native polypeptides in the *E. coli* cytoplasm. GroEL and its accompanying cofactor GroES form a chaperonin complex that helps to prevent misfolding and aggregation of newly synthesised proteins (Thirumalai and Lorimer, 2001). It has been demonstrated that co-expression of GroEL and scFv in *E. coli* increased functional yields. In BL21 *E. coli*, scFv solubility was increased by up to 50 % with chaperone co-expression, which is beneficial for large scale production of recombinant scFv (Veisi et al., 2015). However,

there are conflicting studies that demonstrate no significant improvements following GroEL co expression with scFvs, and instead report that disulfide isomerases DsbC and DsbG are more effective at promoting soluble formation of scFvs (Zhang et al., 2002).

The DnaK/DnaJ/GrpE system is a chaperone complex used to promote correct folding of cytoplasmic proteins in *E. coli*, (Schröder et al., 1993). Improved yield of soluble scFvs has been demonstrated for an anti-domoic acid scFv, although a proportion of inclusion bodies remained present and overproduction of GroESL reduced scFv solubility (Hu et al., 2007). Expression of DnaK/DnaJ/GrpE chaperones with a HER2-targeting scFv with low temperature cultivation synergistically improved scFv solubility, resulting in a four-fold increased yield of soluble scFv protein (Estabragh et al., 2022).

Many described intrabodies expressed in bacteria are identified using phage display libraries in *E. coli,* or using double hybrid technology in yeast through selection against the target protein. Selected candidates are then expressed in an appropriate mammalian cell model. It is well understood that overexpression of mammalian proteins can lead to aggregation in *E. coli* (Baneyx and Mujacic, 2004). The reverse is less covered but is demonstrated to be true in the case of intrabodies. scFv intrabodies selected using phage display libraries in bacteria aggregate in mammalian cell cultures systems. For example, anti-tubulin scFvs that were soluble and non-aggregating in *E. coli,* formed insoluble aggregates in the mammalian cytoplasm (Guglielmi et al., 2011). This paper highlights key differences between the mammalian and bacterial cytoplasm that can be attributed to the differences in scFv solubility in

different expression systems. Highly distinct folding environments, different chaperone systems, redox conditions, and molecular crowding are all contributing factors that may influence scFv solubility in the mammalian cytoplasm (Guglielmi et al., 2011). Evidently, findings or strategies implemented in bacterial expression systems may not translate well to the reducing environment of the mammalian cytoplasm. Likewise, soluble scFvs expressed well in mammalian cultures may not fold well in the bacterial cell, perhaps due to lack of disulfide bond formation or changes to pH.

1.7.4 Fusion partners and Chaperones

A PEST motif is a peptide sequence greater than or equal to twelve residues enriched in proline (P), glutamic acid (E), serine (S), and threonine (T); these motifs typically have a short half-life and have propensity for accelerated proteasomal degradation (Rechsteiner and Rogers, 1996). Addition of a highly charged PEST sequence was demonstrated to significantly increase solubility of intrabodies (Joshi et al., 2012). Further, due to the inherent moderate affinity of the PEST sequence to the proteasome, scFvs were able to target and degrade α-synuclein (Joshi et al., 2012). Although previously, Butler and Messer show that addition of both a PEST and scrambled PEST motif to the anti-hungtingtin had no effect on scFv solubility (Butler and Messer, 2011).

In one of the first studies to adopt net charge engineering as a means of improving scFv solubility, five glutamic acid residues were added to the C-terminus of an A6H-targeting scFv which resulted in a significant increase in solubility and yield following BL21 DE3 *E. coli* (Tan et al., 1998). However, this scFv variant had a propensity to aggregate, and some reduced binding affinity compared to the parent

antibody. Interestingly, data was not provided but the study claims that aggregated species remained in the presence of reducing agent dithiothreitol (DTT), suggesting that this aggregation is independent of disulfide bond formation (Tan et al., 1998).

Adding soluble fusion tags such as maltose binding protein may aid intrabody stabilisation and therefore solubility (Bach et al., 2001). Maltose-binding protein is a common protein fusion tag that can function as a molecular chaperone, promoting solubility and increased stability of an scFv (Hewitt et al., 2011; Reuten et al., 2016). Highly hydrophilic tags such as MBP and NusA, have implemented in scFv construction and improved solubility in bacterial systems, and outperformed scFv fused with signal peptides or Trx peptides (Sun et al., 2012). It was also noted in this study that scFvs began to aggregate after cleavage of their solubility enhancing tags, perhaps limiting the use of these solubility tags in large scale production of soluble scFvs. Fusing an scFv to a soluble tag such as MBP may increase overall scFv solubility and expression yield. However, fusion partners increase molecular weight of the scFv-tag fusion protein, which may limit deliverability of scFvs. Strategies effective in *E. coli* such as addition of solubility tags, can improve bacterial yield but findings are not always predictive of behaviour in the mammalian cytoplasm.

While this approach was successful in reducing the probability of cytoplasmic aggregation of intrabodies, there was a low correlation between predicted net charge and experimentally determined stability. Intrabodies with similar net charges had different aggregation propensity rates, Kvam *et al.,* (2010), indicating that factors beyond net charge are related to scFv aggregation.

1.7.5 Rational Framework Engineering

Rational mutagenesis of framework regions has been implemented in many cases with the aim of optimising scFv solubility with much success. Early work on framework engineering to improve scFv stability showed that increasing thermal stability through modification of framework regions is a key factor for consideration when improving scFv solubility (Wörn and Plückthun, 2001). A key study utilising framework engineering as an scFv solubility optimisation strategy incorporated mutations to the scFv consensus scaffold. A 2–3-fold increase in reporter activity was observed indicating higher protein yield and scFv functionality was maintained (Tanaka and Rabbitts, 2003).

There is an established correlation where increased protein stability correlates with an increase in the proportion of lysine over arginine residues (Warwicker *et al.,* 2014). Substituting lysine for arginine reduced scFv aggregation propensity (Austerberry et al 2019). While charge is maintained in this amino acids substitution, it is possible that arginine substitution in the place of lysines reduce the likelihood that protein-protein collision will lead to aggregation (Austerberry et al., 2019). This study also highlights that solvent exposed arginine residues are suitable candidates for charge swap mutations without identifying aggregation prone or hydrophobic regions.

Plückthun and coworkers examined replacing hydrophobic residues at the variable/constant domain interface with acidic residues. Substitution of Val84 with an aspartic acid in the framework region of an experimental scFv led to a reduction in heat-induced aggregation and was found to increase periplasmic expression 25-fold (Nieba et al., 1997). This earlier study describes the common scFv problem in that

they expose a former variable/constant domain interface containing hydrophobic regions and propose that introduction of negative charge at this site by mutagenesis may mitigate aggregation and improve scFv folding.

CDRs often contain charged hydrophobic residues to facilitate high affinity antigen binding, yet it is these residues that influence solubility and mediate scFv aggregation. Intrabody solubility and aggregation propensity is highly influenced by CDR content (Ewert et al., 2003; Kvam et al., 2010). In particular, CDR3 of the VH domain is at the centre of the antigen binding site, is highly variable and confers most of the interaction surface with the antigen (MacCallum et al., 1996). In some cases, CDR3 mutations have proven to be successful at improving scFv affinity. Mutation in other CDRs may be less disruptive but could require empirical testing on a case-by-case basis, as some mutations in CDRs will impact binding affinity.

Mutating aggregation-prone residues on the scFv surface may facilitate improved solubility. Replacement of non-essential tyrosines in the CDRs significantly improved stability of the scFv and improved binding activity (Zhang et al., 2015). These tyrosine replacements were combined which further improved binding activity, perhaps by reducing hydrophobicity at the binding site. Additionally, by mutating basic residues on the protein surface to acidic residues, scFv folding, half-life and further solubility can be improved (Hugo et al., 2003, 2002).

1.7.6 CDR Grafting

Beyond modifying residues in CDR and framework regions, entire CDR loops can be transplanted into more stable frameworks as a potential optimisation strategy. CDR grafting and rational mutagenesis strategies aim to generate more stable scFvs by either replacing framework regions with a more stable variant or mutating surface-exposed aggregation prone residues to improve stability, (Jung and Plückthun, 1997a; Knappik and Plückthun, 1995; K. Proba et al., 1998). An insoluble scFv may become soluble when frameworks are replaced by intrinsically soluble alternatives (Safdari, 2018). Implementation of this strategy alone risks loss of epitope binding and requires empirical testing for selection of soluble candidates. CDR grafting was explored in detail by Ewert et al., (2004), and proposed that in order for CDR grafting to be successful, an acceptor framework should be distantly related to the donor scFv, to favour more improved biophysical traits. However, this poses a risk of loss of binding affinity unless care is taken to retain certain contact residues or preserve residues just outside of CDR parameters to mitigate this (Ewert et al., 2004).

It was demonstrated that grafting CDRs from aggregate prone scFv onto a more soluble framework enabled improved solubility without dampening binding activity (Öncü et al., 2022). This further supports earlier work that showed that grafting CDRs onto intrinsically soluble human germline frameworks yielded highly soluble scFvs in bacteria (Safdari, 2018). It is unclear if these findings will translate directly to mammalian or *in vivo* applications, where disulfide bond formation and other impeding factors may impact solubility.

CDR grafting is the method by which antigen-binding CDRs of an insoluble scFv can be grafted onto the framework region of an scFv that is well-characterised and reported to confer high stability and solubility (Ewert et al., 2004; Jung and Plückthun, 1997b). However, the repeated success of this technique is uncertain, as the CDRs may contain amino acids that form weak interactions with framework regions, or contribute to scFv folding. Considering this, it may not be a simple case of one soluble scFv framework being suitable for all CDRs. It is evident however that CDR grafting can improve scFv solubility in some cases to an extent.

1.7.7 Disulfide Engineering

The reducing environment of the cell cytoplasm inhibits intradomain disulfide bond formation which normally contributes significantly to the stability of antibody domains. Antibodies and scFvs have a propensity to misfold and aggregate in the cytoplasm due to the inability to form stabilising disulfide bonds (Biocca et al., 1995). 1 % of antibodies were predicted to be successfully expressed in the cytoplasm, although in actuality as few as 0.1 % of those derived from a naïve human spleen cell scFv library were actually stable and functional (Auf der Maur et al., 2004).

Generation of scFvs lacking conserved disulfide bonds that remain functional has proven successful previously (Proba et al., 1998). A fully functional anti-HER2 scFv was generated by replacing cysteines with valine-alanine pairs in both domains. From this work it was suggested that production of cysteine-free scFvs may be possible, if the original scFv was of high thermostability, as thermostability is reduced following complete reduction of both disulfides (Worn and Pluckthun, 2000). It is possible that this optimisation is not viable for particularly unstable scFvs. Typically, disruption of the two conserved disulfide bonds in scFvs reduces thermostability by 4-

5 kcal/mol (Seo et al., 2009). Alternatively, phage display and directed evolution can be employed to identify hyperstable scFv fragment that may fold successfully without a disulfide bond (Proba et al., 1998).

It is possible that maintenance of native disulfide bonds may improve stability and solubility but lead to a reduction in expression. Replacement of cysteines with hydrophobic residues to generate hydrophobic interactions in replacement of disulfide bonds in order to improve expression results in a sharp decrease in antigen-binding affinity (Colby et al., 2004). Directed evolution was then employed to successfully rescue binding affinity, demonstrating that disulfide knockout or cysteine removal may not be a standalone method for improving scFv solubility and expression.

Alternatively, instead of placing a linker between the VH and VL domain, Brinkmann et al., (1993), created a non-native disulfide bond by substituting amino acids in conserved framework regions (residues VH44 and VL102). This led to improved and extended cytotoxic activity in human serum compared to scFv counterparts and increased stability at 37 ^{o}C (Brinkmann et al., 1993). Further, improved scFv stability and reduced aggregation was observed in more recent work, Zhao et al., (2010), where a non-native disulfide bond was introduced to the anti-alfatoxin scFv. However, this optimisation strategy relies on appropriate conditions for disulfide bridge formation such as ShuffleT7 *E. coli.* One study introduced two disulfide bonds between the scFv linker and the variable domains to minimise flexibility of domains and reduce aggregation potential, in which melting temperature was increased by ten degrees (Boucher et al., 2023).

1.7.8 Charge and hydrophobicity tuning

Most cytoplasmic proteins possess a net charge at cytoplasmic pH, consistent with the theory that the cellular proteome has such evolved so that non-specific ionic aggregation is limited (Chan et al., 2006). Where whole molecule charge is equal to buffer pH, proteins will self-associate and aggregate, (Shaw et al., 2001), likely due to loss of electrostatic repulsion and increased hydrophobic interactions. Carrying some net charge is more favourable than no charge in the cytoplasm so it is plausible that engineering net charge is a suitable method to overcome scFv aggregation in the reducing cytoplasm. Intrabody solubility can be improved by engineering an overall negative net charge at cytoplasmic pH and reducing surface hydrophobicity. Ionic repulsion and weak hydrophobic interactions may compensate for impaired intracellular disulfide bond formation and potentially decrease risk of aggregation.

Fusion of highly charged tags to scFv constructs has been well reported and improves scFv solubility (Joshi et al., 2012; Kvam et al., 2010). 3xFLAG tag and SV40 nuclear localisation signal (NLS) tags increased scFv solubility, likely by engineering surface net charge (Kvam et al., 2010). Several groups report improved solubility following addition of highly acidic protein such as transcription elongation factor NusA and MBP (Shaki-Loewenstein et al., 2005; Zheng, 2003). These correlating findings are perhaps due to inhibition of protein aggregation by ionic repulsion, due to the highly acidic nature of the added tags (Zhang et al., 2004). However, this method of charge engineering by tag addition has not been studied to completion and is not completely robust. In the case of the amyloid oligomer-targeting D5 scFv, aggregate formation remained high following 3xFLAG fusion to the scFv (Joshi et al., 2012).

Kabayama et al., further propose that calculation of net charge at pH 6.6, not the physiological pH of 7.4 is more suitable for their ultra stable cytoplasmic antibody (STAND) scFv optimising strategy. Cytoplasmic intrabodies with a low isoelectric point and strong net negative charge at pH 6.6 were stable and functional in the cytoplasm (Kabayama et al., 2020).

Additionally, GRAVY (grand average of hydropathicity) scores are noted as a secondary correlate to net charge for weakly acidic intrabodies suggesting that weak hydrophobic interactions play a role in intrabody stability in the absence of proper disulfide bond formation in the reducing environment. Many functional intrabodies however have been developed that do not require intra/interdomain disulfide bonds (Tanaka and Rabbitts, 2008).

1.7.9 Machine-learning based methods of scFv solubility optimisation

Most recently, computational and AI-guided redesign has advanced the intrabody engineering toolkit. Incorporation of AI and machine learning techniques have been implemented to systematically optimise scFv framework regions while preserving epitope-binding CDRs. With a given scFv backbone structure, AI-guided inverse folding can be used to predict alternative scFv sequences that are conditioned to be more soluble and stable (Dauparas et al., 2022). Tools such as ProteinMPNN can be used to predict alternative sequences for framework regions that fit the given scFv backbone. When running ProteinMPNN, residues in the CDRs can be restricted from editing so that binding affinity is unaffected by sequence redesign. Using ProteinMPNN to predict alternative sequences, a recent study had a 73 % success rate in reformatting insoluble intrabodies to a more soluble form using AI-led

framework redesign (Galindo et al., 2025). Advantages of computational approaches such as this is the reduced experimental burden and empirical testing, partly due to more accurate prediction of *in vitro* solubility.

1.8 Conclusion

The therapeutic use of targeted protein degraders can widen the scope of druggable targets and allow for the regulation of both enzymatic and non-enzymatic processes that are difficult to target with standard small molecule inhibitors (Hughes et al., 2021). BioPROTAC present several advantages over small molecule PROTACs in that there is no need to incorporate a linker domain, accelerating the design process and widening the scope of E3 ligases that can be incorporated into bioPROTAC design (Cyrus et al., 2011; Troup et al., 2020). Incorporating new E3 ligases, both human and bacterial mimics, is essential for further development and exploration into bioPROTAC therapeutics. Incorporating bacterial ligases into PROTAC design is widely under-researched and could be a promising tool for more complete degradation of target substrates, although use of human E3 domains may be preferred to reduce host immunogenicity towards the bioPROTAC.

Research surrounding PROTACs is particularly limited concerning dosing, the ability of PROTACs to cross the blood-brain barrier to access CNS tissues, and the safety and tolerability of PROTAC administration to patients. The exact mechanisms by which proteins are degraded by AUTACs has yet to be well defined and requires further exploration. Autophagy and lysosomal degradation are promising routes for therapeutic degradation in clinical applications due to the high molecular weight of some neuropathological proteins and PROTACs, requiring some protein unfolding for

proteasomal degradation, recently reviewed by (Kocak et al., 2022). To conclude, bioPROTACs present a novel opportunity for achieving targeted protein degradation and the application of bioPROTACs in the context of neurodegenerative disease remains overlooked. Toxic soluble proteins and insoluble aggregating proteins in neurodegenerative are often deemed undruggable and difficult to clear due to impaired proteostasis in the aging population, and developing viral gene therapy delivery systems harnessing bioPROTAC design may have therapeutic advantages.

Almost all scFvs are insoluble in the mammalian cytoplasm, and many aggregate and misfold when expressed in mammalian cells (Cardinale et al., 2001; Fisher and DeLisa, 2009). Various tools and methods have been implemented to improve intracellular solubility and expression of scFv intrabodies, but there is no clear and readily implementable method to make any scFv soluble. It is evident from the literature that scFv whole molecule net charge correlates with intracellular solubility, and it is clear that other factors such as surface hydrophilicity and CDR content influence solubility. Further, efforts to improve scFv expression and solubility may not translate well in the mammalian cytoplasm.

1.8.1 Aims

The aim of this work is to develop bioPROTACs that target SOD1 and α-synuclein, as I hypothesise that targeted degradation of these proteins implicated in ALS and PD could mitigate pathogenesis and ultimately disease progression. To further enhance the potential specificity of these bioPROTACs, I aim to create mutant-specific and conformation-specific bioPROTAC recognition domains using scFvs derived from antibodies that target disease relevant conformers of α-synuclein and

SOD1. In order to do this, I will investigate how to increase the solubility and hence cytoplasmic availability of scFvs and propose a method for reliable antibody reformatting as scFvs.

Chapter II: Materials and Methods

2.1 Cell culture

HEK293T, HEK293S, and NSC34 cells were grown in 6-well plates, 24-well plate, and 10 cm dishes with DMEM supplemented with sodium pyruvate, with 10 % v/v foetal bovine serum (FBS), 100 units/ml penicillin and 100 µg/ml streptomycin (P/S), and 1 % L-glutamine. Cells were incubated at 37 °C at 5 % CO_2 and were routinely split upon 90 % confluency. To passage and prepare plates for experiments, media was aspirated and cells washed once with 5 ml PBS. Media was replaced with 5 ml PBS containing trypsin-EDTA (Gibco) and incubated for 2 minutes at 37 °C. 10 ml of DMEM was added to the cell resuspension solution which was used to seed a new 10 cm dish. 500-800 µL cell resuspension per well was used to seed 6-well plates and 100 µL was used to seed 24-well plates.

2.2 scFv intrabody design

Literature searches, in addition to patents and antibody databases were used to identify antibodies with conformation specific epitopes, evidence of mutation-specific epitopes. Intrabody sequences were designed from publicly available antibody sequences and plasmids synthesised by Genscript or Twist. In addition, SOD1 confirmation-specific antibody sequences were provided from collaborators and are provided in **Appendix.1.**

MS785 antibody sequence data was obtained from hybridoma sequencing outsourced to Pirbright institute. Briefly, 5´-rapid amplification of cDNA ends-ready

cDNA was prepared followed by PCR amplification of the heavy and light chain Ig variable regions. The products were cloned into a sequencing vector and Sanger sequencing was completed. The C4F6 antibody for misfolded SOD1 was sequenced by tryptic digest mass spectrometry as described previously (Rotunno et al., 2014).

10H (GenBank accession no JX430806) and D5E (GenBank accession no JX442980) scFv sequences were already published (Joshi et al., 2012). The scFv sequences were further modified using terminal tags and linker peptides. A full list of derived scFv sequences is presented in **Appendix.1**. Linker peptides, N- and C-termini tags used to construct the scFv intrabody sequences are depicted in **Appendix.2**. Additionally, rational mutagenesis was completed to replace positively charged residues with aspartic acid residues to attempt to improve scFv solubility.

For AI-led scFv design, scFvs were designed in VL-VH orientation, joined by a flexible $(G_4D)_4$ linker. AlphaFold3 was used to generate PDB files of the predicted structures of scFvs (Abramson et al., 2024). These PDB files are used as the input for sequence optimization by proteinMPNN$_{SOL}$ (Dauparas et al., 2022). Using both proteinMPNN$_{SOL}$ 002 and 020 models (trained on the soluble dataset only), 100 alternative sequences per model were generated for each scFv. CDRs, structurally integral residues at the dimer interface, and the flexible linker were restricted from mutation to preserve antigen specificity and structural stability (**Figure 2.1**). AbRSA was used to identify CDRs (Li et al., 2019). According to Chothia numbering the following amino acids were restricted to preserve antigen binding. In the variable heavy domain, amino acids 26-37, 47-56, and 91-102 were restricted from MPNN editing. For the variable light domain, amino acids 24-37, 46-56, and 86-97 were

restricted. In some cases, amino acid biases were applied to modulate net charge and enhance predicted solubility. All MPNN output sequences were analysed for predicted solubility, according to a predictive linear regression model correlating net charge with solubility. High ranking MPNN alternate sequences, with high sequence identity and a predicted solubility of >90 % were selected for experimental validation.

Figure 2.1. Schematic highlighting framework restrictions and CDR loops*. These residues were restricted and unedited by MPNN to maintain antigen specificity and structural stability. Pink represents CDR loops. Cyan represents amino acids in the dimer interface and flexible linker restricted from proteinMPNN editing. Green represents framework regions editable by proteinMPNN. Produced in ChimeraX, using AlphaFold 3 to generate predicted protein structure.*

2.3 Preparation of plasmid DNA

DNA constructs were designed in SnapGene and synthesised by Genscript or Twist Bioscience. 4 µg plasmid DNA was diluted to a final concentration of 50 ng/µL for transformation in BL21 DE3 or Omnimax *E. coli* cells and plated overnight on LB agar containing 100 µg/ml ampicillin. Single colonies were picked 24 hours later and

cultured overnight in LB media for 16 hours. DNA was extracted using the PureYield Plasmid Miniprep system or the PureYield Plasmid MidiPrep system according to the manufacturer's instructions. DNA concentration was determined by NanoDrop.

2.4 Site-directed mutagenesis

Site-directed mutagenesis was performed using Platinum™ SuperFi™ II Mastermix and PCR cycling conditions were set according to the manufacturer's protocol, using Anza™ 10 DpnI to digest template DNA (**Table 2.1**).

Table 2.1. PCR reaction cycling protocols used for site-directed mutagenesis.

PCR cycles	Step	Temperature	Time
1	Initial denature	98	30s
25-30	Denature	98	10s
	Anneal	60	10s
	Extend	72	
1	Final extension	72	5min
		4	indefinitely

2.5 DNA Transfection

Plasmid DNA of interest in pcDNA3.4 or pTWIST vectors were transfected 24 hours after seeding using Lipofectamine 3000 (Invitrogen) or Turbofect (ThermoFisher) according to the manufacturer's instructions. For all transfections, 500 ng and 2000 ng of DNA was added to cells seeded in 24 well plates and 6 well plates

respectively. 6 µg DNA was transfected into 10 cm dishes. For co-transfections, DNA of each plasmid was added at 1:1 ratio (250 ng and 1000 ng per 24- and 6-well plate). HEK293T and 293S cells were incubated for 24 hours and NSC34 cells were incubated for 48-72 hours post-transfection. MG132 and bafilomycin were diluted in DMSO and added to the culture medium of cells 24 hours following transfection, and incubated for 6 hours following MG132 treatment and 24 hours following bafilomycin treatment DMSO was used as a vehicle control.

2.6 Western blot

All samples were sonicated following cell harvesting. Cells were lifted in 100 µL PBS containing protease inhibitor cocktail for 24 well plates and 300 µL for 6-well plates. Sample loading buffer (40 % v/v glycerol, 0.02 % v/v β-mercaptoethanol, 8 % w/v SDS, 0.1 % w/v bromophenol blue) was added and samples were heated to 95 °C for 5 minutes. 10 µL of total protein lysate was loaded into 15 % polyacrylamide gels and SDS-PAGE was run at a constant current of 80 mA for 40 minutes. Proteins were transferred onto a nitrocellulose membrane using iBlot™ 2 Gel Transfer Device (ThermoFisher). Membranes were blocked with 0.5 % w/v skimmed milk (Marvel) and incubated with primary antibodies overnight at room temperature (**Table 2.1**). After washing with TBS-t (50 mM Tris-HCl, 150 mM NaCl, Tween 0.05 %, pH 7.4) the secondary antibody was incubated for 1 hour with subsequent TBS-t washes before ECL detection. In the case of HRP-conjugated primary antibodies, membranes were blocked for 1 hour and incubated in primary antibody for a minimum of 3 hours before subsequent washing and visualisation. *PageRuler prestained protein ladder (Thermo #26616) was used throughout.*

Table 2.1. Antibodies used for Western Blotting

Antibody	Dilution	Catalogue Number	Clone
SOD1	1:2,000	ProteinTech 67480-1	2F10G1
α-synuclein	1:2,000	ProteinTech 66412-1	1B10E9
BH810	1:2,000		
Myc tag (EQKLISEEDL)	1:2,000	Merck 05-724	4A6
IRDye 800CW goat anti-mouse	1:2,000	LI-COR	926-32210,
LI-COR IRDye 680RD goat anti-rabbit	1:2,000	LI-COR	926-68071
Beta-actin	1:2,000	ProteinTech, 66079-1	10625419
HRP-conjugated goat anti-mouse	1:10,000	ProteinTech	SA00001-1
HRP-conjugated goat anti-rabbit	1:10,000	Invitrogen	A16104
FLAG tag	1:200	ProteinTech HRP-66008	8H6A10
HA tag	1:2,000	ProteinTech 81290-1,	6I21
HA tag	1:2,000	ProteinTech 66006-2	1F5C6

2.7 Recombinant expression and purification of α-synuclein

The pRK172-α-syn-TEV-GFP expression plasmid was transformed into BL21 DE3 cells and grown onto LB agar containing 100 µg/ml ampicillin. A single colony was used to inoculate 100 ml of LB media and was incubated at 37 °C, shaking at 220 rpm overnight. 10 ml of this starter culture was used to inoculate 1 L of LB media for α-synuclein expression, for growth at 37 °C with shaking at 180 rpm until the optical density at 600 nm (OD600) reached 0.8 AU. At this point, isopropyl-β-D-1-thiogalactopyranoside (IPTG) was added to the culture to a final concentration of 0.4 mM and the culture was then incubated overnight, shaking at 18 °C. The following day cells were collected by centrifugation at 4,000 g for 20 mins at 4 °C. The pellet was collected and frozen at -20 °C until purification. Cells were resuspended in Purification Buffer A (20 mM Tris-HCl pH 8.0, 1 mM ethylenediaminetetraacetic acid (EDTA)). Cells were lysed by pressure homogenisation using an Emulsiflex. The lysate was incubated at 85 °C for 10 mins and then clarified by centrifugation at 18,000 g for 30 mins at 4 °C. The clarified lysate was applied directly to a 5 mL Q HiTrap anion exchange chromatography column (GE Healthcare Life Sciences) pre-equilibrated with Buffer A. Protein was eluted from the column via gradient elution with Purification Buffer B (Buffer A + 1 M NaCl) followed by a high salt wash. Fractions were analysed by SDS-PAGE and Coomassie staining, and fractions containing α-synuclein were concentrated using a 15 kDa filter. To further purify the sample, size exclusion chromatography was carried out using a Superdex 200 3 G/L column and purification buffer A to remove high molecular weight impurities. Samples were again concentrated using a 15 kDa filter. Concentration of purified protein was determined using a BCA Assay and NanoDrop and purity of protein was visually inspected by

loading 1.75 µg of protein on 15 % polyacrylamide SDS/PAGE gels and staining with Coomassie total protein stain.

2.8 α-synuclein pre-formed fibril generation

Purified α-synuclein was diluted in TBS to a final concentration of 5mg/ml and left shaking at 1000 rpm for 7 days at 37 °C. Every 24 hours, samples were taken and analysed by size exclusion chromatography to monitor aggregation of α-synuclein. A change in peak size could be observed over the seven-day incubation period indicating the loss of soluble α-synuclein and subsequent increase of insoluble aggregated fibrils. NATIVE-PAGE and SDS-PAGE were also used to confirm presence of aggregated fibrils.

2.9 α-synuclein fibril pulldown

HEK293T cells were grown in 10 cm dishes, transfected with 6 µg scFv intrabody DNA, and incubated for 24 hours. Cells were lysed in 1 ml PBS containing protease inhibitor cocktail (Roche EDTA-free, cOmplete), sonicated and then centrifuged at 14,800 g for 45 mins at 4 °C to pellet cell debris. 50 µL of the soluble fraction was retained as the ‘input fraction’. The remainder of the soluble fraction of the cell lysate was split between two tubes: one containing α-synuclein fibrils and one containing TBS only and were left at room temperature for one hour rotating. Samples were centrifuged again at 14,800 g for 45 mins at 4 °C and soluble and insoluble fractions were analysed by SDS/PAGE and Western Blotting. An increased amount of the FLAG-tagged scFv in the insoluble fraction is indicative of interaction between the soluble scFv and insoluble α-synuclein fibrils.

2.10 SOD1 misfolding experiments

For all SOD1 misfolding experiments, cells were washed with PBS containing protease inhibitor cocktail and sonicated, and a Dot Blot was completed, by pipetting 10 µL of sample directly onto nitrocellulose membranes. Once dry, membranes were immediately blocked with 0.5 % w/v skimmed milk for a minimum of one hour and incubated with primary antibodies overnight at room temperature. After washing with TBS-t, the secondary antibody was incubated for 1 hour with subsequent TBS-t washes before ECL detection.

2.11 Solubility testing

To obtain soluble and insoluble fractions, cells were lifted with PBS containing protease inhibitor cocktail and were sonicated, then centrifuged for 45 minutes at 20,000 g at 4 °C. The supernatant (300 µL) was collected, and 100 µL sample loading buffer was added (soluble fraction), and the pellet was resuspended in 300 µL PBS and 100 µL sample buffer was added (insoluble fraction). Samples were prepared for SDS-PAGE and analysed by western blot. To initially test the thermostability of scFvs, total cell lysates were placed in water baths of varying temperatures for 10 minutes and placed back on ice until centrifugation. To test the specificity of α-synuclein scFvs against insoluble aggregates of α-synuclein, pre-formed fibrils prepared as described above were added to the cell lysate and incubated for a minimum of 1 hour at room temperature with rotating. Cell lysates were then centrifuged, and soluble and insoluble fractions were prepared for SDS-PAGE and Western Blotting as described.

2.12 Immunoprecipitation experiments

All immunoprecipitation experiments were completed at room temperature. 20 µL of HA-Trap magnetic agarose beads (Proteintech ATMA-200) were equilibrated in 480 µL binding buffer (25mM Tris-HCl pH 7.4), 150 mM NaCl, 1% NP-40, 1 mM EDTA, 5% glycerol, protease inhibitor cocktail) while cell lysates were being prepared. After 24 hours incubation post transfection, cells were harvested in binding buffer and incubated at room temperature for 30 minutes, pipetting up and down to resuspend cells every 10 minutes. After incubation, cells were centrifuged at 12,000 g for 10 minutes at 20 °C. The supernatant was added to the magnetic beads and incubated with end-over-end rotation for 1 hour at room temperature. Beads were then washed three times with wash buffer (PBS containing protease inhibitor cocktail), before elution with 4x SDS-PAGE sample buffer by heating at 95 °C for 5 minutes.

2.13 Cellular thermal shift assay

HEK293T cells were transfected with scFv variants of interest and incubated for 24 hours. Cells were lifted using 400 µL PBS with protease inhibitor cocktail and aliquoted in 40 µL fractions. Fractions were heated to 35, 40, 45, 50, 55, 60, 65, 70 and 75 °C for five minutes and immediately frozen at -80 °C overnight. Cells were then thawed and sonicated for 120 seconds and centrifuged at 20,000 g for 45 minutes at 4 °C. The soluble fraction was retained and 10 µL SDS-PAGE sample loading buffer added. Samples were then heated to 95 °C for five minutes before SDS-PAGE and western blotting. Method adapted from (Jafari et al., 2014).

2.14 Statistical Analysis

Western blot densitometry quantifications were completed using Empiria Studio (version 3.2.0.186) and data were analysed in Prism 10 (version 10.2.3). Percentage changes and relative abundances were calculated in Excel. A paired sample t-test was used to calculate significant differences between two groups. For example, where level of degradation was assessed between several mutants, a paired t-test was completed to compare the significance between each mutant control and a mutant co-expressed with the bioPROTAC. An ordinary one-way ANOVA was completed to test the significance between the means of 3 or more groups, for example when comparing several bioPROTAC constructs against a single wild-type protein.

Chapter III: A biological proteolysis targeting chimera for α-Synuclein.

3.1 Introduction

Parkinson disease (PD), dementia with Lewy bodies, PD with dementia and multiple-system atrophy are characterised by accumulation of misfolded α-synuclein aggregates in neuronal tissues (Ayers et al., 2022; Kouli et al., 2020; Spillantini et al., 1997). α-synuclein plays a central role in PD pathogenesis, and PD is characterised by the loss of dopaminergic neurons in the substantia nigra and the accumulation of presynaptic protein α-synuclein (Fearnley and Lees, 1991). α-Synuclein is a presynaptic neuronal protein usually involved in neurotransmitter release and vesicle release (Nemani et al., 2010). In PD, due to both environmental and genetic factors, α-synuclein becomes prone to misfolding, insoluble aggregates form and exert toxic effects on the cell. Cellular homeostasis is negatively impacted by impaired vesicle trafficking and protein degradation (Cooper et al., 2006; Winslow et al., 2010). Oxidative stress is increased by accumulation of misfolded α-synuclein, and further exacerbates cellular pathology and death (Hashimoto et al., 1999). Additionally, misfolded α-synuclein can propagate to nearby cells in a prion-like manner, seeding aggregates and contributing to the widespread progressive pathology in the PD brain (Masuda-Suzukake et al., 2013). It is well documented that misfolded α-synuclein is a key component of Lewy body inclusions in PD patients (Spillantini et al., 1998b). Targeted removal of misfolded α-synuclein could aid understanding of disease pathogenesis and offer a new therapeutic development approach.

Proteolysis targeting chimeras (PROTACs) are small molecules that form ternary complexes with a target protein and endogenous E3 ligases. Biological PROTACs (bioPROTACs) are derived from this concept but differ in that they comprise an E3 ligase ubiquitylation domain and target recognition domain fused within a single protein, meaning they are less reliant on host cell machinery Lim *et al.*, (2020), and this E3 proximity facilitates proteasomal degradation of the target protein by bringing ubiquitylation functionality directly to the target. Native proteins or intrabodies derived from nanobodies or antibodies can be used as target recognition domains.

Here, a panel of bioPROTACs were designed targeting α-synuclein. Two of which comprised a NbSyn87 nanobody fused to the CHIP E3 ligase ubiquitylation domain. Nanobodies consist only of a single antigen-binding domain, derived from the variable domain of heavy-chain-alone antibodies (Muyldermans, 2021). With comparatively low molecular weight (~15kDa), nanobodies are promising avenues for gene therapy approaches and bioPROTAC design. Their ability to bypass the blood-brain barrier (BBB) and engage with host protein degradation systems adds to their therapeutic value (Chatterjee et al., 2018). NbSyn87 was used here as a bioPROTAC recognition domain as the nanobody has a high affinity for a distinct epitope within the highly accessible C-terminal domain of α-synuclein (Guilliams et al., 2013). A second bioPROTAC was designed incorporating a VH14 antibody-derived fragment, due its specificity for the non-amyloid component region of α-synuclein, which is critical for the initial aggregation of α-synuclein (Butler et al., 2016a; Chatterjee et al., 2018).

3.1.1 Aim

Develop targeted protein degraders for α-synuclein that can be applied to the study and treatment of α-synucleinopathies.

3.2 Results

3.2.1 Construction of an α-synuclein-targeting bioPROTAC

The anti-α-synuclein nanobody NbSyn87 epitope resides in the C-terminus of α-synuclein (**Figure 3.2.1A**). Fusion of the CHIP ubiquitylation domain (residues 130-303) to the NbSyn87 nanobody aims to bring E3 functionality into proximity of the target α-synuclein. bioPROTACs were designed with the CHIP E3 ubiquitylation domain placed at either the N- or C- terminus with respect to the NbSyn87 nanobody. **Figure 3.2.1B** shows the more effective bioPROTAC with the CHIP E3 domain at the N-terminus. The proposed mechanism of action is that complex formation between bioPROTAC and α-synuclein leads to E2 ubiquitin-conjugating enzyme recruitment and polyubiquitination of the target for proteasomal degradation (**Figure 3.2.1C**). The bioPROTAC may then bind to the next target molecule in proximity, although this has not been directly confirmed. Small molecule PROTACs however are well known to demonstrate sub-stoichiometric catalysis (Bondeson et al., 2015; Mares et al., 2020).

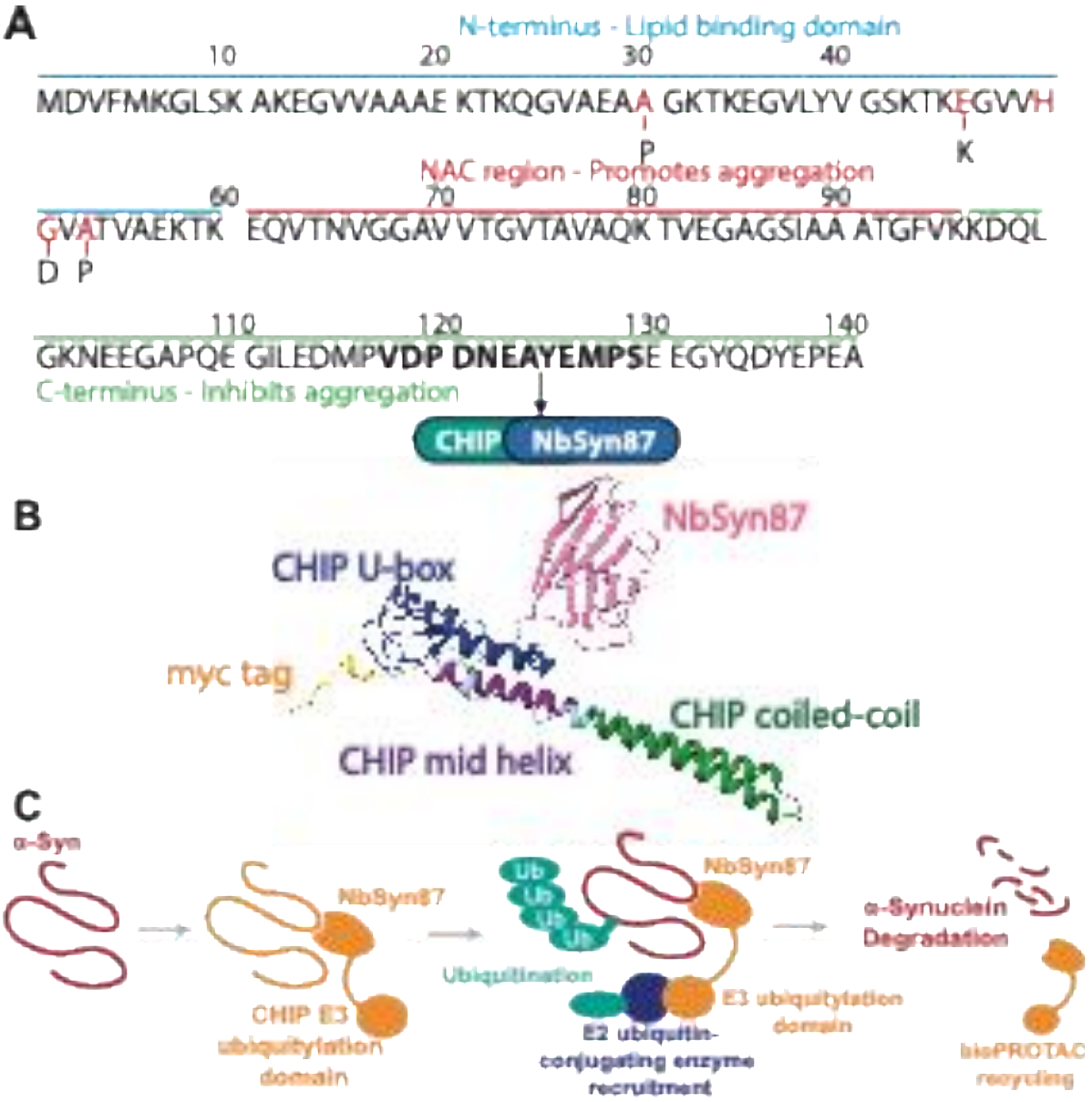

Figure 3.2.1. α-synuclein sequence, bioPROTAC predicted structures and bioPROTAC mechanism of action. A, *Schematic displaying α-synuclein sequence. Domain properties are indicated and select PD-related mutations are shown in red. A generalised structure of the CHIP-NbSyn87 bioPROTAC is depicted and region of NbSyn87 epitope recognition is shown in bold.* ***B,*** *CHIP-NbSyn87 bioPROTAC predicted structure. Orange: myc tag used for western blot detection. Blue; CHIP-Ubox domain. Green; CHIP coiled-coil domain. Pink; NbSyn87 nanobody domain. Produced using AlphaFold 3.* ***C,*** *General bioPROTAC mechanism of action. The CHIP-NbSyn87*

bioPROTAC facilitates close proximity of the α-synuclein target and the CHIP E3 ubiquitylation domain, encouraging degradation utilising host cell machinery. Produced using Adobe Illustrator.

3.2.2 The NbSyn87 bioPROTAC is stably expressed in the cytoplasm

Following bioPROTAC construction and synthesis, the bioPROTAC was expressed in HEK293T cells to determine its solubility, as a poorly soluble bioPROTAC is unlikely to interact and hence degrade it target. The NbSyn87 bioPROTAC was found to be 85.5% soluble (±5%, standard deviation). A CHIP-VH14 bioPROTAC construct was also designed by fusing the CHIP E3 ubiquitylation domain described above with the VH14 nanobody (Chatterjee et al., 2018). The VH14 bioPROTAC was predominantly found in the insoluble fraction of the cell lysate (**Figure 3.2.2**) which may explain why no change in α-synuclein abundance was observed in initial degradation test experiments.

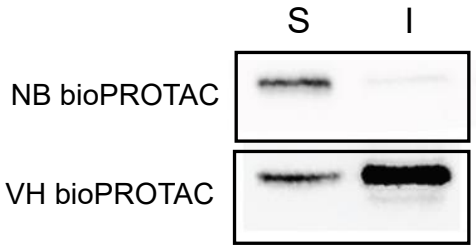

Figure 3.2.2. The NbSyn87 bioPROTAC is high soluble and stably expressed in the cytoplasm. *Additionally, the VH14 was largely insoluble and is therefore less likely to be cytoplasmically available. Shown here are western blots of soluble and insoluble fractions, stained for the myc tag. The NbSyn87 bioPROTAC is more soluble than the VH14 bioPROTAC. HEK293T cells were transfected with either the NbSyn87 or VH14 bioPROTAC and incubated for 24 hours. Cells were harvested and sonicated before*

the soluble and insoluble fractions were separated by centrifugation, prior to SDS-PAGE and western blotting.

3.2.3 NbSyn87 bioPROTAC interacts with transiently expressed α-synuclein

Co-immunoprecipitation was performed using Pierce™ Anti-c-Myc Magnetic Beads (Thermo Scientific™) to test if the CHIP-NbSyn87 bioPROTAC interacts with transiently expressed α-synuclein. α-Synuclein successfully eluted with the myc-tagged CHIP-NbSyn87 bioPROTAC, demonstrating complex formation and interaction in the cell cytoplasm (**Figure 3.2.3**).

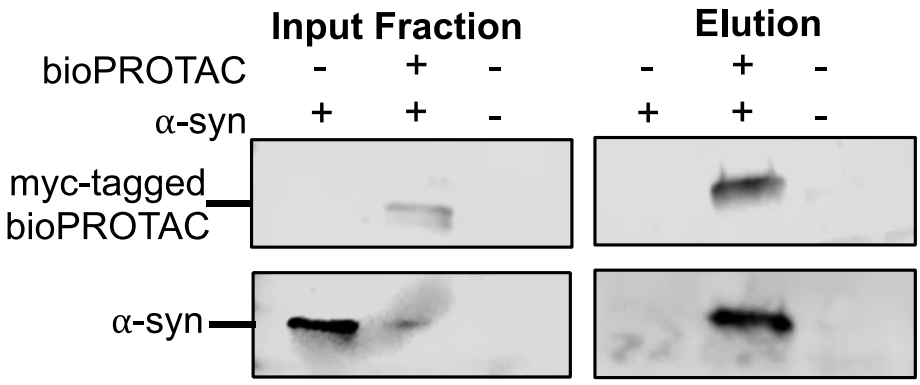

Figure 3.2.3.* α-synuclein *is co-immunoprecipitated with myc-tagged NbSyn87 bioPROTAC, confirming interaction between the bioPROTAC and monomeric* α-*synuclein*. N=2. HEK293T cells were transfected with*** α-synuclein ***and the NbSyn87 bioPROTAC and incubated for 24 hours. Cells were harvested with IP lysis buffer and incubated with myc magnetic beads and incubated for 1 hour at room temperature, before magnetic beads were washed, and elution was performed using 4x SDS-PAGE***

sample loading buffer and heating at 95 degrees for 5 minutes. Input fractions and elution fractions were then analysed by SDS-PAGE and western blotting.

3.2.4 NbSyn87 bioPROTAC-induced reduction of α-synuclein abundance

Co-transfection of α-synuclein and each bioPROTAC in HEK293T cells revealed that placing the E3 domain at the N-terminus yields overall better degradation of the target protein (**Figure 3.2.4A, B**). This construct was selected for further investigation. Overall, a 78% reduction in α-synuclein expression could be observed, (**Figure 3.2.4B**). Non-significant degradation was observed when the NbSyn87 nanobody only was expressed with α-synuclein in line with previous work (Butler et al., 2016a). α-Synuclein abundance was assayed as a function of bioPROTAC abundance and indicated a dose responsive relationship from 0:1 to 1:1 α-synuclein:bioPROTAC coding sequence ratio (**Figure 3.2.4C**).

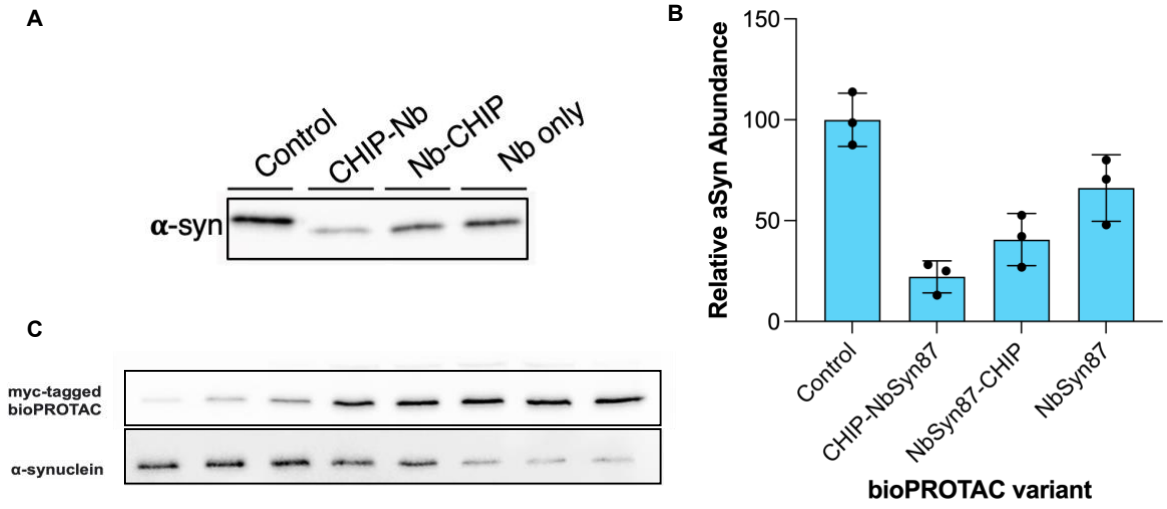

Figure 3.2.4. Placing the E3 ligase ubiquitylation domain on the N or C terminus has different effects on α-synuclein abundance*. HEK293T cells were co-transfected with* α-synuclein *and one of two bioPROTACs: one with the CHIP E3*

domain at the N-terminus (CHIP-NbSyn87) and one bioPROTAC with the CHIP E3 domain at the C-terminus (NbSyn87-CHIP). Cells were also co-transfected with α-synuclein *and the nanobody NbSyn87 only.* ***A****, Western blot showing reduced* α*-synuclein abundance when both CHIP-NbSyn87 and NbSyn87-CHIP are expressed. Some degradation is observed when the NbSyn87 nanobody is expressed alone.* ***B****,* α*-synuclein abundance is reduced in a dose-responsive manner. Different plasmid DNA containing the bioPROTAC was titrated to measure any dose responsive changes to* α-synuclein *abundance.* ***C****, Placing the E3 ubiquitylation domain on the N-terminus significantly reduces* α-synuclein *abundance. Mean relative abundance is shown as a bar chart with standard deviation (error bars) and data points shown in red. N=3, P<0.001, one-way ANOVA.*

NSC-34 cells are a fusion between primary mouse motor neurons and neuroblastoma cells, (Cashman et al., 1992), offering a more relevant genetic background than HEK293T cells and are therefore a more suitable model for testing the NbSyn87 bioPROTAC. Co-transfection experiments at different cell seeding densities revealed that observed clearance in HEK293T models was replicable in NSC34 models. I hypothesised that cell confluency at time of transfection or harvesting could have a notable effect on bioPROTAC-mediated degradation and seeded NSC34 at varying cell densities to observe changes to α-synuclein abundance following bioPROTAC coexpression. When cells were seeded at a density of 75,000 cells per well, total degradation of α-synuclein by the bioPROTAC was observed, and the change in α-synuclein abundance is less prominent at higher seeding densities (**Figure 3.2.5**).

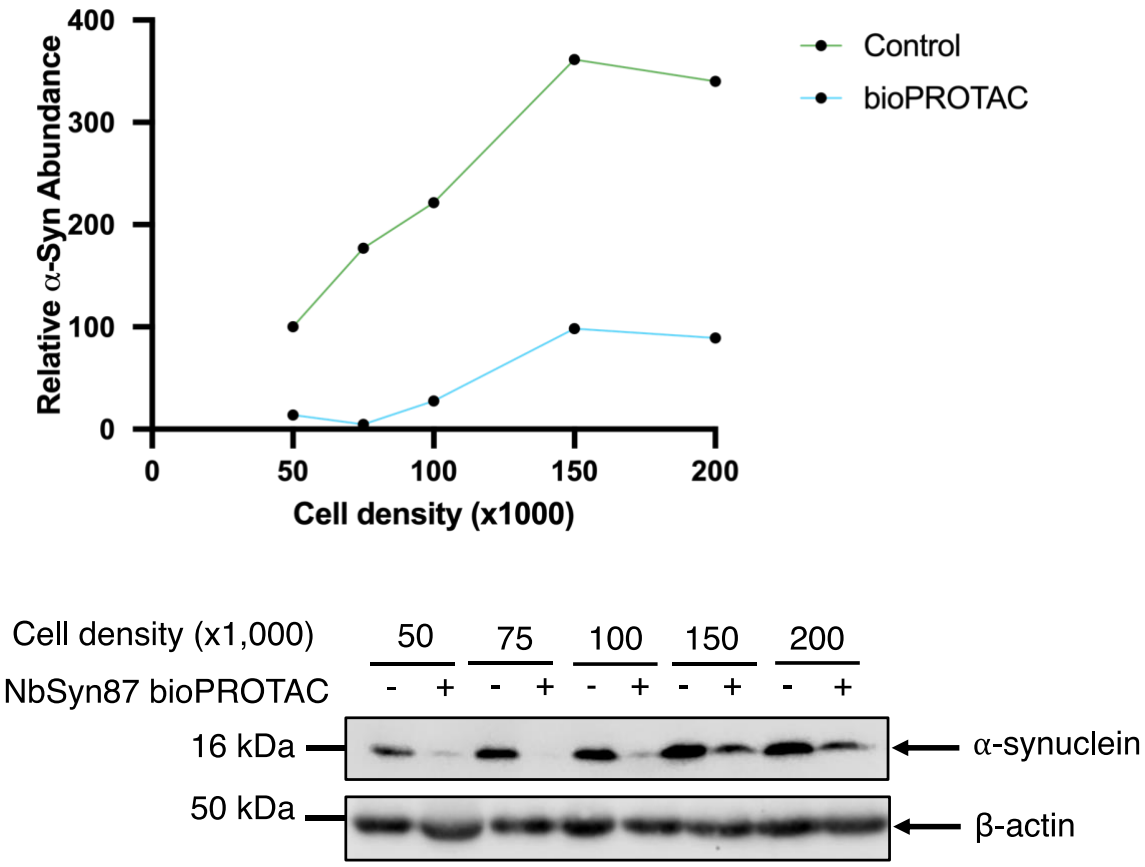

Figure 3.2.5. The NbSyn87 bioPROTAC reduces wildtype α-synuclein abundance in NSC34 cells. A*, Line graph depicts that α-synuclein abundance remains low as cell density increases.* ***B****, Western Blot showing abundance of α-synuclein at different cell densities. Notably, α-synuclein appears to be 100% cleared at a density of 75,000 cells per well. NSC34 cells were transfected with wildtype α-synuclein or plasmid DNA containing α-synuclein and the NbSyn87 bioPROTAC, using a T2A self-cleaving peptide to co-express α-synuclein and the bioPROTAC. Cells were incubated for 72 hours before sample collection before SDS-PAGE and western blotting. N=1. β-actin was used as a loading control.*

3.2.5 NbSyn87 bioPROTAC degrades PD-related mutant α-synuclein

A53 mutations in α-synuclein are linked to familial PD (Polymeropoulos et al., 1997). The NbSyn87 bioPROTAC may also be effective at degrading mutant α-synuclein. Co-expression in HEK293T of mutant α-synuclein and bioPROTAC shows that CHIP-NbSyn87 was effective at degrading mutant α-synuclein associated with familial PD (**Figure 3.2.6A, B**). A53E and A53V mutant α-synuclein abundance was reduced, although this was insignificant due to high variability of α-synuclein abundance in control replicates. There was a significant reduction of A53T abundance with bioPROTAC expression ($p<0.005$). A53T promotes misfolding of α-synuclein, leading to production of insoluble oligomers and fibrils (Sun et al., 2020). As it is likely that NbSyn87 bioPROTAC has a high affinity for monomeric α-synuclein, it may be unable to effectively degrade α-synuclein oligomers or fibrils.

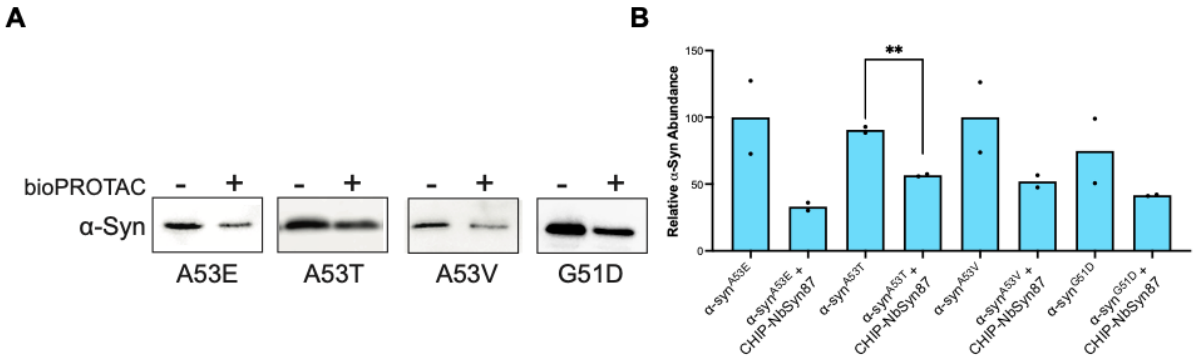

Figure 3.2.6. NbSyn87 bioPROTAC effectively reduces abundance of PD-related mutant α-synuclein*. HEK293T cells were co-transfected with α-synuclein harbouring a point mutation found in Parkinson's disease and the NbSyn87 bioPROTAC that effectively degraded wildtype α-synuclein. Cells were incubated for 24 hours before sample collection before SDS-PAGE and western blotting.* ***A****, Western blot showing change in relative abundance of mutant α-synuclein.* ***B****, Mean changes in relative*

abundance of α-synuclein *depicted in a bar chart with error bars representing standard deviation. N=2. (** = P<0.01, unpaired t-test.)*

3.2.6 Abundance of α-synuclein insoluble aggregates is significantly reduced with bioPROTAC co-expression

Expression of the CHIP-NbSyn87 bioPROTAC significantly decreased levels of insoluble aggregates by 79%, in addition to significantly reducing abundance of soluble α-synuclein (**Figure 3.2.7**). However, in this work transiently expressed α-synuclein was predominantly soluble. Instead, seeding cells with pre-formed insoluble aggregates, generated by fibrillisation of recombinant α-synuclein before directly adding to culture medium would be a more suitable means of testing the ability of the bioPROTAC to clear insoluble aggregates.

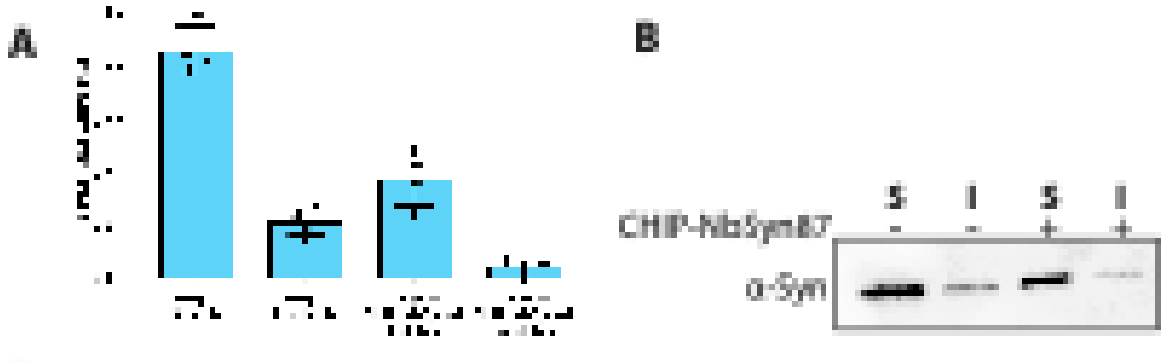

***Figure 3.2.7. The NbSyn87 bioPROTAC significantly reduces abundance of soluble and insoluble aggregates of α-synuclein**. **A**, Levels of relative* α-synuclein *abundance are significantly reduced in test fractions (bioPROTAC expression). **B**, Western blot showing the decreased abundance of* α-synuclein *in the insoluble fraction. Mean relative abundance depicted in a bar chart with standard deviation (error bars) and individual data points (black). P<0.0001, unpaired t-test, N=3. S; soluble. I; insoluble.*

3.2.7 NbSyn87 bioPROTAC efficacy is reduced with autophagy inhibitor treatment

Cells transiently expressing α-synuclein and the NbSyn87 bioPROTAC were treated with bafilomycin, an autophagy inhibitor (Yamamoto et al., 1998). It was found that increasing concentrations of bafilomycin gradually increased abundance of α-synuclein, suggesting less BioPROTAC-catalysed protein degradation (**Figure 3.2.8A, C**). Abundance of α-synuclein does not fully return to control levels which would indicate that α-synuclein is directed to both proteasomal degradation and autophagy for clearance. When the soluble and insoluble fractions of the total cell lysates were examined, the abundance of insoluble α-synuclein aggregates generally increases as bafilomycin concentrations increases. Inhibition of autophagy through bafilomycin treatment leads to the accumulation of insoluble aggregates that are not efficiently cleared by the proteasome. This may indicate that α-synuclein is directed to both proteasomal and autophagy pathways (**Figure 3.2.8B**).

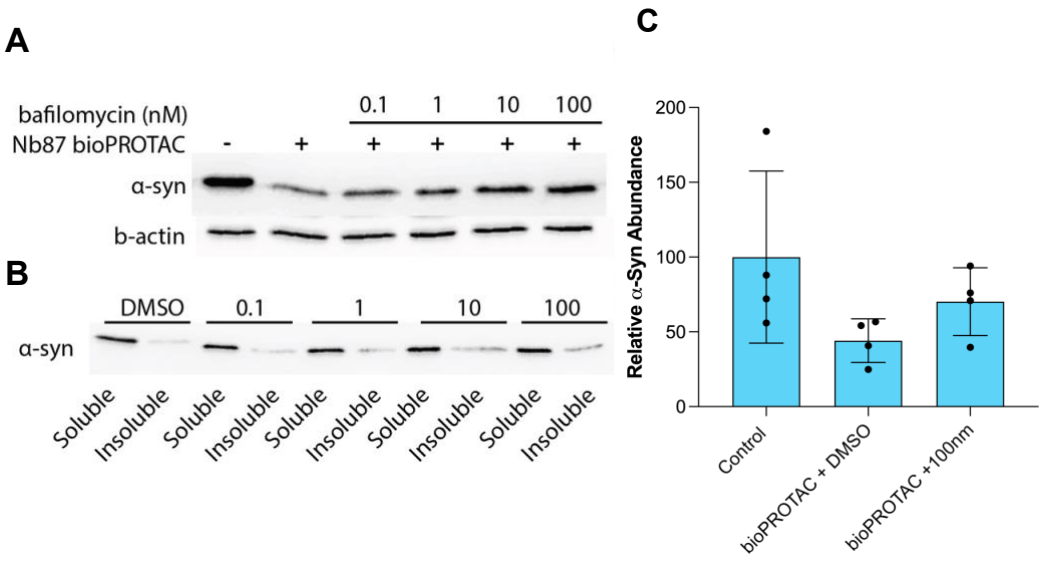

Figure 3.2.8. α-Synuclein is degraded by autophagic degradation in response to NbSyn87 bioPROTAC co-expression. *HEK293T cells were co-transfected with* α-synuclein *and the NbSyn87 bioPROTAC. 6 hours after transfection, cells were incubated with bafilomycin or DMSO as a vehicle control for 16 hours, before samples were collected and either total cell lysates or soluble/insoluble fractions samples were run on SDS-PAGE and western blotting.* ***A****, western blot showing increased abundance of α-synuclein in accordance with increased concentrations of bafilomycin. β-actin levels are unchanged.* ***B****, Soluble and insoluble fractions of total cell lysate following bafilomycin treatment were blotted for α-synuclein, and a modest increase in insoluble α-synuclein is observed.* ***C****, Bar chart showing mean values of total α-synuclein abundance following bioPROTAC expression and DMSO or bafilomycin treatment. Error bars represent standard deviation and data points are shown in black. N=4.*

3.3 Discussion

This work aimed to begin the development of targeted protein degradation therapies for the α-synucleinopathies. Here, I have shown that α-synuclein abundance is significantly reduced by the NbSyn87 bioPROTAC and that levels of insoluble aggregates are reduced by up to 80%. This was observed to be dose responsive. Future work aims to build on this and develop the first panel of confirmation-specific α-synuclein bioPROTACs, using reformatted and modified scFvs as intracellular target recognition domains.

NbSyn87 was chosen as a bioPROTAC recognition domain because the literature provides evidence that the nanobody has high affinity for a distinct epitope within the highly accessible C-terminal domain of α-synuclein (Guilliams et al., 2013). It was also found to have weak affinity for the 26S proteasomal subunit Rpn10, a receptor for poly-ubiquitinated proteins (Gerdes et al., 2020). This weak affinity may facilitate transient interactions between α-synuclein-NbSyn87 complexes and the proteasome, further enhancing likelihood of ubiquitin-mediated proteasomal degradation. These features make it a suitable targeting domain for bioPROTAC design, in addition to its high stability and solubility (El-Turk et al., 2016). α-Synuclein contains several KTKGEV repeats spanning the protein, providing more readily accessible sites for ubiquitination which may increase likelihood of bioPROTAC mediated degradation (Burré et al., 2014). CHIP is highly expressed in the CNS, including dopaminergic neurons (Ballinger et al., 1999; Imai et al., 2002). Further, CHIP has been demonstrated to ubiquitinate α-synuclein (Urushitani et al., 2004), although direct binding affinities for CHIP with α-synuclein have not been quantified.

VH14 was selected for bioPROTAC design, despite being largely insoluble and prone to aggregation (Butler et al., 2016), due to its specificity for the NAC region of α-synuclein. Removal of the NAC region inhibits aggregation of α-synuclein, (Periquet et al., 2007), highlighting its important role in aggregation and making a favourable target for bioPROTAC design. Incorporation of a PEST sequence improved solubility and proteasomal targeting, Joshi et al., (2012), but the VH14-bioPROTAC containing a PEST motif was predominantly expressed in an insoluble state.

Currently, all experiments involve co-expression of the target protein and the bioPROTAC, utilising a P2A self-cleaving peptide to induce cleavage of the 2 proteins (target and bioPROTAC). While P2As are considered the most efficient of the 4 self-cleaving peptides (Kim et al., 2011), a high molecular weight protein 'run-through' is generated so it may be necessary to switch to internal ribosome entry sites (IRES) as a method of protein cleavage for co-expression experiments. Interestingly, these high molecular weight bands are almost undetectable in α-synuclein wildtype experiments where a T2A is used for protein cleavage but is more prominent in α-synuclein mutant experiments which also use a T2A cleavage site, perhaps due to unsuccessful cleavage or lower expression of constructs generated following site-directed mutagenesis. In future bioPROTAC testing experiments, co-transfection of an α-synuclein plasmid and a bioPROTAC plasmid could be completed due to the requirement of high throughput bioPROTAC plasmid development, with several E3 ligases and orientations potentially being combined with each conformation-specific scFv.

Seeding experiments followed perhaps by lentiviral introduction of the bioPROTAC will be useful to further show the efficacy of the bioPROTAC at clearing oligomers and aggregates. Additionally, aggregation assays such as a thioflavin T assay using cell homogenates could be used to generate more data supporting the hypothesis that bioPROTAC expression significantly reduces α-synuclein aggregation (Braun et al., 2021). To test this, cells treated with α-synuclein monomers, oligomers, and preformed-fibrils and the CHIP-NbSyn87 bioPROTAC could be analysed to monitor the extent of aggregation following bioPROTAC expression. PD-related mutants of α-synuclein are known to affect the rate of aggregation of α-synuclein (Stephens et al., 2020).

Evidence shows that α-synuclein may be naturally directed to both autophagy and proteasomal degradation pathways (Webb et al., 2003). In **Figure 3.2.8** standard deviations were high and only a slight increase in α-synuclein abundance was observed. It may be beneficial to use higher concentrations of bafilomycin over a shorter time period as discussed in the literature (Klucken et al., 2012), to observe a more pronounced effect. Conversely, MG132 exposure led to toxicity and cell death, so a shorter incubation period may be necessary to observe the effects of inhibiting proteasomal degradation. Proteasomal inhibition quickly leads to proteoxic stress and apoptosis so these effects may be observed due to long incubation times and accumulation of proteasomal substrates (Pan et al., 2011).

Ongoing testing of the NbSyn87 bioPROTAC's ability to significantly reduce abundance of α-synuclein mutants and wildtype α-synuclein will enable us to show the use of bioPROTACs in the context of neurodegenerative disease therapeutics. It

is essential to confirm efficacy and stability of the CHIP-NbSyn87 in more relevant models such as patient-derived induced pluripotent stem cells (iPSCs) that better represent disease pathology *in vitro.* Testing of bioPROTAC delivery methods such as AAV vectors or emerging lipid nanoparticles strategies in iPSCs is also essential to move this work forward before testing with *in vivo* systems (Agarwal et al., 2024; Yu et al., 2025). It would be imperative to assess confounding factors such as off-target degradation, immune activation and negative impacts on physiological proteostasis such as hindering the degradation of natural E3 substrates or saturating the proteasome (Moreau et al., 2020). In parallel, pharmacokinetic and pharmacodynamic studies are needed to establish dosing and required expression levels (Sun and Liao, 2022).

Targeted protein degradation is a promising therapeutic strategy with possible applications in neurodegenerative disease and several small molecular PROTACs and bioPROTACs have been developed to target neurodegenerative disease targets (Cai et al., 2024; Chisholm et al., 2025; Y. Jiang et al., 2024). In the synucleinopathies such as Parkinson's disease and dementia with Lewy Bodies (DLB), cytoplasmic accumulation of misfolded and aggregated α-synuclein is central to dopaminergic neuron dysfunction and degeneration (Lashuel et al., 2013; Spillantini et al., 1998b). Successful targeted degradation of α-synuclein by CHIP-NbSyn87 bioPROTAC highlights a promising therapeutic avenue for PD, utilising targeted protein clearance to restore proteostasis and potentially alleviate neurodegenerative disease pathology, with the aim of delaying cell death and ultimately disease progression.

Chapter IV: The development of SOD-1 targeting bioPROTACs for amyotrophic lateral sclerosis

4.1 Introduction

Toxic, soluble, misfolded proteins are a central hallmark of neurodegenerative disease and, in some cases, act in a prion-like manner, propagating and seeding aggregates to nearby cells (Münch et al., 2011). Tofersen was recently approved for therapeutic use and is an antisense oligonucleotide which reduces total SOD1 abundance by inducing RNase H–mediated degradation of SOD1 messenger RNA (Miller et al., 2022). While this reduces toxic burden of SOD1 in ALS patients, it also reduces the amount of available wildtype functional protein. To mitigate this, more specific methods of SOD1 degradation that target misfolded conformers or mutant species need to be designed and tested. Selectively removing misfolded or misfolding-prone protein species from cellular spaces could help to improve our understanding of the pathogenesis of diseases such as amyotrophic lateral sclerosis (ALS). A commonality amongst many neurodegenerative disorders such as ALS is that proteostasis is impaired, although the extent and timing of proteostatic disruption can vary between disease and stages of progression (Prell et al., 2012; Saxena et al., 2009). Chemical or biological entities that can perform this function could also have therapeutic uses. This could potentially address shortfalls and hurdles of pharmacological inhibition or degradation of these proteins.

Mutations in the superoxide dismutase 1 (SOD1) gene are found in both sporadic and familial ALS cases (Kiernan et al., 2011). Misfolded SOD1 can aggregate in cells, leading to toxicity and motor neuron degeneration (Deng et al., 1993). The

pathogenesis of SOD1-related disease is often described as a toxic gain of function, with prion-like properties (Ayers et al., 2016). Mutations in SOD1 impair protein maturation and destabilise the protein leading to aberrant self-interactions (Ayers et al., 2017; Lindberg et al., 2005). These properties drive toxic oligomerisation and fibrillisation and lead to motor neuron degeneration (Proctor et al., 2016; Sangwan et al., 2017). Targeting these proteins in their monomeric form could reduce or delay aggregation and hence motor neuron pathology.

Successful BioPROTAC catalysed degradation of α-synuclein indicated this approach may be an adaptable for the degradation of SOD1. A panel of bioPROTACs that target SOD1 were designed based on the interaction domain found in the human copper chaperone for SOD1 (hCCS).

4.1.1 Aim

Develop SOD1-targeting bioPROTACs that efficiently degrade SOD1.

4.2 Results

4.2.1 A CHIP-CCS bioPROTAC was designed to target SOD1

hCCS domain II acts as a molecular chaperone for SOD1 and directly interacts with disulphide reduced wildtype and mutant or disulphide knock-out SOD1 with high affinity (Luchinat et al., 2017). The residues involved in the interface are displayed in **Figure 4.2.1A and Figure 4.2.1B**. Based on this known interaction, a bioPROTAC

was designed incorporating the hCCS domain II and partial D3 domains at the C-terminus and an N-terminal CHIP E3 ubiquitylation domain (**Figure 4.2.1C**).

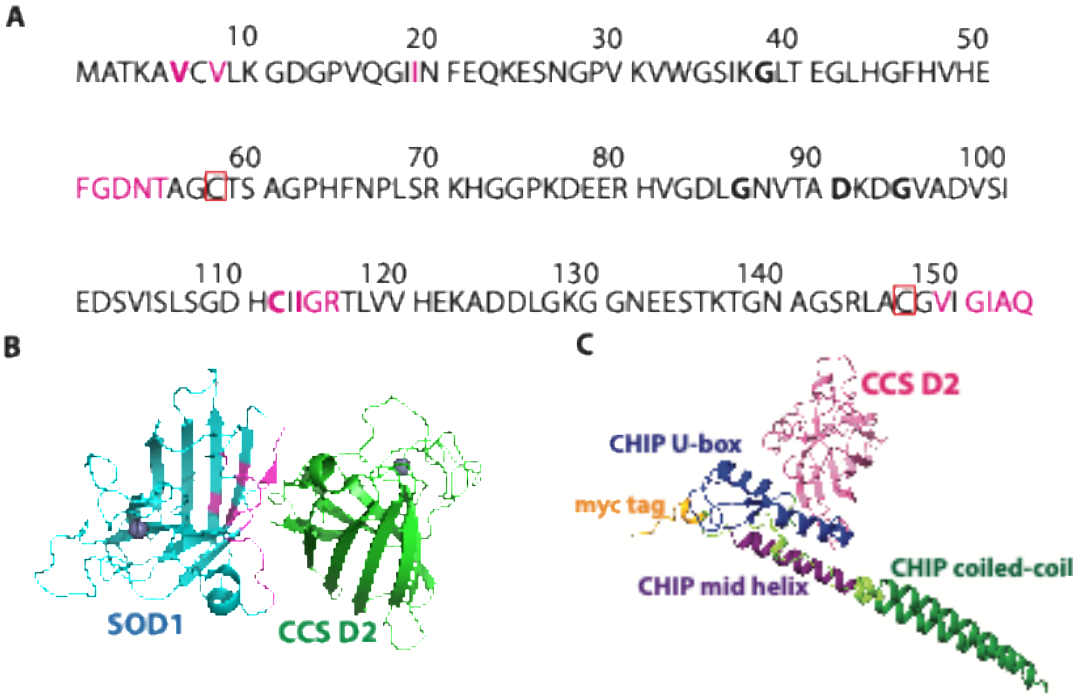

Figure 4.2.1. Schematic representing SOD1 sequence, SOD1-hCCS complex and bioPROTAC construction. ***A***, *The SOD1 amino acid sequence is displayed. ALS-related mutations of interest assessed in this work are shown in bold. Amino acids involved in the interaction between hCCS domain II and SOD1 are highlighted in pink. Cysteines responsible for disulfide bridge formation have been highlighted in red boxes.* ***B***, *SOD1 and CCS domain II interaction (Sala et al., 2019; PDB 6FOL). Shown in pink are residues involved in the interaction interface (>4Å from binding site). C, The CHIP-hCCS bioPROTAC predicted structure is shown. Pink; CCS domain II. Blue; CHIP U-box domain. Purple; CHIP mid helix. Green; CHIP coiled coil domain. Orange; myc tag for detection via western blot.*

4.2.2 The CHIP-CCS bioPROTAC is stably expressed in the cytoplasm

BioPROTAC solubility is an essential consideration. A bioPROTAC with poor solubility is likely to aggregate and not be available for interaction with target proteins. Alongside the CHIP-hCCS bioPROTAC (**Figure 4.2.1**), a second bioPROTAC was designed using the same CHIP E3 ubiquitylation domain at the N-terminus and misfolding-specific SOD1 nanobody Nb54 at the C-terminus (Kumar et al., 2022). It was hypothesised that this bioPROTAC would be highly soluble based on incorporation of the single-domain nanobody and the known solubility of CHIP and CHIP-CCS. However, the CHIP-Nb54 bioPROTAC was considerably less soluble than the CHIP-CCS bioPROTAC and is therefore likely to be less bioavailable (**Figure 4.2.2**). Abundance and solubility of SOD1 remained unchanged in this replicate, possibly indicating absence of interaction and unsuccessful degradation (**Figure 4.2.2**).

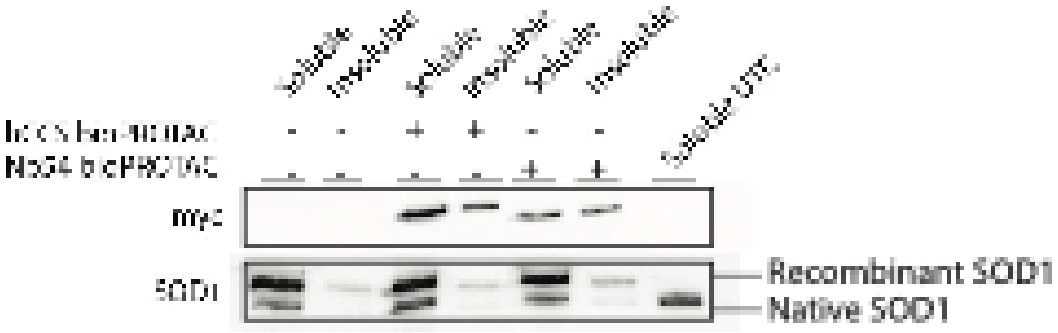

Figure 4.2.2. The CHIP-CCS bioPROTAC is highly soluble and stably expressed in the cytoplasm. *The CHIP-Nb54 bioPROTAC is a less suitable candidate for a bioPROTAC, as it is less soluble than the CHIP-CCS bioPROTAC and therefore less bioavailable. HEK293T cells were transfected with SOD1 plasmid DNA and either the CHIP-Nb54 bioPROTAC or CHIP-CCS bioPROTAC. Soluble and insoluble fractions were obtained by centrifuging before SDS-PAGE and western blotting for SOD1 and*

the myc tag. Western blot probing for the myc tag shows that a larger proportion of the Nb54 bioPROTAC resides in the insoluble fraction. The CHIP-CCS bioPROTAC is predominantly soluble. Western blot probing for SOD1 shows that a larger abundance of recombinant wildtype SOD1 is found in the insoluble fraction. Endogenous SOD1 is found entirely in the soluble fraction. N=1. UTC; untransfected control.

4.2.3 CHIP-CCS bioPROTAC reduces abundance of misfolded SOD1

Changes to abundance of misfolded SOD1 in the presence of the hCCS bioPROTAC was tested by dot blot and probing for misfolded-SOD1 with antibody B8H10 (**Figure 4.2.3**). Several ALS-related SOD1 variants exhibited significant decreases in SOD1 misfolding in response to bioPROTAC coexpression, with low standard deviations (**Figure 4.2.3**). There was no statistical significance for changes in $SOD1^{WT}$ and $SOD1^{I113T}$ misfolding. The relative signal from western blot detection using anti-8BH10 antibody was low for $SOD1^{WT}$. Insignificant changes to $SOD1^{WT}$ misfolding should be expected as the wildtype protein has a lower propensity to misfold and aggregate than the mutant protein.

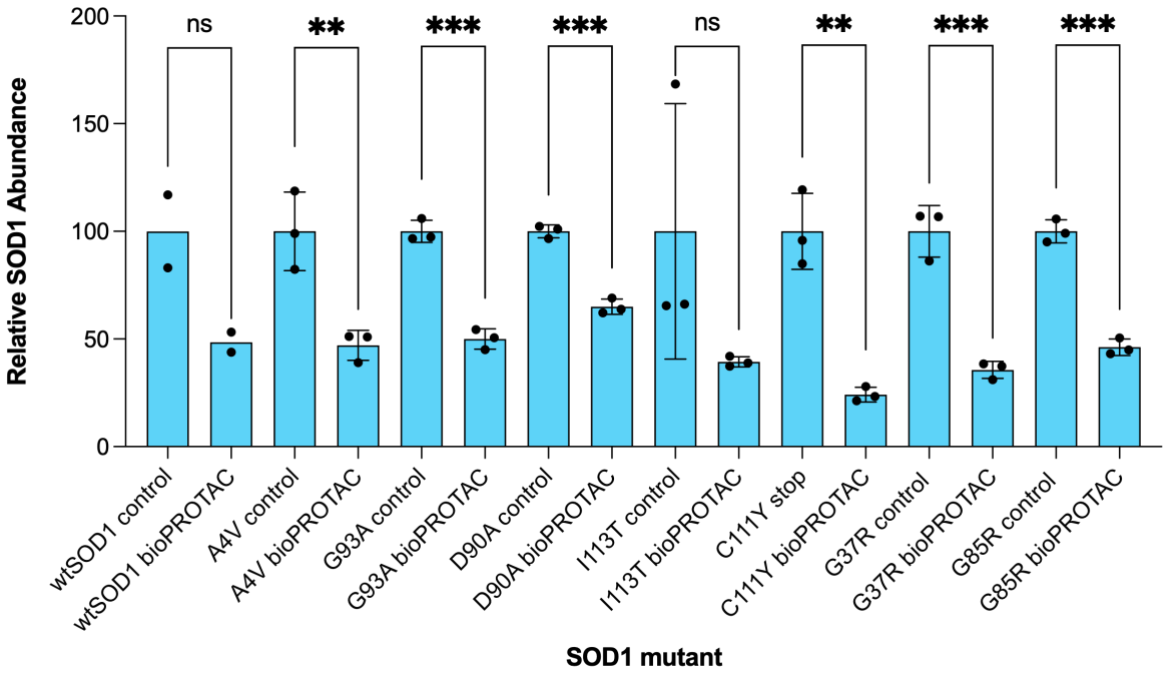

Figure 4.2.3. The CHIP-CCS bioPROTAC reduces SOD1 misfolding. *Abundance of SOD1 probed with misfolding-specific antibody is reduced following bioPROTAC expression. HEK293T cells were transfect with both wildtype and ALS-mutant SOD1, and the CHIP-CCS bioPROTAC in test samples. Cells were incubated for 24 hours post transfection before a dot blot was used to probe for misfolded SOD1-specifc antibody 8BH10. Bar chart represents mean relative abundance of misfolded SOD1 for wildtype and ALS-related mutants, with and without co-expression of the CHIP-CCS bioPROTAC. Where N =3, standard deviations are represented by error bars. Data points are shown in black. An unpaired t-test was completed for each SOD1 variant and the respective control and test populations (N=3) (SOD1^{WT}: N=2). NS = non-significant. * = P<0.05, ** = P<0.01, *** = P<0.005.*

4.2.4 The CHIP-CCS bioPROTAC reduces SOD1 aggregation

It was observed that levels of misfolded SOD1 are significantly reduced by the CHIP-CCS bioPROTAC, while total SOD1 degradation was not significantly decreased and had high mutant to mutant variability. A selection of ALS-SOD1 mutants were co-expressed with the CHIP-CCS bioPROTAC in HEK293T cells and the soluble and insoluble fractions were collected to identify changes in levels of insoluble aggregates of SOD1. Here, a reduction of insoluble SOD1 aggregates for $SOD1^{G93A}$ and $SOD1^{D90A}$ was observed, (**Figure 4.2.4**) which is more likely due to disulphide reduced SOD1 stabilisation by the CCS domain II rather than direction to proteasomal degradation.

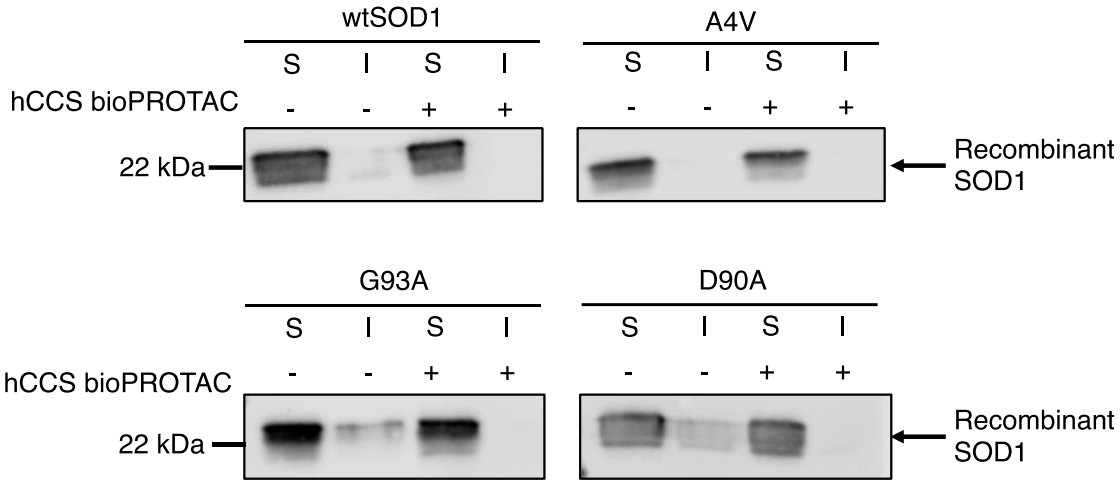

Figure 4.2.4. CHIP-CCS bioPROTAC reduces abundance of insoluble SOD1. *A reduction of insoluble SOD1 abundance with no significant change to total SOD1 abundance indicates that the CHIP-CCS bioPROTAC is likely stabilising SOD1 and is ineffective at directing SOD1 to proteasomal degradation. HEK293T cells were transfected with SOD1 variants: wildtype (A), A4V (B), G93A (C), D90A (D), and co-transfected with the CHIP-CCS bioPROTAC. Cells were incubated for 24 hours before*

centrifuging for 1 hour at 4°C to separate the PBS-soluble and insoluble fractions. Abundance of SOD1 was analysed by western blotting. S; soluble fraction. I; insoluble fraction. N=1.

4.2.5 The CHIP-CCS bioPROTAC degrades wtSOD1

This CHIP-hCCS bioPROTAC modestly reduced wildtype SOD1 abundance in HEK293T cells (**Figure 4.2.5**). Reduced degradation of wildtype SOD1 was observed when expressing the CHIP E3 ubiquitylation domain alone. A SOD1-CHIP fusion was co-expressed with wildtype SOD1 to assess if SOD1 dimerisation could facilitate targeted degradation by bringing the fused CHIP E3 into proximity with the dimer, but degradation was variable and non-significant (**Figure 4.2.5**).

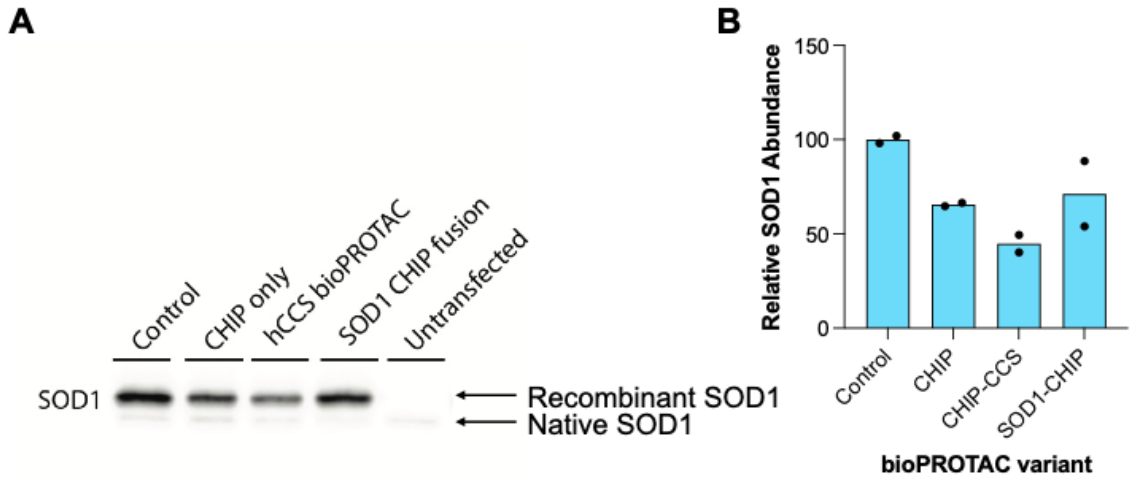

Figure 4.2.5. Wildtype SOD1 abundance is reduced following CHIP-CCS bioPROTAC expression*. SOD1 dimerisation does not facilitate targeted degradation in HEK293T cells. Cells were transfected with SOD1 and the following constructs: CHIP E3 ubiquitylation domain, hCCS bioPROTAC (CHIP E3 ubiquitylation domain and hCCS D2 fusion), and a SOD1 CHIP E3 domain fusion.* ***A****, Western blot showing*

*changes in SOD1 abundance with co-transfection of different constructs. **B**, Bar chart depicting mean relative abundance of SOD1 following co-expression with the hCCS bioPROTAC and constructs. Error bars represent standard deviation and data points are shown in black. N=2, ns.*

4.2.6 CHIP-CCS bioPROTAC reduces total abundance of SOD-ALS mutants with high replicate variability and limited efficacy

The hCCS bioPROTAC was tested against seven ALS-related SOD1 variants spanning the length of the protein. Varying degrees of degradation, largely similar to that observed for $SOD1^{WT}$, were observed (**Figure 4.2.6**). No statistically significant changes to SOD1 abundance were observed in the cases of $SOD1^{D90A}$ and $SOD1^{I113T}$. Of all ALS-related SOD1 mutations tested, $SOD1^{A4V}$ abundance decreased the most when the bioPROTAC was expressed. However, $SOD1^{A4V}$ has a shorter half-life and is quickly turned over, which may contribute to the greater change in total SOD1 abundance (Farrawell and Yerbury, 2021).

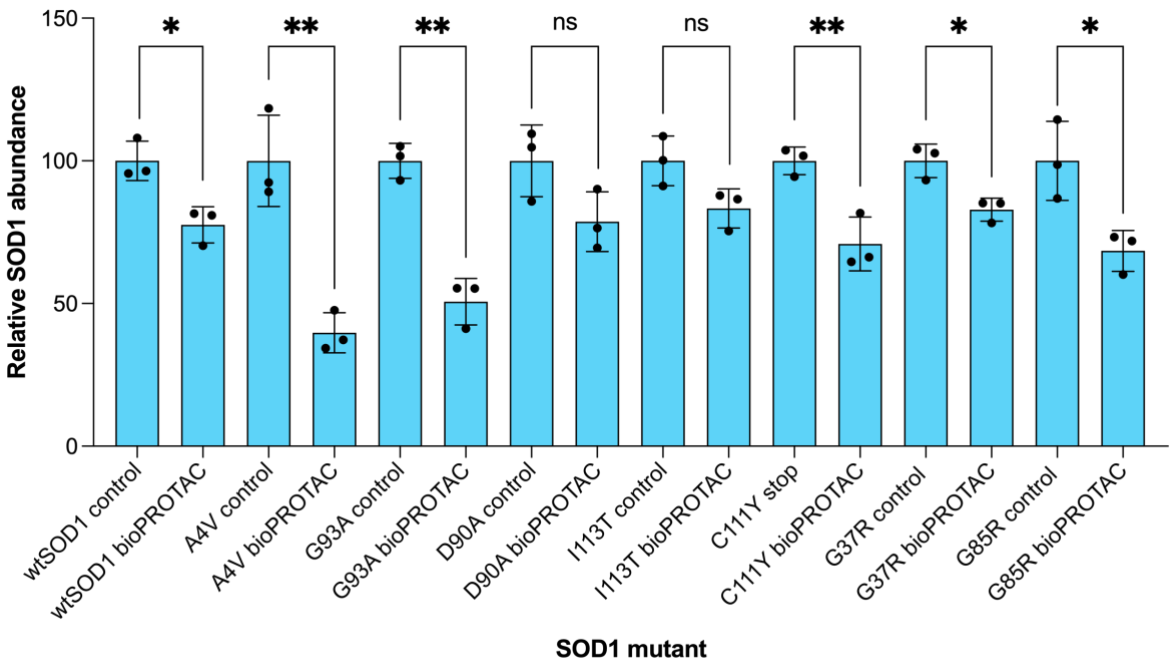

Figure 4.2.6. Wildtype and mutant SOD1 are modestly degraded by the hCCS bioPROTAC in HEK293T cells. *HEK293T cells were transfected with wildtype or mutant SOD1 (control), or a cotransfection with a SOD1 variant and the hCCS bioPROTAC was completed (bioPROTAC), and cells were incubated for 24 hours. Cells were harvested and samples prepared for SDS-PAGE and western blotting. Average change in abundance between control and test replicates is shown as percentage change with standard deviations. A paired sample t-test was conducted between the control and bioPROTAC test means of each ALS-related SOD1 mutant, N=3. * = P<0.05. ** = P<0.01. NS = nonsignificant.*

Percentage change of SOD1 abundance was highly variable. In some cases degradation was not observable, or there was a high degree of variability between both technical and biological replicates. Variable degradation of SOD1 in HEK293T cells is reported in the literature, and it is suggested variable transgene expression across HEK293T population may give rise to high variability in degradation of SOD1

(Kumar et al., 2022). To test if SOD1 overexpression in HEK293T cells was a factor in casusing inefficent SOD1 degradation, $SOD1^{A4V}$ and $SOD1^{G93A}$ degradation by the CHIP-CCS bioPROTAC was also tested in HEK293S cells, due to their high transfection efficiency yet lower protein expression due to the lack of an SV40 large T antigen (Thomas and Smart, 2005). The mean change in relative abundance of SOD1 was higher in HEK293S cells for both $SOD1^{A4V}$ and $SOD1^{G93A}$, although standard deviations were higher in both cases. $SOD1^{A4V}$ clearance was not statistically significant (**Figure 4.2.7**).

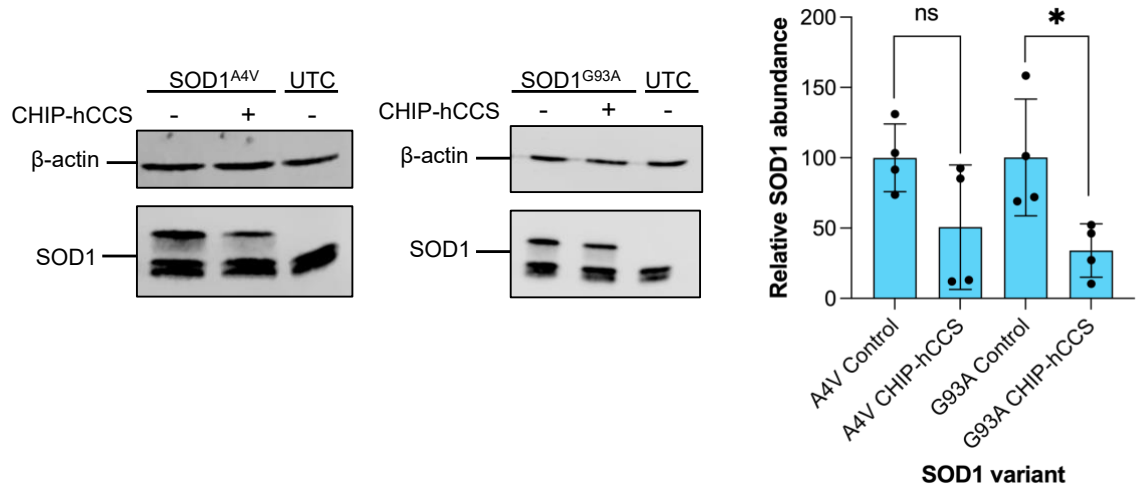

Figure 4.2.7. $SOD1^{A4V}$ and $SOD1^{G93A}$ are degraded by the hCCS bioPROTAC in HEK293S cells. *HEK293S cells were transfected with $SOD1^{A4V}$ or $SOD1^{G93A}$ and the hCCS bioPROTAC and cells were incubated for 24 hours before SDS-PAGE and western blotting as described.* ***A****, western blot showing $SOD1^{A4V}$ degradation in HEK293S cells.* ***B****, western blot showing $SOD1^{G93A}$ degradation in HEK293S cells.* ***C****, Bar chart depict mean releative abundance of $SOD1^{A4V}$ and $SOD1^{G93A}$ with and without bioPROTAC co-expression. Average change in abundance between control and test replicates is shown as percentage change with standard deviation (error bars) and replicate data points are shown (black). A paired sample t-test was conducted between the control and test means of each ALS-related SOD1 mutant shown, N=4.*

** = P<0.05. NS = nonsignificant. UTC; untransfected control. β-actin was used as an internal loading control.*

4.2.7 CHIP-hCCS bioPROTAC increases mutant SOD1 abundance in NSC34 cells

All SOD1 mutants and $SOD1^{WT}$ were also expressed with the hCCS bioPROTAC in NSC34 cells to further determine if SOD1 overexpression was causing variability in results obtained from HEK293T experimental data. Interestingly, a significant increase in SOD1 abundance was observed following CHIP-hCCS bioPROTAC in NSC34 cells (**Figure 4.2.8**). This increase was significant in all mutant SOD1 tests excluding $SOD1^{G85R}$, likely due to low $SOD1^{G85R}$ expression levels which can be expected due to metal ion deficieny and accelerated protein turnover (Cao et al., 2008).

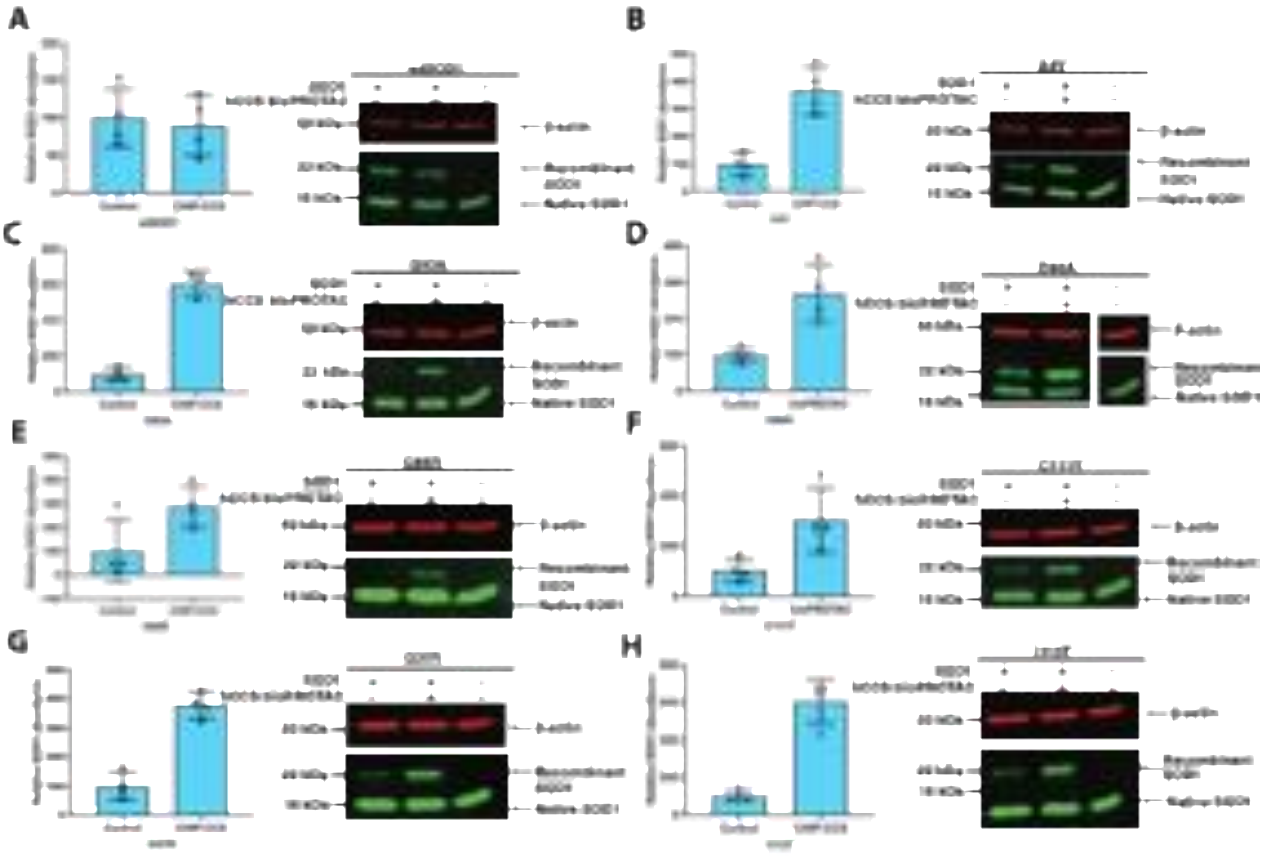

Figure 4.2.8. CHIP-hCCS bioPROTAC stabilises mutant SOD1 expression in NSC34 cells. *A, $SOD1^{WT}$. B, $SOD1^{A4V}$. C, $SOD1^{G93A}$. D, $SOD1^{D90A}$. E, $SOD1^{I113T}$. F, $SOD1^{C111Y}$.G, $SOD1^{G37R}$. H, $SOD1^{G85R}$. NSC-34 cells were transfected with SOD1 variants and the CHIP-hCCS bioPROTAC and incubated for 72 hours, before sample collection and preparation for SDS-PAGE and western blotting. Bar charts represent mean relative abundance of SOD1 following normalisation to β-actin, in which individual data points are shown, and error bars represent standard deviation. NS = non-significant. * = P<0.05, ** = P<0.01, *** = P<0.005. **** = P<0.001. Paired-sample t-test, N=4. β-actin was used as an internal loading control.*

4.3 Discussion

This work aimed to develop a targeted bioPROTAC for SOD1-amyotrophic lateral sclerosis (SOD1-ALS). To achieve this, a panel of bioPROTACs utilising the CHIP E3 ubiquitylation domain and SOD-1 targeting domains (CCS and Nb54) were designed and tested in non-neuronal and neuron-like cell models. CHIP-CCS was shown to express in soluble form and interact with its target. SOD1 misfolding was significantly reduced by the CHIP–CCS bioPROTAC, and total SOD1 abundance was decreased in some case for ALS-related SOD1 mutants, although this was highly variable across biological repeats. I found that while the CHIP-CCS bioPROTAC was able to effectively interact with mutant SOD1 and stabilise misfolded SOD1 in HEK293T and NSC34 cell models, the bioPROTAC was ineffective at degrading all ALS-related SOD1 mutants tested.

The hCCS-CHIP construct was rationally designed around two characterised interactions. hCCS acts as a molecular chaperone that directly binds both wild-type and mutant SOD1, and promotes maturation by transferring copper and catalysing intramolecular disulphide bridge formation (Casareno et al., 1998) Meanwhile CHIP is an E3 ligase known to interact with SOD1 and promote proteasomal degradation of both wild-type and mutant forms (Urushitani et al., 2004). In this context the hCCS domain II which is homologous to SOD1 is an appealing candidate for bioPROTAC design. Further, the CCS domain II is a known stabiliser of SOD1 and promotes disorder-to-order transitions through molecular chaperoning (Luchinat et al., 2017). However, it may be that these properties in fact hinder bioPROTAC efficacy. I hypothesise that the binding affinity between hCCS and SOD1 may be too strong and the bioPROTAC is not able to release SOD1 following ubiquitination machinery

recruitment, which would suggest that the cascade of multiple SOD1 ubiquitination and degradation by a single bioPROTAC molecule is slowed or halted. I tested this hypothesis by repeating the experiments in NSC34 cells due to reduced protein expression of NSC34 cells in comparison to HEK293T models, and observed increased SOD1 abundance following bioPROTAC expression. This is further evidence that the bioPROTAC is interacting and stabilising SOD1 but not effectively ubiquitinating and degrading SOD1. Investigating ubiquitination of the target through in vitro ubiquitination assays, proximity ligation assays or probing for K63-linked ubiquination using K63-targeting antibodies would provide evidence of ubiquitination status.

Efficient bioPROTAC mediated degradation may in fact rely on transient and therefore lower affinity interactions with the target. In future work, *in silico* structural prediction analysis could enable selection of point mutations that disrupt hydrogen bonding at the SOD1-hCCS domain II interface in order to weaken but not inhibit interaction between the bioPROTAC and its target. In turn, this may produce a more transient interaction between the CHIP-CCS bioPROTAC.

A further constraint of this bioPROTAC-SOD1 interaction may be poor lysine accessibility. Successful polyubiquitination requires accessible ubiquitination sites on the target protein, such as lysine residues or the primary methionine residue, and it may be that SOD1-CCS binding prevents access to these residues due to poor flexibility or steric hindrance, preventing CHIP from polyubiquitinating the target. Significant increases in SOD1 abundance in NSC34 cells indicate that the CCS-D2 domain of the bioPROTAC is effectively interacting with and stabilising SOD1,

meaning it may be a poor substrate for the proteasome due to this stabilisation. To test if SOD1 overexpression in HEK293T cells was a factor causing high variations in degradation capability and high standard deviations, SOD1 degradation by the CHIP-CCS bioPROTAC was tested in in HEK293T cells. It is suggested that variable transgene expression across HEK293T population may give rise to high variability in degradation of SOD1 (Kumar et al., 2022). While SOD1 abundance was reduced by the CHIP-CCS bioPROTAC in HEK293S cells, there was again high variability between replicates and expression of recombinant SOD1 was low.

$SOD1^{D90A}$ exhibited lower reductions in SOD1 misfolding compared to other SOD1 mutants in HEK293T cell models. This mutation displays similar biophysical properties to $SOD1^{WT}$ and produces SOD1 inclusions similar to that of misfolded $SOD1^{WT}$ (Forsberg et al., 2010). Both $SOD1^{I113T}$ misfolding and degradation was not statistically significant, and total reduction in SOD1 abundance was low. $SOD1^{I113T}$ has low disease penetrance and a similar structure to the wildtype protein, which could be why similar changes to levels of misfolded SOD1 and total SOD1 abundance are observed for $SOD1^{WT}$ and $SOD1^{I113T}$ (Hough et al., 2004).

Nb54 and Nb61 nanobodies were selected for their propensity to degrade mutant SOD1 more effectively than $SOD1^{WT}$ (Kumar et al., 2022). A CHIP-Nb54 bioPROTAC was designed and expressed in HEK293T cell although no change in $SOD1^{A4V}$ or $SOD1^{G93A}$ abundance was observed. It is also possible that the Nb54 target recognition domain could be incorporated into new bioPROTAC design with different E3 ligases to see if solubility can be improved. Nb54 and Nb61 nanobodies exhibited a selective reactivity to misfolded SOD1 in previous studies, (Kumar et al.,

2022). SOD1 misfolding experiments using this bioPROTAC are also necessary to determine if misfolded mutant SOD1 can be targeted by this bioPROTAC. Bacterial E3 ligase mimetics have also been incorporated into targeted protein degradation strategies, exhibiting highly potent target degradation with little variability compared to other human E3 ligases in the literature (Ludwicki et al., 2019). CCS-containing bioPROTACs were designed with several other human E3 ligase ubiquitylation domains and incorporating IpaH9.8 bacterial E3 ligase (Wang *et al.,* 2023), to test if there would be a greater reduction in SOD1 abundance (data not shown). No change in SOD1 abundance was observed following CHIP-IpaH9.8 expression with wildtype SOD1 in HEK293T cells. It is clear that appropriate recognition domain selection is vital for efficient E3 activation degradation. Successful SOD1-targeting bioPROTACs are being developed using the CHIP E3 ubiquitylation domain, further indicating that the recognition domains here may not be suitable for bioPROTAC construction (Chisholm et al., 2025).

SOD1-ALS is a rapidly progressive and fatal neurodegenerative disease affecting the motor neurons. Mutations in SOD1 lead to formation of toxic aggregates that contribute to neuron death, impair various cellular homeostatic processes and induce oxidative stress (Taylor et al., 2016; Wang et al., 2008). However, functional SOD1 retains a crucial role in mitigating oxidative damage by catalysing dismutation of superoxide free radicals (Corson et al., 1998). Therefore, it is favourable to develop targeted therapies that are specific to misfolded or mutant SOD1, and preserving functional SOD1 will help enable the cell to mitigate the effects of oxidative damage and neuropathology, thus slowing disease progression. Misfolded aggregates of SOD1 exhibit a prion-like nature, as toxic aggregates seed nearby cells and cause

widespread pathology, McAlary *et al.,* (2019), so the development of therapies that specifically target misfolded or aggregated SOD1 for its degradation may in turn slow or halt the progression of the disease.

Targeted protein degradation therapies such as those described here offer a potential avenue for developing effective and safer treatments for ALS that spare functional wildtype protein and slow the progression of this rapid-onset disease. Several small molecule PROTACs and bioPROTACs have been developed to target neurodegenerative disease (Cai et al., 2024). A panel of mutant SOD1-specific scFvs were developed that can be used as bioPROTAC target recognitions domain in future work. While the CHIP-CCS bioPROTAC described here was not successful at significantly reducing wildtype and mutant SOD1 abundance, insights into bioPROTAC design considerations were obtained from this investigation. From this work it can be concluded that a bioPROTAC recognition domain must be soluble, bind with moderate affinity and avoid stabilising the target protein.

Chapter V: Development of a strategy to reliably repurpose antibodies as soluble functional intrabodies

5.1 Introduction

The rapid growth of monoclonal antibody technology development has produced high-affinity binders against a range of disease-causing protein conformers (Briney et al., 2019; Carter and Rajpal, 2022). The inability of antibodies to bind intracellular toxic species including disease-related conformers has motivated efforts to reformat them into intracellular antibodies, or intrabodies, for direct therapeutic intervention. While potentially applicable as intracellular immunotherapies, a single chain variable fragment (scFv) can also be used as a bioPROTAC recognition domain, bringing E3 ligase and host degradation machinery into close proximity with mutant- or confirmation-specific forms of a target protein. Antibodies with distinct confirmation- and mutation-specific epitopes have been reformatted here as soluble scFv intrabodies that can be used in the application of intracellular targeted therapeutics. In doing so, this work contributed to the development of an implementable strategy that reliably repurposes any antibody as a functional intrabody.

To generate scFv constructs, the variable heavy (VH) and variable light (VL) chain sequences of each parent monoclonal antibody were identified through published sequences, patents, hybridoma sequencing or mass spectrometry (**Figure 5.1.1A**). Complementarity determining regions (CDRs) are retained and a flexible peptide linker is used to connect VH and VL domains without impacting the antigen binding site (**Figure 5.1.1B**). The VH and VL domain were connected by a $(G_4S)_4$ linker in unmodified scFvs (**Figure 5.1.1C; top**) and a $(G_4D)_4$ linker was used for scFvs made

with a set of standard modifications (**Figure 5.1.1C; middle**). These standard modifications refer to the addition of a N-terminal FLAG tag and modified linker with a reduce net charge (**Figure 5.1.1C; middle**). In some cases, further aspartic acid substitutions were added to decrease whole molecule net charge (**Figure 5.1.1C; bottom**).

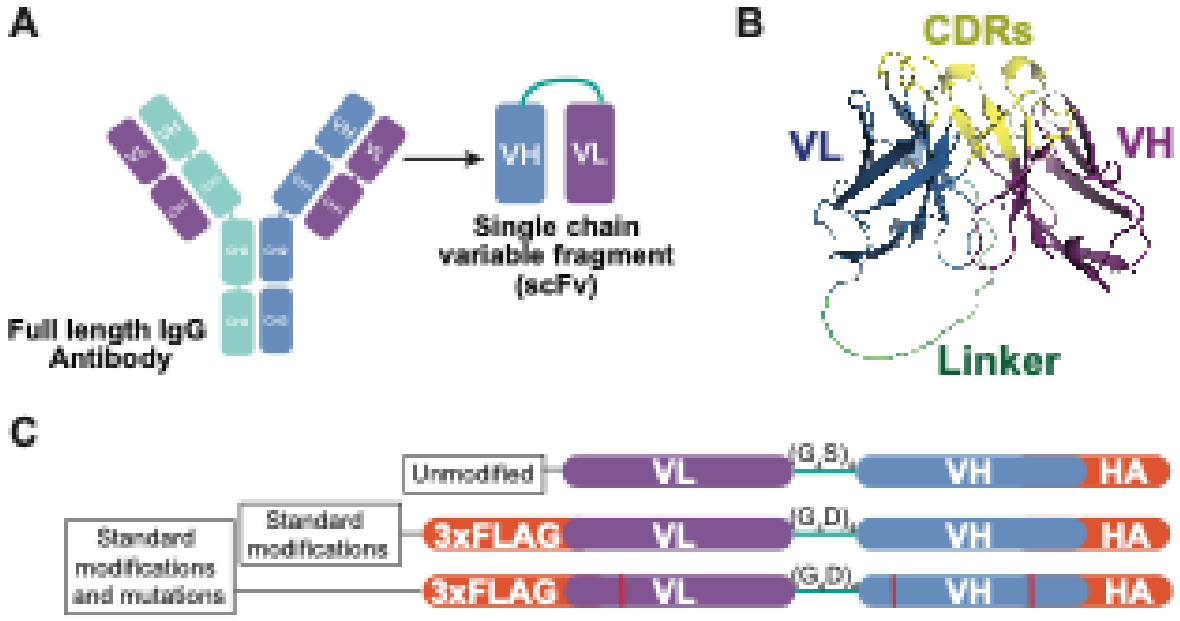

Figure 5.1.1. scFv construction and modification. ***A****, Schematic depicting scFv derivation from full length antibodies.* ***B****, Depicted is the AlphaFold predicted structure of the AMF7-63 scFv. The VH domain is shown in blue and the VL domain is shown in purple. Yellow indicates CDRs (complementarity determining regions) and the* $(G_4D)_4$ *linker is shown in green.* ***C****, Schematic further depicting scFv constructions with different sets of modifications. 'Unmodified' scFvs were constructed in VL-VH or VH-VL orientation with the commonly used* $(G_4S)_4$ *linker and a C-terminal HA tag for detection by western blot. A panel of scFvs were designed with 'standard modifications': an N-terminal 3xFLAG tag and a* $(G_4D)_4$ *linker and a C-terminal HA tag. In some cases, scFvs with standard modifications were further modified by introducing framework aspartic acid substitutions.*

Soluble α-synuclein oligomers and insoluble aggregates are implicated in neurodegenerative disease such as PD due to their neurotoxicity and prion-like properties (Masuda-Suzukake et al., 2013; van Rooijen et al., 2010). Similarly, mutant and misfolded SOD1 monomers acquire toxic properties in a gain of function manner, driving oxidative stress and motor neuron degeneration (Münch et al., 2011b; Vande Velde et al., 2008). In this chapter, a panel of confirmation-specific antibodies targeting monomeric, oligomeric and aggregate forms of α-synuclein were selected for redesign as functional intrabodies (**Table 5.1.1**). A further panel of misfolded SOD1-specific scFv intrabodies were designed with the aim of creating a selection of available intrabodies with distinct target epitopes (**Table 5.1.2**). A strategy for rational repurposing of conformation-specific antibodies into soluble, functional intrabodies has been developed and is described here. Candidate antibodies were reformatted into scFvs using a modified $(G_4D)_4$ linker, and in some cases rational mutagenesis was competed to improve solubility. Solubility was defined as the percentage of expressed scFv in the PBS soluble fraction, determined by western blotting.

Table 5.1.1. α-synuclein specific antibodies and their affinity for quaternary structures.

Antibody	Specificity	Reference
D5E	Oligomer	Emadi *et al.,* 2007
10H	Oligomer	Emadi *et al.,* 2009
Syn-O2	Oligomer>fibril	Kumar *et al.,* 2020
PRX002 (Prasinezumab)	Monomer	Games *et al.,* 2014
BIIB054 (Cinpanemab)	Fibril>oligomer>monomer	Weihofen *et al.,* 2019

Table 5.1.2. Misfolded SOD1 antibodies used in this work and their known epitopes and immunogens.

Antibody	Epitope/Target	Immunogen	Reference
a-miSOD1	Lys75-Gly81	Lys75-Gly81	Maier *et al.,* 2018
SE21	Ser102-His110	Glu100-Thre116	Bakavayev *et al.,* 2021
C4F6	Asp90-Ala93	Ala1-Gln153	Urushitani *et al.,* 2007
MS785	Leu8-Val14	Cys6-Gly16	Fujisawa *et al.,* 2012
AMF763	Not known	Asp124-Gly141	Pickles *et al.,* 2016

5.1.1Aims

Establish a strategy to reliably reformat antibodies as soluble intrabodies and in doing so develop a panel of scFv intrabodies against α-synuclein conformers and misfolded SOD1 for intracellular therapeutic application.

5.2 Results

5.2.1 scFv solubility optimisation

5.2.1.1 Solubility is not significantly impacted in disulphide knockout variants

Cysteine residues are required for disulphide bond formation in proteins such as scFvs, where intrasubunit disulphide bonds contribute towards stabilisation of the protein (Goto and Hamaguchi, 1979). To determine if disulphide bond formation is critical for intracellular scFv stability, all cysteines in the AMF7-63 VL-VH and 10H VL-VH constructs were replaced with alanines, a smaller non-polar residue that does not have the necessary sulphur atom for disulphide bond formation. No observable effect on solubility was measured between the 10H scFv and the cysteine knockout variant, meaning that the scFv is unimpacted by absence of a disulphide bond between VL and VH domains (**Figure 5.2.1A, B).** In contrast, solubility of the AMF7-63 scFv decreased by 20%, however this was not statistically significant (**Figure 5.2.1C, D**). This suggests that disulphide bond formation may be important for the structural stability of the scFv. Interestingly, the multiple banding pattern observed from the AMF7-63 VL-VH scFv is not present in the cysteine knockout variant, perhaps due to the loss of oxidation of a fifth accessory cysteine that is present in the AMF7-63 scFv sequence that does not form a disulphide bond. Due to the finding that the AMF7-63 cysteine knockout scFv was less soluble than the AMF7-63 scFv, removal of cysteines

was not pursued as a solubility optimisation tool. Cysteine knockout does not significantly improve solubility but can decrease solubility in some cases, therefore all subsequent constructs were designed with all disulphide bond-forming cysteines in place.

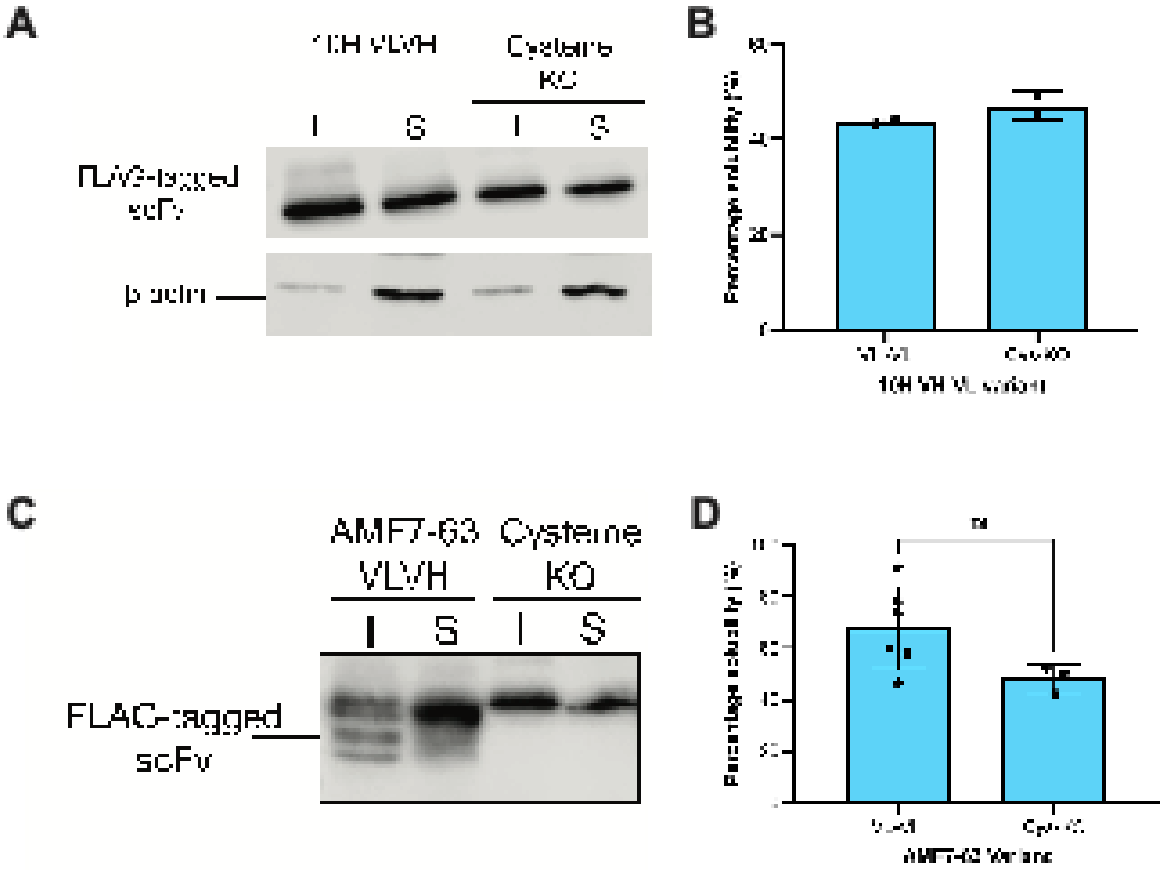

Figure 5.2.1. Cysteine knockout substitution has no significant impact on scFv solubility. ***A***, *western blot and* ***B***, *bar chart representing mean solubility values of 10H scFv variants. No observable difference between wild type 10H scFv and the cysteine knockout scFv was found.* ***C*** *western blot and* ***D,*** *bar chart representing mean solubility values of AMF7-63 scFv variants, no statistically significant reduction in solubility was observed following replacement of cysteines with alanines in the AMF7-63 scFv. scFvs described here were transfected into HEK293T cells and incubated for 24 hours. Cells were harvested and sonicated before the soluble and insoluble fractions were*

separated by centrifugation, prior to SDS-PAGE and western blotting. Bar charts represent mean solubility values of each scFv variant with standard deviation (error bars) and data points (black).

5.2.1.2 scFv variable domain orientation has an impact on solubility

scFvs can be synthesised in two orientations, denoted VH-VL and VL-VH where VH-VL represents the variable heavy domain at the N-terminus and VL-VH represents the opposite (**Figure 5.2.2**). The order in which scFv domains are translated when the scFv folds has a variable effect on biophysical characteristics, and both VL-VH and VH-VL orientations appear favourable in different cases across the literature (reviewed by Sandomenico et al., 2020).

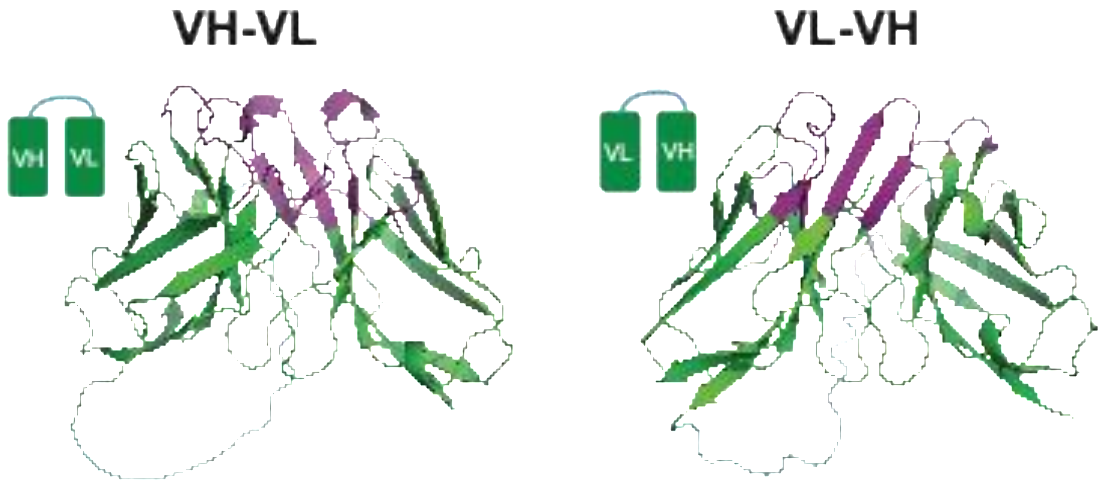

Figure 5.2.2. Predicted structures of the AMF7-63 scFv in both VH-VL and VL-VH orientation*. In the VH-VL orientation, the Variable heavy domain is at the N-terminus and resides at the C-terminus in the VL-VH orientation. AlphaFold 3 was used to generated predicted structures which were visualised in ChimeraX.*

The effect of domain orientation on solubility was examined in order to assess if there are any consistent trends for future scFv design. AMF7-63 and Syn-O2 scFvs were designed in both VH-VL and VL-VH orientations and the solubility was compared to examine effect of domain orientation on scFv solubility. In both cases, the VL-VH oriented scFv was found to be more soluble than the respective VH-VL orientation (**Figure 5.2.3A, B**). This work assessing scFv solubility and domain orientation contributed to a larger comparative analysis, which showed that VH-VL scFv intrabodies with a positively charged VH domain had an overall reduced solubility in comparison to their VL-VH counterparts (**Figure 5.2.3C**). When VH domains carried a net charge of zero or lower, VH-VL$\%_{sol}$/VLVH$\%_{sol}$ ratio was near one, indicating there was no difference between VH-VL and VL-VH solubility. In this analysis, VL-VH scFvs were found to be overall more soluble and based on these findings, scFvs were designed in VL-VH orientation in most cases. In this larger analysis, there were no cases by which VH-VL oriented scFvs were significantly more soluble than VL-VH counterparts.

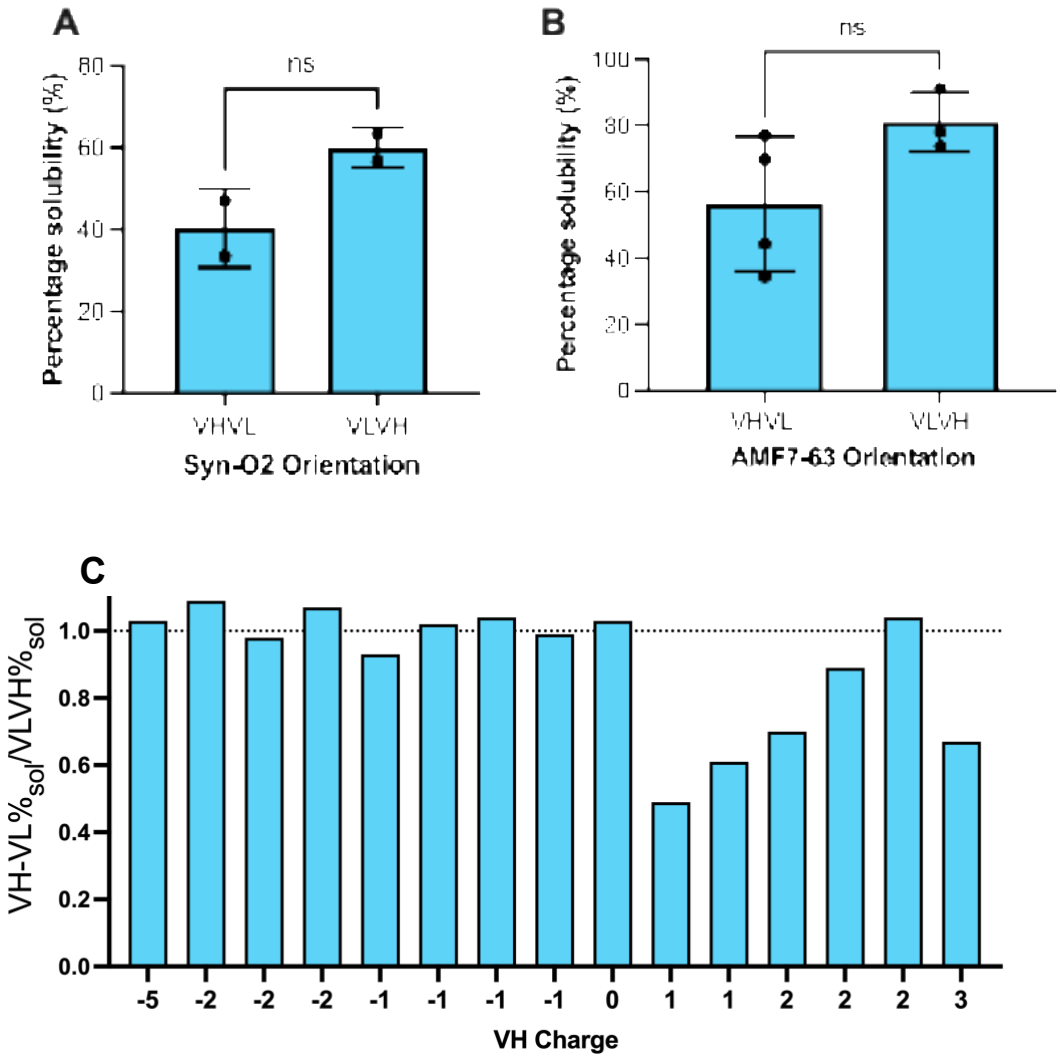

Figure 5.2.3. The VLVH scFv orientation is more soluble in select cases. *scFv orientation was tested to assess impact on solubility. The VLVH oriented AMF7-63 and Syn-O2 scFvs were more soluble than VHVL counterparts, although this was not found to be statistically significant.* ***A****, SynO2 scFv solubility (P = 0.1222, ns).* ***B****, AMF7-63 solubility (P = 0.1118, ns).* ***C****, The ratio of VH-VL:VL-VH solubility for fifteen scFv intrabodies with varying VH charge (shown on the X-axis). scFvs in either VH-VL or VL-VH orientation were designed and transfected into HEK293T cells and incubated for 24 hours. Cells were harvested and sonicated before the soluble and insoluble fractions were separated by centrifugation, prior to SDS-PAGE and western blotting.*

Bar charts represent mean solubility values of each scFv variant with standard deviation (error bars) and data points (black).

It may be that a more positively charged VH domain requires molecular chaperoning intracellularly by its respective VL domain which is not possible if the VH domain is translated first. The effect of domain orientation on scFv solubility has variable reports across the literature. While some studies report VH-VL scFvs are more soluble in bacterial expression systems, Kim et al., (2008) others report that VL-VH is more soluble in bacterial systems such as Shuffle T7 *E. coli*, which promotes disulphide bond formation (Koçer et al., 2021). Recent reports present evidence that an scFv in VL-VH orientation was more soluble in *in vivo* models, (Anraku et al., 2025). I hypothesise that when a more positively charged VH domain is translated first the scFv is less soluble, and that when the net charge of the VH and VL domains are equal scFv domain orientation has no significant effect on scFv solubility. The net charges of VH and VL domains may account for the contrasting findings in these studies.

5.2.1.3 Reducing charge through interdomain linker modification significantly improves solubility

To determine whether scFv constructs could be optimised to improve solubility through easily implementable changes, two different linker configurations were compared. Most commonly, a $(G_4S)_4$ linker is implemented due to its high flexibility, solubility and minimal steric hindrance (Huston et al., 1988). By replacing serine residues with aspartic acid, the whole molecule net charge is reduced by four without

changing the scFv framework sequence. It was hypothesised that modifying the linker peptide to reduce whole molecule net charge will improve scFv solubility.

Cinpanemab (BIIB-054) is a monoclonal antibody with a high affinity for aggregated α-synuclein, in addition to oligomeric and monomeric forms (Weihofen et al., 2019). However the SPARK trial reported no clinical benefit and cinpanemab therapeutic development was discontinued (Lang et al., 2022). This antibody could be repurposed as an intrabody for intracellular use. Of all α-synuclein targeting scFvs tested, BIIB-054 displayed the highest solubility and had the lowest whole molecule net charge. An unmodified construct was 45% soluble (± 18.5%, SD), and incorporation of an N-terminal 3xFLAG tag increased solubility to 73% (± 8.5%) (**Figure 5.2.4**). Addition of FLAG and 3xFLAG tags improve scFv solubility (Kabayama et al., 2020; Kvam et al., 2010). In the case of BIIB-054, incorporation of both the N-terminal 3xFLAG tag and a $(G_4D)_4$ linker significantly increased solubility to 93.4% (± 2.5%), ($p<0.005$, unpaired t-test) (**Figure 5.2.4**). From this finding, all scFvs described in this work were developed with the $(G_4D)_4$ linker with the aim of improving solubility without editing the scFv sequence.

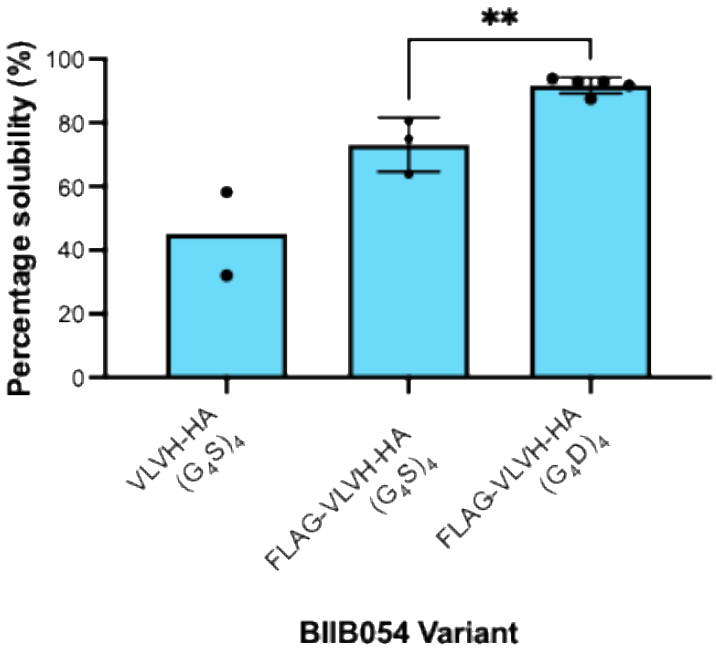

Figure 5.2.4. The incorporation of aspartic acid substitutions into the flexible linker peptide significantly improves scFv solubility. *HEK293T cells were transfected with the following BIIB054-VHVL constructs: An unmodified scFv containing a $(G_4S)_4$ linker and a C-terminal HA tag (unmodified). Second, an scFv containing the terminal FLAG and HA tags, and a $(G_4S)_4$ linker. Third, a modified scFv containing a FLAG and HA tag, along with a $(G_4D)_4$ linker (standard modifications). Cells were then incubated for 24 hours. Cells were harvested and sonicated before the soluble and insoluble fractions were separated by centrifugation, prior to SDS-PAGE and western blotting. Bar chart representing mean solubility values of each scFv variant with standard deviation (error bars) and data points (black). (** = P<0.005, unpaired t-test.)*

5.2.1.4 Reformatted scFv intrabodies can display very high thermostability

To test the thermodynamic stability of the BIIB-054 scFv, cell lysates were heated to a range of temperatures, and the solubility of the expressed scFv was analysed by SDS-PAGE and western blot. BIIB-054 scFv solubility began to decrease at approximately 60 ºC, but unexpectedly returned to its highly soluble state at 80 and 90 ºC, (**Figure 5.2.5A**). However, in the presence of dithiothreitol (DTT), solubility of the scFv again considerably decreased at 60 ºC but did not re-increase at higher temperatures (**Figure 5.2.5B**). The scFv solubility in the presence of DTT does not decrease below 36% however, indicating that even at these temperatures there is a considerable fraction of the protein that remained soluble. While the BIIB-054 scFv remains soluble, this experiment does not assess if the scFv is correctly folded, so it cannot be determined if BIIB-054 remains correctly folded in the absence of disulphide bond formation in a reducing environment. It is clear that beyond 60 ºC and in a reducing environment, solubility of the scFv decreases, but in an oxidising environment, the solubility returns back to 92% (N=1) at 90 ºC, (**Figure 5.2.5C**). Proteins are negatively charged at a buffer pH above their theoretical pI. Increased temperature reduces buffer pH, and proteins display the least solubility and are prone to self-association and aggregation when solution pH corresponds to their pI (Arakawa and Timasheff, 1985). Therefore, it is possible that where BIIB-054 solubility decreases at approximately 60 ºC, the buffer reaches a pH equal to BIIB-054 theoretical pI.

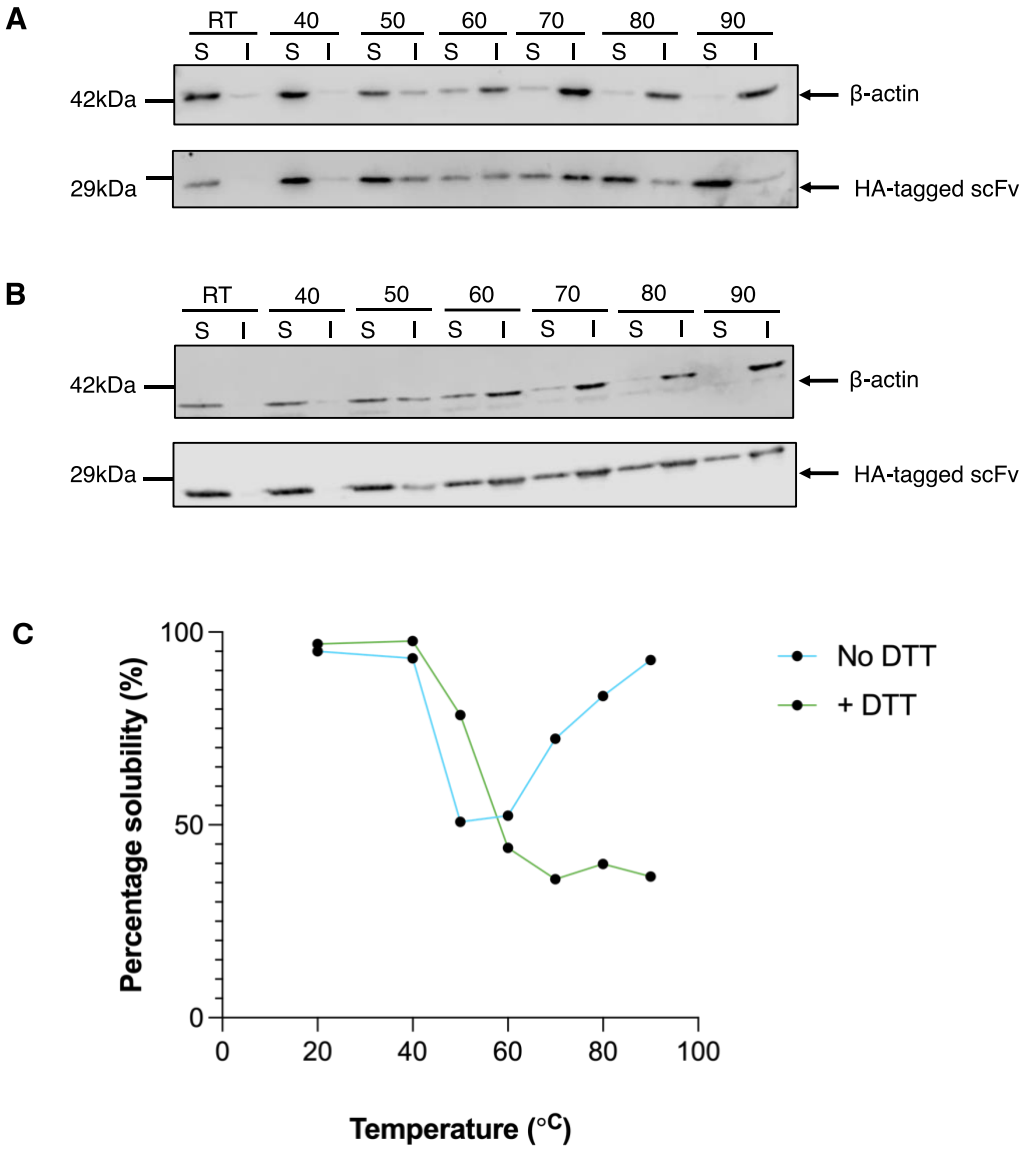

Figure 5.2.5. The BIIB-054 scFv exhibits very high thermostability. *In the presence of a reducing agent (DTT), solubility is reduced at higher temperatures.* ***A****, Western blot showing that the scFv is predominantly soluble at temperatures of 80 and 90 °C, with a reduced solubility at 50 and 60 °C.* ***B****, In the presence of 40 mM DTT, solubility of the scFv is reduced at around 50-60 °C and solubility further decreases as temperature increases.* ***C****, Line graph comparing percentage solubility of the BIIB-054 scFv with and without DTT in the lysis buffer. 10 cm dishes of HEK293T cells were transfected with the BIIB-054 scFv and incubated for 24 hours, before cell harvesting and aliquoting the total cell lysate into seven microcentrifuge tubes. Each*

tube was incubated at a different temperature (see above) and placed onto ice prior to centrifugation. Solubility of scFv was analysed by SDS-PAGE and Western Blotting. N=1.

5.2.2 AMF7-63 case study: solubility optimisation and retained specificity

5.2.2.1 Solubility of AMF7-63 can be increased by reducing whole molecule net charge using tag addition, linker modification and framework substitutions

AMF7-63 is a misfolding specific antibody with affinity for residues 125-142 found in the electrostatic loop region of human SOD1 (Pickles et al., 2016). This epitope is normally sequestered in the correctly folded wildtype SOD1 structure (Vande Velde et al., 2008). In some cases, addition of charged terminal peptide tags was insufficient to generate a highly soluble scFv. I hypothesised that whole molecule net charge remained high, and solubility could be further improved by replacing positively charged residues (lysine or arginine) with a negatively charged aspartic acid residue. Excluding a conserved salt bridge between VL domain R/K61-D82 and VH domain R/K66-D86 (denoted by Chothia numbering), most positively charged residues generally remain surface exposed when the scFv is folded. As they project into solvent and do not effect folding of the core Ig-fold interface, these solvent-exposed sites in the variable framework regions are rational areas to introduce negative charge through mutagenesis.

AMF7-63 demonstrated poor solubility and was selected for this broad scanning mutagenesis experiment. A panel of AMF7-63 scFvs each containing a different

aspartic acid substitution spanning the scFv were designed and their solubility tested (**Figure 5.2.6**). The net charge of each scFv is reduced by two, and the aim of this investigation was to identify positively charged residues that could be mutated to improve solubility. In doing so, I further tested the hypothesis that whole molecule net charge negatively correlated with scFv solubility and was a good predictive model. Interestingly in the case of AMF7-63, some mutations decrease the solubility of the scFv, though it was not statistically significant (**Figure5.2.6**). There is some likelihood that this is due to variability expected in transient expression in cell lines, and more biological replicates would be needed to better understand if there is a marked decrease for some mutations or it is due to nonsignificant variability between replicates.

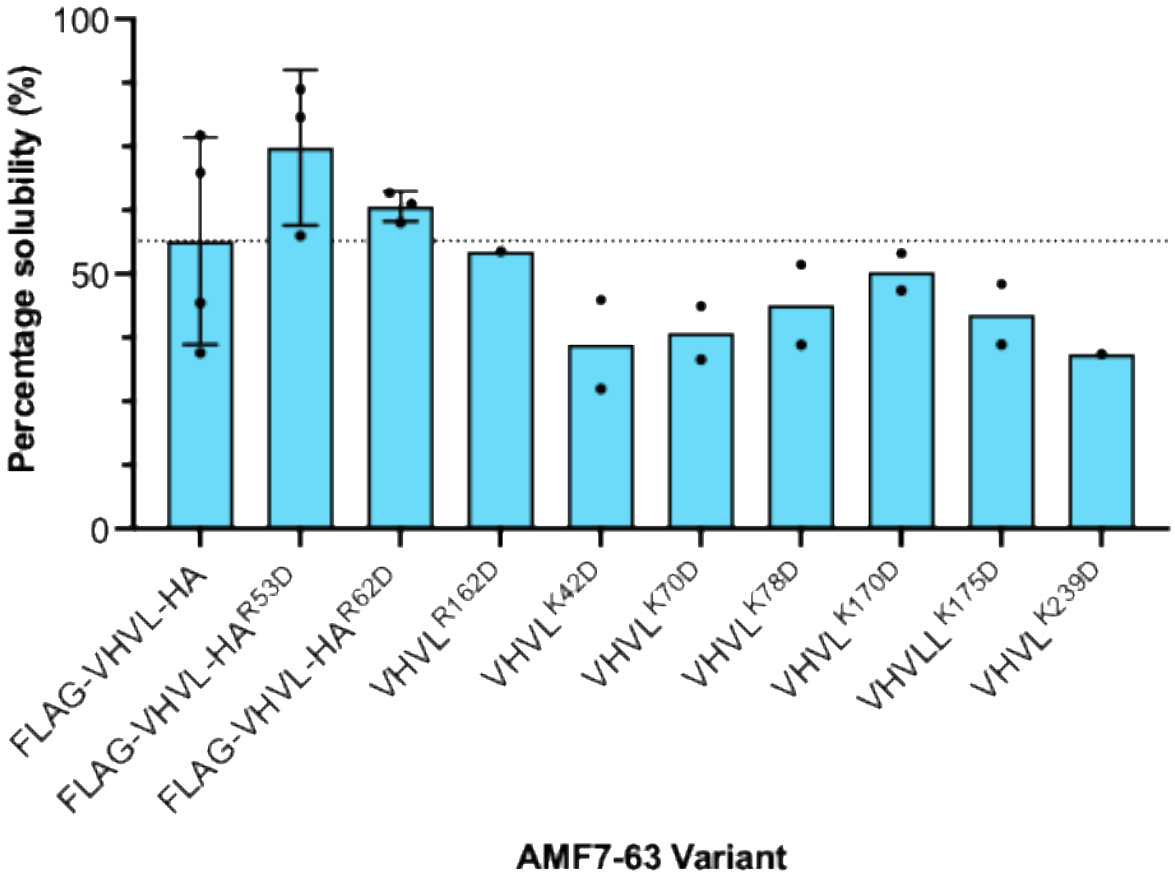

Figure 5.2.6. Replacing a positively charged residue with a negatively charged aspartic acid can have a positive effect on solubility. *Bar chart depicting the solubility of variants of the AMF7-63 scFv. Solubility was most significantly increased by mutations AMF7-63^{R53D} and AMF7-63^{R62D}. HEK293T cells were transfected with wildtype AMF7-63 variants and those containing standard modifications plus one mutation that replaces either a lysine or arginine with aspartic acid. Cells were incubated for 24 hours. Soluble and insoluble fractions were collected prior to SDS-PAGE and western blotting. Bar charts represent mean percentage solubility with standard deviation (error bars) and data points (black). A dotted line indicates the mean percentage solubility of the AMF7-63 scFv variant that contains a modified peptide linker plus N- and C-termini tags.*

Out of all tested mutations (**Figure 5.2.6**), AMF7-63^{R53D} and AMF7-63 ^{R62D} mutants were determined to have a higher mean average solubility than the standard VHVL scFv with terminal 3xFLAG and HA tags and $(G_4D)_4$ linker (**Figure 5.2.7A & B**). When AMF7-63 is reformatted as an scFv with a C-terminal HA tag and $(G_4S)_4$ linker, the scFv exhibited 6.9% (± 4.5%) solubility. The addition of an N-terminal 3xFLAG tag, and modified $(G_4D)_4$ linker increased scFv solubility to 58.4% (± 20.3%), demonstrating that scFv solubility can be significantly improved by introducing an N-terminal 3xFLAG tag and a modified linker peptide (**Figure 5.2.7A & B**). Next, I determined if the increased solubility introduced by point mutations that swap positively charged residues for a negatively charged aspartic acid had a cumulative effect. An scFv was created by site directed mutagenesis containing standard modifications, plus mutations at both the 53rd and 62nd amino acid. Introducing a second aspartic mutation further reduces theoretic isoelectric point at physiologic pH and reduces net charge (**Figure 5.2.7 C & D**)**.** Here, I found that incorporating both aspartic acid mutations at Arg53 and Arg62 increased scFv solubility to 97% (± 1.6%) resulting in a 14-fold increase in comparison to the unmodified scFv (**Figure 5.2.7B**). This aligns with the hypothesis that reducing negative net charge increases solubility of scFvs, and proves that we can achieve near 100% solubility by introducing several point mutations into the scFv along with our standard modifications to decrease whole molecule net charge. By comparing the net charge and solubility of these AMF7-63 variants, a negative correlation can be observed, supporting our findings that a lower whole molecule net charge has an inverse relationship with scFv solubility (**Figure 5.2.7D**).

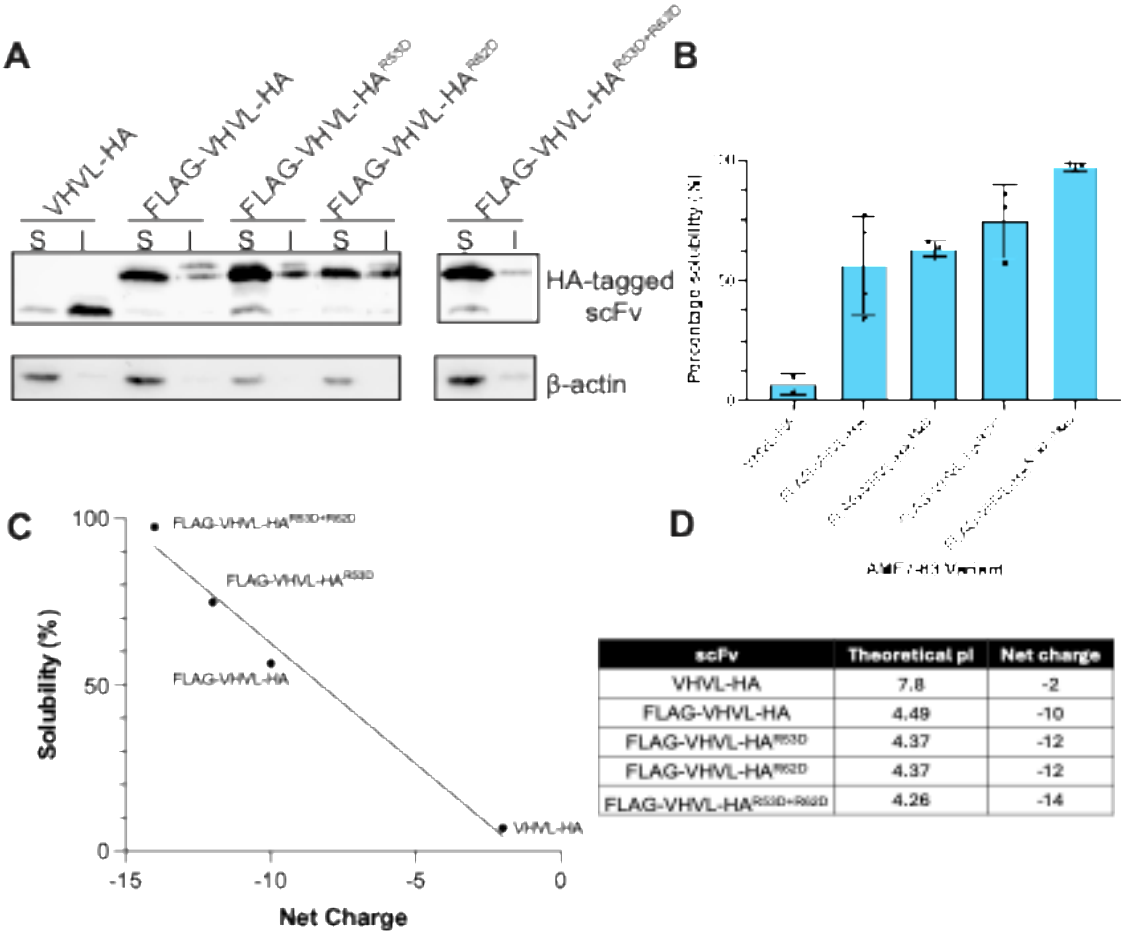

scFv	Theoretical pI	Net charge
VHVL-HA	7.8	-2
FLAG-VHVL-HA	4.49	-10
FLAG-VHVL-HA^{R53D}	4.37	-12
FLAG-VHVL-HA^{R62D}	4.37	-12
FLAG-VHVL-HA$^{R53D+R62D}$	4.26	-14

Figure 5.2.7. A more negative whole molecule net charge correlates with increased scFv solubility. A*, Western Blot showing that a greater proportion of the FLAG-tagged scFv is found in the soluble fraction when negative net charge is increased. β-actin is used as a control as it predominantly remains in the soluble fraction. Briefly, HEK293T cells were transfected with AMF7-63 scFv variants and were then incubated for 24 hours. Cells were harvested and sonicated before the soluble and insoluble fractions were separated by centrifugation, prior to SDS-PAGE and western blotting.* ***B****, Bar chart depicting mean percentage solubility of each AMF7-63 VH-VL variant with standard deviations (error bars) and replicate date points*

(black). P<0.0001, one-way ANOVA. ***C****, Line graph plotting negative net charge of modified AMF7-63 scFvs against their mean solubility in HEK293T experiments. A more negative net charge correlates with increased scFv solubility.* R^2 *= 0.9818.* ***D****, Table depicting the theoretical isoelectric point and negative net charge of each AMF7-63 scFv variant, as predicted by Expasy ProtParam.*

5.2.2.2 Whole molecule net charge is predictive of scFv solubility

The results described in this chapter herein contributed to a larger scale analysis of scFv charge and solubility, where a predictive linear regression model was established. To calculate percentage solubility, the equation below derived from the given linear regression can be used to predict scFv solubility (**Figure 5.2.8**).

$$= -(4.6237 \times net\ charge) + 8.2469$$

A negative correlation (R^2 = 0.75) over the charge range +3 to -20 was observed between whole molecule net charge and scFv solubility, obtained from testing the solubility of 45 scFv intrabodies following transient expression in HEK293T cells, including those described here. From this work, it can be concluded that a scFv should have a whole molecule net charge of -15 or lower in order to have achieve high intracellular solubility (>80%). The protocol for scFv reformatting described in this work allows for initial construct design success without the need for production and testing of a larger panel of candidate proteins based on this relationship between whole molecule net charge and solubility.

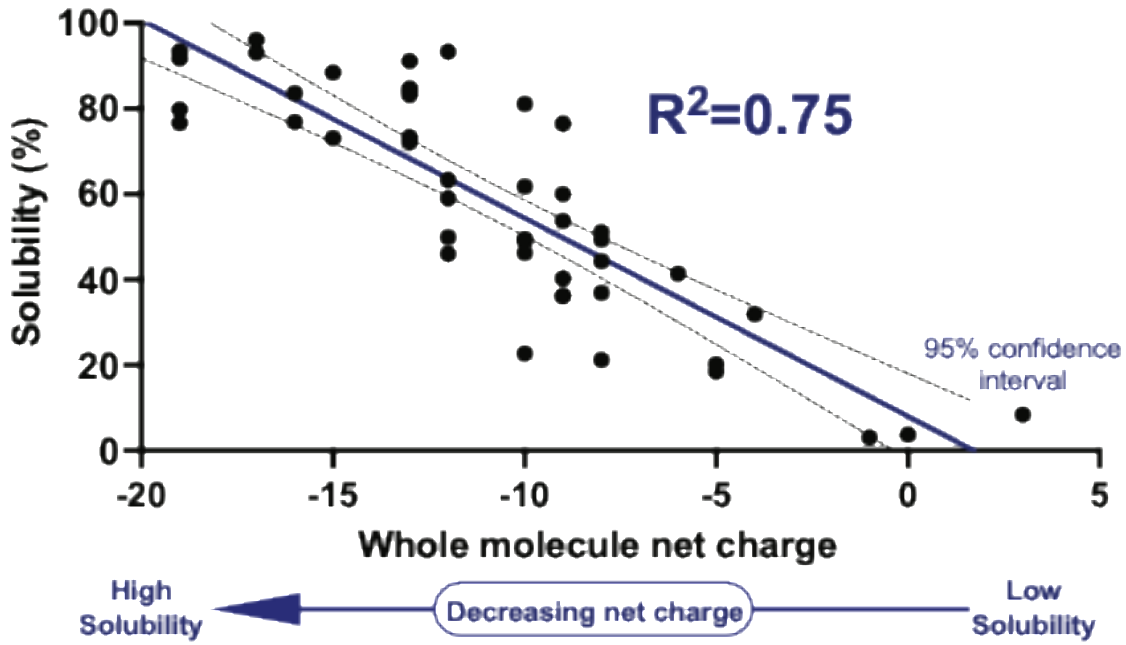

Figure 5.2.8. scFv intrabody solubility negatively correlates with whole molecule net charge. *Results from this chapter contributed to the above analysis where a negative linear correlation was identified between whole molecule net charge and solubility. Data points (black) represent mean solubility values of scFvs expressed in HEK293T cells as described (n≥2), for 45 different scFv intrabodies. Solubility of several scFvs targeting proteins implicated in neurodegenerative disease were tested by Rushba Shahzad, Kimia Aghasolemaini and Gareth Wright (O'Shea et al., 2025). Linear regression analysis is shown in blue and bands for 95 % confidence intervals are shown.*

5.2.2.3 Modified AMF7-63 scFvs retain parent mutant specificity demonstrated by co-immunoprecipitation

Next, it was essential to determine if these more soluble AMF7-63 scFv variants retained their parent antibody specificity. A HA-tag magnetic bead co-immunoprecipitation was completed to confirm interaction with AMF7-63 and ALS-mutant SOD1. Initially I tested if the AMF7-63 scFv variant with standard modifications (3xFLAG and HA tags, modified linker) retained parent antibody specificity. It was observed that the scFv immunoprecipitated with $SOD1^{A4V}$ and $SOD1^{G93A}$, but not wildtype SOD1, confirming its mutant specificity (**Figure 5.2.10A**). To confirm if AMF7-63^{R53D} and AMF7-63^{R62D} mutations affect scFv binding, a further immunoprecipitation reaction with $SOD1^{A4V}$ was completed. Both AMF7-63^{R53D} and AMF7-63^{R62D} successfully precipitated $SOD1^{A4V}$ (**Figure 5.2.9B**).

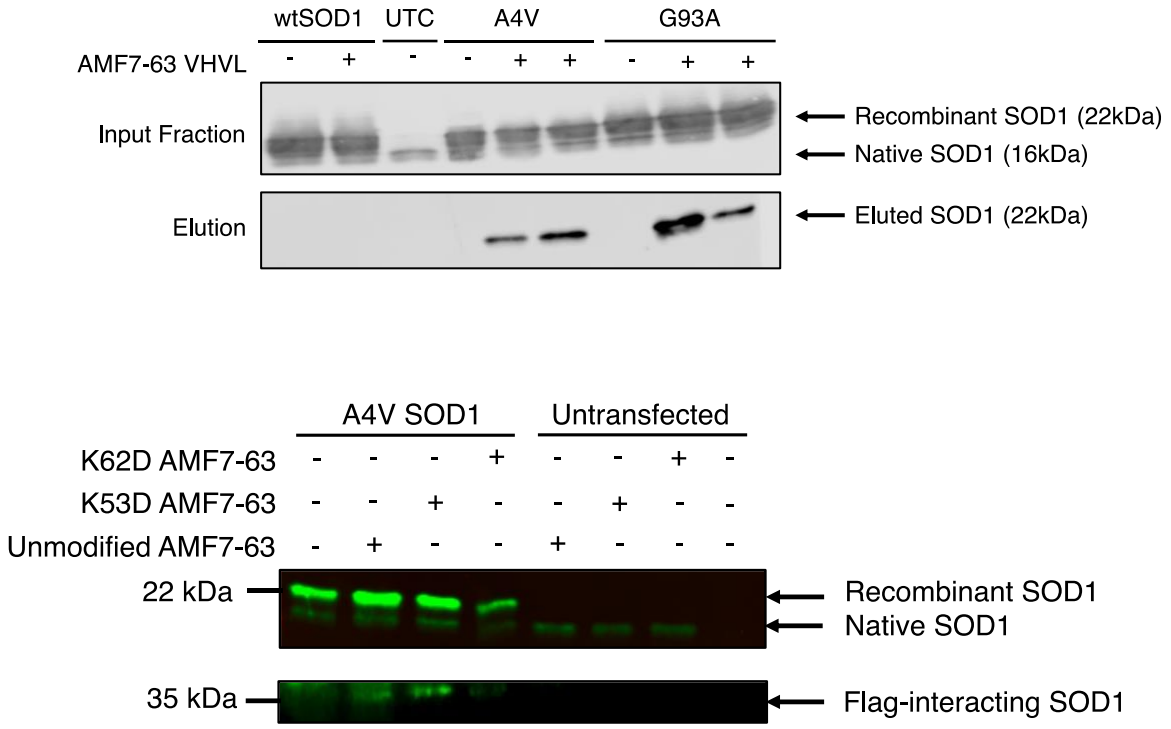

Figure 5.2.9. AMF7-63 scFv variant harbouring substitution mutations retain their parent antibody specificity for mutant SOD1. A*; SOD1^{A4V} and SOD1^{G93A} are pulled down with AMF7-63 VH-VL, while wtSOD1 does not interact with AMF7-63 VH-VL. N=3. HEK293T cells were co transfected with wildtype SOD1, SOD1^{A4V} and SOD1^{G93A}, and the VH-VL AMF7-63 scFv, or the by AMF7-63^{R53D} and AMF7-63^{R62D} variants, and were incubated for 24 hours before immunoprecipitation with magnetic beads. Input and elution fractions were analysed by SDS-PAGE and western blotting. B, SOD1^{A4V} is pulled down by AMF7-63^{R53D} and AMF7-63^{R62D}. N=1. HEK293T cells were co transfected with SOD1^{A4V} and the VH-VL AMF7-63^{R53D} and AMF7-63^{R62D} modified scFvs, and were incubated for 24 before immunoprecipitation with magnetic beads. Input and elution fractions were analysed by SDS-PAGE and western blotting. UTC; untransfected control.*

The AMF7-63$^{R53D+R62D}$ scFv co-immunoprecipitated with SOD1^{A4V} confirming that cumulative rational mutagenesis does not affect binding specificity and can be a useful tool in developing soluble scFvs (**Figure 5.2.10A**). This mutation was then also co-transfected with some less common SOD1 ALS-linked mutants, and the modified scFv was successfully eluted with SOD1^{C111Y} and SOD1^{I113T}. The modified AMF7-63 scFv did not elute with the wild type-like variant SOD1^{D90A}, further showcasing its specificity for misfolded conformations of SOD1 (**Figure 5.2.10B**).

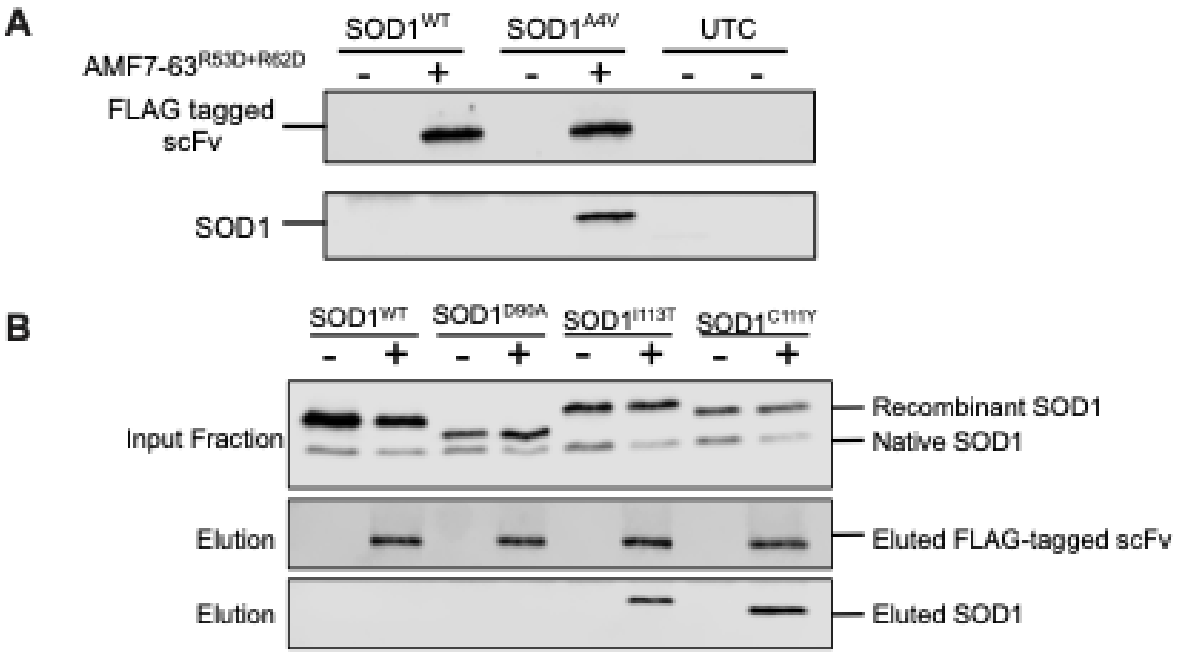

Figure 5.2.10. SOD1 ALS-linked mutants are pulled down with the modified AMF763$^{R53D+R62D}$scFv, but SOD1^{WT} and SOD1^{D90A} do not interact with the modified scFv, displaying maintained mutant-specific epitope recognition. A*, Western blots depicting elution from magnetic beads following the pull-down*

experiment. Recombinant SOD1^{A4V} is pulled down with the modified scFv and wildtype SOD1 is not eluted with the scFv. ***B****, Western blots depicting cell lysates or 'input fractions' of each experimental condition and elution from magnetic beads following the pull-down experiment. Only recombinant SOD1^{I113T} and SOD1^{C111Y} is only pulled down with the modified scFv. HEK293T cells were co transfected with wildtype SOD1, SOD1^{A4V}, SOD1^{D90A,} SOD1^{I113T}, SOD1^{C111Y}, and the VH-VL AMF763$^{R53D+R62D}$scFv, incubated for 24 hours before immunoprecipitation with HA-tag magnetic beads. Input and elution fractions were analysed by SDS-PAGE and western blotting. UTC; untransfected control.*

5.2.2.4 Thermostability of AMF7-63 is unimpacted by rational mutagenesis to framework and CDR regions

To determine whether the rational mutations added to the AMF7-63 scFv had an effect on thermostability, the scFv variants were heated to different temperatures and the abundance of soluble protein at each temperature analysed by western blotting. While AMF763$^{R53D+R62D}$ appeared more abundant (**Figure 5.2.11A**), it appears that abundance of soluble protein began to decrease at approximately 40-45 ^{o}C for all scFv variants (**Figure 5.2.11B**). It can be suggested that introduced mutations have no detrimental effect to thermal stability and are unlikely to cause scFv misfolding or lead to aggregation at physiological temperatures.

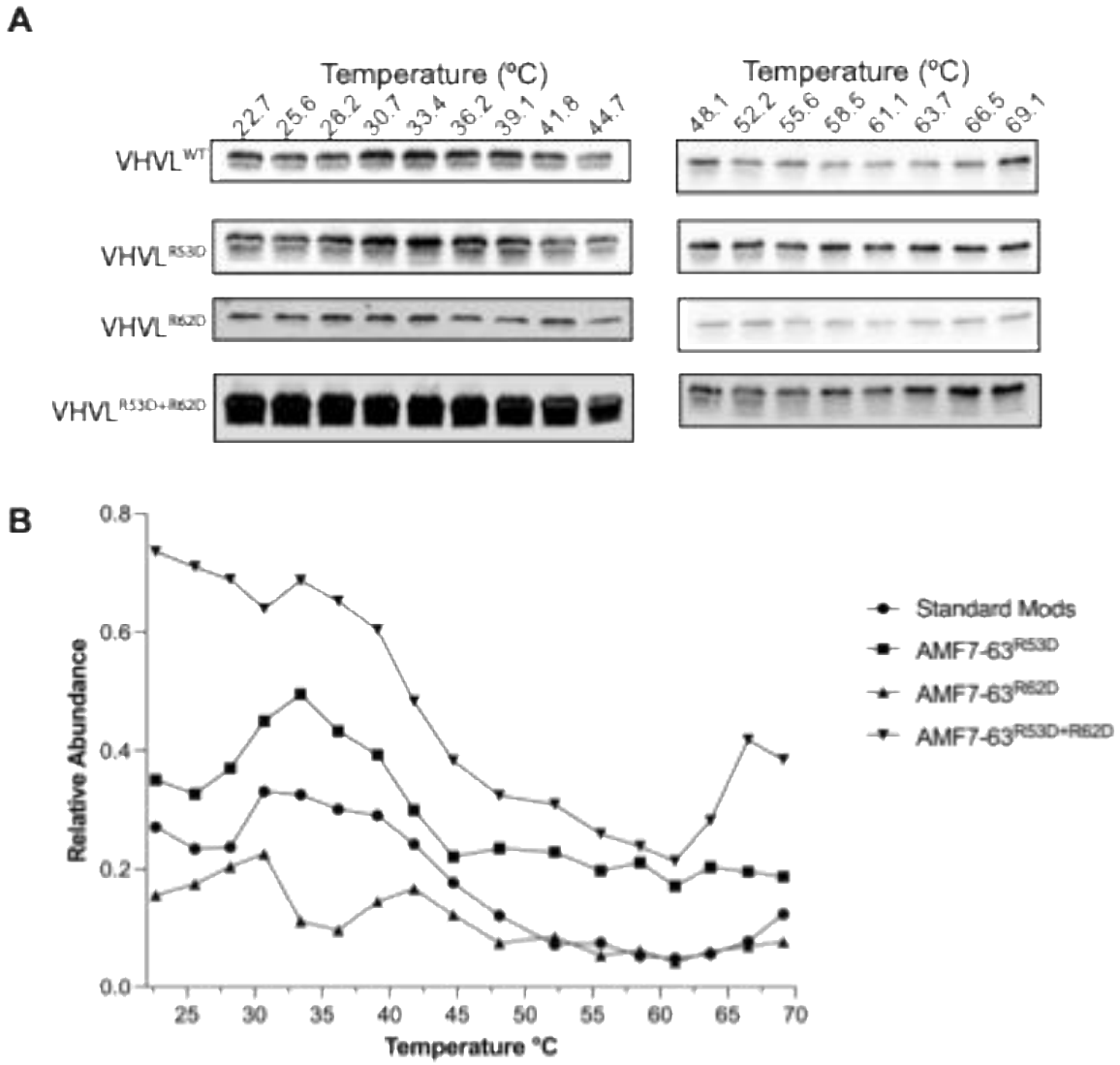

Figure 5.2.11. Thermostability of the AMF7-63 scFv is not impacted by rational mutagenesis. A*, Western blots depicting abundance of each soluble fraction the AMF7-63 scFv variants at increasing temperatures.* ***B****, Line graph depicting relative abundances of AMF7-63 scFv variants in the soluble fraction. While abundance markedly decreases at approximately 40-45 °C, relative soluble abundance remains highest for AMF7-63$^{R53D+R62D}$. HEK293T cells were transfected with the above variants and incubated for 24 hours. Cells were harvested and fractions of the cell lysate were heated at varying temperatures, from 22 to 70 °C. The soluble fractions were obtained by centrifugation and analysed by SDS-PAGE and western blotting. N=1.*

5.2.3 AI-driven inverse folding to optimise scFv solubility

5.2.3.1 AI-driven inverse folding generates abundant, soluble scFvs with improved thermostability

Inverse protein folding computational approaches can be used to predict alternate amino acid sequences that correctly fold into a 3D shape corresponding to the given protein backbone, often downstream of structural prediction methods such as AlphaFold or RFDiffusion. Deep learning models such as proteinMPNN$_{SOL}$, which was trained on a soluble protein dataset, can be used to predict alternate more soluble sequences (Dauparas et al., 2022). The success of ProteinMPNN implementation to antibodies and other proteins prompted the application of ProteinMPNN to poorly soluble scFvs described in this work. Recent work has established the use of ProteinMPNN in *de novo* antibody and protein design and development of protein nanomaterials (Alamo et al., 2025; de Haas et al., 2023; Li et al., 2024). I aimed to investigate if ProteinMPNN$_{SOL}$ could be used to further improve scFv solubility where human redesign efforts based on whole molecule net charge failed.

To ensure preservation of antigen binding specificity, residues encompassing the CDRs were restricted from alteration by proteinMPNN$_{SOL}$, according to Chothia numbering of antibody domains. The linker peptide was also restricted from proteinMPNN$_{SOL}$ alteration to ensure that charge and flexibility of the linker are retained. To further ensure antigen binding affinity and maintain structural integrity,

residues within the dimerisation interface were fixed through visual inspection of predicted structures, (**Figure 5.2.12**).

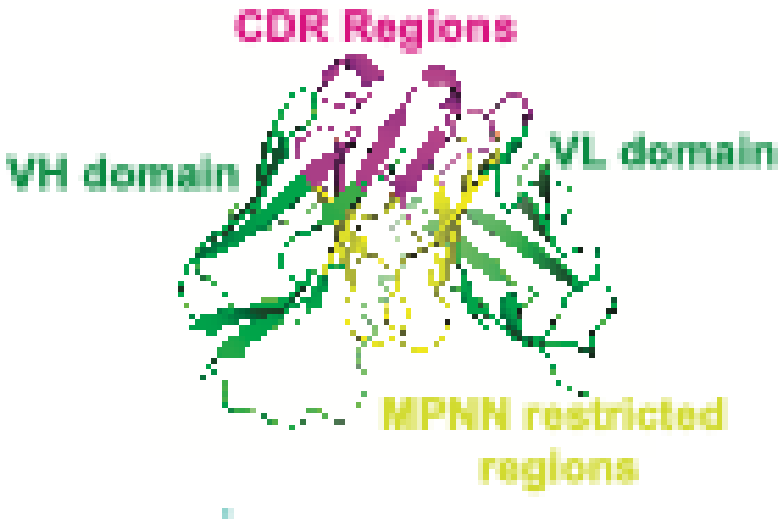

Figure 5.2.12. AlphaFold predicted structure of an scFv in VL-VH orientation, depicting regions restricted from alternative proteinMPNN prediction. *Shown in pink are complementarity determining regions. Residues comprising the dimer interface are highlighted in yellow and were restricted from proteinMPNN alteration to preserve stability of the scFv. VH and VL domains are shown in green.*

The 10H and MS785 scFvs exhibited poor solubility compared to scFv counterparts with the same or similar whole molecule net charge, indicating that solubility is perhaps hindered by other physiochemical or biophysical factors. In this work, protein $MPNN_{SOL}$ was used to generate alternative scFv sequences for 10H and MS785. Two protein MPNN models with different noise levels were used to generate scFvs sequences: $proteinMPNN_{SOL}^{002}$ and $proteinMPNN_{SOL}^{020}$ representing 0.02Å and 0.20Å model noise respectively. The 0.20Å model has a greater degree of flexibility in terms of which amino acid residues can occupy a given space on the protein backbone, whereas the 0.02Å model is more restrictive.

Upon solubility testing of proteinMPNN outputs for the MS785 scFv sequence, both proteinMPNN$_{SOL}^{002}$ and proteinMPNN$_{SOL}^{020}$ exhibited high solubility (**Figure 5.2.13A, B**). The solubility of both MS785 MPNN constructs were significantly higher than the solubility of a scFv designed using rational mutagenesis and addition of terminal tags to reduce net charge (human redesign).

Interestingly, the proteinMPNN$_{SOL}^{020}$ MS785 scFv variant demonstrated considerably increased abundance compared to the proteinMPNN$_{SOL}^{002}$ variant and other human redesigned variants (**Figure 5.2.13A**). However, this finding was not replicable for 10H, where the proteinMPNN$_{SOL}^{002}$ scFv variant displayed higher solubility than proteinMPNN$_{SOL}^{020}$ and human designed 10H scFv variants (**Figure 5.2.14**). The 10H scFv has an affinity for oligomeric α-synuclein and is reported to exhibit poor solubility (Emadi *et al.,* 2009). The 10H scFv was found to be 31.96% soluble (± 5.49%) with standard modifications before MPNN redesign, demonstrating a 2.3-fold increase in protein abundant in the soluble fraction, and a 15-fold increase in soluble protein compared to the unmodified scFv.

In the case of both 10H and MS785, the proteinMPNN$_{SOL}^{020}$ scFv variant demonstrated considerably higher thermostability than other scFv variant counterparts (**Figure 5.2.15A & B**) demonstrating the ability of proteinMPNN to generate more soluble and thermodynamically stable proteins.

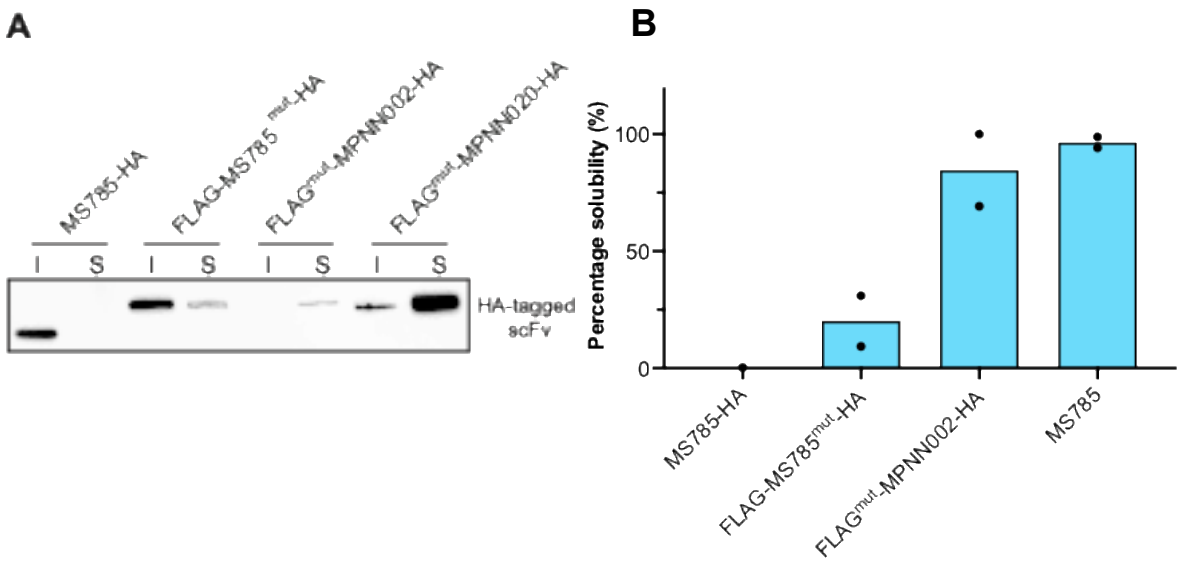

Figure 5.2.13. MS785 scFv solubility and abundance is increased following AI-led inverse folding and protein redesign. ***A****, Western blot and* ***B****, bar chart representing increased solubility of A-redesigned MS785 scFvs. The proteinMPNN$_{SOL}^{020}$ variant is considerably more abundant then the proteinMPNN$_{SOL}^{002}$ variant. HEK293T cells were transfected with an MS785 scFv variant (human or AI-led design constructs) and incubated for 24 hours. Cells were harvested and sonicated before the soluble and insoluble fractions were separated by centrifugation, prior to SDS-PAGE and Western Blotting. Bar chart represents mean solubility values of each scFv variant with standard deviation (error bars) and data points (black).*

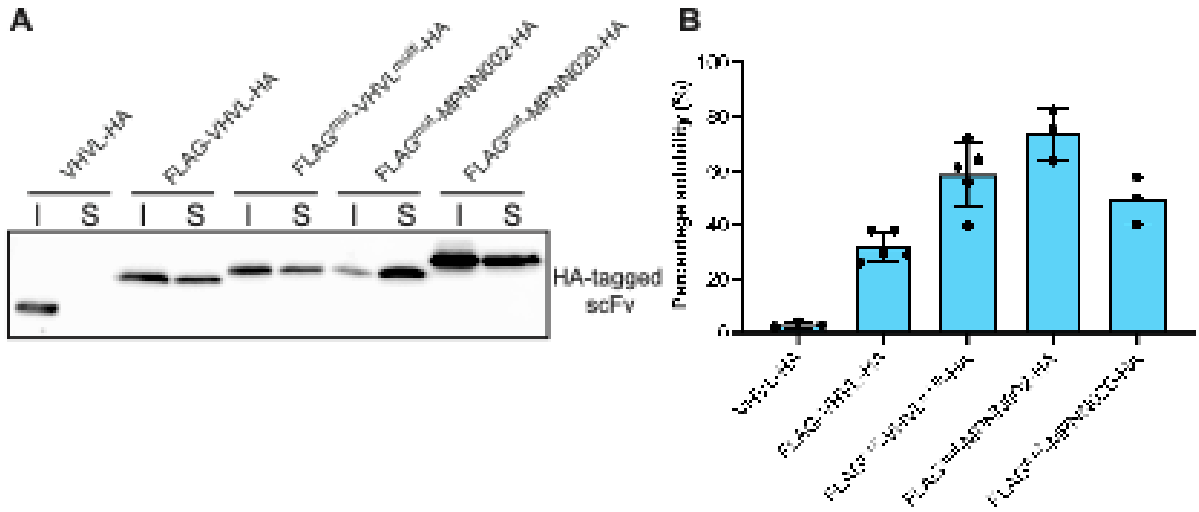

Figure 5.2.14. 10H scFv solubility is increased using a proteinMPNN$_{SOL}^{002}$-generated sequence. A, *western blot and* ***B****, bar chart representing increased solubility of AI-redesigned 10H scFvs. Interestingly, the proteinMPNN$_{SOL}^{002}$ scFv variant is most soluble. HEK293T cells were transfected with a 10H scFv variant (human or AI-led design constructs) and incubated for 24 hours. Samples were prepared for analysis by western blotting as described. Bar chart represents mean solubility values of each scFv variant with standard deviation (error bars) and data points (black).*

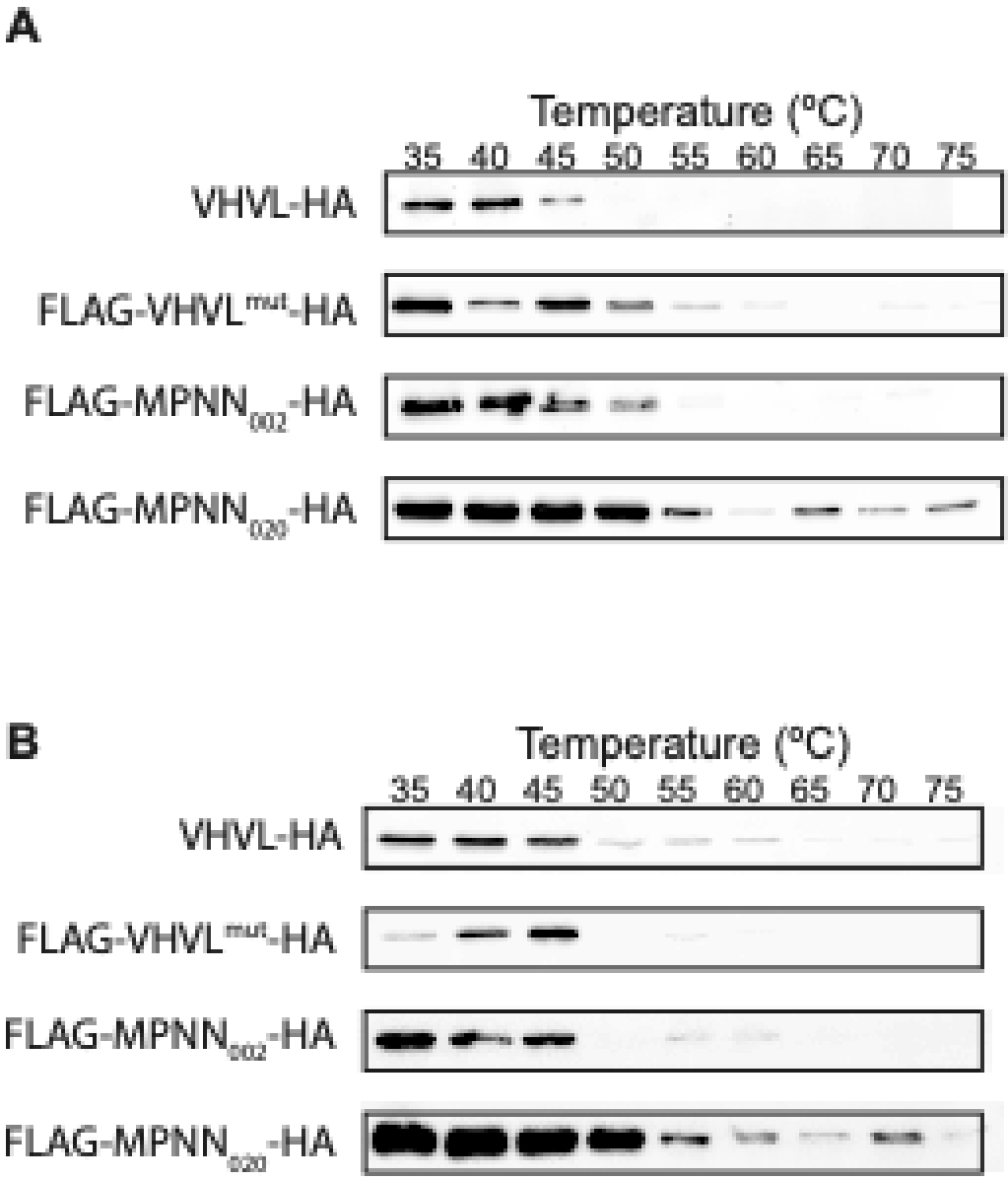

Figure 5.2.15. scFv thermal stability is increased following AI-led inverse folding and redesign. *A, western blot demonstrating increased thermostability of the AI-redesigned MS785 scFv utilising proteinMPNN$_{SOL}$ (020 model). B, Western blot demonstrating increased thermostability of the 10H AI-redesigned MS785 scFv utilising proteinMPNN$_{SOL}$ (020 model). In both cases, the scFv designed using proteinMPNN$_{SOL}$ (020 model) appears to be more abundant at physiological*

temperatures and remains soluble at higher temperatures than human redesigned scFvs. scFv human and AI-redesigned variants were transfected into HEK293T cells and incubated for 24 hours. Cell lysates were incubated to varying temperatures using a gradient heat block for five minutes before freezing at -80 ºC. The following day, the soluble fractions were obtained by centrifugation as described and abundance of scFv at each temperature was analysed by western blotting.

5.2.3.2 Parent antibody specificity is retained following AI-led redesign of scFv framework regions

MS785 scFv has a high affinity for misfolded SOD1 (Fujisawa *et al.,* 2012). The AI-redesigned variant generated using proteinMPNN$_{SOL}^{020}$ was found to be highly abundant and solubility was increased over 300-fold in comparison to the unmodified scFv. To test if the mutant specificity of the parent antibody was retained following AI-led scFv redesign, a co-immunoprecipitation reaction between SOD1^{A4V} and MS785$_{SOL}^{020}$ was completed and SOD1^{A4V} was eluted with the scFv (**Figure 5.2.16**). Additionally, a range of binding buffers with differing pH and salt concentrations were tested for the same immunoprecipitation reaction to determine optimum conditions for protein elution. Physiological pH and salt concentration was found to be optimum upon visual inspection (**Figure 5.2.16**).

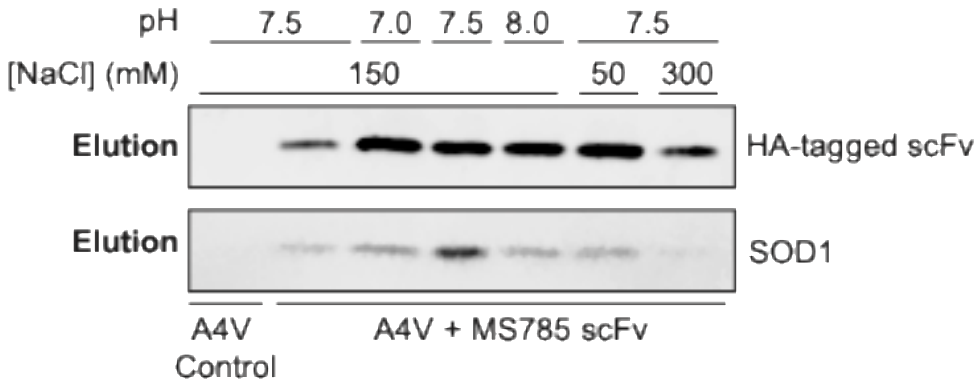

Figure 5.2.16. Immunoprecipitation of SOD1^{A4V} with MS785 is most efficient at physiological pH and salt concentrations. *Western blot depicting co-immunoprecipitation of SOD1^{A4V} by the MS785 modified scFv, redesigned by proteinMPNN$_{SOL}$ (020 model). The immunoprecipitation protocol was followed as described, but all stages requiring binding buffer were tested with a range of buffers containing the listed pH and salt concentration. Immobilised protein was eluted according to the described protocol and analysed by western blotting.*

5.2.4 Applications of soluble intracellular scFvs

5.2.4.1 A panel of soluble SOD1-targeting scFvs with distinct epitopes were developed which retain mutant specificity

Establishment of a reliable reformatting method to turn any antibody into a soluble intrabody allowed production of a panel anti-SOD1 scFvs derived from conformation specific antibodies. Each scFv contains a 3xFLAG and HA tag, a modified $(G_4D)_4$ linker and where necessary rational mutagenesis of surface exposed positively charged residues to aspartic acid to lower whole molecule net charge or

redesigned by inverse folding. Sequences are provided in **Appendix 1**. C4F6, SE21 and a-miSOD1 and the MPNN-designed MS785 scFvs demonstrated high solubility (**Figure 5.2.17A**). The SOD1 conformation-specific intrabodies described target five distinct epitopes in the SOD1 monomer (**Figure 5.2.17B**). To test if this panel of scFvs retain their specificity for misfolded SOD1 conformers, an immunoprecipitation reaction was completed with $SOD1^{WT}$, $SOD1^{A4V}$, $SOD1^{G93A}$ and $SOD1^{D90A}$. All SOD1-targeting scFvs described were eluted with $SOD1^{A4V}$ and $SOD1^{G93A}$ (**Figure 5.2.17C**). Co-immunoprecipitation for the wildtype recombinant SOD1 and the wild type like $SOD1^{D90A}$ mutant were unsuccessful, indicating the retained misfolded conformation specificity of these SOD1 scFvs (**Figure 5.2.17B**).

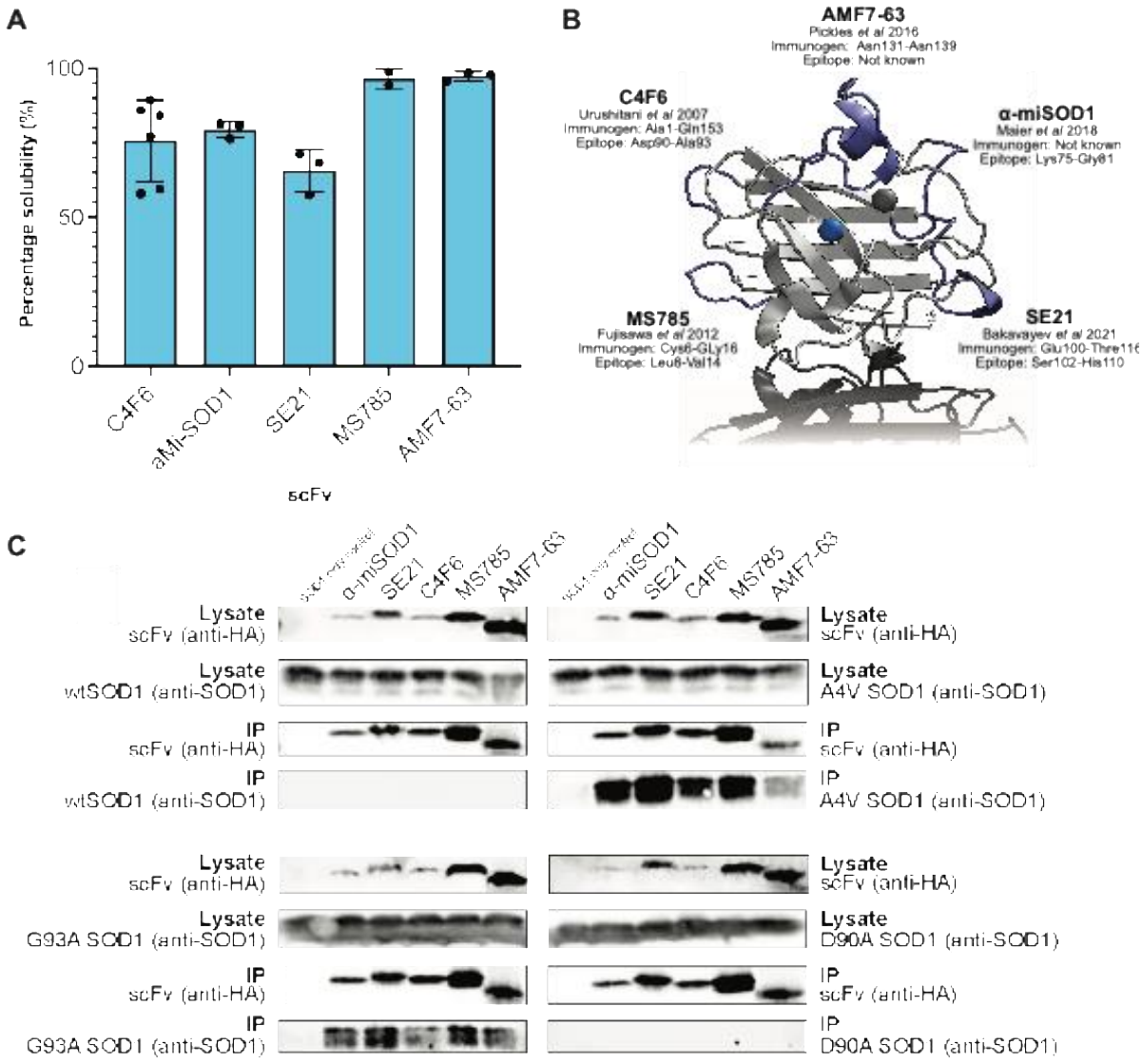

Figure 5.2.17. Reformatted state-specific scFv intrabodies retain parent antibody mutant specificity. A, *Assessment of solubility of a panel of misfolding-specific scFvs. scFvs described here were transfected into HEK293T cells and incubated for 24 hours. Cells were harvested and sonicated before the soluble and insoluble fractions were separated by centrifugation, prior to SDS-PAGE and western blotting. Bar charts represent mean solubility values of each scFv variant with standard deviation (error bars) and data points (black).* ***B****, The chosen SOD1 conformation-specific intrabodies target five distinct epitopes in the SOD1 monomer here shown on*

the fully metalated disulphide intact form and are reported to be ALS-mutant specific antibodies. ***C,*** *Assessment of mutation-specific interactions between scFv intrabodies and wildtype, A4V, G93A, and D90A SOD1. Briefly, HEK293T cells were co-transfected with an scFv variant and a SOD1 mutant and incubated for 24 hours. Cells were harvested with binding buffer and the soluble fraction incubated with HA magnetic beads for 1 hour rotating at room temperature, before magnetic beads were washed and bound protein was eluted using 4x SDS-PAGE sample loading buffer and heating to 95 °C for five minutes. Input fractions and elution fractions were then analysed by SDS-PAGE and western blotting. Immunoprecipitation was observed for the A4V and G93A SOD1 mutants, but not for wildtype recombinant SOD1 and the wildtype-like D90A variant.*

5.2.4.2 A panel of confirmation-specific α-synuclein -targeting scFvs were developed and retain parent antibody specificity

A panel of scFvs were designed targeting oligomeric and aggregated α-synuclein based on commercial and research antibodies. A negatively charged FLAG tag, HA tag, and a $(G_4D)_4$ linker were added to promote solubility, as it was predicted that solubility without these modifications would be low due to higher whole molecule net charges. Despite the addition of these tags, scFv solubility remained poor (below 70% soluble), excluding BIIB-054 VH-VL and BIIB-054 VL-VH (**Figure 5.2.18**). For most scFvs, domain orientation had no significant effect on scFv solubility. In the case of Syn-O2, the VL-VH scFv variant was 20% more soluble than VH-VL although this was deemed insignificant (p=0.1222, unpaired t-test). D5E and 10H are previously published scFvs and described to exhibit high solubility (Emadi et al., 2009, 2007).

However, in this work D5E and 10H displayed 36.9% ± 10.7% and 49.4% ± 10.7% solubility respectively, perhaps due to the use of more physiologically relevant buffers that do not contain detergents. Additionally, a 10H VLVH scFv was synthesised and tested but it was found that there was no significant effect on solubility when domain orientation was changed (**Figure 5.2.18**).

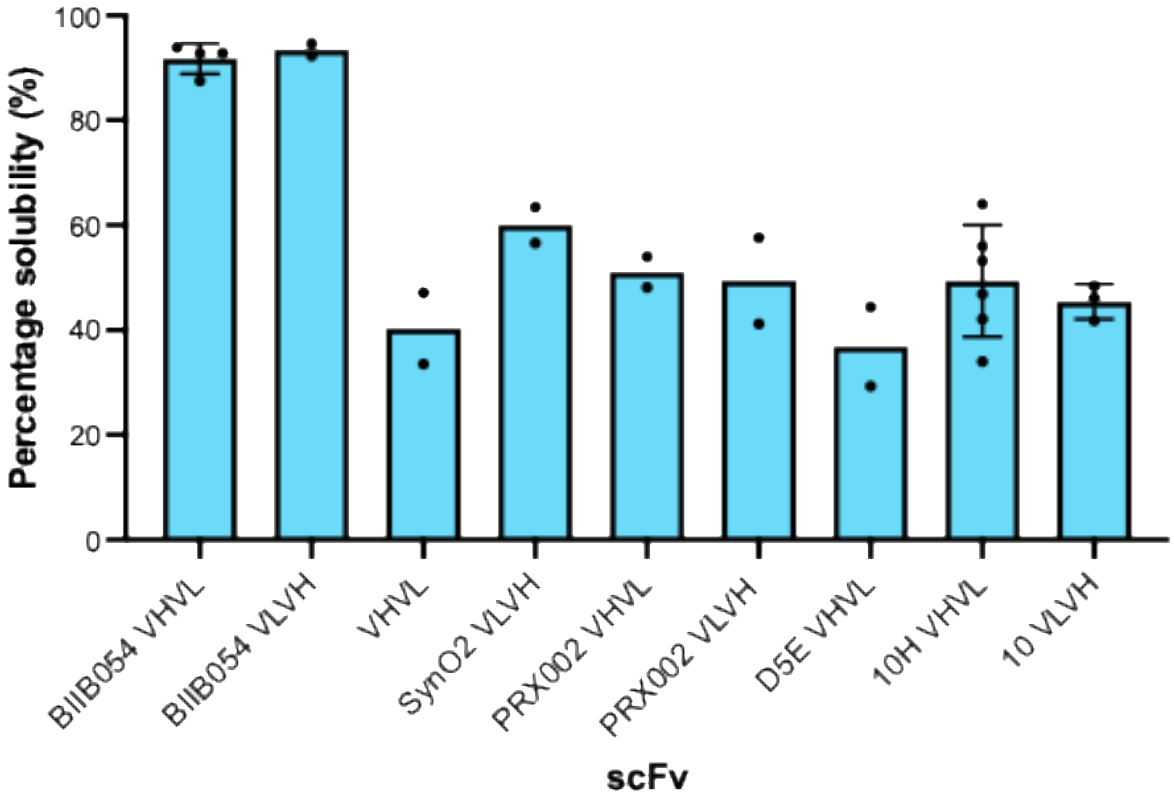

Figure 5.2.18. A panel of confirmation-specific* α-synuclein *targeting scFvs were designed and their solubility was tested*. HEK293T cells were transfected with an scFv variant and incubated for 24 hours. Each scFv variant described here contains an N-terminal 3xFLAG tag, a $(G_4D)_4$ linker, and C-terminal HA tag. Cells were harvested and sonicated before the soluble and insoluble fractions were separated by centrifugation, prior to SDS-PAGE and Western Blotting. Bar chart represents mean*

solubility values of each scFv variant with standard deviation (error bars) and data points (black).

α-Synuclein remains almost completely soluble in this cell model. Oligomeric or fibrillar states are likely absent or perhaps present at undetectable levels. Co-immunoprecipitation following co-expression of α-synuclein and scFvs revealed that PRX002 and BIIB-054 interact with transiently expressed α-synuclein (**Figure 5.2.19**). The PRX002 and BIIB-054 antibodies display some affinity for monomeric α-synuclein, which is retained when reformatted as scFvs here (Games et al., 2014; Weihofen et al., 2019). It is possible that transiently expressed α-synuclein in the HEK293T cell model employed here remains in the monomeric form, as oligomer-specific scFvs do not interact with α-synuclein in this immunoprecipitation experiment. It can therefore be deduced, that BIIB-054 and PRX002 scFvs are interacting and eluting with monomeric forms of α-synuclein, supported by the absence of interaction with α-synuclein and oligomer-targeting scFvs. Additionally, solubility of the PRX002 scFv significantly increased when expressed with α-synuclein, (**Figure 5.2.20**), which is indicative of an interaction between PRX002 and α-synuclein, stabilising the scFv and increasing solubility.

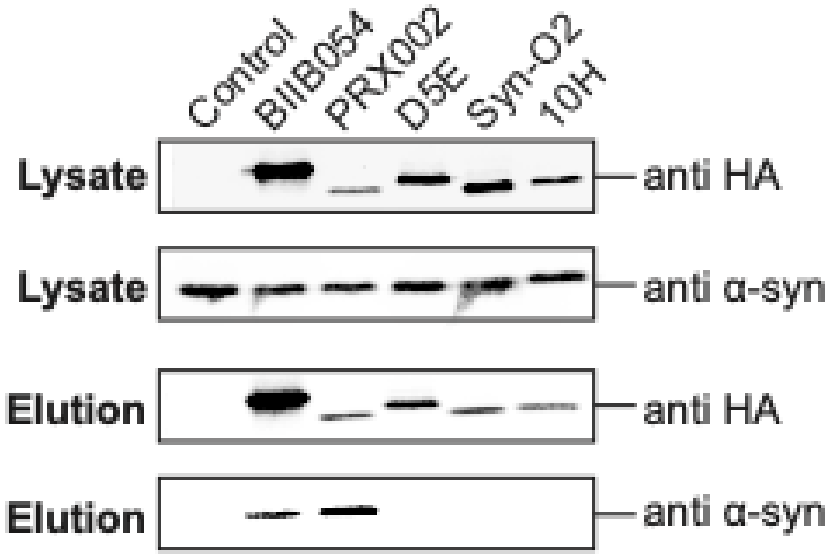

Figure 5.2.19. scFvs retain state specific recognition of conformation-specific parent antibodies. *Immunoprecipitation and western blotting for α-synuclein reveals that BIIB-054 and PRX002 bind to monomeric transiently expressed α-synuclein, while no interaction could be observed between α-synuclein and D5E, Syn-O2 and 10H, which to be specific to oligomeric and aggregated alpha synuclein states. Briefly, HEK293T cells were co-transfected with an scFv variant and α-synuclein and incubated for 24 hours. Cells were harvesting with binding buffer and the soluble fraction incubated with HA magnetic beads for 1 hour rotating at room temperature, before magnetic beads were washed and bound protein was eluted using 4x SDS-PAGE sample loading buffer and heating to 95 degrees for 5 minutes. Input fractions and elution fractions were then analysed by SDS-PAGE and Western Blotting.*

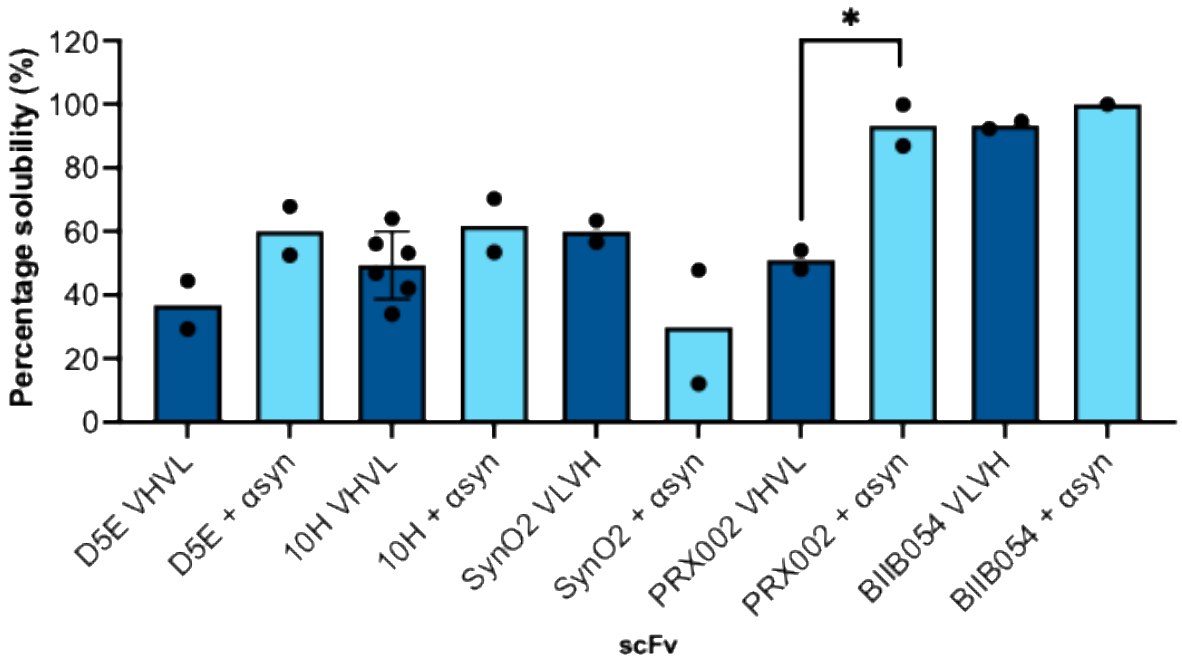

Figure 5.2.20. PRX002 solubility is significantly increased when co-expressed with transiently expressed monomeric α-synuclein. *HEK293T cells were transfected with an scFv variant and α-synuclein and incubated for 24 hours. Cells were harvested and sonicated before the soluble and insoluble fractions were separated by centrifugation, prior to SDS-PAGE and western blotting. Bar chart represents mean solubility values of each scFv variant with standard deviation (error bars) and data points (black). Navy bars represent scFv solubility alone and blue bars represent scFv solubility when expressed with α-synuclein. PRX002 solubility was significantly increased; P = 0.0270, unpaired t-test, N = 2. All other changes in scFv solubility when expressed with α-synuclein were non-significant (P>0.05.)*

The BIIB-054 scFv is derived from the aggregate-specific antibody (Weihofen et al., 2019). A fibril pull-down assay showed that soluble scFv separates into the insoluble fraction on addition of α-synuclein fibrils. This confirms specificity is retained when cinpanemab is reformatted as a scFv intrabody (**Figure 5.2.21**). β-actin is a

typically stable and soluble protein, and remained in the soluble fraction with α-synuclein pre-formed fibril incubation (**Figure 5.2.21**).

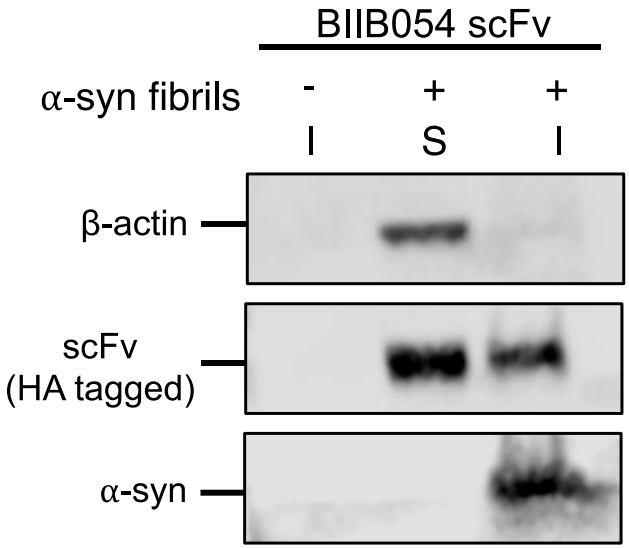

Figure 5.2.21. Assessment of oligomeric state specific interaction between pre-formed α-synuclein fibrils and the BIIB-054 scFv. *The highly soluble BIIB-054 scFv is pulled into the insoluble fraction when incubated with* α-synuclein *fibrils. Western blot probing for* α-synuclein *shows that fibrils are insoluble. β-actin is typically soluble, is not known to interact with* α-synuclein *fibrils, and is used as a control indicating that the pull-down of the scFv is specific. An increased amount of the HA-tagged scFv in the insoluble fraction indicates that the BIIB-054 is binding to the pre-formed fibrils. HEK293T cells grown in 10 cm dishes were transfected with the BIIB-054 scFv and incubated for 24 hours. The absence of detectable scFv in the insoluble fraction in the absence of pre-formed fibrils is used as an additional control to indicate that this is interaction is specific to fibrillar aggregates. The total cell lysate was aliquoted into microcentrifuge tubes, and* α-synuclein *fibrils (test) or TBS (control) were added to the tubes and incubated at room temperature with end-over-end rotating. Samples were*

centrifuged to separate soluble and insoluble fractions and analysed by SDS-PAGE and western blotting. N=2.

5.3 Discussion

The relationship between net negative surface charge and protein solubility is well documented and understood (Kramer et al., 2012). Adding fusion tags or mutations to complementarity determining regions has been shown to improve scFv solubility. The STAND approach demonstrates that adding a 3xFLAG tag to scFv sequences increases their solubility without changing framework or CDR sequence (Kabayama et al., 2020). Other work suggests that introducing negatively charged mutations to framework or CDR regions can also improve solubility (Joshi et al., 2012; Kvam et al., 2010). Aspartate scanning through CDR loops and introducing CDR mutations has been demonstrated to increase aggregation resistance (Dudgeon et al., 2012). However, this may be a less favourable approach due to the possibility of loss of epitope binding affinity. Here, I describe an easily implementable strategy to develop 'off-the-shelf' soluble scFv intrabodies. Though not significant in these findings, the VL-VH domain orientation is preferred for scFv intrabody design due to an increase in whole molecule solubility. In a larger scale analysis, VL-VH scFv intrabodies were significantly more soluble than VH-VL counterparts when the net charge of the VH domain was 0 or above. In cases where the VH domain was negatively charged, there was no significant difference between VH-VL and VL-VH scFv solubility. Then, through incorporation of a charged flexible peptide linker such as $(G_4D)_4$, a 3xFLAG at the N-terminus of the scFv and a HA tag at the C terminus, net charge can be considerably reduced and thereby solubility increased. If the net charge of an scFv protein is particularly high despite use of charged tags and interdomain linkers, the sequence

could then be redesigned by inversely folding using proteinMPNN$_{SOL}$, using the 020 model and fixing residue positions that comprise the CDR regions, domain interface and linker peptide. From the proteinMPNN$_{SOL}$ outputs, a sequence with the highest predicted solubility and highest proteinMPNN$_{SOL}$ ranking was selected for synthesis. While cumulative rational mutagenesis improves solubility, as demonstrated in the case of AMF7-63, the site-directed mutagenesis approach is time consuming and, in the cases, described here (MS785 and 10H) yields a less soluble and less abundant protein.

The AMF7-63 antibody, (Pickles *et al.,* 2016), was reformatted as an scFv in both VH-VL and VL-VH orientations. Solubility testing revealed that the scFv is more soluble in the VL-VH orientation, however it was not statistically significant. In a larger-scale analysis, VL-VH scFv intrabodies were significantly more soluble than VH-VL counterparts when the VH domain's net charge was neutral or positive, whereas no significant difference was observed when the VH domain carried a negative charge. It is clear however that scFv orientation and VH domain net charge has some marked effect on solubility and hence cytoplasmic stability. I hypothesise that is likely due to the way in which the translated protein leaves the ribosome, as it could be that when a more positively charged VH domain of an scFv comes off the ribosome before its more negatively charged VL chaperone, this may increase the likelihood of the protein to misfold and aggregate.

For proof-of-concept purposes, asparagine and lysine scanning of the VH-VL scFv was completed and aspartic acid mutations were introduced at a single site with the goal of decreasing net charge of the scFv. Introducing one point mutation had a

noticeable effect on solubility, and epitope recognition of $SOD1^{A4V}$ was maintained. To further confirm the hypothesis that decreased net charge directly correlated with improved scFv solubility, a second mutation was added to confirm if there was a cumulative effect. Solubility testing revealed that increasing a second aspartic acid mutation increased scFv solubility to near 100%. Mutant specific parent antibody epitope recognition was retained in the double mutant AMF7-63 scFv, making this a useful a bioPROTAC target recognition domain.

Recently, results from a phase II clinical trial testing cinpanemab (BIIB-054) as a disease-modifying treatment for PD showed no significant changes in clinical measures of disease progression when compared to placebo groups (Lang et al., 2022). Most recently, Biogen chose to discontinue development of cinpanemab. Another monoclonal antibody targeting aggregated α-synuclein is also being investigated for its use as a disease modifying PD therapeutic. PRX002, referred to as prasinezumab, also targets aggregated α-synuclein but has high affinity for the C-terminus and binds to both monomeric and aggregated α-synuclein (Pagano et al., 2022). Both antibodies were reformatted as scFvs and found to co-immunoprecipitate with monomeric transiently expressed α-synuclein (**Figure 5.2.19**) this demonstrates retained affinity for the α-synuclein monomers, although further study is needed to determine if the PRX002 scFv binds to fibrillar α-synuclein.

D5E, 10H, and Syn-O2 have affinities for oligomeric conformers of α-synuclein (Emadi et al., 2009, 2007; Kumar et al., 2020). Experiments where α-synuclein oligomers are generated and co expressed with these scFvs are necessary to confirm state specific recognition, although the unsuccessful immunoprecipitation of

monomeric α-synuclein with these scFvs indicates that these scFvs do not bind non-specifically to the transiently expressed monomer (**Figure 5.2.19**). Interestingly, solubility of the PRX002 scFv significantly increased when co-expressed with monomeric α-synuclein in HEK293T cell experiments, which is indicative of an interaction and hence stabilisation of the PRX002 scFv (**Figure 5.2.20**).

It is evident that some data points fall outside of the 95% confidence interval in the linear regression model displayed in **Figure 5.2.6**, suggesting that whole molecule net charge is not the only factor influencing scFv solubility. It is possible that surface hydrophilicity may impact scFv solubility in the cytoplasm. MS785 and 10H scFvs demonstrated poor solubility despite human redesign efforts such as such as addition of negatively charged linkers and terminal tags, and incorporation of several aspartic acid substitution. The 10H multi scFv was predicted to exhibit 100% solubility according to our linear regression model and exhibited 58% solubility, further reinforcing that whole molecule net charge is not the only factor influencing solubility in these cases. ProteinMPNN was used to predict alternative soluble sequences while restricting CDRs and dimer interface regions. ProteinMPNN generated scFvs that demonstrated high solubility and increased thermostability. In the case of MS785, parent antibody epitope recognition was maintained and the modified scFv co-immunoprecipitated with $SOD1^{A4V}$. ProteinMPNN has been known to increase surface hydrophilicity, (Goverde et al., 2024), so it is plausible that proteinMPNN was able to improve scFv surface hydrophilicity whilst reducing whole molecule net charge to generate an scFv more soluble than that of human redesign.

Highly soluble confirmation-specific scFvs have great therapeutic value. To advance this work towards clinical trials and move towards scFv-based therapies for treatment of neurodegenerative diseases the long-term stability and effect on cell viability must be investigated in more clinically relevant models such as patient-derived iPSCs before moving forward to *in vivo* systems. The scFv optimisation strategies described here must be validated in patient-derived iPSC neuron cultures and *in vivo*, to confirm solubility and stability in physiologically relevant systems. Importantly, pharmacokinetic studies are necessary to understand scFv half-life and clearance mechanisms before advancing with therapeutic design. The development of efficient delivery methods, such as viral vectors, lipid nanoparticles and exosomes (J. Jiang et al., 2024; Kou et al., 2011; Wong et al., 2017) must be designed and tested and the effects of long term scFv expression evaluated.

5.3.1 Conclusion

scFv intrabodies described here were derived from monoclonal antibodies or were obtained through hybridoma sequencing. While some are used in research, some have been implemented in stage II and stage III clinical trials. This work described the development of a systematic strategy to reformat any available antibody as a highly soluble and intracellularly stable scFv, based on the discovery of a strong negative correlation between net charge and scFv solubility in cell models.

Chapter VI: Conclusions

The collective origins of neurodegenerative diseases such as ALS and PD are predominantly intracellular. While some studies propose that cellular toxicity is attributed to only the aggregated form of protein, others document that this may be a protective process and that soluble precursors are the most neurotoxic form. Targeting these soluble toxic oligomers may be preferential therapeutically, preventing their aggregation. In ALS, misfolded and aggregation prone toxic SOD1 species are causative of motor neuron degeneration through mechanisms such as oxidative stress, protein aggregation and prion-like propagation (Münch et al., 2011b; Vande Velde et al., 2008). α-Synuclein undergoes a fibrillization and aggregation process that creates Lewy body inclusions in dopaminergic neurons (Vidović and Rikalovic, 2022). These aggregates drive neuronal dysfunction, however if it is not fully elucidated whether the toxic soluble oligomers or insoluble aggregates are the drivers of dopaminergic neuron degeneration and disease. Targeting intracellular toxic precursors may be a viable therapeutic strategy, preventing prion propagation or delaying aggregation.

Effective bioPROTAC design requires careful consideration of protein target along with recognition and ubiquitylation domain selection. α-synuclein has a half-life of 16-48 hours (Cuervo et al., 2004; Ho et al., 2020; Mathieson et al., 2018) while disulfide-reduced SOD1 exhibits a comparatively short half-life of six hours (Jonsson et al., 2006). α-Synuclein is efficiently degraded by the CHIP-NbSyn87 bioPROTAC while SOD1 was not degraded and in NSC34 cells increased in abundance using an identical ubiquitylation strategy. It seems target proteins with longer half-lives are

preferred candidates for bioPROTAC degradation; a concept demonstrated for small molecule PROTACs (Riching et al., 2018; Vetma et al., 2024). Longer substrate half-lives may provide more opportunity for bioPROTAC binding, ubiquitin transfer and degradation. NbSyn87 binds to α-synuclein with high affinity, comparable to that of hCCS domain II suggesting that the relationship between binding affinity and bioPROTAC efficacy may be complex (Guilliams et al., 2013). However, the most obvious difference between these cases is the impact of the recognition domain; NbSyn87 contributes to degradation while hCCS domain II stabilises its target (Luchinat et al., 2017). NbSyn87 is not known to impact α-synuclein structure while hCCS domain II acts as a molecular chaperone for SOD1 (Luchinat et al., 2017).

NbSyn87 does have a weak affinity for proteasomal subunit Rpn10, which further drives proteasome-mediated degradation of α-synuclein, and may be a contributing factor for the efficient degradation by the CHIP-NbSyn87 bioPROTAC (Gerdes et al., 2020). α-Synuclein contains several KTKGEV repeats spanning the protein, providing more readily accessible sites for ubiquitination which may increase likelihood of bioPROTAC mediated degradation (Burré et al., 2014). Substrate flexibility and target protein lysine accessibility are essential for effective ubiquitination. It may also be possible that recognition domain interactions protect key lysine residues from ubiquitination by preventing access and mitigated by high conformational freedom of the target.

Efficient bioPROTAC mediated degradation relies on transient interactions with the target rather than high binding affinity interactions that stabilise the target. These high affinity stabilising interactions may prevent the bioPROTAC from dissociating to

then bind to additional substrates and prevent successive ubiquitination. From this I conclude that a bioPROTAC recognition domain must be highly soluble, bind with moderate affinity and avoid stabilising the target protein.

Targeted protein degradation is a promising therapeutic strategy with possible applications in neurodegenerative disease. Several small molecular PROTACs and bioPROTACs have been developed to target proteins implicated in neurodegenerative diseases (Cai et al., 2024; Carton et al., 2025; Chisholm et al., 2025). In the synucleinopathies such as Parkinson's disease and dementia with Lewy Bodies (DLB), cytoplasmic accumulation of misfolded and aggregated α-synuclein is central to dopaminergic neuron dysfunction and degeneration, (Lashuel et al., 2013; Spillantini et al., 1998b). The successful targeted degradation of α-synuclein by the CHIP-NbSyn87 bioPROTAC highlights a promising therapeutic avenue for PD, utilising targeted protein clearance to restore proteostasis and potentially alleviate neurodegenerative disease pathology, with the aim of delaying cell death and ultimately disease progression. Future work investigating if degradation of the target protein is solely bioPROTAC dependent is essential to confirm efficacy. Additional positive controls such as catalytically inactive bioPROTAC mutants that inhibit E3 activity would enable determination of the mechanism of action for α-synuclein clearance. In addition, other proteasome inhibitors or E1 inhibitors that prevent UPS degradation could be used to confirm the route of bioPROTAC-mediated degradation.

Conformation specific antibodies have been used to study misfolded and mutant forms of SOD1, providing new insight into the distribution and localisation of misfolded SOD1 species (Ayers et al., 2016; Bakavayev et al., 2023; Fujisawa et al.,

2012; Maier et al., 2018; Pickles et al., 2016). Importantly, this degree of specificity allows for the differentiation between wildtype and mutant SOD1, which could allow for the development of targeted therapeutics that spare the functional wildtype SOD1. Similarly, in the context of PD, conformation-specific antibody development has furthered the understanding of α-synuclein aggregation and cellular pathology. Conformation-specific antibodies such as D5E, 10H, SynO2, PRX002 and BIIB054 described in this work selectively recognise oligomeric or fibrillar α-synuclein , allowing characterisation of α-synuclein in different disease states and also now serve as candidates for clinical trials (Emadi et al., 2009, 2007; Games et al., 2014; Kumar et al., 2020; Weihofen et al., 2019).

This work presents an approach for bringing these interactions inside the cell, by repurposing these antibodies as functional soluble intrabodies. However, this can be applied to antibody targeting any intracellular protein. Importantly, repurposing antibodies as functional intrabodies may address shortfalls where small molecule drugs are ineffective. The described relationship between whole molecule net charge and solubility is established and the research to optimise previously insoluble intrabodies extensive (Kabayama et al., 2020; Kvam et al., 2010). The work presented here systematically combines several of these strategies within a reproducible reformatting pipeline based on the establishment of a correlation between net charge and solubility in the cytoplasm. The observation that scFvs with a more neutral or positive VH domain charge were significantly more soluble in the VL–VH orientation, provides insight that scFv domain orientation should be considered in intrabody design. Further, this work provides evidence that more negatively charged linker

domains can significantly improve solubility without editing the scFv framework and can be readily implemented in scFv construction.

In future work, it is imperative to assess the capacity of scFvs to alter disease-relevant phenotypes and move beyond target engagement. This includes determining if candidate scFvs reduce protein aggregation and improve neuronal survival in more physiologically relevant disease models such as patient derived induced pluripotent stem cells (iPSCs) that better recapitulate disease pathology. Later extending this work into *in vivo* systems to further investigate scFv efficacy, safety, and delivery method in a physiological context will advance intrabodies towards clinical trials, as a potential therapy for currently untreatable neurodegenerative disorders.

References

Abhinandan, K.R., Martin, A.C.R., 2008. Analysis and improvements to Kabat and structurally correct numbering of antibody variable domains. Mol Immunol 45, 3832–3839. https://doi.org/10.1016/j.molimm.2008.05.022

Abramson, J., Adler, J., Dunger, J., Evans, R., Green, T., Pritzel, A., Ronneberger, O., Willmore, L., Ballard, A.J., Bambrick, J., Bodenstein, S.W., Evans, D.A., Hung, C.-C., O'Neill, M., Reiman, D., Tunyasuvunakool, K., Wu, Z., Žemgulytė, A., Arvaniti, E., Beattie, C., Bertolli, O., Bridgland, A., Cherepanov, A., Congreve, M., Cowen-Rivers, A.I., Cowie, A., Figurnov, M., Fuchs, F.B., Gladman, H., Jain, R., Khan, Y.A., Low, C.M.R., Perlin, K., Potapenko, A., Savy, P., Singh, S., Stecula, A., Thillaisundaram, A., Tong, C., Yakneen, S., Zhong, E.D., Zielinski, M., Žídek, A., Bapst, V., Kohli, P., Jaderberg, M., Hassabis, D., Jumper, J.M., 2024. Accurate structure prediction of biomolecular interactions with AlphaFold 3. Nature 630, 493–500. https://doi.org/10.1038/s41586-024-07487-w

Agarwal, P., Reid, D.L., Amiji, M., 2024. CNS delivery of targeted protein degraders. Journal of Controlled Release 372, 661–673. https://doi.org/10.1016/j.jconrel.2024.06.057

Alamo, D. del, Frick, R., Truan, D., Karpiak, J., 2025. Adapting ProteinMPNN for antibody design without retraining. https://doi.org/10.1101/2025.05.09.653228

Andrews, J.A., Jackson, C.E., Heiman-Patterson, T.D., Bettica, P., Brooks, B.R., Pioro, E.P., 2020. Real-world evidence of riluzole effectiveness in treating amyotrophic lateral sclerosis. Amyotroph Lateral Scler Frontotemporal Degener 21, 509–518. https://doi.org/10.1080/21678421.2020.1771734

Anraku, Y., Kita, S., Onodera, T., Sato, A., Tadokoro, T., Ito, S., Adachi, Y., Kotaki, R., Suzuki, Tateki, Sasaki, J., Shiwa-Sudo, N., Iwata-Yoshikawa, N., Nagata, N., Kobayashi, S., Kazuki, Y., Oshimura, M., Nomura, T., Sasaki, M., Orba, Y., Suzuki, Tadaki, Sawa, H., Hashiguchi, T., Fukuhara, H., Takahashi, Y., Maenaka, K., 2025. Structural and virological identification of neutralizing antibody footprint provides insights into therapeutic antibody design against SARS-CoV-2 variants. Commun Biol 8, 483. https://doi.org/10.1038/s42003-025-07827-0

Arima, K., Mizutani, T., Alim, M.A., Tonozuka-Uehara, H., Izumiyama, Y., Hirai, S., Uéda, K., 2000. NACP/alpha-synuclein and tau constitute two distinctive subsets of filaments in the same neuronal inclusions in brains from a family of parkinsonism and dementia with Lewy bodies: double-immunolabeling fluorescence and electron microscopic studies. Acta Neuropathol 100, 115–121. https://doi.org/10.1007/s004010050002

Armstrong, M.J., Okun, M.S., 2020. Diagnosis and Treatment of Parkinson Disease: A Review. JAMA 323, 548–560. https://doi.org/10.1001/jama.2019.22360

Arslan, M., Karadag, M., Onal, E., Gelinci, E., Cakan-Akdogan, G., Kalyoncu, S., 2022. Effect of non-repetitive linker on in vitro and in vivo properties of an anti-VEGF scFv. Sci Rep 12, 5449. https://doi.org/10.1038/s41598-022-09324-4

Auf der Maur, A., Tissot, K., Barberis, A., 2004. Antigen-independent selection of intracellular stable antibody frameworks. Methods, Intrabodies 34, 215–224. https://doi.org/10.1016/j.ymeth.2004.04.004

Ayers, J.I., Fromholt, S.E., O'Neal, V.M., Diamond, J.H., Borchelt, D.R., 2016. Prion-like propagation of mutant SOD1 misfolding and motor neuron disease spread

along neuroanatomical pathways. Acta Neuropathol 131, 103–114. https://doi.org/10.1007/s00401-015-1514-0

Ayers, J.I., Lee, J., Monteiro, O., Woerman, A.L., Lazar, A.A., Condello, C., Paras, N.A., Prusiner, S.B., 2022. Different α-synuclein prion strains cause dementia with Lewy bodies and multiple system atrophy. Proceedings of the National Academy of Sciences 119, e2113489119. https://doi.org/10.1073/pnas.2113489119

Ayers, J.I., McMahon, B., Gill, S., Lelie, H.L., Fromholt, S., Brown, H., Valentine, J.S., Whitelegge, J.P., Borchelt, D.R., 2017. Relationship between mutant SOD1 maturation and inclusion formation in cell models. J Neurochem 140, 140–150. https://doi.org/10.1111/jnc.13864

Bach, H., Mazor, Y., Shaky, S., Shoham-Lev, A., Berdichevsky, Y., Gutnick, D.L., Benhar, I., 2001. Escherichia coli maltose-binding protein as a molecular chaperone for recombinant intracellular cytoplasmic single-chain antibodies. J Mol Biol 312, 79–93. https://doi.org/10.1006/jmbi.2001.4914

Bakavayev, S., Stavsky, A., Argueti-Ostrovsky, S., Yehezkel, G., Fridmann-Sirkis, Y., Barak, Z., Gitler, D., Israelson, A., Engel, S., 2023. Blocking an epitope of misfolded SOD1 ameliorates disease phenotype in a model of amyotrophic lateral sclerosis. Brain 146, 4594–4607. https://doi.org/10.1093/brain/awad222

Ballinger, C.A., Connell, P., Wu, Y., Hu, Z., Thompson, L.J., Yin, L.-Y., Patterson, C., 1999. Identification of CHIP, a Novel Tetratricopeptide Repeat-Containing Protein That Interacts with Heat Shock Proteins and Negatively Regulates Chaperone Functions. Mol Cell Biol 19, 4535–4545. https://doi.org/10.1128/mcb.19.6.4535

Baneyx, F., Mujacic, M., 2004. Recombinant protein folding and misfolding in Escherichia coli. Nat Biotechnol 22, 1399–1408. https://doi.org/10.1038/nbt1029

Banik, S.M., Pedram, K., Wisnovsky, S., Ahn, G., Riley, N.M., Bertozzi, C.R., 2020. Lysosome-targeting chimaeras for degradation of extracellular proteins. Nature 584, 291–297. https://doi.org/10.1038/s41586-020-2545-9

Bendor, J.T., Logan, T.P., Edwards, R.H., 2013. The Function of α-Synuclein. Neuron 79, 1044–1066. https://doi.org/10.1016/j.neuron.2013.09.004

Bensimon, G., Lacomblez, L., Meininger, V., 1994. A controlled trial of riluzole in amyotrophic lateral sclerosis. ALS/Riluzole Study Group. N Engl J Med 330, 585–591. https://doi.org/10.1056/NEJM199403033300901

Bery, N., Miller, A., Rabbitts, T., 2020. A potent KRAS macromolecule degrader specifically targeting tumours with mutant KRAS. Nat Commun 11, 3233. https://doi.org/10.1038/s41467-020-17022-w

Biocca, S., Ruberti, F., Tafani, M., Pierandrel-Amaldi, P., Cattaneo, A., 1995. Redox State of Single Chain Fv Fragments Targeted to the Endoplasmic Reticulum, Cytosol and Mitochondria. Nat Biotechnol 13, 1110–1115. https://doi.org/10.1038/nbt1095-1110

Bird, R.E., Hardman, K.D., Jacobson, J.W., Johnson, S., Kaufman, B.M., Lee, S.M., Lee, T., Pope, S.H., Riordan, G.S., Whitlow, M., 1988. Single-chain antigen-binding proteins. Science 242, 423–426. https://doi.org/10.1126/science.3140379

Blokhuis, A.M., Groen, E.J.N., Koppers, M., van den Berg, L.H., Pasterkamp, R.J., 2013. Protein aggregation in amyotrophic lateral sclerosis. Acta Neuropathol 125, 777–794. https://doi.org/10.1007/s00401-013-1125-6

Bondeson, D.P., Mares, A., Smith, I.E.D., Ko, E., Campos, S., Miah, A.H., Mulholland, K.E., Routly, N., Buckley, D.L., Gustafson, J.L., Zinn, N., Grandi, P., Shimamura, S., Bergamini, G., Faelth-Savitski, M., Bantscheff, M., Cox, C., Gordon, D.A., Willard, R.R., Flanagan, J.J., Casillas, L.N., Votta, B.J., den Besten, W., Famm, K., Kruidenier, L., Carter, P.S., Harling, J.D., Churcher, I., Crews, C.M., 2015. Catalytic in vivo protein knockdown by small-molecule PROTACs. Nat Chem Biol 11, 611–617. https://doi.org/10.1038/nchembio.1858

Boucher, L.E., Prinslow, E.G., Feldkamp, M., Yi, F., Nanjunda, R., Wu, S.-J., Liu, T., Lacy, E.R., Jacobs, S., Kozlyuk, N., Del Rosario, B., Wu, B., Aquino, P., Davidson, R.C., Heyne, S., Mazzanti, N., Testa, J., Diem, M.D., Gorre, E., Mahan, A., Nanda, H., Gunawardena, H.P., Gervais, A., Armstrong, A.A., Teplyakov, A., Huang, C., Zwolak, A., Chowdhury, P., Cheung, W.C., Luo, J., 2023. “Stapling” scFv for multispecific biotherapeutics of superior properties. MAbs 15, 2195517. https://doi.org/10.1080/19420862.2023.2195517

Boylan, K., 2015. Familial Amyotrophic Lateral Sclerosis. Neurol Clin 33, 807–830. https://doi.org/10.1016/j.ncl.2015.07.001

Braun, A.R., Liao, E.E., Horvath, M., Kalra, P., Acosta, K., Young, M.C., Kochen, N.N., Lo, C.H., Brown, R., Evans, M.D., Pomerantz, W.C.K., Rhoades, E., Luk, K., Cornea, R.L., Thomas, D.D., Sachs, J.N., 2021. Potent inhibitors of toxic alpha-synuclein identified via cellular time-resolved FRET biosensors. npj Parkinsons Dis. 7, 52. https://doi.org/10.1038/s41531-021-00195-6

Briney, B., Inderbitzin, A., Joyce, C., Burton, D.R., 2019. Commonality despite exceptional diversity in the baseline human antibody repertoire. Nature 566, 393–397. https://doi.org/10.1038/s41586-019-0879-y

Brinkmann, U., Reiter, Y., Jung, S.H., Lee, B., Pastan, I., 1993. A recombinant immunotoxin containing a disulfide-stabilized Fv fragment. Proc Natl Acad Sci U S A 90, 7538–7542. https://doi.org/10.1073/pnas.90.16.7538

Bruijn, L.I., Houseweart, M.K., Kato, S., Anderson, K.L., Anderson, S.D., Ohama, E., Reaume, A.G., Scott, R.W., Cleveland, D.W., 1998. Aggregation and motor neuron toxicity of an ALS-linked SOD1 mutant independent from wild-type SOD1. Science 281, 1851–1854. https://doi.org/10.1126/science.281.5384.1851

Brys, M., Fanning, L., Hung, S., Ellenbogen, A., Penner, N., Yang, M., Welch, M., Koenig, E., David, E., Fox, T., Makh, S., Aldred, J., Goodman, I., Pepinsky, B., Liu, Y., Graham, D., Weihofen, A., Cedarbaum, J.M., 2019. Randomized phase I clinical trial of anti–α-synuclein antibody BIIB054. Mov Disord 34, 1154–1163. https://doi.org/10.1002/mds.27738

Buckley, D.L., Crews, C.M., 2014. Small-Molecule Control of Intracellular Protein Levels through Modulation of the Ubiquitin Proteasome System. Angewandte Chemie International Edition 53, 2312–2330. https://doi.org/10.1002/anie.201307761

Buckley, D.L., Van Molle, I., Gareiss, P.C., Tae, H.S., Michel, J., Noblin, D.J., Jorgensen, W.L., Ciulli, A., Crews, C.M., 2012. Targeting the von Hippel–Lindau E3 Ubiquitin Ligase Using Small Molecules To Disrupt the VHL/HIF-1α Interaction. J. Am. Chem. Soc. 134, 4465–4468. https://doi.org/10.1021/ja209924v

Burré, J., Sharma, M., Südhof, T.C., 2014. α-Synuclein assembles into higher-order multimers upon membrane binding to promote SNARE complex formation.

Proc Natl Acad Sci U S A 111, E4274-4283. https://doi.org/10.1073/pnas.1416598111

Burré, J., Sharma, M., Tsetsenis, T., Buchman, V., Etherton, M.R., Südhof, T.C., 2010. Alpha-synuclein promotes SNARE-complex assembly in vivo and in vitro. Science 329, 1663–1667. https://doi.org/10.1126/science.1195227

Butler, D.C., Joshi, S.N., Genst, E.D., Baghel, A.S., Dobson, C.M., Messer, A., 2016a. Bifunctional Anti-Non-Amyloid Component α-Synuclein Nanobodies Are Protective In Situ. PLOS ONE 11, e0165964. https://doi.org/10.1371/journal.pone.0165964

Butler, D.C., Joshi, S.N., Genst, E.D., Baghel, A.S., Dobson, C.M., Messer, A., 2016b. Bifunctional Anti-Non-Amyloid Component α-Synuclein Nanobodies Are Protective In Situ. PLoS One 11, e0165964. https://doi.org/10.1371/journal.pone.0165964

Butler, D.C., Messer, A., 2011. Bifunctional Anti-Huntingtin Proteasome-Directed Intrabodies Mediate Efficient Degradation of Mutant Huntingtin Exon 1 Protein Fragments. PLoS One 6, e29199. https://doi.org/10.1371/journal.pone.0029199

Cacace, A.M., Chandler, J., Flanagan, J. j., Berlin, M., Cadelina, G., Pizzano, J., Bookbinder, M., Crews, C. m., Crew, A. p., Taylor, I., Houston, J., 2019. O5-04-05: A New Therapeutic Strategy for Tauopathies: Discovery of Highly Potent Brain Penetrant Protactm Degrader Molecules That Target Pathologic Tau Protein Species. Alzheimer's & Dementia 15, P1624–P1624. https://doi.org/10.1016/j.jalz.2019.06.4856

Caggiu, E., Arru, G., Hosseini, S., Niegowska, M., Sechi, G., Zarbo, I.R., Sechi, L.A., 2019. Inflammation, Infectious Triggers, and Parkinson's Disease. Front. Neurol. 10. https://doi.org/10.3389/fneur.2019.00122

Cai, Z., Yang, Z., Li, H., Fang, Y., 2024. Research progress of PROTACs for neurodegenerative diseases therapy. Bioorganic Chemistry 147, 107386. https://doi.org/10.1016/j.bioorg.2024.107386

Cao, X., Antonyuk, S.V., Seetharaman, S.V., Whitson, L.J., Taylor, A.B., Holloway, S.P., Strange, R.W., Doucette, P.A., Valentine, J.S., Tiwari, A., Hayward, L.J., Padua, S., Cohlberg, J.A., Hasnain, S.S., Hart, P.J., 2008. Structures of the G85R Variant of SOD1 in Familial Amyotrophic Lateral Sclerosis. J Biol Chem 283, 16169–16177. https://doi.org/10.1074/jbc.M801522200

Cardinale, A., Filesi, I., Biocca, S., 2001. Aggresome formation by anti-Ras intracellular scFv fragments. European Journal of Biochemistry 268, 268–277. https://doi.org/10.1046/j.1432-1033.2001.01876.x

Carlson, J.R., 1988. A new means of inducibly inactivating a cellular protein. Mol Cell Biol 8, 2638–2646. https://doi.org/10.1128/mcb.8.6.2638-2646.1988

Carter, P.J., Rajpal, A., 2022. Designing antibodies as therapeutics. Cell 185, 2789–2805. https://doi.org/10.1016/j.cell.2022.05.029

Carton, B., Gelders, G., Sathe, G., Kocaturk, N.M., Roth, S., Macartney, T.J., Elsen, J.V., Muynck, L.D., Buist, A., Moechars, D., Sapkota, G.P., 2025. Targeted degradation of α-synuclein prevents PFF-induced aggregation. https://doi.org/10.1101/2025.04.15.648905

Casareno, R.L., Waggoner, D., Gitlin, J.D., 1998. The copper chaperone CCS directly interacts with copper/zinc superoxide dismutase. J Biol Chem 273, 23625–23628. https://doi.org/10.1074/jbc.273.37.23625

Cashman, N.R., Durham, H.D., Blusztajn, J.K., Oda, K., Tabira, T., Shaw, I.T., Dahrouge, S., Antel, J.P., 1992. Neuroblastoma × spinal cord (NSC) hybrid cell lines resemble developing motor neurons. Developmental Dynamics 194, 209–221. https://doi.org/10.1002/aja.1001940306

Chan, P., Lovrić, J., Warwicker, J., 2006. Subcellular pH and predicted pH-dependent features of proteins. PROTEOMICS 6, 3494–3501. https://doi.org/10.1002/pmic.200500534

Chao, G., Lau, W.L., Hackel, B.J., Sazinsky, S.L., Lippow, S.M., Wittrup, K.D., 2006. Isolating and engineering human antibodies using yeast surface display. Nat Protoc 1, 755–768. https://doi.org/10.1038/nprot.2006.94

Chatterjee, D., Bhatt, M., Butler, D., De Genst, E., Dobson, C.M., Messer, A., Kordower, J.H., 2018. Proteasome-targeted nanobodies alleviate pathology and functional decline in an α-synuclein-based Parkinson's disease model. npj Parkinson's Disease 4, 25. https://doi.org/10.1038/s41531-018-0062-4

Chen, X., Zaro, J.L., Shen, W.-C., 2013. Fusion protein linkers: property, design and functionality. Adv Drug Deliv Rev 65, 1357–1369. https://doi.org/10.1016/j.addr.2012.09.039

Chen, Y.-J., Wu, H., Shen, X.-Z., 2016. The ubiquitin-proteasome system and its potential application in hepatocellular carcinoma therapy. Cancer Lett 379, 245–252. https://doi.org/10.1016/j.canlet.2015.06.023

Chisholm, C.G., Bartlett, R., Brown, M.L., Proctor, E.-J., Farrawell, N.E., Gorman, J., Delerue, F., Ittner, L.M., Vine-Perrow, K.L., Ecroyd, H., Cashman, N.R., Saunders, D.N., McAlary, L., Lum, J.S., Yerbury, J.J., 2025. Development of a targeted BioPROTAC degrader selective for misfolded SOD1. Nat Commun 16, 9713. https://doi.org/10.1038/s41467-025-65481-w

Chothia, C., Lesk, A.M., 1987. Canonical structures for the hypervariable regions of immunoglobulins. J Mol Biol 196, 901–917. https://doi.org/10.1016/0022-2836(87)90412-8

Chou, K.L., Stacy, M., Simuni, T., Miyasaki, J., Oertel, W.H., Sethi, K., Fernandez, H.H., Stocchi, F., 2018. The spectrum of “off” in Parkinson’s disease: What have we learned over 40 years? Parkinsonism & Related Disorders 51, 9–16. https://doi.org/10.1016/j.parkreldis.2018.02.001

Christ, D., Famm, K., Winter, G., 2007. Repertoires of aggregation-resistant human antibody domains. Protein Eng Des Sel 20, 413–416. https://doi.org/10.1093/protein/gzm037

Chu, T.-T., Gao, N., Li, Q.-Q., Chen, P.-G., Yang, X.-F., Chen, Y.-X., Zhao, Y.-F., Li, Y.-M., 2016a. Specific Knockdown of Endogenous Tau Protein by Peptide-Directed Ubiquitin-Proteasome Degradation. Cell Chemical Biology 23, 453–461. https://doi.org/10.1016/j.chembiol.2016.02.016

Chu, T.-T., Gao, N., Li, Q.-Q., Chen, P.-G., Yang, X.-F., Chen, Y.-X., Zhao, Y.-F., Li, Y.-M., 2016b. Specific Knockdown of Endogenous Tau Protein by Peptide-Directed Ubiquitin-Proteasome Degradation. Cell Chemical Biology 23, 453–461. https://doi.org/10.1016/j.chembiol.2016.02.016

Colby, D.W., Chu, Y., Cassady, J.P., Duennwald, M., Zazulak, H., Webster, J.M., Messer, A., Lindquist, S., Ingram, V.M., Wittrup, K.D., 2004. Potent inhibition of huntingtin aggregation and cytotoxicity by a disulfide bond-free single-domain intracellular antibody. Proceedings of the National Academy of Sciences 101, 17616–17621. https://doi.org/10.1073/pnas.0408134101

Collins, I., Wang, H., Caldwell, J.J., Chopra, R., 2017. Chemical approaches to targeted protein degradation through modulation of the ubiquitin–proteasome pathway. Biochem J 474, 1127–1147. https://doi.org/10.1042/BCJ20160762

Cooper, A.A., Gitler, A.D., Cashikar, A., Haynes, C.M., Hill, K.J., Bhullar, B., Liu, K., Xu, K., Strathearn, K.E., Liu, F., Cao, S., Caldwell, K.A., Caldwell, G.A., Marsischky, G., Kolodner, R.D., Labaer, J., Rochet, J.-C., Bonini, N.M., Lindquist, S., 2006. Alpha-synuclein blocks ER-Golgi traffic and Rab1 rescues neuron loss in Parkinson's models. Science 313, 324–328. https://doi.org/10.1126/science.1129462

Corson, L.B., Strain, J.J., Culotta, V.C., Cleveland, D.W., 1998. Chaperone-facilitated copper binding is a property common to several classes of familial amyotrophic lateral sclerosis-linked superoxide dismutase mutants. Proc Natl Acad Sci U S A 95, 6361–6366. https://doi.org/10.1073/pnas.95.11.6361

Corvol, J.-C., Artaud, F., Cormier-Dequaire, F., Rascol, O., Durif, F., Derkinderen, P., Marques, A.-R., Bourdain, F., Brandel, J.-P., Pico, F., Lacomblez, L., Bonnet, C., Brefel-Courbon, C., Ory-Magne, F., Grabli, D., Klebe, S., Mangone, G., You, H., Mesnage, V., Lee, P.-C., Brice, A., Vidailhet, M., Elbaz, A., 2018. Longitudinal analysis of impulse control disorders in Parkinson disease. Neurology 91, e189–e201. https://doi.org/10.1212/WNL.0000000000005816

Cuervo, A.M., Stefanis, L., Fredenburg, R., Lansbury, P.T., Sulzer, D., 2004. Impaired degradation of mutant alpha-synuclein by chaperone-mediated autophagy. Science 305, 1292–1295. https://doi.org/10.1126/science.1101738

Cyrus, K., Wehenkel, M., Choi, E.-Y., Han, H.-J., Lee, H., Swanson, H., Kim, K.-B., 2011. Impact of linker length on the activity of PROTACs. Mol. BioSyst. 7, 359–364. https://doi.org/10.1039/C0MB00074D

Damgaard, R.B., 2021. The ubiquitin system: from cell signalling to disease biology and new therapeutic opportunities. Cell Death Differ 28, 423–426. https://doi.org/10.1038/s41418-020-00703-w

Dauparas, J., Anishchenko, I., Bennett, N., Bai, H., Ragotte, R.J., Milles, L.F., Wicky, B.I.M., Courbet, A., de Haas, R.J., Bethel, N., Leung, P.J.Y., Huddy, T.F., Pellock, S., Tischer, D., Chan, F., Koepnick, B., Nguyen, H., Kang, A., Sankaran, B., Bera, A.K., King, N.P., Baker, D., 2022. Robust deep learning based protein sequence design using ProteinMPNN. Science 378, 49–56. https://doi.org/10.1126/science.add2187

de Haas, R.J., Brunette, N., Goodson, A., Dauparas, J., Yi, S.Y., Yang, E.C., Dowling, Q., Nguyen, H., Kang, A., Bera, A.K., Sankaran, B., de Vries, R., Baker, D., King, N.P., 2023. Rapid and automated design of two-component protein nanomaterials using ProteinMPNN. bioRxiv 2023.08.04.551935. https://doi.org/10.1101/2023.08.04.551935

Deng, H.X., Hentati, A., Tainer, J.A., Iqbal, Z., Cayabyab, A., Hung, W.Y., Getzoff, E.D., Hu, P., Herzfeldt, B., Roos, R.P., 1993. Amyotrophic lateral sclerosis and structural defects in Cu,Zn superoxide dismutase. Science 261, 1047–1051. https://doi.org/10.1126/science.8351519

Deng, Z., Lim, J., Wang, Q., Purtell, K., Wu, S., Palomo, G.M., Tan, H., Manfredi, G., Zhao, Y., Peng, J., Hu, B., Chen, S., Yue, Z., 2019. ALS-FTLD-linked mutations of SQSTM1/p62 disrupt selective autophagy and NFE2L2/NRF2 anti-oxidative stress pathway. Autophagy 16, 917–931. https://doi.org/10.1080/15548627.2019.1644076

Denizci Öncü, M., Balcıoğlu, B.K., Özgür, B., Öztürk, H.Ü., Serhatlı, M., Işık, Ş., Erdağ, B., Dinler Doğanay, G., Özdemir Bahadır, A., 2022. Structure-based

engineering of an antiangiogenic scFv antibody for soluble production in E. coli without loss of activity. Biotechnol Appl Biochem 69, 2122–2137. https://doi.org/10.1002/bab.2273

Douglass, E.F.Jr., Miller, C.J., Sparer, G., Shapiro, H., Spiegel, D.A., 2013. A Comprehensive Mathematical Model for Three-Body Binding Equilibria. J. Am. Chem. Soc. 135, 6092–6099. https://doi.org/10.1021/ja311795d

Du, X., Xie, X., Liu, R., 2020. The Role of α-Synuclein Oligomers in Parkinson's Disease. International Journal of Molecular Sciences 21. https://doi.org/10.3390/ijms21228645

Dudgeon, K., Famm, K., Christ, D., 2009. Sequence determinants of protein aggregation in human VH domains. Protein Eng Des Sel 22, 217–220. https://doi.org/10.1093/protein/gzn059

Dudgeon, K., Rouet, R., Kokmeijer, I., Schofield, P., Stolp, J., Langley, D., Stock, D., Christ, D., 2012. General strategy for the generation of human antibody variable domains with increased aggregation resistance. Proc Natl Acad Sci U S A 109, 10879–10884. https://doi.org/10.1073/pnas.1202866109

Durães, F., Pinto, M., Sousa, E., 2018. Old Drugs as New Treatments for Neurodegenerative Diseases. Pharmaceuticals (Basel) 11, 44. https://doi.org/10.3390/ph11020044

Edelman, G.M., 1973. Antibody structure and molecular immunology. Science 180, 830–840. https://doi.org/10.1126/science.180.4088.830

Ellis, R.J., 2001. Macromolecular crowding: obvious but underappreciated. Trends Biochem Sci 26, 597–604. https://doi.org/10.1016/s0968-0004(01)01938-7

El-Turk, F., Newby, F.N., De Genst, E., Guilliams, T., Sprules, T., Mittermaier, A., Dobson, C.M., Vendruscolo, M., 2016. Structural Effects of Two Camelid

Nanobodies Directed to Distinct C-Terminal Epitopes on α-Synuclein. Biochemistry 55, 3116–3122. https://doi.org/10.1021/acs.biochem.6b00149

Emadi, S., Barkhordarian, H., Wang, M.S., Schulz, P., Sierks, M.R., 2007. Isolation of a human single chain antibody fragment against oligomeric α-synuclein that inhibits aggregation and prevents α-synuclein induced toxicity. J Mol Biol 368, 1132–1144. https://doi.org/10.1016/j.jmb.2007.02.089

Emadi, S., Kasturirangan, S., Wang, M.S., Schulz, P., Sierks, M.R., 2009. Detecting Morphologically Distinct Oligomeric Forms of α-Synuclein. J Biol Chem 284, 11048–11058. https://doi.org/10.1074/jbc.M806559200

Emin, D., Zhang, Y.P., Lobanova, E., Miller, A., Li, X., Xia, Z., Dakin, H., Sideris, D.I., Lam, J.Y.L., Ranasinghe, R.T., Kouli, A., Zhao, Y., De, S., Knowles, T.P.J., Vendruscolo, M., Ruggeri, F.S., Aigbirhio, F.I., Williams-Gray, C.H., Klenerman, D., 2022. Small soluble α-synuclein aggregates are the toxic species in Parkinson's disease. Nat Commun 13, 5512. https://doi.org/10.1038/s41467-022-33252-6

Erkkinen, M.G., Kim, M.-O., Geschwind, M.D., 2018. Clinical Neurology and Epidemiology of the Major Neurodegenerative Diseases. Cold Spring Harb Perspect Biol 10, a033118. https://doi.org/10.1101/cshperspect.a033118

Estabragh, A.M., Sadeghi, H.M.M., Akbari, V., 2022. Co-Expression of Chaperones for Improvement of Soluble Expression and Purification of An Anti-HER2 scFv in Escherichia Coli. Adv Biomed Res 11, 117. https://doi.org/10.4103/abr.abr_351_21

Ewert, S., Honegger, A., Plückthun, A., 2004. Stability improvement of antibodies for extracellular and intracellular applications: CDR grafting to stable frameworks

and structure-based framework engineering. Methods 34, 184–199. https://doi.org/10.1016/j.ymeth.2004.04.007

Ewert, S., Honegger, A., Plückthun, A., 2003. Structure-based improvement of the biophysical properties of immunoglobulin VH domains with a generalizable approach. Biochemistry 42, 1517–1528. https://doi.org/10.1021/bi026448p

Famm, K., Hansen, L., Christ, D., Winter, G., 2008. Thermodynamically stable aggregation-resistant antibody domains through directed evolution. J Mol Biol 376, 926–931. https://doi.org/10.1016/j.jmb.2007.10.075

Fang, T., Al Khleifat, A., Meurgey, J.-H., Jones, A., Leigh, P.N., Bensimon, G., Al-Chalabi, A., 2018. Stage at which riluzole treatment prolongs survival in patients with amyotrophic lateral sclerosis: a retrospective analysis of data from a dose-ranging study. Lancet Neurol 17, 416–422. https://doi.org/10.1016/S1474-4422(18)30054-1

Farrawell, N.E., Yerbury, J.J., 2021. Mutant Cu/Zn Superoxide Dismutase (A4V) Turnover Is Altered in Cells Containing Inclusions. Front Mol Neurosci 14, 771911. https://doi.org/10.3389/fnmol.2021.771911

FEARNLEY, J.M., LEES, A.J., 1991. AGEING AND PARKINSON'S DISEASE: SUBSTANTIA NIGRA REGIONAL SELECTIVITY. Brain 114, 2283–2301. https://doi.org/10.1093/brain/114.5.2283

Finan, C., Gaulton, A., Kruger, F.A., Lumbers, R.T., Shah, T., Engmann, J., Galver, L., Kelley, R., Karlsson, A., Santos, R., Overington, J.P., Hingorani, A.D., Casas, J.P., 2017. The druggable genome and support for target identification and validation in drug development. Science Translational Medicine 9, eaag1166. https://doi.org/10.1126/scitranslmed.aag1166

Fisher, A., DeLisa, M.P., 2009. Efficient isolation of soluble intracellular single-chain antibodies using the twin-arginine translocation machinery. J Mol Biol 385, 299–311. https://doi.org/10.1016/j.jmb.2008.10.051

Flick, K., Raasi, S., Zhang, H., Yen, J.L., Kaiser, P., 2006. A ubiquitin-interacting motif protects polyubiquitinated Met4 from degradation by the 26S proteasome. Nat Cell Biol 8, 509–515. https://doi.org/10.1038/ncb1402

Forsberg, K., Graffmo, K., Pakkenberg, B., Weber, M., Nielsen, M., Marklund, S., Brännström, T., Andersen, P.M., 2019. Misfolded SOD1 inclusions in patients with mutations in C9orf72 and other ALS/FTD-associated genes. J Neurol Neurosurg Psychiatry 90, 861–869. https://doi.org/10.1136/jnnp-2018-319386

Forsberg, K., Jonsson, P.A., Andersen, P.M., Bergemalm, D., Graffmo, K.S., Hultdin, M., Jacobsson, J., Rosquist, R., Marklund, S.L., Brännström, T., 2010. Novel antibodies reveal inclusions containing non-native SOD1 in sporadic ALS patients. PLoS One 5, e11552. https://doi.org/10.1371/journal.pone.0011552

Fujisawa, T., Homma, K., Yamaguchi, N., Kadowaki, H., Tsuburaya, N., Naguro, I., Matsuzawa, A., Takeda, K., Takahashi, Y., Goto, J., Tsuji, S., Nishitoh, H., Ichijo, H., 2012. A novel monoclonal antibody reveals a conformational alteration shared by amyotrophic lateral sclerosis-linked SOD1 mutants. Ann Neurol 72, 739–749. https://doi.org/10.1002/ana.23668

Galindo, G., Maejima, D., DeRoo, J., Burlingham, S.R., Fixen, G., Morisaki, T., Febvre, H.P., Hasbrook, R., Zhao, N., Ghosh, S., Mayton, E.H., Snow, C.D., Geiss, B.J., Ohkawa, Y., Sato, Y., Kimura, H., Stasevich, T.J., 2025. AI-assisted protein design to rapidly convert antibody sequences to intrabodies targeting diverse peptides and histone modifications. https://doi.org/10.1101/2025.02.06.636921

Games, D., Valera, E., Spencer, B., Rockenstein, E., Mante, M., Adame, A., Patrick, C., Ubhi, K., Nuber, S., Sacayon, P., Zago, W., Seubert, P., Barbour, R., Schenk, D., Masliah, E., 2014. Reducing C-Terminal-Truncated Alpha-Synuclein by Immunotherapy Attenuates Neurodegeneration and Propagation in Parkinson's Disease-Like Models. J Neurosci 34, 9441–9454. https://doi.org/10.1523/JNEUROSCI.5314-13.2014

Gerdes, C., Waal, N., Offner, T., Fornasiero, E.F., Wender, N., Verbarg, H., Manzini, I., Trenkwalder, C., Mollenhauer, B., Strohäker, T., Zweckstetter, M., Becker, S., Rizzoli, S.O., Basmanav, F.B., Opazo, F., 2020. A nanobody-based fluorescent reporter reveals human α-synuclein in the cell cytosol. Nat Commun 11, 2729. https://doi.org/10.1038/s41467-020-16575-0

Gil, D., Schrum, A.G., 2013. Strategies to stabilize compact folding and minimize aggregation of antibody-based fragments. Adv Biosci Biotechnol 4, 73–84. https://doi.org/10.4236/abb.2013.44A011

Go, E.B., Lee, J.H., Cho, J.H., Kwon, N.H., Choi, J., Kwon, I., 2024. Enhanced therapeutic potential of antibody fragment via IEDDA-mediated site-specific albumin conjugation. J Biol Eng 18, 23. https://doi.org/10.1186/s13036-024-00418-3

Gosink, M.M., Vierstra, R.D., 1995. Redirecting the specificity of ubiquitination by modifying ubiquitin-conjugating enzymes. Proc Natl Acad Sci U S A 92, 9117–9121. https://doi.org/10.1073/pnas.92.20.9117

Goto, Y., Hamaguchi, K., 1979. The Role of the Intrachain Disulfide Bond in the Conformation and Stability of the Constant Fragment of the Immunoglobulin Light Chain. The Journal of Biochemistry 86, 1433–1441.

Graff, C.P., Chester, K., Begent, R., Wittrup, K.D., 2004. Directed evolution of an anti-carcinoembryonic antigen scFv with a 4-day monovalent dissociation half-time at 37 degrees C. Protein Eng Des Sel 17, 293–304. https://doi.org/10.1093/protein/gzh038

Guglielmi, L., Denis, V., Vezzio-Vié, N., Bec, N., Dariavach, P., Larroque, C., Martineau, P., 2011. Selection for intrabody solubility in mammalian cells using GFP fusions. Protein Eng Des Sel 24, 873–881. https://doi.org/10.1093/protein/gzr049

Guilliams, T., El-Turk, F., Buell, A.K., O'Day, E.M., Aprile, F.A., Esbjörner, E.K., Vendruscolo, M., Cremades, N., Pardon, E., Wyns, L., Welland, M.E., Steyaert, J., Christodoulou, J., Dobson, C.M., De Genst, E., 2013. Nanobodies Raised against Monomeric α-Synuclein Distinguish between Fibrils at Different Maturation Stages. Journal of Molecular Biology 425, 2397–2411. https://doi.org/10.1016/j.jmb.2013.01.040

Guo, F., Liu, X., Cai, H., Le, W., 2017. Autophagy in neurodegenerative diseases: pathogenesis and therapy. Brain Pathol 28, 3–13. https://doi.org/10.1111/bpa.12545

Haass, C., Selkoe, D.J., 2007. Soluble protein oligomers in neurodegeneration: lessons from the Alzheimer's amyloid β-peptide. Nat Rev Mol Cell Biol 8, 101–112. https://doi.org/10.1038/nrm2101

Hashimoto, M., Hsu, L.J., Xia, Y., Takeda, A., Sisk, A., Sundsmo, M., Masliah, E., 1999. Oxidative stress induces amyloid-like aggregate formation of NACP/alpha-synuclein in vitro. Neuroreport 10, 717–721. https://doi.org/10.1097/00001756-199903170-00011

Hayhurst, A., Harris, W.J., 1999. Escherichia coli skp chaperone coexpression improves solubility and phage display of single-chain antibody fragments. Protein Expr Purif 15, 336–343. https://doi.org/10.1006/prep.1999.1035

Hennecke, F., Krebber, C., Plückthun, A., 1998. Non-repetitive single-chain Fv linkers selected by selectively infective phage (SIP) technology. Protein Eng 11, 405–410. https://doi.org/10.1093/protein/11.5.405

Hewitt, S.N., Choi, R., Kelley, A., Crowther, G.J., Napuli, A.J., Van Voorhis, W.C., 2011. Expression of proteins in Escherichia coli as fusions with maltose-binding protein to rescue non-expressed targets in a high-throughput protein-expression and purification pipeline. Acta Cryst F 67, 1006–1009. https://doi.org/10.1107/S1744309111022159

Hitti, F.L., Ramayya, A.G., McShane, B.J., Yang, A.I., Vaughan, K.A., Baltuch, G.H., 2019. Long-term outcomes following deep brain stimulation for Parkinson's disease. Journal of Neurosurgery 132, 205–210. https://doi.org/10.3171/2018.8.JNS182081

Ho, P.W.-L., Leung ,Chi-Ting, Liu ,Huifang, Pang ,Shirley Yin-Yu, Lam ,Colin Siu-Chi, Xian ,Jiawen, Li ,Lingfei, Kung ,Michelle Hiu-Wai, Ramsden ,David Boyer, and Ho, S.-L., 2020. Age-dependent accumulation of oligomeric SNCA/α-synuclein from impaired degradation in mutant LRRK2 knockin mouse model of Parkinson disease: role for therapeutic activation of chaperone-mediated autophagy (CMA). Autophagy 16, 347–370. https://doi.org/10.1080/15548627.2019.1603545

Hollenstein, D.M., Kraft, C., 2020. Autophagosomes are formed at a distinct cellular structure. Curr Opin Cell Biol 65, 50–57. https://doi.org/10.1016/j.ceb.2020.02.012

Honegger, A., Malebranche, A.D., Röthlisberger, D., Plückthun, A., 2009. The influence of the framework core residues on the biophysical properties of immunoglobulin heavy chain variable domains. Protein Eng Des Sel 22, 121–134. https://doi.org/10.1093/protein/gzn077

Hopkins, A.L., Groom, C.R., 2002. The druggable genome. Nat Rev Drug Discov 1, 727–730. https://doi.org/10.1038/nrd892

Hough, M.A., Grossmann, J.G., Antonyuk, S.V., Strange, R.W., Doucette, P.A., Rodriguez, J.A., Whitson, L.J., Hart, P.J., Hayward, L.J., Valentine, J.S., Hasnain, S.S., 2004. Dimer destabilization in superoxide dismutase may result in disease-causing properties: structures of motor neuron disease mutants. Proc Natl Acad Sci U S A 101, 5976–5981. https://doi.org/10.1073/pnas.0305143101

Hsu, J.H.-R., Rasmusson, T., Robinson, J., Pachl, F., Read, J., Kawatkar, S., O' Donovan, D.H., Bagal, S., Code, E., Rawlins, P., Argyrou, A., Tomlinson, R., Gao, N., Zhu, X., Chiarparin, E., Jacques, K., Shen, M., Woods, H., Bednarski, E., Wilson, D.M., Drew, L., Castaldi, M.P., Fawell, S., Bloecher, A., 2020. EED-Targeted PROTACs Degrade EED, EZH2, and SUZ12 in the PRC2 Complex. Cell Chemical Biology 27, 41-46.e17. https://doi.org/10.1016/j.chembiol.2019.11.004

Hu, X., O'Hara, L., White, S., Magner, E., Kane, M., Wall, J.G., 2007. Optimisation of production of a domoic acid-binding scFv antibody fragment in Escherichia coli using molecular chaperones and functional immobilisation on a mesoporous silicate support. Protein Expr Purif 52, 194–201. https://doi.org/10.1016/j.pep.2006.08.009

Huang, M., Liu, Y.U., Yao, X., Qin, D., Su, H., 2024. Variability in SOD1-associated amyotrophic lateral sclerosis: geographic patterns, clinical heterogeneity, molecular alterations, and therapeutic implications. Transl Neurodegener 13, 28. https://doi.org/10.1186/s40035-024-00416-x

Hudson, P.J., Kortt, A.A., 1999. High avidity scFv multimers; diabodies and triabodies. J Immunol Methods 231, 177–189. https://doi.org/10.1016/s0022-1759(99)00157-x

Hughes, S.J., Testa, A., Thompson, N., Churcher, I., 2021. The rise and rise of protein degradation: Opportunities and challenges ahead. Drug Discovery Today 26, 2889–2897. https://doi.org/10.1016/j.drudis.2021.08.006

Hugo, N., Lafont, V., Beukes, M., Altschuh, D., 2002. Functional aspects of co-variant surface charges in an antibody fragment. Protein Science 11, 2697–2705. https://doi.org/10.1110/ps.0209302

Hugo, N., Weidenhaupt, M., Beukes, M., Xu, B., Janson, J. -C., Vernet, T., Altschuh, D., 2003. VL position 34 is a key determinant for the engineering of stable antibodies with fast dissociation rates. Protein Engineering 16, 381–386. https://doi.org/10.1093/protein/gzg042

Huston, J.S., Levinson, D., Mudgett-Hunter, M., Tai, M.S., Novotný, J., Margolies, M.N., Ridge, R.J., Bruccoleri, R.E., Haber, E., Crea, R., 1988. Protein engineering of antibody binding sites: recovery of specific activity in an anti-digoxin single-chain Fv analogue produced in Escherichia coli. Proc Natl Acad Sci U S A 85, 5879–5883. https://doi.org/10.1073/pnas.85.16.5879

Imai, Y., Soda, M., Hatakeyama, S., Akagi, T., Hashikawa, T., Nakayama, K.I., Takahashi, R., 2002. CHIP is associated with Parkin, a gene responsible for

familial Parkinson's disease, and enhances its ubiquitin ligase activity. Mol Cell 10, 55–67. https://doi.org/10.1016/s1097-2765(02)00583-x

Jafari, R., Almqvist, H., Axelsson, H., Ignatushchenko, M., Lundbäck, T., Nordlund, P., Molina, D.M., 2014. The cellular thermal shift assay for evaluating drug target interactions in cells. Nat Protoc 9, 2100–2122. https://doi.org/10.1038/nprot.2014.138

Jespers, L., Schon, O., Famm, K., Winter, G., 2004. Aggregation-resistant domain antibodies selected on phage by heat denaturation. Nat Biotechnol 22, 1161–1165. https://doi.org/10.1038/nbt1000

Ji, C.H., Kim, H.Y., Lee, M.J., Heo, A.J., Park, D.Y., Lim, S., Shin, S., Ganipisetti, S., Yang, W.S., Jung, C.A., Kim, K.Y., Jeong, E.H., Park, S.H., Bin Kim, S., Lee, S.J., Na, J.E., Kang, J.I., Chi, H.M., Kim, H.T., Kim, Y.K., Kim, B.Y., Kwon, Y.T., 2022. The AUTOTAC chemical biology platform for targeted protein degradation via the autophagy-lysosome system. Nat Commun 13, 904. https://doi.org/10.1038/s41467-022-28520-4

Jiang, J., Lu, Y., Chu, J., Zhang, X., Xu, C., Liu, S., Wan, Z., Wang, J., Zhang, L., Liu, K., Liu, Z., Yang, A., Ren, X., Zhang, R., 2024. Anti-EGFR ScFv functionalized exosomes delivering LPCAT1 specific siRNAs for inhibition of lung cancer brain metastases. Journal of Nanobiotechnology 22, 159. https://doi.org/10.1186/s12951-024-02414-7

Jiang, Y., Lin, Y., Tetlow, A.M., Pan, R., Ji, C., Kong, X.-P., Congdon, E.E., Sigurdsson, E.M., 2024. Single-domain antibody-based protein degrader for synucleinopathies. Molecular Neurodegeneration 19, 44. https://doi.org/10.1186/s13024-024-00730-y

Jones, P.T., Dear, P.H., Foote, J., Neuberger, M.S., Winter, G., 1986. Replacing the complementarity-determining regions in a human antibody with those from a mouse. Nature 321, 522–525. https://doi.org/10.1038/321522a0

Jonsson, P.A., Graffmo, K.S., Andersen, P.M., Brännström, T., Lindberg, M., Oliveberg, M., Marklund, S.L., 2006. Disulphide-reduced superoxide dismutase-1 in CNS of transgenic amyotrophic lateral sclerosis models. Brain 129, 451–464. https://doi.org/10.1093/brain/awh704

Joshi, S.N., Butler, D.C., Messer, A., 2012. Fusion to a highly charged proteasomal retargeting sequence increases soluble cytoplasmic expression and efficacy of diverse anti-synuclein intrabodies. MAbs 4, 686–693. https://doi.org/10.4161/mabs.21696

Jung, S., Plückthun, A., 1997a. Improving in vivo folding and stability of a single-chain Fv antibody fragment by loop grafting. Protein Eng 10, 959–966. https://doi.org/10.1093/protein/10.8.959

Jung, S., Plückthun, A., 1997b. Improving in vivo folding and stability of a single-chain Fv antibody fragment by loop grafting. Protein Eng 10, 959–966. https://doi.org/10.1093/protein/10.8.959

Kabat, E.A., Wu, T.T., 1971. Attempts to locate complementarity-determining residues in the variable positions of light and heavy chains. Ann N Y Acad Sci 190, 382–393. https://doi.org/10.1111/j.1749-6632.1971.tb13550.x

Kabayama, H., Takeuchi, M., Tokushige, N., Muramatsu, S., Kabayama, M., Fukuda, M., Yamada, Y., Mikoshiba, K., 2020. An ultra-stable cytoplasmic antibody engineered for in vivo applications. Nat Commun 11, 336. https://doi.org/10.1038/s41467-019-13654-9

Kargbo, R.B., 2020. PROTAC-Mediated Degradation of KRAS Protein for Anticancer Therapeutics. ACS Med. Chem. Lett. 11, 5–6. https://doi.org/10.1021/acsmedchemlett.9b00584

Kelm, J.M., Pandey, D.S., Malin, E., Kansou, H., Arora, S., Kumar, R., Gavande, N.S., 2023. PROTAC'ing oncoproteins: targeted protein degradation for cancer therapy. Molecular Cancer 22, 62. https://doi.org/10.1186/s12943-022-01707-5

Kiernan, M.C., Vucic, S., Cheah, B.C., Turner, M.R., Eisen, A., Hardiman, O., Burrell, J.R., Zoing, M.C., 2011. Amyotrophic lateral sclerosis. Lancet 377, 942–955. https://doi.org/10.1016/S0140-6736(10)61156-7

Kim, J.H., Lee, S.-R., Li, L.-H., Park, H.-J., Park, J.-H., Lee, K.Y., Kim, M.-K., Shin, B.A., Choi, S.-Y., 2011. High cleavage efficiency of a 2A peptide derived from porcine teschovirus-1 in human cell lines, zebrafish and mice. PLoS One 6, e18556. https://doi.org/10.1371/journal.pone.0018556

Kim, Y.-J., Neelamegam, R., Heo, M.-A., Edwardraja, S., Paik, H.-J., Lee, S.-G., 2008. Improving the productivity of single-chain Fv antibody against c-Met by rearranging the order of its variable domains. J Microbiol Biotechnol 18, 1186–1190.

Kitada, T., Asakawa, S., Hattori, N., Matsumine, H., Yamamura, Y., Minoshima, S., Yokochi, M., Mizuno, Y., Shimizu, N., 1998. Mutations in the parkin gene cause autosomal recessive juvenile parkinsonism. Nature 392, 605–608. https://doi.org/10.1038/33416

Klucken, J., Poehler, A.-M., Ebrahimi-Fakhari, D., Schneider, J., Nuber, S., Rockenstein, E., Schlötzer-Schrehardt, U., Hyman, B.T., McLean, P.J., Masliah, E., Winkler, J., 2012. Alpha-synuclein aggregation involves a

bafilomycin A 1-sensitive autophagy pathway. Autophagy 8, 754–766. https://doi.org/10.4161/auto.19371

Knappik, A., Plückthun, A., 1995. Engineered turns of a recombinant antibody improve its *in vivo* folding. Protein Eng Des Sel 8, 81–89. https://doi.org/10.1093/protein/8.1.81

Kocak, M., Ezazi Erdi, S., Jorba, G., Maestro, I., Farrés, J., Kirkin, V., Martinez, A., Pless, O., 2022. Targeting autophagy in disease: established and new strategies. Autophagy 18, 473–495. https://doi.org/10.1080/15548627.2021.1936359

Koçer, İ., Cox, E.C., DeLisa, M.P., Çelik, E., 2021. Effects of variable domain orientation on anti-HER2 single-chain variable fragment antibody expressed in the Escherichia coli cytoplasm. Biotechnol Prog 37, e3102. https://doi.org/10.1002/btpr.3102

Komander, D., 2009. The emerging complexity of protein ubiquitination. Biochem Soc Trans 37, 937–953. https://doi.org/10.1042/BST0370937

Komander, D., Rape, M., 2012. The ubiquitin code. Annu Rev Biochem 81, 203–229. https://doi.org/10.1146/annurev-biochem-060310-170328

Kou, J., Kim, H., Pattanayak, A., Song, M., Lim, J.-E., Taguchi, H., Paul, S., Cirrito, J.R., Ponnazhagan, S., Fukuchi, K., 2011. Anti-Aβ single-chain antibody brain delivery via AAV reduces amyloid load but may increase cerebral hemorrhages in an Alzheimer mouse model. J Alzheimers Dis 27, 23–38. https://doi.org/10.3233/JAD-2011-110230

Kouli, A., Camacho, M., Allinson, K., Williams-Gray, C.H., 2020. Neuroinflammation and protein pathology in Parkinson's disease dementia. Acta Neuropathologica Communications 8, 211. https://doi.org/10.1186/s40478-020-01083-5

Kouli, A., Torsney, K.M., Kuan, W.-L., 2018. Parkinson's Disease: Etiology, Neuropathology, and Pathogenesis, in: Stoker, T.B., Greenland, J.C. (Eds.), Parkinson's Disease: Pathogenesis and Clinical Aspects. Codon Publications, Brisbane (AU).

Kramer, R.M., Shende, V.R., Motl, N., Pace, C.N., Scholtz, J.M., 2012. Toward a molecular understanding of protein solubility: increased negative surface charge correlates with increased solubility. Biophys J 102, 1907–1915. https://doi.org/10.1016/j.bpj.2012.01.060

Krüger, R., Kuhn, W., Müller, T., Woitalla, D., Graeber, M., Kösel, S., Przuntek, H., Epplen, J.T., Schöls, L., Riess, O., 1998. Ala30Pro mutation in the gene encoding alpha-synuclein in Parkinson's disease. Nat Genet 18, 106–108. https://doi.org/10.1038/ng0298-106

Kuma, A., Komatsu, M., Mizushima, N., 2017. Autophagy-monitoring and autophagy-deficient mice. Autophagy 13, 1619–1628. https://doi.org/10.1080/15548627.2017.1343770

Kumar, M.S., Fowler-Magaw, M.E., Kulick, D., Boopathy, S., Gadd, D.H., Rotunno, M., Douthwright, C., Golebiowski, D., Yusuf, I., Xu, Z., Brown, R.H., Sena-Esteves, M., O'Neil, A.L., Bosco, D.A., 2022. Anti-SOD1 Nanobodies That Stabilize Misfolded SOD1 Proteins Also Promote Neurite Outgrowth in Mutant SOD1 Human Neurons. Int J Mol Sci 23, 16013. https://doi.org/10.3390/ijms232416013

Kumar, S.T., Jagannath, S., Francois, C., Vanderstichele, H., Stoops, E., Lashuel, H.A., 2020. How specific are the conformation-specific α-synuclein antibodies? Characterization and validation of 16 α-synuclein conformation-specific antibodies using well-characterized preparations of α-synuclein monomers,

fibrils and oligomers with distinct structures and morphology. Neurobiol Dis 146, 105086. https://doi.org/10.1016/j.nbd.2020.105086

Kvam, E., Sierks, M.R., Shoemaker, C.B., Messer, A., 2010. Physico-chemical determinants of soluble intrabody expression in mammalian cell cytoplasm. Protein Eng Des Sel 23, 489–498. https://doi.org/10.1093/protein/gzq022

Lang, A.E., Siderowf, A.D., Macklin, E.A., Poewe, W., Brooks, D.J., Fernandez, H.H., Rascol, O., Giladi, N., Stocchi, F., Tanner, C.M., Postuma, R.B., Simon, D.K., Tolosa, E., Mollenhauer, B., Cedarbaum, J.M., Fraser, K., Xiao, J., Evans, K.C., Graham, D.L., Sapir, I., Inra, J., Hutchison, R.M., Yang, M., Fox, T., Haeberlein, S.B., Dam, T., 2022. Trial of Cinpanemab in Early Parkinson's Disease. New England Journal of Medicine 387, 408–420. https://doi.org/10.1056/NEJMoa2203395

Lashuel, H.A., Overk, C.R., Oueslati, A., Masliah, E., 2013. The many faces of α-synuclein: from structure and toxicity to therapeutic target. Nat Rev Neurosci 14, 38–48. https://doi.org/10.1038/nrn3406

Layfield, R., Lowe, J., Bedford, L., 2005. The ubiquitin-proteasome system and neurodegenerative disorders. Essays Biochem 41, 157–171. https://doi.org/10.1042/EB0410157

Lefranc, M.P., Giudicelli, V., Ginestoux, C., Bodmer, J., Müller, W., Bontrop, R., Lemaitre, M., Malik, A., Barbié, V., Chaume, D., 1999. IMGT, the international ImMunoGeneTics database. Nucleic Acids Res 27, 209–212. https://doi.org/10.1093/nar/27.1.209

Li, J.-Q., Tan, L., Yu, J.-T., 2014. The role of the LRRK2 gene in Parkinsonism. Mol Neurodegener 9, 47. https://doi.org/10.1186/1750-1326-9-47

Li, L., Chen, S., Miao, Z., Liu, Y., Liu, X., Xiao, Z.-X., Cao, Y., 2019. AbRSA: A robust tool for antibody numbering. Protein Sci 28, 1524–1531. https://doi.org/10.1002/pro.3633

Li, W., Li, J., Bao, J., 2011. Microautophagy: lesser-known self-eating. Cell Mol Life Sci 69, 1125–1136. https://doi.org/10.1007/s00018-011-0865-5

Li, Y., Jiao, W., Liu, R., Deng, X., Zhu, F., Xue, W., 2024. Expanding the sequence spaces of synthetic binding protein using deep learning-based framework ProteinMPNN. Front. Comput. Sci. 19, 195903. https://doi.org/10.1007/s11704-024-31060-3

Lim, S., Khoo, R., Peh, K.M., Teo, J., Chang, S.C., Ng, S., Beilhartz, G.L., Melnyk, R.A., Johannes, C.W., Brown, C.J., Lane, D.P., Henry, B., Partridge, A.W., 2020. bioPROTACs as versatile modulators of intracellular therapeutic targets including proliferating cell nuclear antigen (PCNA). Proc Natl Acad Sci U S A 117, 5791–5800. https://doi.org/10.1073/pnas.1920251117

Lindberg, M.J., Byström, R., Boknäs, N., Andersen, P.M., Oliveberg, M., 2005. Systematically perturbed folding patterns of amyotrophic lateral sclerosis (ALS)-associated SOD1 mutants. Proceedings of the National Academy of Sciences 102, 9754–9759. https://doi.org/10.1073/pnas.0501957102

Liu, X., Kalogeropulou, A.F., Domingos, S., Makukhin, N., Nirujogi, R.S., Singh, F., Shpiro, N., Saalfrank, A., Sammler, E., Ganley, I.G., Moreira, R., Alessi, D.R., Ciulli, A., 2022. Discovery of XL01126: A Potent, Fast, Cooperative, Selective, Orally Bioavailable, and Blood-Brain Barrier Penetrant PROTAC Degrader of Leucine-Rich Repeat Kinase 2. J Am Chem Soc 144, 16930–16952. https://doi.org/10.1021/jacs.2c05499

Luchinat, E., Barbieri, L., Banci, L., 2017. A molecular chaperone activity of CCS restores the maturation of SOD1 fALS mutants. Sci Rep 7, 17433. https://doi.org/10.1038/s41598-017-17815-y

Ludwicki, M.B., Li, J., Stephens, E.A., Roberts, R.W., Koide, S., Hammond, P.T., DeLisa, M.P., 2019. Broad-Spectrum Proteome Editing with an Engineered Bacterial Ubiquitin Ligase Mimic. ACS Cent. Sci. 5, 852–866. https://doi.org/10.1021/acscentsci.9b00127

Luz, D., Shiga, E.A., Chen, G., Quintilio, W., Andrade, F.B., Maranhão, A.Q., Caetano, B.A., Mitsunari, T., Silva, M.A., Rocha, L.B., Moro, A.M., Sidhu, S.S., Piazza, R.M.F., 2018. Structural Changes in Stx1 Engineering Monoclonal Antibody Improves Its Functionality as Diagnostic Tool for a Rapid Latex Agglutination Test. Antibodies (Basel) 7, 9. https://doi.org/10.3390/antib7010009

MacCallum, R.M., Martin, A.C., Thornton, J.M., 1996. Antibody-antigen interactions: contact analysis and binding site topography. J Mol Biol 262, 732–745. https://doi.org/10.1006/jmbi.1996.0548

Maier, M., Welt, T., Wirth, F., Montrasio, F., Preisig, D., McAfoose, J., Vieira, F.G., Kulic, L., Späni, C., Stehle, T., Perrin, S., Weber, M., Hock, C., Nitsch, R.M., Grimm, J., 2018. A human-derived antibody targets misfolded SOD1 and ameliorates motor symptoms in mouse models of amyotrophic lateral sclerosis. Sci Transl Med 10, eaah3924. https://doi.org/10.1126/scitranslmed.aah3924

Maniaci, C., Hughes, S.J., Testa, A., Chen, W., Lamont, D.J., Rocha, S., Alessi, D.R., Romeo, R., Ciulli, A., 2017. Homo-PROTACs: bivalent small-molecule dimerizers of the VHL E3 ubiquitin ligase to induce self-degradation. Nat Commun 8, 830. https://doi.org/10.1038/s41467-017-00954-1

Mares, A., Miah, A.H., Smith, I.E.D., Rackham, M., Thawani, A.R., Cryan, J., Haile, P.A., Votta, B.J., Beal, A.M., Capriotti, C., Reilly, M.A., Fisher, D.T., Zinn, N., Bantscheff, M., MacDonald, T.T., Vossenkamper, A., Dace, P., Churcher, I., Benowitz, A.B., Watt, G., Denyer, J., Scott-Stevens, P., Harling, J.D., 2020. Extended pharmacodynamic responses observed upon PROTAC-mediated degradation of RIPK2. Commun Biol 3, 140. https://doi.org/10.1038/s42003-020-0868-6

Maroteaux, L., Scheller, R.H., 1991. The rat brain synucleins; family of proteins transiently associated with neuronal membrane. Molecular Brain Research 11, 335–343. https://doi.org/10.1016/0169-328X(91)90043-W

Marras, C., Beck, J.C., Bower, J.H., Roberts, E., Ritz, B., Ross, G.W., Abbott, R.D., Savica, R., Van Den Eeden, S.K., Willis, A.W., Tanner, C.M., 2018. Prevalence of Parkinson's disease across North America. npj Parkinson's Disease 4, 21. https://doi.org/10.1038/s41531-018-0058-0

Masrori, P., Van Damme, P., 2020. Amyotrophic lateral sclerosis: a clinical review. European Journal of Neurology 27, 1918–1929. https://doi.org/10.1111/ene.14393

Masuda-Suzukake, M., Nonaka, T., Hosokawa, M., Oikawa, T., Arai, T., Akiyama, H., Mann, D.M.A., Hasegawa, M., 2013. Prion-like spreading of pathological α-synuclein in brain. Brain 136, 1128–1138. https://doi.org/10.1093/brain/awt037

Mathieson, T., Franken, H., Kosinski, J., Kurzawa, N., Zinn, N., Sweetman, G., Poeckel, D., Ratnu, V.S., Schramm, M., Becher, I., Steidel, M., Noh, K.-M., Bergamini, G., Beck, M., Bantscheff, M., Savitski, M.M., 2018. Systematic analysis of protein turnover in primary cells. Nat Commun 9, 689. https://doi.org/10.1038/s41467-018-03106-1

McAlary, L., Plotkin, S.S., Yerbury, J.J., Cashman, N.R., 2019. Prion-Like Propagation of Protein Misfolding and Aggregation in Amyotrophic Lateral Sclerosis. Front Mol Neurosci 12, 262. https://doi.org/10.3389/fnmol.2019.00262

McCampbell, A., Cole, T., Wegener, A.J., Tomassy, G.S., Setnicka, A., Farley, B.J., Schoch, K.M., Hoye, M.L., Shabsovich, M., Sun, L., Luo, Y., Zhang, M., Comfort, N., Wang, B., Amacker, J., Thankamony, S., Salzman, D.W., Cudkowicz, M., Graham, D.L., Bennett, C.F., Kordasiewicz, H.B., Swayze, E.E., Miller, T.M., 2018. Antisense oligonucleotides extend survival and reverse decrement in muscle response in ALS models. J Clin Invest 128, 3558–3567. https://doi.org/10.1172/JCI99081

Meade, R.M., Allen, S.G., Williams, C., Tang, T.M.S., Crump, M.P., Mason, J.M., 2023. An N-terminal alpha-synuclein fragment binds lipid vesicles to modulate lipid-induced aggregation. Cell Reports Physical Science 4, 101563. https://doi.org/10.1016/j.xcrp.2023.101563

Miller, B.R., Demarest, S.J., Lugovskoy, A., Huang, F., Wu, X., Snyder, W.B., Croner, L.J., Wang, N., Amatucci, A., Michaelson, J.S., Glaser, S.M., 2010. Stability engineering of scFvs for the development of bispecific and multivalent antibodies. Protein Eng Des Sel 23, 549–557. https://doi.org/10.1093/protein/gzq028

Miller, T.M., Cudkowicz, M.E., Genge, A., Shaw, P.J., Sobue, G., Bucelli, R.C., Chiò, A., Damme, P.V., Ludolph, A.C., Glass, J.D., Andrews, J.A., Babu, S., Benatar, M., McDermott, C.J., Cochrane, T., Chary, S., Chew, S., Zhu, H., Wu, F., Nestorov, I., Graham, D., Sun, P., McNeill, M., Fanning, L., Ferguson, T.A., Fradette, S., 2022. Trial of Antisense Oligonucleotide Tofersen for SOD1 ALS.

New England Journal of Medicine 387, 1099–1110. https://doi.org/10.1056/NEJMoa2204705

Moreau, K., Coen, M., Zhang, A.X., Pachl, F., Castaldi, M.P., Dahl, G., Boyd, H., Scott, C., Newham, P., 2020. Proteolysis-targeting chimeras in drug development: A safety perspective. Br J Pharmacol 177, 1709–1718. https://doi.org/10.1111/bph.15014

Morreale, F.E., Walden, H., 2016. Types of Ubiquitin Ligases. Cell 165, 248-248.e1. https://doi.org/10.1016/j.cell.2016.03.003

Mulder, M.P.C., Witting, K.F., Ovaa, H., 2020. Cracking the Ubiquitin Code: The Ubiquitin Toolbox. Curr Issues Mol Biol 37, 1–20. https://doi.org/10.21775/cimb.037.001

Mullard, A., 2018. Pfizer exits neuroscience. Nature Reviews Drug Discovery 17, 86–86. https://doi.org/10.1038/nrd.2018.16

Münch, C., O'Brien, J., Bertolotti, A., 2011a. Prion-like propagation of mutant superoxide dismutase-1 misfolding in neuronal cells. Proceedings of the National Academy of Sciences 108, 3548–3553. https://doi.org/10.1073/pnas.1017275108

Münch, C., O'Brien, J., Bertolotti, A., 2011b. Prion-like propagation of mutant superoxide dismutase-1 misfolding in neuronal cells. Proc Natl Acad Sci U S A 108, 3548–3553. https://doi.org/10.1073/pnas.1017275108

Muyldermans, S., 2021. A guide to: generation and design of nanobodies. FEBS J 288, 2084–2102. https://doi.org/10.1111/febs.15515

Neklesa, T., Snyder, L.B., Willard, R.R., Vitale, N., Pizzano, J., Gordon, D.A., Bookbinder, M., Macaluso, J., Dong, H., Ferraro, C., Wang, G., Wang, J., Crews, C.M., Houston, J., Crew, A.P., Taylor, I., 2019. ARV-110: An oral

androgen receptor PROTAC degrader for prostate cancer. JCO 37, 259–259. https://doi.org/10.1200/JCO.2019.37.7_suppl.259

Neklesa, T.K., Winkler, J.D., Crews, C.M., 2017. Targeted protein degradation by PROTACs. Pharmacology & Therapeutics 174, 138–144. https://doi.org/10.1016/j.pharmthera.2017.02.027

Nemani, V.M., Lu, W., Berge, V., Nakamura, K., Onoa, B., Lee, M.K., Chaudhry, F.A., Nicoll, R.A., Edwards, R.H., 2010. Increased expression of alpha-synuclein reduces neurotransmitter release by inhibiting synaptic vesicle reclustering after endocytosis. Neuron 65, 66–79. https://doi.org/10.1016/j.neuron.2009.12.023

Nieba, L., Honegger, A., Krebber, C., Plückthun, A., 1997. Disrupting the hydrophobic patches at the antibody variable/constant domain interface: improved in vivo folding and physical characterization of an engineered scFv fragment. Protein Eng 10, 435–444. https://doi.org/10.1093/protein/10.4.435

Notkins, A.L., 2004. Polyreactivity of antibody molecules. Trends in Immunology 25, 174–179. https://doi.org/10.1016/j.it.2004.02.004

O'Shea, C.M., Shahzad, R., Aghasoleimani, K., Newman, S., Panmanee, J., Schalkwyk, L.C., Brooke, G.N., Benson, F.E., Trimmer, J.S., Bosco, D.A., Fujisawa, T., Ichijo, H., Cashman, N.R., Engel, S., Wright, G.S.A., 2025. Reliable repurposing of the antibody interactome inside the cell. https://doi.org/10.1101/2025.11.16.688718

Pagano, G., Boess, F.G., Taylor, K.I., Ricci, B., Mollenhauer, B., Poewe, W., Boulay, A., Anzures-Cabrera, J., Vogt, A., Marchesi, M., Post, A., Nikolcheva, T., Kinney, G.G., Zago, W.M., Ness, D.K., Svoboda, H., Britschgi, M., Ostrowitzki, S., Simuni, T., Marek, K., Koller, M., Sevigny, J., Doody, R., Fontoura, P.,

Umbricht, D., Bonni, A., PASADENA Investigators, Prasinezumab Study Group, 2021. A Phase II Study to Evaluate the Safety and Efficacy of Prasinezumab in Early Parkinson's Disease (PASADENA): Rationale, Design, and Baseline Data. Front Neurol 12, 705407. https://doi.org/10.3389/fneur.2021.705407

Pagano, G., Taylor, K.I., Anzures Cabrera, J., Simuni, T., Marek, K., Postuma, R.B., Pavese, N., Stocchi, F., Brockmann, K., Svoboda, H., Trundell, D., Monnet, A., Doody, R., Fontoura, P., Kerchner, G.A., Brundin, P., Nikolcheva, T., Bonni, A., 2024. Prasinezumab slows motor progression in rapidly progressing early-stage Parkinson's disease. Nat Med 30, 1096–1103. https://doi.org/10.1038/s41591-024-02886-y

Pagano, G., Taylor, K.I., Anzures-Cabrera, J., Marchesi, M., Simuni, T., Marek, K., Postuma, R.B., Pavese, N., Stocchi, F., Azulay, J.-P., Mollenhauer, B., López-Manzanares, L., Russell, D.S., Boyd, J.T., Nicholas, A.P., Luquin, M.R., Hauser, R.A., Gasser, T., Poewe, W., Ricci, B., Boulay, A., Vogt, A., Boess, F.G., Dukart, J., D'Urso, G., Finch, R., Zanigni, S., Monnet, A., Pross, N., Hahn, A., Svoboda, H., Britschgi, M., Lipsmeier, F., Volkova-Volkmar, E., Lindemann, M., Dziadek, S., Holiga, Š., Rukina, D., Kustermann, T., Kerchner, G.A., Fontoura, P., Umbricht, D., Doody, R., Nikolcheva, T., Bonni, A., 2022. Trial of Prasinezumab in Early-Stage Parkinson's Disease. New England Journal of Medicine 387, 421–432. https://doi.org/10.1056/NEJMoa2202867

Paiva, S.-L., Crews, C.M., 2019. Targeted protein degradation: elements of PROTAC design. Curr Opin Chem Biol 50, 111–119. https://doi.org/10.1016/j.cbpa.2019.02.022

Pan, J.-A., Ullman, E., Dou, Z., Zong, W.-X., 2011. Inhibition of Protein Degradation Induces Apoptosis through a Microtubule-Associated Protein 1 Light Chain 3-Mediated Activation of Caspase-8 at Intracellular Membranes ▿. Mol Cell Biol 31, 3158–3170. https://doi.org/10.1128/MCB.05460-11

Paré, B., Lehmann, M., Beaudin, M., Nordström, U., Saikali, S., Julien, J.-P., Gilthorpe, J.D., Marklund, S.L., Cashman, N.R., Andersen, P.M., Forsberg, K., Dupré, N., Gould, P., Brännström, T., Gros-Louis, F., 2018. Misfolded SOD1 pathology in sporadic Amyotrophic Lateral Sclerosis. Sci Rep 8, 14223. https://doi.org/10.1038/s41598-018-31773-z

Park, D., Izaguirre, J., Coffey, R., Xu, H., 2022. Modeling the Effect of Cooperativity in Ternary Complex Formation and Targeted Protein Degradation Mediated by Heterobifunctional Degraders. ACS Bio Med Chem Au 3, 74–86. https://doi.org/10.1021/acsbiomedchemau.2c00037

Parzych, K.R., Klionsky, D.J., 2014. An Overview of Autophagy: Morphology, Mechanism, and Regulation. Antioxid Redox Signal 20, 460–473. https://doi.org/10.1089/ars.2013.5371

Pei, J., Pan, X., Wang, A., Shuai, W., Bu, F., Tang, P., Zhang, S., Zhang, Y., Wang, G., Ouyang, L., 2021. Developing potent LC3-targeting AUTAC tools for protein degradation with selective autophagy. Chem. Commun. 57, 13194–13197. https://doi.org/10.1039/D1CC04661F

Periquet, M., Fulga, T., Myllykangas, L., Schlossmacher, M.G., Feany, M.B., 2007. Aggregated α-Synuclein Mediates Dopaminergic Neurotoxicity In Vivo. J. Neurosci. 27, 3338–3346. https://doi.org/10.1523/JNEUROSCI.0285-07.2007

Pettersson, M., Crews, C.M., 2019. PROteolysis TArgeting Chimeras (PROTACs) - Past, present and future. Drug Discov Today Technol 31, 15–27. https://doi.org/10.1016/j.ddtec.2019.01.002

Pickles, S., Semmler, S., Broom, H.R., Destroismaisons, L., Legroux, L., Arbour, N., Meiering, E., Cashman, N.R., Vande Velde, C., 2016. ALS-linked misfolded SOD1 species have divergent impacts on mitochondria. Acta Neuropathol Commun 4, 43. https://doi.org/10.1186/s40478-016-0313-8

Polonelli, L., Pontón, J., Elguezabal, N., Moragues, M.D., Casoli, C., Pilotti, E., Ronzi, P., Dobroff, A.S., Rodrigues, E.G., Juliano, M.A., Maffei, D.L., Magliani, W., Conti, S., Travassos, L.R., 2008. Antibody Complementarity-Determining Regions (CDRs) Can Display Differential Antimicrobial, Antiviral and Antitumor Activities. PLoS One 3, e2371. https://doi.org/10.1371/journal.pone.0002371

Polymeropoulos, M.H., Lavedan, C., Leroy, E., Ide, S.E., Dehejia, A., Dutra, A., Pike, B., Root, H., Rubenstein, J., Boyer, R., Stenroos, E.S., Chandrasekharappa, S., Athanassiadou, A., Papapetropoulos, T., Johnson, W.G., Lazzarini, A.M., Duvoisin, R.C., Di Iorio, G., Golbe, L.I., Nussbaum, R.L., 1997. Mutation in the alpha-synuclein gene identified in families with Parkinson's disease. Science 276, 2045–2047. https://doi.org/10.1126/science.276.5321.2045

Pondal, M., Marras, C., Miyasaki, J., Moro, E., Armstrong, M.J., Strafella, A.P., Shah, B.B., Fox, S., Prashanth, L.K., Phielipp, N., Lang, A.E., 2013. Clinical features of dopamine agonist withdrawal syndrome in a movement disorders clinic. J Neurol Neurosurg Psychiatry 84, 130–135. https://doi.org/10.1136/jnnp-2012-302684

Potjewyd, F.M., Axtman, A.D., 2021. Exploration of Aberrant E3 Ligases Implicated in Alzheimer's Disease and Development of Chemical Tools to Modulate Their

Function. Front Cell Neurosci 15, 768655. https://doi.org/10.3389/fncel.2021.768655

Powell, J.E., Lim, C.K.W., Krishnan, R., McCallister, T.X., Saporito-Magriña, C., Zeballos, M.A., McPheron, G.D., Gaj, T., 2022. Targeted gene silencing in the nervous system with CRISPR-Cas13. Sci Adv 8, eabk2485. https://doi.org/10.1126/sciadv.abk2485

Prell, T., Lautenschläger, J., Witte, O.W., Carri, M.T., Grosskreutz, J., 2012. The unfolded protein response in models of human mutant G93A amyotrophic lateral sclerosis. European Journal of Neuroscience 35, 652–660. https://doi.org/10.1111/j.1460-9568.2012.08008.x

Proba, K., Wörn, A., Honegger, A., Plückthun, A., 1998. Antibody scFv fragments without disulfide bonds made by molecular evolution. J Mol Biol 275, 245–253. https://doi.org/10.1006/jmbi.1997.1457

Proba, Karl, Wörn, A., Honegger, A., Plückthun, A., 1998. Antibody scFv fragments without disulfide bonds, made by molecular evolution1. Journal of Molecular Biology 275, 245–253. https://doi.org/10.1006/jmbi.1997.1457

Proctor, E.A., Fee, L., Tao, Y., Redler, R.L., Fay, J.M., Zhang, Y., Lv, Z., Mercer, I.P., Deshmukh, M., Lyubchenko, Y.L., Dokholyan, N.V., 2016. Nonnative SOD1 trimer is toxic to motor neurons in a model of amyotrophic lateral sclerosis. Proc Natl Acad Sci U S A 113, 614–619. https://doi.org/10.1073/pnas.1516725113

Rambacher, K.M., Calabrese, M.F., Yamaguchi, M., 2021. Perspectives on the development of first-in-class protein degraders. Future Med Chem 13, 1203–1226. https://doi.org/10.4155/fmc-2021-0033

Rana, A., Nikam, T., Sreepathi, B., Saraf, S.A., Awasthi, S., 2025. The Aggregation Continuum of α-Synuclein and Its Relevance to Brain Aging. ACS Chem. Neurosci. 16, 3634–3652. https://doi.org/10.1021/acschemneuro.5c00356

Rechsteiner, M., Rogers, S.W., 1996. PEST sequences and regulation by proteolysis. Trends Biochem Sci 21, 267–271.

Reuten, R., Nikodemus, D., Oliveira, M.B., Patel, T.R., Brachvogel, B., Breloy, I., Stetefeld, J., Koch, M., 2016. Maltose-Binding Protein (MBP), a Secretion-Enhancing Tag for Mammalian Protein Expression Systems. PLoS One 11, e0152386. https://doi.org/10.1371/journal.pone.0152386

Riching, K.M., Mahan, S., Corona, C.R., McDougall, M., Vasta, J.D., Robers, M.B., Urh, M., Daniels, D.L., 2018. Quantitative Live-Cell Kinetic Degradation and Mechanistic Profiling of PROTAC Mode of Action. ACS Chem. Biol. 13, 2758–2770. https://doi.org/10.1021/acschembio.8b00692

Rinaldi, C., Wood, M.J.A., 2018. Antisense oligonucleotides: the next frontier for treatment of neurological disorders. Nat Rev Neurol 14, 9–21. https://doi.org/10.1038/nrneurol.2017.148

Rotunno, M.S., Auclair, J.R., Maniatis, S., Shaffer, S.A., Agar, J., Bosco, D.A., 2014. Identification of a Misfolded Region in Superoxide Dismutase 1 That Is Exposed in Amyotrophic Lateral Sclerosis. The Journal of Biological Chemistry 289, 28527. https://doi.org/10.1074/jbc.M114.581801

Rousseau, A., Bertolotti, A., 2018. Regulation of proteasome assembly and activity in health and disease. Nat Rev Mol Cell Biol 19, 697–712. https://doi.org/10.1038/s41580-018-0040-z

Rowland, L.P., Shneider, N.A., 2001. Amyotrophic lateral sclerosis. N Engl J Med 344, 1688–1700. https://doi.org/10.1056/NEJM200105313442207

Saez, I., Vilchez, D., 2014. The Mechanistic Links Between Proteasome Activity, Aging and Age-related Diseases. Curr Genomics 15, 38–51. https://doi.org/10.2174/1389202915011403061133 44

Safdari, Y., 2018. Engineering of single chain antibodies for solubility. International Immunopharmacology 55, 86–97. https://doi.org/10.1016/j.intimp.2017.11.046

Saibil, H., 2013. Chaperone machines for protein folding, unfolding and disaggregation. Nat Rev Mol Cell Biol 14, 630–642. https://doi.org/10.1038/nrm3658

Sakamoto, K.M., Kim, K.B., Kumagai, A., Mercurio, F., Crews, C.M., Deshaies, R.J., 2001. Protacs: chimeric molecules that target proteins to the Skp1-Cullin-F box complex for ubiquitination and degradation. Proc Natl Acad Sci U S A 98, 8554–8559. https://doi.org/10.1073/pnas.141230798

Sala, F.A., Wright, G.S.A., Antonyuk, S.V., Garratt, R.C., Hasnain, S.S., 2019. Molecular recognition and maturation of SOD1 by its evolutionarily destabilised cognate chaperone hCCS. PLOS Biology 17, e3000141. https://doi.org/10.1371/journal.pbio.3000141

Salat, D., Tolosa, E., 2013. Levodopa in the treatment of Parkinson's disease: current status and new developments. J Parkinsons Dis 3, 255–269. https://doi.org/10.3233/JPD-130186

Sanderson, J.B., De, S., Jiang, H., Rovere, M., Jin, M., Zaccagnini, L., Hays Watson, A., De Boni, L., Lagomarsino, V.N., Young-Pearse, T.L., Liu, X., Pochapsky, T.C., Hyman, B.T., Dickson, D.W., Klenerman, D., Selkoe, D.J., Bartels, T., 2020. Analysis of α-synuclein species enriched from cerebral cortex of humans with sporadic dementia with Lewy bodies. Brain Commun 2, fcaa010. https://doi.org/10.1093/braincomms/fcaa010

Sandomenico, A., Sivaccumar, J.P., Ruvo, M., 2020. Evolution of Escherichia coli Expression System in Producing Antibody Recombinant Fragments. Int J Mol Sci 21, 6324. https://doi.org/10.3390/ijms21176324

Sangwan, S., Zhao, A., Adams, K.L., Jayson, C.K., Sawaya, M.R., Guenther, E.L., Pan, A.C., Ngo, J., Moore, D.M., Soriaga, A.B., Do, T.D., Goldschmidt, L., Nelson, R., Bowers, M.T., Koehler, C.M., Shaw, D.E., Novitch, B.G., Eisenberg, D.S., 2017. Atomic structure of a toxic, oligomeric segment of SOD1 linked to amyotrophic lateral sclerosis (ALS). Proc Natl Acad Sci U S A 114, 8770–8775. https://doi.org/10.1073/pnas.1705091114

Sato, H., Arawaka, S., Hara, S., Fukushima, S., Koga, K., Koyama, S., Kato, T., 2011. Authentically Phosphorylated α-Synuclein at Ser129 Accelerates Neurodegeneration in a Rat Model of Familial Parkinson's Disease. J Neurosci 31, 16884–16894. https://doi.org/10.1523/JNEUROSCI.3967-11.2011

Sau, D., De Biasi, S., Vitellaro-Zuccarello, L., Riso, P., Guarnieri, S., Porrini, M., Simeoni, S., Crippa, V., Onesto, E., Palazzolo, I., Rusmini, P., Bolzoni, E., Bendotti, C., Poletti, A., 2007. Mutation of SOD1 in ALS: a gain of a loss of function. Hum Mol Genet 16, 1604–1618. https://doi.org/10.1093/hmg/ddm110

Saxena, S., Cabuy, E., Caroni, P., 2009. A role for motoneuron subtype-selective ER stress in disease manifestations of FALS mice. Nat Neurosci 12, 627–636. https://doi.org/10.1038/nn.2297

Schaefer, J.V., Plückthun, A., 2012. Transfer of engineered biophysical properties between different antibody formats and expression systems. Protein Eng Des Sel 25, 485–506. https://doi.org/10.1093/protein/gzs039

Schneekloth, J.S.Jr., Fonseca, F.N., Koldobskiy, M., Mandal, A., Deshaies, R., Sakamoto, K., Crews, C.M., 2004. Chemical Genetic Control of Protein Levels:

Selective in Vivo Targeted Degradation. J. Am. Chem. Soc. 126, 3748–3754. https://doi.org/10.1021/ja039025z

Schröder, H., Langer, T., Hartl, F.U., Bukau, B., 1993. DnaK, DnaJ and GrpE form a cellular chaperone machinery capable of repairing heat-induced protein damage. EMBO J 12, 4137–4144. https://doi.org/10.1002/j.1460-2075.1993.tb06097.x

Seo, M.J., Jeong, K.J., Leysath, C.E., Ellington, A.D., Iverson, B.L., Georgiou, G., 2009. Engineering antibody fragments to fold in the absence of disulfide bonds. Protein Sci 18, 259–267. https://doi.org/10.1002/pro.31

Shaki-Loewenstein, S., Zfania, R., Hyland, S., Wels, W.S., Benhar, I., 2005. A universal strategy for stable intracellular antibodies. Journal of Immunological Methods 303, 19–39. https://doi.org/10.1016/j.jim.2005.05.004

Shaw, K.L., Grimsley, G.R., Yakovlev, G.I., Makarov, A.A., Pace, C.N., 2001. The effect of net charge on the solubility, activity, and stability of ribonuclease Sa. Protein Sci 10, 1206–1215. https://doi.org/10.1110/ps.440101

Shaw, P.J., Tomkins, J., Slade, J.Y., Usher, P., Curtis, A., Bushby, K., Ince, P.G., 1997. CNS tissue Cu/Zn superoxide dismutase (SOD1) mutations in motor neurone disease (MND). Neuroreport 8, 3923–3927. https://doi.org/10.1097/00001756-199712220-00016

Shi, S., Li, L., Chen, K., Liu, X., 2004. [Identification of the mutation of SOD1 gene in a familial amyotrophic lateral sclerosis]. Zhonghua Yi Xue Yi Chuan Xue Za Zhi 21, 149–152.

Sievers, Q.L., Petzold, G., Bunker, R.D., Renneville, A., Słabicki, M., Liddicoat, B.J., Abdulrahman, W., Mikkelsen, T., Ebert, B.L., Thomä, N.H., 2018. Defining the

human C2H2 zinc finger degrome targeted by thalidomide analogs through CRBN. Science 362, eaat0572. https://doi.org/10.1126/science.aat0572

Sinha, R.A., Singh, B.K., Yen, P.M., 2017. Reciprocal Crosstalk Between Autophagic and Endocrine Signaling in Metabolic Homeostasis. Endocr Rev 38, 69–102. https://doi.org/10.1210/er.2016-1103

Snyder, L.B., Neklesa, T.K., Willard, R.R., Gordon, D.A., Pizzano, J., Vitale, N., Robling, K., Dorso, M.A., Moghrabi, W., Landrette, S., Gedrich, R., Lee, S.H., Taylor, I.C.A., Houston, J.G., 2025. Preclinical Evaluation of Bavdegalutamide (ARV-110), a Novel PROteolysis TArgeting Chimera Androgen Receptor Degrader. Mol Cancer Ther 24, 511–522. https://doi.org/10.1158/1535-7163.MCT-23-0655

Spillantini, M.G., Crowther, R.A., Jakes, R., Hasegawa, M., Goedert, M., 1998a. α-Synuclein in filamentous inclusions of Lewy bodies from Parkinson's disease and dementia with Lewy bodies. Proc Natl Acad Sci U S A 95, 6469–6473. https://doi.org/10.1073/pnas.95.11.6469

Spillantini, M.G., Crowther, R.A., Jakes, R., Hasegawa, M., Goedert, M., 1998b. α-Synuclein in filamentous inclusions of Lewy bodies from Parkinson's disease and dementia with Lewy bodies. Proc Natl Acad Sci U S A 95, 6469–6473. https://doi.org/10.1073/pnas.95.11.6469

Spillantini, M.G., Schmidt, M.L., Lee, V.M.-Y., Trojanowski, J.Q., Jakes, R., Goedert, M., 1997. α-Synuclein in Lewy bodies. Nature 388, 839–840. https://doi.org/10.1038/42166

Stephens, A.D., Zacharopoulou, M., Moons, R., Fusco, G., Seetaloo, N., Chiki, A., Woodhams, P.J., Mela, I., Lashuel, H.A., Phillips, J.J., De Simone, A., Sobott, F., Schierle, G.S.K., 2020. Extent of N-terminus exposure of monomeric alpha-

synuclein determines its aggregation propensity. Nat Commun 11, 2820. https://doi.org/10.1038/s41467-020-16564-3

Su, D., Cui, Y., He, C., Yin, P., Bai, R., Zhu, J., Lam, J.S.T., Zhang, J., Yan, R., Zheng, X., Wu, J., Zhao, D., Wang, A., Zhou, M., Feng, T., 2025. Projections for prevalence of Parkinson's disease and its driving factors in 195 countries and territories to 2050: modelling study of Global Burden of Disease Study 2021. BMJ 388, e080952. https://doi.org/10.1136/bmj-2024-080952

Sun, K., Liao, M.Z., 2022. Clinical Pharmacology Considerations on Recombinant Adeno-Associated Virus–Based Gene Therapy. The Journal of Clinical Pharmacology 62, S79–S94. https://doi.org/10.1002/jcph.2141

Sun, W., Xie, J., Lin, H., Mi, S., Li, Z., Hua, F., Hu, Z., 2012. A combined strategy improves the solubility of aggregation-prone single-chain variable fragment antibodies. Protein Expression and Purification 83, 21–29. https://doi.org/10.1016/j.pep.2012.02.006

Sun, Y., Hou, S., Zhao, K., Long, H., Liu, Z., Gao, J., Zhang, Y., Su, X.-D., Li, D., Liu, C., 2020. Cryo-EM structure of full-length α-synuclein amyloid fibril with Parkinson's disease familial A53T mutation. Cell Res 30, 360–362. https://doi.org/10.1038/s41422-020-0299-4

Sung, V.W., Nicholas, A.P., 2013. Nonmotor symptoms in Parkinson's disease: expanding the view of Parkinson's disease beyond a pure motor, pure dopaminergic problem. Neurol Clin 31, S1-16. https://doi.org/10.1016/j.ncl.2013.04.013

Takahashi, D., Arimoto, H., 2021. Selective autophagy as the basis of autophagy-based degraders. Cell Chem Biol 28, 1061–1071. https://doi.org/10.1016/j.chembiol.2021.05.006

Takahashi, D., Moriyama, J., Nakamura, T., Miki, E., Takahashi, E., Sato, A., Akaike, T., Itto-Nakama, K., Arimoto, H., 2019. AUTACs: Cargo-Specific Degraders Using Selective Autophagy. Mol Cell 76, 797-810.e10. https://doi.org/10.1016/j.molcel.2019.09.009

Tan, P.H., Chu, V., Stray, J.E., Hamlin, D.K., Pettit, D., Wilbur, D.S., Vessella, R.L., Stayton, P.S., 1998. Engineering the isoelectric point of a renal cell carcinoma targeting antibody greatly enhances scFv solubility. Immunotechnology 4, 107–114. https://doi.org/10.1016/s1380-2933(98)00011-6

Tanaka, T., Rabbitts, T.H., 2008. Functional intracellular antibody fragments do not require invariant intra-domain disulfide bonds. J Mol Biol 376, 749–757. https://doi.org/10.1016/j.jmb.2007.11.085

Taylor, J.P., Brown, R.H., Cleveland, D.W., 2016. Decoding ALS: from genes to mechanism. Nature 539, 197–206. https://doi.org/10.1038/nature20413

Teillaud, J.L., Desaymard, C., Giusti, A.M., Haseltine, B., Pollock, R.R., Yelton, D.E., Zack, D.J., Scharff, M.D., 1983. Monoclonal antibodies reveal the structural basis of antibody diversity. Science 222, 721–726. https://doi.org/10.1126/science.6356353

Thirumalai, D., Lorimer, G.H., 2001. Chaperonin-mediated protein folding. Annu Rev Biophys Biomol Struct 30, 245–269. https://doi.org/10.1146/annurev.biophys.30.1.245

Thomas, P., Smart, T.G., 2005. HEK293 cell line: a vehicle for the expression of recombinant proteins. J Pharmacol Toxicol Methods 51, 187–200. https://doi.org/10.1016/j.vascn.2004.08.014

Tomoshige, S., Ishikawa, M., 2021. PROTACs and Other Chemical Protein Degradation Technologies for the Treatment of Neurodegenerative Disorders.

Angewandte Chemie International Edition 60, 3346–3354. https://doi.org/10.1002/anie.202004746

Tomoshige, S., Nomura, S., Ohgane, K., Hashimoto, Y., Ishikawa, M., 2017. Discovery of Small Molecules that Induce the Degradation of Huntingtin. Angew Chem Int Ed Engl 56, 11530–11533. https://doi.org/10.1002/anie.201706529

Troup, R.I., Fallan, C., Baud, M.G.J., 2020. Current strategies for the design of PROTAC linkers: a critical review. Explor Target Antitumor Ther 1, 273–312. https://doi.org/10.37349/etat.2020.00018

Urushitani, M., Kurisu, J., Tateno, M., Hatakeyama, S., Nakayama, K.-I., Kato, S., Takahashi, R., 2004. CHIP promotes proteasomal degradation of familial ALS-linked mutant SOD1 by ubiquitinating Hsp/Hsc70. Journal of Neurochemistry 90, 231–244. https://doi.org/10.1111/j.1471-4159.2004.02486.x

Valente, E.M., Abou-Sleiman, P.M., Caputo, V., Muqit, M.M.K., Harvey, K., Gispert, S., Ali, Z., Del Turco, D., Bentivoglio, A.R., Healy, D.G., Albanese, A., Nussbaum, R., González-Maldonado, R., Deller, T., Salvi, S., Cortelli, P., Gilks, W.P., Latchman, D.S., Harvey, R.J., Dallapiccola, B., Auburger, G., Wood, N.W., 2004. Hereditary early-onset Parkinson's disease caused by mutations in PINK1. Science 304, 1158–1160. https://doi.org/10.1126/science.1096284

Van Bulck, M., Sierra-Magro, A., Alarcon-Gil, J., Perez-Castillo, A., Morales-Garcia, J.A., 2019. Novel Approaches for the Treatment of Alzheimer's and Parkinson's Disease. Int J Mol Sci 20, 719. https://doi.org/10.3390/ijms20030719

van Rooijen, B.D., Claessens, M.M.A.E., Subramaniam, V., 2010. Membrane Permeabilization by Oligomeric α-Synuclein: In Search of the Mechanism. PLoS One 5, e14292. https://doi.org/10.1371/journal.pone.0014292

Vande Velde, C., Miller, T.M., Cashman, N.R., Cleveland, D.W., 2008. Selective association of misfolded ALS-linked mutant SOD1 with the cytoplasmic face of mitochondria. Proc Natl Acad Sci U S A 105, 4022–4027. https://doi.org/10.1073/pnas.0712209105

Varshavsky, A., 2019. N-degron and C-degron pathways of protein degradation. Proc Natl Acad Sci U S A 116, 358–366. https://doi.org/10.1073/pnas.1816596116

Vasta, R., De Mattei, F., Tafaro, S., Canosa, A., Manera, U., Grassano, M., Palumbo, F., Cabras, S., Matteoni, E., Di Pede, F., Zocco, G., Pellegrino, G., Minerva, E., Pascariu, D., Iazzolino, B., Callegaro, S., Fuda, G., Salamone, P., De Marchi, F., Mazzini, L., Moglia, C., Calvo, A., Chiò, A., 2025. Changes to Average Survival of Patients With Amyotrophic Lateral Sclerosis (1995–2018). Neurology 104, e213467. https://doi.org/10.1212/WNL.0000000000213467

Veisi, K., Farajnia, S., Zarghami, N., Khoram Khorshid, H.R., Samadi, N., Ahdi Khosroshahi, S., Zarei Jaliani, H., 2015. Chaperone-Assisted Soluble Expression of a Humanized Anti-EGFR ScFv Antibody in E. Coli. Adv Pharm Bull 5, 621–627. https://doi.org/10.15171/apb.2015.084

Vetma, V., Casarez-Perez, L., Eliaš, J., Stingu, A., Kombara, A., Gmaschitz, T., Braun, N., Ciftci, T., Dahmann, G., Diers, E., Gerstberger, T., Greb, P., Kidd, G., Kofink, C., Puoti, I., Spiteri, V., Trainor, N., Westermaier, Y., Whitworth, C., Ciulli, A., Farnaby, W., McAulay, K., Frost, A.B., Chessum, N., Koegl, M., 2024. Confounding factors in targeted degradation of short-lived proteins. https://doi.org/10.1101/2024.02.19.581012

Vidović, M., Rikalovic, M.G., 2022. Alpha-Synuclein Aggregation Pathway in Parkinson's Disease: Current Status and Novel Therapeutic Approaches. Cells 11, 1732. https://doi.org/10.3390/cells11111732

Vincow, E.S., Merrihew, G., Thomas, R.E., Shulman, N.J., Beyer, R.P., MacCoss, M.J., Pallanck, L.J., 2013. The PINK1–Parkin pathway promotes both mitophagy and selective respiratory chain turnover in vivo. Proc Natl Acad Sci U S A 110, 6400–6405. https://doi.org/10.1073/pnas.1221132110

Vogiatzis, S., Celestino, M., Trevisan, M., Magro, G., Del Vecchio, C., Erdengiz, D., Palù, G., Parolin, C., Maguire-Zeiss, K., Calistri, A., 2021. Lentiviral Vectors Expressing Chimeric NEDD4 Ubiquitin Ligases: An Innovative Approach for Interfering with Alpha-Synuclein Accumulation. Cells 10, 3256. https://doi.org/10.3390/cells10113256

Wakabayashi, K., Hayashi, S., Yoshimoto, M., Kudo, H., Takahashi, H., 2000. NACP/α-synuclein-positive filamentous inclusions in astrocytes and oligodendrocytes of Parkinson's disease brains. Acta Neuropathol 99, 14–20. https://doi.org/10.1007/PL00007400

Wang, C., Zheng, C., Wang, H., Zhang, L., Liu, Z., Xu, P., 2022. The state of the art of PROTAC technologies for drug discovery. Eur J Med Chem 235, 114290. https://doi.org/10.1016/j.ejmech.2022.114290

Wang, J., Zhang, M., Liu, S., He, Z., Wang, R., Liang, M., An, Y., Jiang, C., Song, C., Ning, Z., Yin, F., Huang, H., Li, Z., Ye, Y., 2023. Targeting UBE2C for degradation by bioPROTACs based on bacterial E3 ligase. Chinese Chemical Letters 34, 107732. https://doi.org/10.1016/j.cclet.2022.08.012

Wang, Q., Johnson, J.L., Agar, N.Y.R., Agar, J.N., 2008. Protein Aggregation and Protein Instability Govern Familial Amyotrophic Lateral Sclerosis Patient Survival. PLOS Biology 6, e170. https://doi.org/10.1371/journal.pbio.0060170

Wang, T., Badran, A.H., Huang, T.P., Liu, D.R., 2018. Continuous directed evolution of proteins with improved soluble expression. Nat Chem Biol 14, 972–980. https://doi.org/10.1038/s41589-018-0121-5

Wang, W., Perovic, I., Chittuluru, J., Kaganovich, A., Nguyen, L.T.T., Liao, J., Auclair, J.R., Johnson, D., Landeru, A., Simorellis, A.K., Ju, S., Cookson, M.R., Asturias, F.J., Agar, J.N., Webb, B.N., Kang, C., Ringe, D., Petsko, G.A., Pochapsky, T.C., Hoang, Q.Q., 2011. A soluble α-synuclein construct forms a dynamic tetramer. Proc. Natl. Acad. Sci. U.S.A. 108, 17797–17802. https://doi.org/10.1073/pnas.1113260108

Wang, W., Zhou, Q., Jiang, T., Li, S., Ye, J., Zheng, J., Wang, X., Liu, Y., Deng, M., Ke, D., Wang, Q., Wang, Y., Wang, J.-Z., 2021. A novel small-molecule PROTAC selectively promotes tau clearance to improve cognitive functions in Alzheimer-like models. Theranostics 11, 5279–5295. https://doi.org/10.7150/thno.55680

Wang, Y., Yuan, W., Guo, S., Li, Q., Chen, X., Li, C., Liu, Q., Sun, L., Chen, Z., Yuan, Z., Luo, C., Chen, S., Tong, S., Nassal, M., Wen, Y.-M., Wang, Y.-X., 2022. A 33-residue peptide tag increases solubility and stability of Escherichia coli produced single-chain antibody fragments. Nat Commun 13, 4614. https://doi.org/10.1038/s41467-022-32423-9

Webb, J.L., Ravikumar, B., Atkins, J., Skepper, J.N., Rubinsztein, D.C., 2003. Alpha-Synuclein is degraded by both autophagy and the proteasome. J Biol Chem 278, 25009–25013. https://doi.org/10.1074/jbc.M300227200

Weihofen, A., Liu, Y., Arndt, J.W., Huy, C., Quan, C., Smith, B.A., Baeriswyl, J.-L., Cavegn, N., Senn, L., Su, L., Marsh, G., Auluck, P.K., Montrasio, F., Nitsch, R.M., Hirst, W.D., Cedarbaum, J.M., Pepinsky, R.B., Grimm, J., Weinreb, P.H.,

2019. Development of an aggregate-selective, human-derived α-synuclein antibody BIIB054 that ameliorates disease phenotypes in Parkinson's disease models. Neurobiol Dis 124, 276–288. https://doi.org/10.1016/j.nbd.2018.10.016

Wenzhi, Y., Xiangyi, L., Dongsheng, F., 2024. The prion-like effect and prion-like protein targeting strategy in amyotrophic lateral sclerosis. Heliyon 10, e34963. https://doi.org/10.1016/j.heliyon.2024.e34963

Winslow, A.R., Chen, C.-W., Corrochano, S., Acevedo-Arozena, A., Gordon, D.E., Peden, A.A., Lichtenberg, M., Menzies, F.M., Ravikumar, B., Imarisio, S., Brown, S., O'Kane, C.J., Rubinsztein, D.C., 2010. α-Synuclein impairs macroautophagy: implications for Parkinson's disease. J Cell Biol 190, 1023–1037. https://doi.org/10.1083/jcb.201003122

Wong, P., Li, L., Chea, J., Delgado, M.K., Crow, D., Poku, E., Szpikowska, B., Bowles, N., Channappa, D., Colcher, D., Wong, J.Y.C., Shively, J.E., Yazaki, P.J., 2017. PET imaging of 64Cu-DOTA-scFv-anti-PSMA lipid nanoparticles (LNPs): Enhanced tumor targeting over anti-PSMA scFv or untargeted LNPs. Nucl Med Biol 47, 62–68. https://doi.org/10.1016/j.nucmedbio.2017.01.004

Wörn, A., Plückthun, A., 2001. Stability engineering of antibody single-chain Fv fragments. J Mol Biol 305, 989–1010. https://doi.org/10.1006/jmbi.2000.4265

Wörn, A., Plückthun, A., 1998a. Mutual stabilization of VL and VH in single-chain antibody fragments, investigated with mutants engineered for stability. Biochemistry 37, 13120–13127. https://doi.org/10.1021/bi980712q

Wörn, A., Plückthun, A., 1998b. An intrinsically stable antibody scFv fragment can tolerate the loss of both disulfide bonds and fold correctly. FEBS Lett 427, 357–361. https://doi.org/10.1016/s0014-5793(98)00463-3

Xiao, B., Tan, E.-K., 2025. Prasinezumab slows motor progression in Parkinsons disease: beyond the clinical data. npj Parkinsons Dis. 11, 31. https://doi.org/10.1038/s41531-025-00886-4

Xu, J.L., Davis, M.M., 2000. Diversity in the CDR3 region of V(H) is sufficient for most antibody specificities. Immunity 13, 37–45. https://doi.org/10.1016/s1074-7613(00)00006-6

Yamamoto, A., Tagawa, Y., Yoshimori, T., Moriyama, Y., Masaki, R., Tashiro, Y., 1998. Bafilomycin A1 prevents maturation of autophagic vacuoles by inhibiting fusion between autophagosomes and lysosomes in rat hepatoma cell line, H-4-II-E cells. Cell Struct Funct 23, 33–42. https://doi.org/10.1247/csf.23.33

Yu, Y., Hu, W., Xu, Y., Xu, H., Gao, J., 2025. Advancements in delivery Systems for Proteolysis-Targeting Chimeras (PROTACs): Overcoming challenges and expanding biomedical applications. Journal of Controlled Release 382, 113719. https://doi.org/10.1016/j.jconrel.2025.113719

Yusakul, G., Sakamoto, S., Pongkitwitoon, B., Tanaka, H., Morimoto, S., 2016. Effect of linker length between variable domains of single chain variable fragment antibody against daidzin on its reactivity. Biosci. Biotechnol. Biochem. 80, 1306–1312. https://doi.org/10.1080/09168451.2016.1156482

Zhang, K., Geddie, M.L., Kohli, N., Kornaga, T., Kirpotin, D.B., Jiao, Y., Rennard, R., Drummond, D.C., Nielsen, U.B., Xu, L., Lugovskoy, A.A., 2015. Comprehensive optimization of a single-chain variable domain antibody fragment as a targeting ligand for a cytotoxic nanoparticle. MAbs 7, 42–52. https://doi.org/10.4161/19420862.2014.985933

Zhang, T., Liu, C., Li, W., Kuang, J., Qiu, X.-Y., Min, L., Zhu, L., 2022. Targeted protein degradation in mammalian cells: A promising avenue toward future. Comput Struct Biotechnol J 20, 5477–5489. https://doi.org/10.1016/j.csbj.2022.09.038

Zhang, Y.-B., Howitt, J., McCorkle, S., Lawrence, P., Springer, K., Freimuth, P., 2004. Protein aggregation during overexpression limited by peptide extensions with large net negative charge. Protein Expression and Purification 36, 207–216. https://doi.org/10.1016/j.pep.2004.04.020

Zhang, Z., Li, Z.-H., Wang, F., Fang, M., Yin, C.-C., Zhou, Z.-Y., Lin, Q., Huang, H.-L., 2002. Overexpression of DsbC and DsbG markedly improves soluble and functional expression of single-chain Fv antibodies in *Escherichia coli*. Protein Expression and Purification 26, 218–228. https://doi.org/10.1016/S1046-5928(02)00502-8

Zhao, H.L., Yao, X.Q., Xue, C., Wang, Y., Xiong, X.H., Liu, Z.M., 2008. Increasing the homogeneity, stability and activity of human serum albumin and interferon-α2b fusion protein by linker engineering. Protein Expression and Purification 61, 73–77. https://doi.org/10.1016/j.pep.2008.04.013

Zhao, J.-X., Yang, L., Gu, Z.-N., Chen, H.-Q., Tian, F.-W., Chen, Y.-Q., Zhang, H., Chen, W., 2010. Stabilization of the Single-Chain Fragment Variable by an Interdomain Disulfide Bond and Its Effect on Antibody Affinity. Int J Mol Sci 12, 1–11. https://doi.org/10.3390/ijms12010001

Zheng, J., Tian, N., Liu, F., Zhang, Y., Su, J., Gao, Y., Deng, M., Wei, L., Ye, J., Li, H., Wang, J.-Z., 2021. A novel dephosphorylation targeting chimera selectively promoting tau removal in tauopathies. Sig Transduct Target Ther 6, 269. https://doi.org/10.1038/s41392-021-00669-2

Zheng, L., 2003. Production of a Functional Catalytic Antibody ScFv-NusA Fusion Protein in Bacterial Cytoplasm. Journal of Biochemistry 133, 577–581. https://doi.org/10.1093/jb/mvg074

Zhu, Y., Duan, C., Lü, L., Gao, H., Zhao, C., Yu, S., Uéda, K., Chan, P., Yang, H., 2011. α-Synuclein overexpression impairs mitochondrial function by associating with adenylate translocator. Int J Biochem Cell Biol 43, 732–741. https://doi.org/10.1016/j.biocel.2011.01.014

Appendices

Appendix 1. Full scFv variable heavy and light domain sequences. CDRS are indicated by underlined text.

Antibody name	Variable heavy domain	Reference
D5E	EVQLLESGGGLVQPGGSLRLSCAAS*GFTFSS* *Y*AMSWVRQAPGKGLEWVSSI*GQKGGG*TEYA DSVKGRFTISRDNSKNTLYLQMNSLRAEDTAV YYCAK*HFENFDY*WGQGTLVTVSSG	Joshi *et al.,* 2012
10H	EVQLLESGGGLVQPGGSLRLSCAAS*GFTFSS* *Y*AMSWVRQAPGKGLEWVSNI*SSAGKGLEWV* *SSIDDSGAS*TYYADSVKGRFTISRDNSKNTLYL QMNSLRAEDTAVYYCAK*DSASFDY*WGQGTLV TVSS	Joshi *et al*., 2012
Syn-O2	EVQLVESGGGLVQPKGSLKLSCAAS*GFTFNT* *Y*AMHWVRQAPGKGLEWVARI*RSKSSNYA*TYY ADSVKDRFTISRDDSQSMLYLQMNNLKTEDTA MYYCVR*PLKWYFDV*WGTGTTVTVSS	Kumar *et al*., 2020
BIIB054	EVQLVESGGGLVEPGGSLRLSCAVS*GFDFEK* *A*WMSWVRQAPGQGLQWVARI*KSTADGGT*TS YAAPVEGRFIISRDDSRNMLYLQMNSLKTEDT AVYYCTS*AH*WGQGTLVTVSSA	Weihofen *et al.,* 2019
PRX002	EVQLVESGGGLVQPGGSLRLSCAAS*GFTFSN* *Y*GMSWVRQAPGKGLEWVASI*SSGGGS*TYYP DNVKGRFTISRDDAKNSLYLQMNSLRAEDTAV YYCAR*GGAGIDY*WGQGTLVTVSSA	Games *et al.,* 2014

	Variable light domain	
D5E	DIQMTQSPSSLSASVGDRVTITC*RASQSISSYL N*WYQQKPGKAPKLLIY*AASHLQS*GVPSRFSG SGSGTDFTLTISSLQPEDFATYYC*QQTRRPPS T*FGQGTKVEIK	Joshi *et al.,* 2012
10H	TDIQMTQSPSSLSASVGDRVTITC*RASQSISSY LN*WYQQKPGKAPKLLIY*TASSLQS*GVPSRFSG SGSGTDFTLTISSLQPEDFATYYC*QQSAASPS T*FGQGTKVEIKR	Joshi *et al*., 2012
Syn-O2	QIVLTQSPAILSASPGEKVTMTC*SASSTVNY*M HWYQQKSGTSPKIWIY*DTSKLAS*GVPARFSG SGSWTSYSLTISSMEAEDAATYYC*QQWNSNP PT*FGAGTKLELK	Kumar *et al*., 2020
BIIB054	SYELTQPPSVSVSPGQTARITC*SGEALPMQFA H*WYQQRPGKAPVIVVY*KDSERPS*GVPERFSG SSSGTTATLTITGVQAEDEADYYC*QSPDSTNT YEV*FGGGTKLTVL	Weihofen *et al.,* 2019
PRX002	DIQMTQSPSSLSASVGDRVTITC*KSIQTLLYSS NQKNYLA*WFQQKPGKAPKLLIY*WASIRKS*GVP SRFSGSGSGTDFTLTISSLQPEDLATYYC*QQY YSYPLT*FGGGTKLEIK	Games *et al.,* 2014

	Variable heavy domain	**Reference**
α-miSOD1	EVQLVESGGDLVDPGGSLDLSCVAS*GFTFSNY*WMHWVRQAPGQRPVWVSRT*NTDGRN*TAYADYAKGRFTISRDNADSTLYLQLNSLRAEDTAVYFCAR*LRRNVADQITHNYYMDV*WGKGTLVTVSS	Maier *et al.,* 2016
C4F6	EVQLVETGGGLVQPDGSLKLSCAAS*GFTFNTN*AMNWVRQAPGKGLEWVARI*RSKSNNYA*TYYADSVKDRFIISRDDSQSMLYLQMNNLKTEDTAMYYCMR*APSNDFVY*WGQGTLVTVSAA	Urushitani *et al.,* 2007
AMF7-63	QSVGESGGGLVTPGTPLTLTCTVS*GFSLSSY*GVSWVRQAPGKGLEYIGFI*STRGN*PYYASWAKGRFTISKTSTTVDLKITSPTTEDTATYFCAG*ATVVGDSI*WGPGTLVTVSS	Pickles *et al.,* 2016
SE21	QIQLVQSGPELKKPGESVSISCEAS*GYTFTDS*AIHWVKQAPGEGLKYMGWI*NTYTGK*PTYADDFKGRFVFSLEASASTAKLQISNLKSEDTATFFCAR*SVYSYDGTFYRYFLDA*WGQGASVTVSS	Bakavayev *et al.,* 2021
MS785	AVQLVESGGGLVQPKESLKISCAAS*GFTFSDT*AMYWVRQAPGRGLEWVARI*RAKPYNYA*TYYADSVKGRFTISRDDSKSMVYLQMDNLKTEDTAMYYCTA*EGGYSGWYFDF*WGPGTMVTVSS	Fujisawa *et al.,* 2012

	Variable light domain	
α-miSOD1	EIVLTQSPGSLAVSLGERATINC*KSSQTVLYNN KNYLA*WYQQKPGQPPKLLIS*WASSRES*GVPD RFSGSGSGTDFTLTISSLQAEDVAVYYC*QHYY GTPVT*FGGGTKVEID	Maier *et al.,* 2016
C4F6	DIVMTQAAPSVPVTPGESVSISC*DSSKSLLHS NGNTYLY*WFLQRPGQSPQLLIY*RMSNLAS*GV PDRFSGSGSGTAFTLRISRVEAEDVGVYYC*M QHLEYPLT*FGAGTKLELK	Urushitani *et al.,* 2007
AMF7-63	QVLTQTASSVSAAVGGTVTISC*QSSQSVYKGY WQA*WYQQKPGQPPKLLIY*ETSTLAS*GVPSRF SGSGSGTQFTLTISGVQCDDAATYYC*AGGYS NNIYT*FGGGTEVVVK	Pickles *et al.,* 2016
SE21	ADTVLTQSPALAVSPGEKVTISC*RASESVSKHI H*WFQQKSGQQPTLLIY*LASSLES*GVPARFSGS GSGTDFTLTIDPVEADDTATYYC*QQSWNDPW T*FGGGTKLELK	Bakavayev *et al.,* 2021
MS785	EIVLTQSPTTMAASPGEKVTLTC*RATSSVSYM Y*WYQQKSGTSPKLWIY*DTSKLAS*GVPNRFSG SGSGTSYSLTVSSMETEDTATYYC*QQGRSFP PT*FGGGTKLELK	Fujisawa *et al.,* 2012

Appendix 2. Sequences of plasmid design features used in generating plasmid DNA containing the target protein and bioPROTAC, or used in generating scFv plasmid DNA*. T2A and P2A sequences are used to cleave the translated protein*

between the bioPROTAC and target protein. Linkers are used to connect VH-VL domains of intrabodies or connect E3 ubiquitylation domains with recognition sequences where necessary. Myc tags are incorporated for bioPROTAC detection by Western Blotting and myc pulldowns. FLAG and HA tags can also be used in this way but were used to increase the overall net negative charge of intrabodies.

Name	**Sequence**	**Molecular Weight**	**Theoretical pI**
P2A	ATNFSLLKQAGDVEENPGP	1.98kDa	4.14
T2A	EGRGSLLTCGDVEENPGP	1.82kDa	4.00
G4S	GGGGSGGGGSGGGGS	0.96kDa	5.52
G4D	GGDGGGGDGGGGDGGGDGG	1.04kDa	3.42
3x FLAG	DYKDHDGDYKDHDIDYKDDDDK	2.73kDa	4.16
HA	YPYDVPDYA	1.10kDa	3.56
myc	EQKLISEEDL	1.20kDa	4.00
Partial D3	GLFQNPKQI	1.04kDa	8.75